The Role of the Bone Marrow Niche and G-CSF in Osteochondral Repair

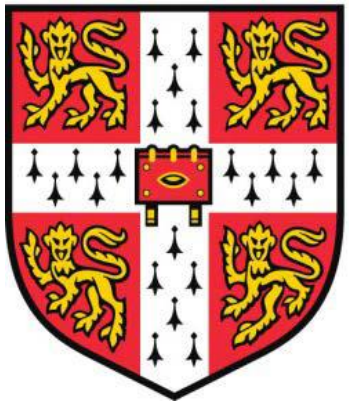

Francesca Emily Beaton

Queens' College

Division of Trauma and Orthopaedic Research, Department of Surgery

University of Cambridge

September 2018

This dissertation is submitted for the degree of Doctor of Philosophy

THE ROLE OF THE BONE MARROW NICHE AND G-CSF IN OSTEOCHONDRAL REPAIR

Francesca Emily Beaton

Osteoarthritis is a debilitating condition with an increasing global burden. Regenerative strategies to treat damaged articular cartilage aim to relieve pain and maintain joint function. Procedures for osteochondral repair, such as drilling or microfracture of the subchondral bone, are thought to restore cartilage by delivering bone marrow cells to the defect site. However, the specific identity or contribution of these cells to the repair process is not well understood.

Mesenchymal stem/stromal cells are thought to contribute to tissue repair by either progenitor or trophic action. In the bone marrow niche mesenchymal stem/stromal cells (BMSCs) contribute to haematopoietic stem and progenitor cell (HSPC) maintenance and the dynamics of this are disrupted by osteochondral repair procedures. In addition, the bone marrow niche can be further manipulated by the HSPC mobilising agent granulocyte-colony stimulating factor (G-CSF). This cytokine has previously been shown to improve the repair of osteochondral tissues, however, the cellular mechanisms underlying this response are poorly described. This thesis investigates BMSC and HSPC interactions in bone and cartilage repair, and the mechanism by which G-CSF may act to improve repair outcomes.

To look at BMSC–HSPC interactions a co-culture system was designed and then used to demonstrate that HSPCs inhibit the differentiation of BMSCs towards osteogenic and chondrogenic lineages. To explore the interaction and role of these cells *in vivo* during osteochondral repair, a mouse defect model was established. Defects were 729 (± 42.6) µm wide at the articular surface, occupied 41.6 (± 2.5) % of the width of the patella groove and penetrated 1205 (± 58.6) µm into the distal femur. The coefficient of variation (CV) for each parameter was below 6%. The area of injury demonstrated regenerated articular cartilage, an observation not previously described in the typically poor healing C57BL/6 strain of mice. Further, cells known to respond to G-CSF were seen to have specific spatial profiles in the osteochondral repair tissue over time. For example, at 24 hours post-surgery, defect sites were filled with a blood clot within which neutrophils (anti-NIMP) were embedded. After 1 week, these cells were no longer present within the injury whilst macrophages (anti-CD68) had infiltrated the wound site having previously been rarely observed at 24hrs.

To begin to understand the role of BMSCs in this repair model, Nestin-GFP reporter mice were studied. GFP signal was detected at the defect site at 24 hours after injury. Mice

treated with G-CSF showed an increase in Nestin-driven GFP in their spleens. In addition, GFP was detected in the defect of G-CSF treated mice at 4 days post-surgery.

To explore the role of G-CSF on BMSCs directly, in vitro techniques were used. These studies demonstrated the presence of a functional G-CSF receptor in the non-haematopoietic bone marrow-derived BMSCs. The impact on MSC cell function was explored, including proliferation and differentiation, showing minimal impact and suggesting a more likely role for G-CSF in the regulation of the trophic activity of BMSCs.

The data presented in this thesis further illustrates that the cross talk of multiple bone marrow cell types influences their cell fate. The osteochondral model developed during these studies can be exploited further to investigate the role of individual cell types during repair. In addition, the studies presented here illustrate that the actions of G-CSF are likely exerted on a diverse range of cell types during the repair process and a better understanding of the mechanism of action will allow greater precision, translation and clinical utility.

DECLARATION OF ORIGINALITY

This thesis is the result of my own work and includes nothing which is the outcome of work done in collaboration, except where indicated in the text or acknowledgements.

This research was conducted under the supervision of Professor Andrew McCaskie and Dr Mark Birch between October 2014 and September 2018. This work is not substantially the same as any that I have submitted, or, is being concurrently submitted for a degree or diploma or other qualification at the University of Cambridge or any other University or similar institution. I further state that no substantial part of my dissertation has already been submitted, or, is being concurrently submitted for any such degree, diploma or other qualification at the University of Cambridge or any other University of similar institution.

This thesis does not exceed the 60,000 word limit in accordance with the Degree Committee for the School of Clinical Medicine.

ACKNOWLEDGEMENTS

Firstly, I would like to thank each of my supervisors. Professor Andrew McCaskie for his ideas, support and leadership of the department, and Dr Mark Birch for his time, guidance and expertise. Secondly, thank you to other members of the group; Dr Virginia Piombo and Dr Frances Henson for their help in setting up the mouse work and Karin Newell for all her help in assisting me with the animal surgeries, making the process as smooth as possible. I am grateful to Dr Roger Brooks and Dr Nigel Loveridge for their support and thoughtful contributions which have enabled me to look at problems and results from multiple perspectives.

I would like to thank all other members both past and present of the group that I have had the opportunity to work with or alongside, for their professional guidance, teamwork in running the lab and encouragement during the ups and downs of PhD life – especially Niina Hopper and Sarah Lindsay. I like to thank Sophie Frankham-Wells, my fellow PhD starter, with whom I worked closely in our first year pulling together our previous experiences to kick-start our PhDs. I would especially like to thank my other fellow PhD students, Anna Albiero and Ciara Whitty. Their friendship and encouragement over the last four years has been invaluable as well as the scientific discussion and their contagious enthusiasm for research.

I gratefully acknowledge Arthritis UK and the University of Cambridge Clinical School, who provided the funding which made this PhD possible. Thank you to the patients and medical staff at Addenbrooke's Hospital for providing tissue donations. I'd also like thank the team in Phenomics for their help and Simon Mendez Ferrer and his group for the kind gift of transgenic mice.

Thanks to Julia, my scientific buddy outside of the Cambridge bubble, thank you for always asking and showing an interest in my work. This also goes for my housemate Sarah, your encouragement and support are invaluable. Your advice and the late night scientific discussions after long days in the lab has helped my PhD thesis to take shape.

Thank you to my school friends, their ability to take me thoughts away from PhD life and make great memories has been priceless. A special thanks to my oldest friends Amanda, Charlotte and Emily. Being bridesmaid for Amanda and Matt, and Emily and Alex, are major highlights of the last couple of years. I look forward to another 18 years of friendship.

Lastly, I would like to thank my family. My grandparents who instilled in me the attitude to never stop learning and to continue to push yourself throughout life. My brother, Stefano and my parents who have supported me every step of the way. I could not have achieved this without your love and encouragement.

CONTENTS

FIGURES

TABLES

ABBREVIATIONS

7-ADD	7-Aminoactinomycin D
ACI	Autologous Chondrocyte Implantation
AGM	Aorta-Gonad-Mesonephros
αMEM	Minimum Essential Medium Eagle Alpha Modification
ANOVA	Analysis of Variance
APC	Allophycocyanin
ATCC	American Type Culture Collection
BFU-E	Burst Forming Unit-Erythroid
Bglap	Bone Gamma-Carboxyglutamic Acid-containing Protein
BMSC	Bone marrow (mesenchymal) Stem/Stromal Cell
bp	base pair
BSA	Bovine Serum Albumin
cDNA	Complementary Deoxyribonucleic Acid
CFU-C	Colony Forming Unit-Cell
CFU-E	Colony Forming Unit-Erythroid
CFU-F	Colony Forming Units-Fibroblast
CFU-GEMM	Colony Forming Unit-Granulocyte, Macrophage, Erythroid and Megakaryocyte
CFU-M	Colony Forming Unit-Macrophage
c-Kit	Mast/Stem Cell Growth Factor Receptor
Col1a	Type I collagen
Col2a	Type II collagen
Csf3r	Colony Stimulating Factor 3 Receptor (G-CSF R)
CST	Cell Signalling Technologies
CXCL12	Stromal cell-derived factor 1
CXCR4	C-X-C chemokine receptor type 4
CXCR7	C-X-C chemokine receptor type 7
DAB	3,3'-diaminobenzidine
DAPI	4′,6-diamidino-2-phenylindole
DMEM	Dulbecco's Modified Eagle Medium
DMMB	Dimethylmethylene Blue
ECM	Extracellular Martrix
EDTA	Ethylenediaminetetraacetic Acid
eGFP	enchnaced Green Fluorescent Protein
FACS	Fluorescence-Activated Cell Sorting
FCS	Foetal Calf Serum
Flt3	Fms like Tyrosine Kinase 3

G-CSF	Granulocyte Colony Stimulating Factor
G-CSF R	Granulocyte Colony Stimulating Factor Receptor
GFP	Green Fluorescent Protein
HA	Hyaluronic Acid
Hck	Tyrosine-Protein Kinase HCK
HCl	Hydrochloric Acid
HPC	Haematopoietic Progenitor Cell
HPRT	Hypoxanthine Phosphoribosyltransferase 1
HRP	Horseradish Peroxidase
HSC	Haematopoietic Stem Cell
HSPC	Haematopoietic Stem and Progenitor Cell
IgG	Immunoglobulin
IHC	Immunohistochemistry
IL-6	Interleukin 6
ISCT	International Society for Cellular Therapy
JAK2/STAT3	Janus Kinase 2/Signal Transducer and Activator Of Transcription 3
LSK	Lineage, Stem cells antigen-1, Mast/Stem Cell Growth Factor Receptor
MACS	Magnetic-Activated Cell Sorting
MAPK/ERK	Mitogen Activated Protein Kinase/Extracellular Signal Regulated Kinase
MSC	Mesenchymal Stem/Stromal Cell
NaCl	Sodium Chloride
NHS	National Health Service
NICE	National Institute for Health and Care Excellence
OA	Osteoarthritis
PBS	Phosphate Buffered Saline
PCR	Polymerase Chain Reaction
PI3K/AKT	Phosphoinositide 3-kinase/Protein kinase B
PTPRC	Protein Tyrosine Phosphatase, Receptor Type, C
qRT-PCR	Quantitative Real-Time Polymerase Chain Reaction
RNA	Ribonucleic Acid
RPMI	Roswell Park Memorial Institute medium
Runx2	Runt-related transcription factor 2
Sca-1	Stem cells antigen-1
SCF	Stem cell factor
SDF	Stromal cell-derived factor 1
sMSCs	Synovial Mesenchymal Stem/stromal Cells
UK	United Kingdom
WHO	World Health Organization

1. INTRODUCTION

1.1. Osteoarthritis: The Clinical Challenge

Osteoarthritis (OA) is a degenerative musculoskeletal condition characterised by the progressive loss of articular cartilage, associated wear on nearby bone, degradation of local cellular structures, and inflammation. Its prevalence continues to increase and joint replacement remains the mainstay of treatment for end-stage disease. It is generally believed that untreated focal cartilage defects, for example caused by trauma, progress towards OA through a cascade of events. Early treating of these defects may hold the key to preventing subsequent progression to extensive cartilage degradation and the need for surgical intervention. While there are several techniques currently used in clinical practice, none are thought to be optimal.

1.1.1. Epidemiology and the cost of OA

OA has a multifactorial aetiology, considered to be the result of an interplay between systemic and environmental factors (Sandell, 2012; Chen et al., 2017; Mobasheri et al., 2017). Age is a major risk factor, with radiological evidence of the disease evident in most individuals aged over 65 years. In general, there is a negative correlation between age and the innate ability to maintain and repair tissues throughout the body. Furthermore, with regard to the joint, increased age is associated with an increased chance of joint trauma and biomechanical changes to joints as well as decreased physical activity, which can lead to decreased muscle strength and joint stability (OARSI, 2016).

On the other hand, it is widely accepted that trauma and overuse of joints, particularly by participants in sports or physical jobs associated with high impact or twisting loading, can lead to damage that predisposes the joint to OA (Buckwalter, 2003). Cartilage lesions are generally thought to progress to early OA (Gelber et al., 2000; Anderson et al., 2011). The likelihood of this may be affected by other factors such as genetic predisposition and obesity (Abramson and Attur, 2009; Sandell, 2012; Zengini et al., 2018).

The World Health Organization estimates that 9.6% of men and 18.0% of women over 60 years of age worldwide have significant clinical problems characteristic of symptomatic osteoarthritis (WHO, 2016). The United Nations predicted that the number of people aged 60 years or over is expected to more than double by 2050 (United Nations, 2017). Therefore, given that age is a primary risk factor, OA is set to become an increasing economic burden to healthcare systems. In addition, the intangible impact upon a patient's quality of life can be significant, with loss of function of the affected joint(s) and associated limitations to an individual's daily activities. This has the potential to result in depression, reduced social interaction and suboptimal workplace performance (Wieland et al., 2005;

OARSI, 2016). Whilst not life-threatening, OA can have significant impact on physical and mental health. It is therefore an increasingly important area for clinical intervention.

1.1.2. Diagnosis

Osteoarthritis can usually be diagnosed using a patient's medical history and a clinical examination (Sinusas, 2012). Plain radiography can detect joint space narrowing and bone changes including osteophytes, subchondral sclerosis and subchondral cysts, see Figure 1-1. The Kellgren-Lawrence scale is commonly used to categorise the disease progression from radiographs assigning a grade from 0 to 4, which correlates to increasing severity of OA; Grade 0 signifying no presence of OA and Grade 4 signifying severe OA (Kohn, Sassoon and Fernando, 2016). Advanced 3D imaging techniques are also used to show soft tissue and other local changes.

Patients commonly present themselves with secondary symptoms (including joint pain and a limited and/or painful range of movement in the joint) which occur long after initiation of OA. Ordinarily, OA affects joints in an asymmetrical manner; a singular joint can be affected but often multiple joints display some degree of degeneration.

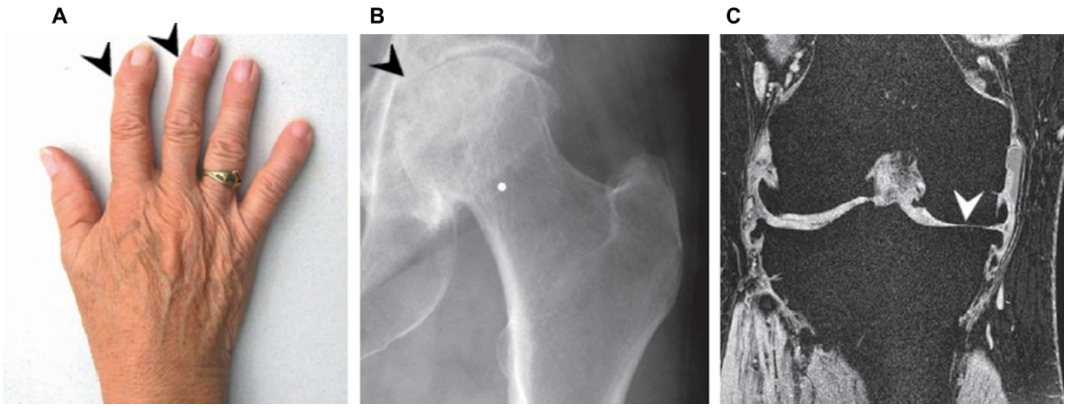

Figure 1-1 -The appearance of osteoarthritis.
(A) Deformities in the joints of the fingers are visible (black arrowheads), (B) narrowing of the hip joint space is observed using plain radiography (black arrowhead), (C) MRI shows the loss of the cartilage on the medial side of the knee (white arrowhead). (Image adapted from Bijlsma et al. 2011).

1.1.3. Pathological observations

OA is a disease of synovial joints, with pathological changes seen in the majority of the joint tissues including cartilage, subchondral bone, synovium, tendons, and muscles. Synovial joints are unique from other joints due to the presence of synovial fluid-filled capsules surrounding the joints, which allow for a wide range of movements.

The most defining feature of OA is the loss of articular cartilage matrix. Hyaline articular cartilage lining the distal ends of bones forms the articulating surface, which functions to

allow smooth low friction movement of the skeleton, distributing mechanical loads across the bone surface. It is a highly organised/structured tissue consisting of macromolecules and specialised proteins, which retain water, resulting in high tensile strength and flexibility (Gosset et al., 2008).

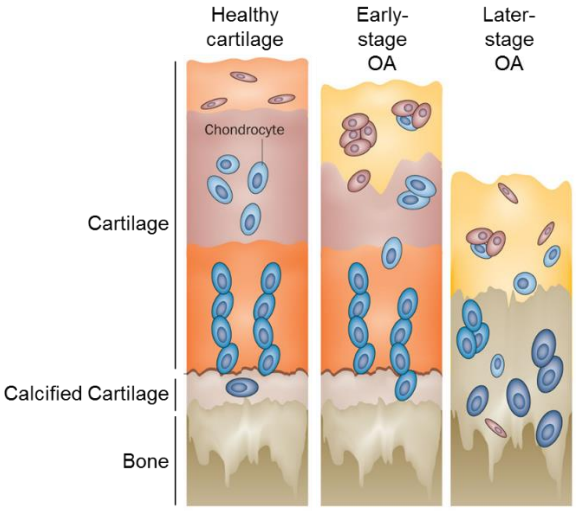

Figure 1-2 - Schematic of healthy and OA cartilage at early and later stages of disease progression.
Early OA is characterised by the loss of the superficial layer but as disease progresses the zonal architecture of the articular cartilage is lost and chondrocyte distribution is disrupted (image adapted from Jiang and Tuan, 2015).

Articular cartilage loss results from the breakdown of matrix proteoglycans and collagen, which are degraded by the action of proteolytic enzymes. It is believed that while limited pericellular remodelling of cartilage matrix can occur throughout life the extensive cartilage loss observed in OA results from a shift to a more catabolic chondrocyte phenotype. Alongside the loss of extracellular proteins, changes in chondrocyte morphology and spatial distribution can also be seen macroscopically (see Figure 1-2). Those in the superficial layer of articular cartilage become clustered, whilst those in the deeper and calcified layers undergo apoptosis (Zhang et al., 2016).

Changes in the bone underlying damaged cartilage also occur, including increased bone turnover and remodelling (Figure 1-3) (Li et al., 2013). This has been associated with microdamage in the bone, but it remains unclear if microdamage is an initiating event or the response to the overlying cartilage degradation (Madry, van Dijk and Mueller-Gerbl, 2010). Bone marrow oedema-like lesions and subchondral bone cysts are additional histopathological alterations in the subchondral bone (Kwoh, 2013; MacKay et al., 2018).

Bone outgrowths, termed osteophytes, are a pathological feature commonly observed in late stage OA. These are present at the margins of the joint in non-weight bearing zones, and are therefore not proximal to chondral lesions (Wieland et al., 2005; Li et al., 2013).

Their presence is thought to be controlled by growth factors elevated in OA, supporting the notion that OA is a joint disease, and not simply a disease of the cartilage (Steinberg et al., 2018). In addition to growth factors, cytokines and chemokines are also increased in OA. These molecules can affect matrix degradation and the repair equilibrium, exacerbating disease progression (Fellows et al., 2016).

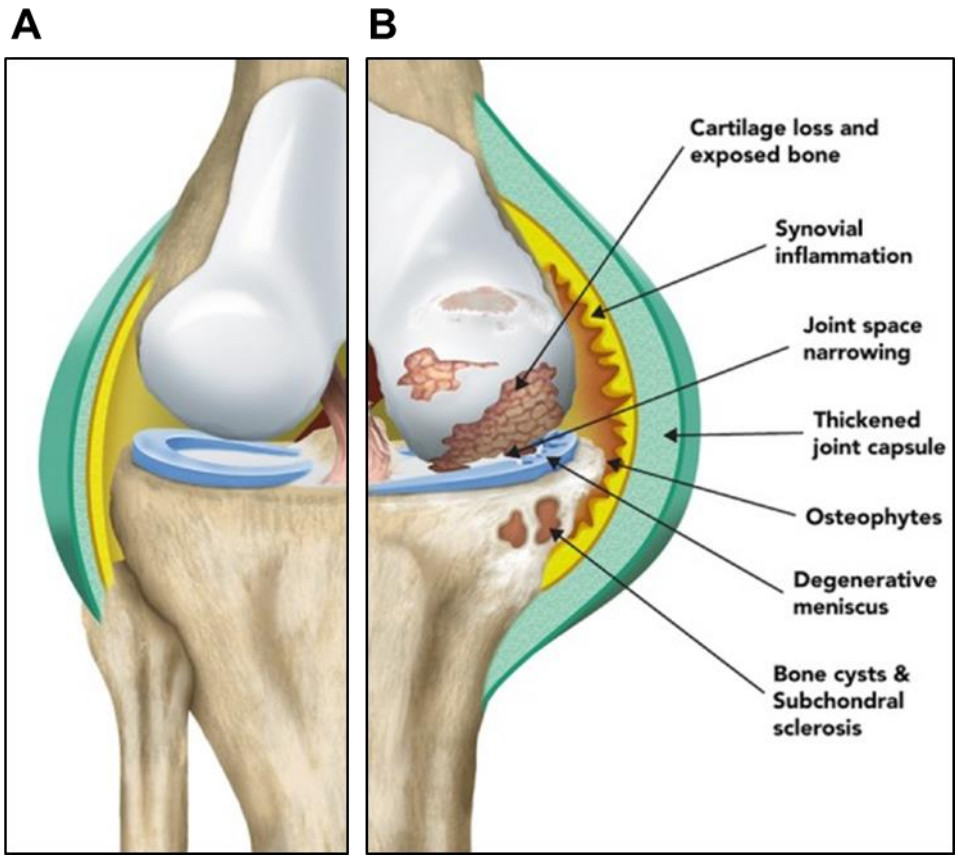

Figure 1-3 – Schematic describing the tissue changes and degeneration of an osteoarthritic knee
(A) A healthy knee joint with complete covering of articular cartilage and no synovial inflammation. (B) Degeneration of articular cartilage, synovial inflammation and bone changes are depicted (image adapted from Cibrián Uhalte et al., 2017).

1.1.4. Current treatment strategies for OA

A stepped-care approach is the most widely-used treatment strategy for OA (Sinusas, 2012), focusing on reduction of pain and improved function of affected joints (Zhang et al., 2016). A lack of disease modifying-drugs (pharmaceuticals) has led to conservative treatments for OA, such as first line analgesics, used to target symptoms, rather than an approach aimed at reducing disease progression (Wieland et al., 2005; Driban et al., 2010). Alongside these pharmacological strategies, physical therapy, bracing and splinting of the joint, weight loss, and exercise have been shown to have significant clinical benefit by supporting and strengthening the joint (Sinusas, 2012; Marenah et al., 2018).

As the disease progresses and the effect upon a patient's daily activities becomes strongly apparent, surgical intervention becomes appropriate (ARUK, 2013). Currently the most effective procedure is total joint replacement, but other surgical procedures are also used as preliminary measures.

1.1.5. Patient stratification and the need for a new strategy

One might expect that for effective treatment and the ability to halt disease progression, a thorough understanding of the pathological process would be required. In the field of musculoskeletal repair, however, this is not the way treatment strategies have classically developed. The pathogenesis profile of OA is therefore yet to be fully elucidated.

The reasons behind this can be strongly associated with the mainstay of OA treatment; the joint replacement. Since the 1960s, (Charnley, 1961) this treatment has answered the need for a solution to the disabling effects of OA. However, this approach has fundamental limitations; it initially masks the symptoms using analgesia and then waits for the condition to be 'bad enough' to warrant surgery. This has major cost effects, on both patients and the healthcare system (Marenah et al., 2018). Additionally, in more recent years the failure of this treatment to be curative has become evident. Approximately 5% of patients who have a total hip replacement or total knee replacement over the age of 70 years will require revision surgery and significantly, this increases to 35 % for men in their early 50s (Bayliss et al., 2017). With an ever-increasing life expectancy (resulting from advances in the treatment of conditions which were once life-threatening), increasing healthcare costs, increasing prevalence of risk factors (e.g., obesity), and growing expectations of patients, the need for a more permanent solution to treat OA has become apparent (Driban et al., 2010).

Although OA is now accepted to be a heterogeneous disease, it is still unstratified and grouped clinically as a single condition with the same common endpoint of joint replacement for practically all patients. For improvement in outcomes, it is becoming more widely accepted that there is merit in clinically stratifying patients and evolving subset, or even personalised, medical approaches, whether these be surgical treatments or the development of disease-modifying drugs.

The best method to stratify OA, however, is unclear. OA is considered highly heterogeneous and alongside variables relating to the initiation of OA and genetics, joints vary in terms of clinical symptoms and biochemical temporal profiles (Driban et al., 2010; Kraus et al., 2015; Mobasheri et al., 2017). Mechanism of onset is perhaps the most obvious way to sub-categorise OA. Whilst age related-OA is difficult to predict, patients who have an increased risk of secondary OA due to joint trauma or genetical predisposition might identify younger patients at an early stage of disease progression (pre-OA) where early intervention is indicated (Ryd et al., 2015). Furthermore, one could

consider this the demographic most in need of a cure or at minimum a long-term solution, as opposed to the current best option of mid-length joint replacement.

1.2. Trauma Induced Chondral Defects

Joint trauma, either to the cartilage directly or to the other structures of the joint have been shown to substantially increase the risk of OA accounting for 12% of all cases (Gelber et al., 2000). These can be either single or repetitive injuries and include any kind of acute physical trauma such as a sports injury, vehicle accident or fall. The pathogenesis and transition from a chondral defect to established OA is not well-characterised, with limited evidence as to which lesions are likely to progress to OA (Punzi et al., 2016). One potential route is through changes in biomechanics. Even a small cartilage defect, or change in gait due to damage to ligaments, tendons or other joint tissues, has the potential to change the biomechanical properties of the joint. This alters the load distribution on the articular surface and the strains on the joint tissues (Gomoll et al., 2010). These changes increase the likelihood of widespread cartilage degeneration by affecting joint movement, mechanical wear and attrition of opposing surfaces as well as the formation of loose debris. At the cellular level, the damage of cartilage can be characterised by cell death and inflammatory events that can affect the biology of the entire joint compartment (Punzi et al., 2016).

Patients presenting to clinicians with OA that was initiated from a joint trauma injury are on average over 10 years younger than those whom progress to OA from an alternative aetiology (Gelber et al., 2000). Whilst total joint replacement is effective for established degenerated joints, this treatment strategy is not viable for this younger patient group before extensive OA changes develop. These patients ideally require a life-long treatment to regain full use of their joint and to reduce their risk of progression to OA. This would be achieved by re-establishing a normal articular surface (Caldwell and Wang, 2015; Zhang et al., 2016). Furthermore, before OA onset these patients have a relatively ‘normal’ joint environment compared with a chronic OA joint. It is perhaps then obvious to try and intervene at this stage to repair the injured tissue rather than wait and treat a disease of the whole joint.

To summarise, it is widely considered that a less invasive intervention, earlier in disease progression, which can regenerate damaged articular cartilage, would be more effective in these patients. Importantly, it is in these individuals that one may have the best chance of developing a curative regenerative treatment.

1.3. Cartilage Regeneration

Several approaches are being investigated for the regeneration and long-term repair of articular cartilage (Marenah et al., 2018). These include the use of scaffolds and the transplantation of cells, with the aim to improve or replace the low innate capacity of cartilage to regenerate. Nevertheless, the clear dominance of joint replacements partly reflects the difficulties that have been encountered trying to address this need.

First, it is worth considering what the ideal situation would be. The answer is simple: to restore the tissue to its pre-trauma or pre-disease state. Consequently, there would be a lack of scar formation following repair, which, for most adult tissues is not achieved by endogenous healing. In the case of cartilage, scar formation is particularly problematic as it can disrupt the smooth articular surface and lack full integration with the surrounding cartilage. This can have detrimental implications, disrupting the mechanical properties that allow for even loading of the joint and pain free movement (Tiku and Sabaawy, 2015). This has been the primary difficulty in the field; establishing cartilage that displays mechanical and functional characteristics that are comparable with native articular cartilage and result in pain free movement.

1.3.1. Basic cartilage biology

To design new strategies, a good understanding of the tissue of interest is first required. Articular cartilage contains a single cell type, the chondrocyte. These cells are individually isolated within lacunae surrounded by extracellular matrix (ECM). Relative to the volume of the tissue, chondrocytes are sparsely distributed, and rely predominantly on diffusion for nutritional support. These cells are responsible for producing, sustaining and degrading the ECM (Gosset et al., 2008). The chondrocytes of articular cartilage are distinct from chondrocytes located in other cartilaginous tissues, such as the ear and nasal septum, in terms of the matrix they produce. The two main macromolecules in articular cartilage matrix are produced by these cells: the large proteoglycan aggrecan and type II collagen. However, articular cartilage is not homogenous and displays a zonal structure with four distinct zones: superficial, transitional (middle), deep, and calcified (Figure 1-4). Each zone has unique properties relating to cell density and morphology, collagen fibre orientation, and biomolecular composition (Fox, Bedi and Rodeo, 2009).

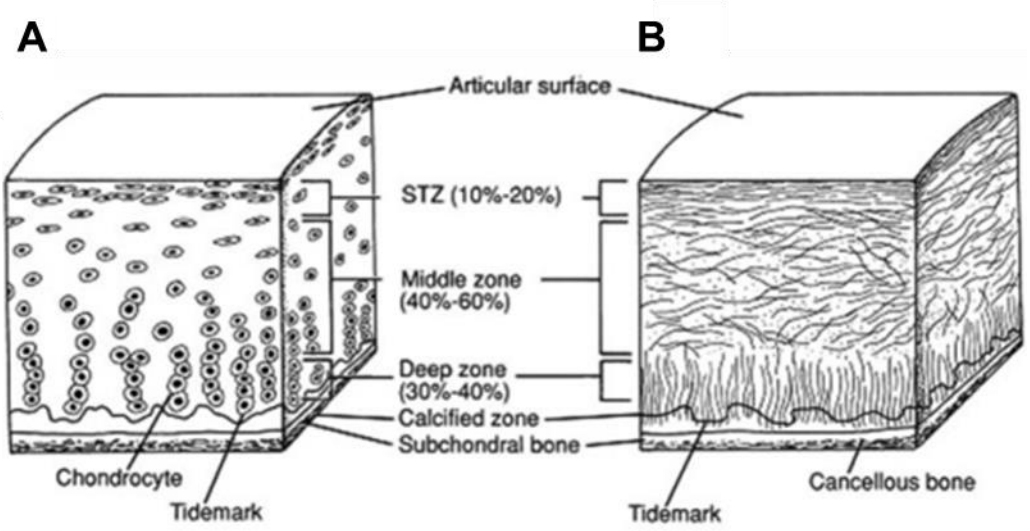

Figure 1-4 – Schematic describing the architecture of articular cartilage
Cross-sectional diagram showing the zonal structure of healthy articular cartilage with differing cellular (A) and collagen fibre compositions (B) (image adapted from Fox, Bedi and Rodeo, 2009).

The superficial layer of articular cartilage, which directly apposes the other articular surface in the synovial joint, contains cells which are flat in shape and produce large amounts of proteoglycans including aggrecan, lubricin and proteoglycan 4 (PRG4) (Tiku and Sabaawy, 2015). These glycoproteins maintain the integrity of the superficial zone, whilst providing lubrication and resistance to shear stresses. This is fundamental to protect and maintain the deeper cartilage layers.

Below the superficial zone, in the middle zone, chondrocytes are rounder and surrounded by randomly organized collagen type I fibrils, whilst in the deep zone these cells are ellipsoid and stacked in cell columns parallel to the collagen fibres orientated perpendicular to the articular surface. This deep zone has the highest proteoglycan content and the lowest water concentration and is believed to provide an important role in the distribution of aggrecan and collagen ensuring cartilage can maintain its mechanical function. Below this layer, cartilage is calcified acting as a transitional zone by anchoring the overlying hyaline cartilage to the subchondral bone. Containing hypertrophic chondrocytes, this zone is separated from other layers of cartilage by the ‘tidemark’ boundary marking the mineralisation front.

The ECM of each of these layers is continually remodelled through normal tissue turnover with chondrocytes replacing lost macromolecules (Goldring and Marcu, 2009). Whilst metabolically active, chondrocytes rarely divide after skeletal growth is complete. Dogma has long held that the cartilage lacks a progenitor cell population. In recent years however, this has been challenged by multiple research groups and the superficial zone of articular cartilage has been reported to contain cells with stem-like properties (Dowthwaite et al., 2004; Hattori, Oxford and Reddi, 2007; Williams et al., 2010). It is therefore suggested

that articular cartilage has a resident population of cells with the potential under certain circumstances to regenerate the tissue.

1.3.2. Endogenous repair of defects

Articular cartilage defects are generally centred on load bearing areas and can be limited to the cartilage as chondral defects or extend into the bone when they are termed osteochondral defects (Brittberg et al., 1994). It has long been argued that defects solely of the cartilage have little capacity to repair, with the characteristics of cartilage suspected to be the primary problem. The isolation of individual chondrocytes, with a lack of proliferation and migration ability, was first proposed in the 18th century to be the compounding factor restricting the ability of the cartilage to heal spontaneously (Marmotti et al., 2013a). Articular cartilage has since been considered to have a poor intrinsic regeneration potential attributed to its low cellularity, lack of vascularity and the dense, hydrated extracellular matrix that inhibits cellular migration in and around the tissue.

Alongside the identification of chondro-progenitors, there is now evidence that the cartilage does attempt some level of repair. Molecular processes such as the expression of proteases and the release of growth factors which occur in other wounds do exist (Tiku and Sabaawy, 2015). Furthermore, studies in OA have demonstrated an increase in matrix synthesis as well as cell proliferation - with clusters of chondrocytes forming at the borders of the damaged cartilage. These clusters of six or more chondrocytes residing in one large lacuna are considered a hallmark of OA. Seol et al., (2012) published evidence that localised chondrocyte death activates clonogenic cells to migrate towards the injury boundary (Seol et al., 2012). Importantly, however, it is not yet known if this proliferative response is a true attempt at endogenous regeneration by the cells of the cartilage (Lotz et al., 2010). As a consequence, it is worth noting that, although it is well reported that chondral defects fail to heal, it may simply be that those that successfully heal are not clinically investigated.

Whilst the regenerative capacity of chondral-only defects is unclear, osteochondral defects (see Figure 1-5), which bleed on penetration of the underlying subchondral bone, are well accepted to generate a level of endogenous repair. If small enough, it is thought that these defects can heal spontaneously (Lydon, Getgood and Henson, 2017).

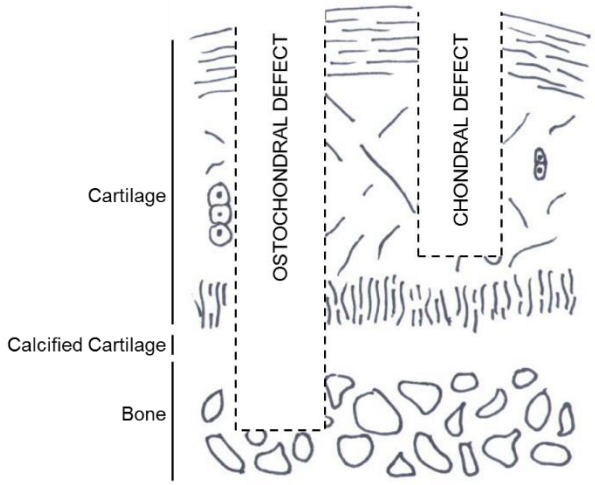

Figure 1-5 – Schematic of osteochondral and chondral defects
Depiction of the difference in depth of osteochondral and chondral defects. The former penetrates through the calcified cartilage into the subchondral bone whereas chondral defects only damage the overlying articular cartilage.

The bone marrow that fills the cavity of the long bones and lies beneath the subchondral bone plate is a well-characterised microenvironment. Bone marrow has long been used as a source for cellular therapy because it contains an array of different cells; from mature differentiated cells, to cells more 'stem-like' in nature which harbour multipotent potential. These properties make it a primary site for stem cell and tissue regeneration research. Cell types include inflammatory cell progenitors, haematopoietic stem cells and vascular progenitors all of which are thought to contribute to wound repair. Further, multipotent cells capable of differentiating into cartilage and bone are present; mesenchymal stem/stromal cells. Which cells of the bone marrow play a role in the endogenous repair of osteochondral defects is yet to be fully elucidated, but much research surrounds the recruitment, migration and cell therapy usage of this latter cell type into the defect site.

Unfortunately, unlike the ideal and original hyaline cartilage, the fibrocartilage produced by the repair of osteochondral defects lacks the highly organised structure and biomechanical properties of healthy hyaline articular cartilage. It can be considered scar tissue, lacking some aspects of the biomechanical properties believed necessary for durable long-term repair. However, the formation of a scar is an improvement on a wound and is considered to be superior to a chondral defect. Surgeons aim to replicate this endogenous repair capability using bone marrow stimulation techniques such as microdrilling and microfracture.

1.3.3. Mimicking endogenous repair using the microfracture technique

Microdrilling was first developed by Pridie in 1959 (Pridie and Gordon, 1959) where damaged cartilage is debrided to the level of the subchondral bone, and a drill is used to

bore through to the marrow cavity. Pressure within the marrow cavity leads to extrusion of blood and bone marrow into the defect site to form a clot. The microfacture technique was subsequently developed in the 1980s by Steadman (Steadman et al., 1997) where an awl is used rather than a microdrill as used in microdrilling (see Figure 1-6).

The ultimate intention of bone marrow stimulation techniques is to bring about the endogenous repair seen in naturally occurring osteochondral defects. Unfortunately, like the naturally-occurring repair tissue, the surgically-induced defects result in the formation of fibrocartilage-like repair tissue (Caldwell and Wang, 2015). It is recognised, however, that the microfracture technique while beneficial in providing effective short-term functional improvement to patients, (Mithoefer et al., 2009) it is not a long-term solution. This is due to concerns in the durability of the repair that is thought to be unable to withstand the demands of everyday activities resulting in the return of clinical symptoms (Fellows et al., 2016).

Currently this technique is used in patients who are preferably younger than 45 years of age, have a body mass index below 30, and have experienced symptoms for less than one year. Contraindications include degenerative joint diseases and axial malalignment (Steadman, Rodkey and Briggs, 2010). For this reason, microfracture addresses a patient stratification category that identifies early trauma-induced cartilage defects, being useful as a preventive measure against the development of OA in the affected joint.

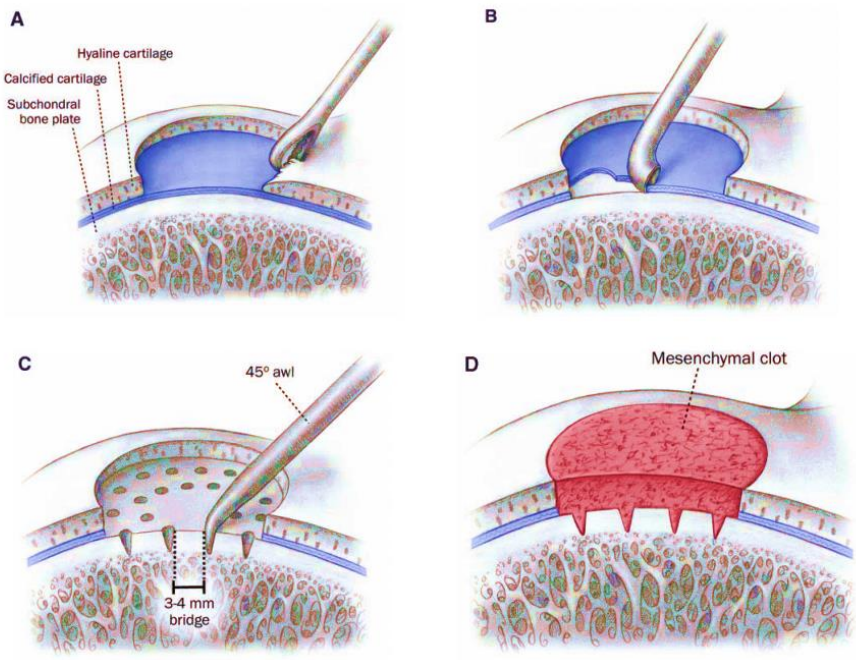

Figure 1-6 - Microfracture surgical technique.
(A) Debridement to generate a clear margin, (B) Removal of calcified cartilage, (C) Microfracture penetration within the cartilage defect, (D) Penetration through to the bone marrow results in filling of the defect with a mesenchymal blood and bone marrow clot (image adapted from Mithoefer et al., 2009).

1.4. The Relationship between Cartilage and Bone

Bone marrow stimulation techniques like microfracture disrupt the structure and mechanical integrity of subchondral bone. This is believed to play a part in the healing response of the osteochondral tissues as bone and cartilage are tightly coupled; the disruption of either tissue can have adverse effects on the other. For example, some cartilage defects have been linked to changes in the underlying bone, such as in osteochondritis dissecans (Gomoll et al., 2010) and malalignment of joints (Li et al., 2013). Further, it has been proposed that cross-talk and physical connections between cartilage and its underlying bone could be partly responsible for the pathogenesis of OA (Li et al., 2013). This highlights the important interplay between these two tissues. As the understanding of these interactions improves, cartilage defects are being increasingly viewed as a problem of the entire osteochondral unit, rather than limited to the surface cartilage alone (Gomoll et al., 2010). Here, the development of the bone, the synovial joint and articular cartilage will be discussed.

1.4.1. The development of bone

Alongside their relationship in the adult skeleton, cartilage and bone also have a close connection in terms of developmental biology. Understanding developmental biology is considered critical in the field of regenerative medicine, as it is the process a regenerative treatment ideally recapitulates. It is therefore worthwhile to briefly overview this process.

Developmental biology describes the formation of three germ layers during embryogenesis; the ectoderm, mesoderm, and endoderm. Individual skeletal segments develop through either intramembraneous ossification or endochondral ossification (Mackie, Tatarczuch and Mirams, 2011). The flat facial bones develop via the former, whereby bone is lain directly onto fibrous connective tissue. Long bones of the skeleton, on the other hand, develop by endochondral ossification that differs as a temporary cartilage scaffold precedes the formation of bone. This second ossification method will be discussed further in section 1.4.2.1 due to its relevance to long bone and bone marrow formation.

1.4.2. Synovial joint and articular cartilage development

The cartilaginous model (the anlagen) of the appendicular skeleton is formed from the lateral plate mesoderm by condensations at the limb bud, forming rod-like structures of a temporary cartilage scaffold, sheathed by perichondrium. This is a continuous and uninterrupted structure until segmentation occurs where a stripe of mesenchymal tissue forms the joint interzone beginning synovial joint formation (Archer, Dowthwaite and Francis-West, 2003; Koyama et al., 2008; De Bari, Kurth and Augello, 2010). Subsequently, the interzone divides into three layers to generate the joint cavity. The two

outermost layers contribute to the adult articular cartilage and the inner layer, alongside surrounding mesenchyme, contributes to multiple joint tissues including the synovial membrane, menisci and ligaments as well as superficial zone chondrocytes. The contribution to the adjacent long bone cartilaginous shaft, on the other hand, is negligible.

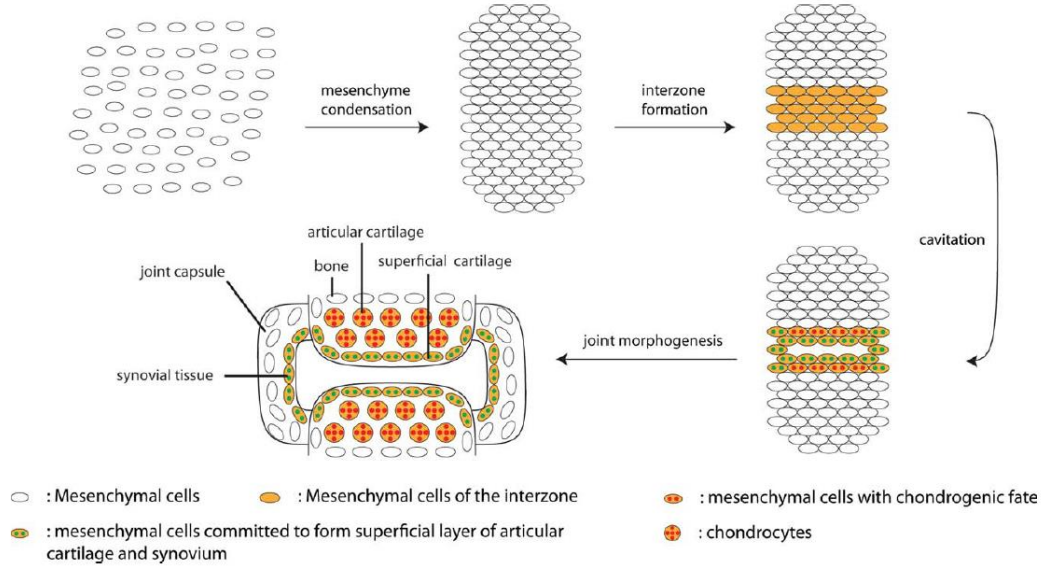

Figure 1-7 – Synovial joint development
Schematic representation of synovial joint development that begins by cavitation of the mesenchyme limb bud at the interzone. Cells of the interzone subsequently contribute to the tissues of the articular cartilage and synovial lining (image from De Bari, Kurth and Augello, 2010).

1.4.2.1. Endochondral ossification

The formation of the synovial joint occurs simultaneously with the initiation of endochondral ossification of the cartilaginous scaffold. Limb bud cells differentiate into chondrocytes, proliferate, mature and undergo hypertrophy within each condensation. The scaffold structure is then ossified and replaced by bone, a process that is achieved by the coordinated action of a number of different cell types (Mackie et al., 2008).

At the onset of ossification, vasculature invades and tissue mineralises before bone remodelling occurs (Sivaraj and Adams, 2016). Remodelling is a process where old bone is resorbed by osteoclasts (phagocytic multinucleated cells derived from the monocytic haematopoietic lineage) and new bone laid down by osteoblasts (large cuboidal cells which are very active protein secretors, derived from the mesenchymal stem cells). As this remodelling takes place, large-calibre sinusoid-type blood vessels form and haematopoietic progenitors home to this microenvironment leading to the formation of bone marrow.

Bone remodelling continues throughout life to maintain the structural integrity of the skeleton. Consequently, 5-10% of the skeleton is replaced every year after skeletal growth

is complete and concordantly this process repairs ‘wear and tear’ microdamage. Furthermore, it is noteworthy that this process of endochondral ossification is an example of a developmental process that re-occurs in the adult, during fracture healing where a cartilaginous callus forms followed by mineralisation to regenerate the bone (Baron and Kneissel, 2013; Sims and Martin, 2014).

1.5. Mesenchymal Stromal / Stem Cell

Both chondrocytes, bone forming osteoblasts and other mature cells of bone (osteocytes and bone-lining cells) are thought to be derived from a common multipotent progenitor. Discovery of the existence of this cell type built momentum in the 1960s. Firstly, Tavassoli and Crosby (1968) established that postnatal bone marrow suspensions (devoid of bone) has an inherent osteogenic potential. Friedenstein and co-workers followed this with a series of seminal studies demonstrating this was associated with a subpopulation of bone marrow cells (Friedenstein et al., 1968; Owen and Friedenstein, 1988). Further, these cells were able to form ectopic ossicles comprising of multiple skeletal tissues, including bone, cartilage and haematopoietic bone marrow when transplanted under the renal capsule (Tavassoli and Crosby, 1968). Thus, the hypothesis that these tissues were derived from a single progenitor cell population was born. Over time, this progenitor population has been refined to describe an adherent non-haematopoietic cell type that is capable of self-renewal and demonstrates multipotency – commonly described as a Mesenchymal Stromal / Stem Cell (MSC).

1.5.1. Identifying MSCs

1.5.1.1. In vitro

MSCs are now commonly defined by their adherence to plastic, their ability to form fibroblastic colony forming units (CFU-F) *in vitro* (indicative of self-renewal) and their osteogenic, chondrogenic and adipogenic *in vitro* potential (indicative of multi-potency), as demonstrated by the production of mineralised, polyanionic, and hydrophobic material respectively (Bianco et al., 2013).

In 2006, the International Society for Cellular Therapy (ISCT) published a seminal paper proposing a profile of cell surface markers in an attempt to improve comparability across MSC research (Dominici et al., 2006). Surface markers are a modern staple of biology, used to help identify and classify cells. However, although many markers have been reported to identify MSCs, no single marker is uniquely expressed by these cells. Much research has gone into looking for an elusive definitive MSC marker and there is currently a whole array under investigation. The ISCT paper defines a minimal criteria for MSCs: positive phenotypic expression of surface molecules CD105, CD90 and CD73, whilst negative for pan leukocyte (CD45), endothelial or primitive haematopoietic (CD34),

monocytic (CD14 or CD11b), B cell (CD79a or CD19), and lacking the expression of HLA class II (Dominici et al., 2006).

These criteria have been adopted as best practice and are widely used as a retrospective identification strategy of culture expanded cells (De Bari, Kurth and Augello, 2010; da Silva Meirelles, Caplan and Nardi, 2008). A key insufficiency of the phenotypic analysis conducted in many papers is the reporting of global expression of these markers across the cell population under investigation rather than characterisation to the level of the single cell. Dominici et al. (2006) suggest that multicolour analysis would be optimal, but little has been published as to whether individual cells express the entire set of ICTS markers.

1.5.1.2. In vivo

To date most of the work on MSCs has been based *in vitro* on plastic adherent, culture expanded cell populations and a true *in vivo* correlate of these cells has yet to be identified. To understand the *in vivo* biology of MSCs there is a need for the ability to locate and track their role in their native environment. Dominici and colleagues' (2006) focused on *ex vivo* identification of MSCs and to date the research community has yet to find a consensus on *in vivo* identification. This lies in part down to the lack of a single (unique) marker. Markers that have been suggested include leptin receptor and nestin (Wang et al., 2014).

1.5.2. MSC terminology

The appropriate name for these cells remains controversial. Friedenstein and Owen called this cell type an osteogenic stem cell (Friedenstein, Chailakhyan and Gerasimov, 1987) and then a bone marrow stromal stem cell (Owen and Friedenstein, 1988). In 1991 Caplan coined the term mesenchymal stem cell based on these studies and *in vitro* evidence that these cells could differentiate *in vitro* into other mesenchymal lineages (Caplan, 1991).

1.5.2.1. Derived from the mesoderm?

Whilst bone marrow MSCs can be considered the 'conventional' MSC, being the first tissue from which these cells were identified (Friedenstein, Chailakhyan and Gerasimov, 1987). Cells that adhere to plastic, form CFU-Fs and are tri-potent have since been isolated from most connective tissues including skeletal muscle (Uccelli, Moretta and Pistoia, 2008) and placenta tissue (Talwadekar, Kale and Limaye, 2015). With this ability to isolate from these tissues, research have also shown an ability to differentiate MSCs *in vitro* isolated from different tissues down other mesoderm lineages, for example myogenic (Drost et al., 2009). One could therefore postulate that the MSC represents a common progenitor of all non-epithelial, non-haematopoietic tissues that are developmentally derived from the mesoderm.

In addition to differentiation down mesodermal lineages other than skeletal tissues, reports have also been made of differentiation of MSCs to cells classically defined as cells of ectodermal origin; such as neurons (Scuteri et al., 2011) and epithelial skin cells (Păunescu et al., 2007). One therefore might claim that MSCs are capable of differentiation down numerous lineages of all three developmental layers. However, there are reasons to be hesitant to reach this conclusion. Namely, culture conditions can fundamentally alter cell properties. It is well accepted that *in vitro* conditions are unable to replicate the environment found in a cell's original anatomical location and in biology generally, it is recognised that cells can be induced to undergo differentiation by reprogramming *in vitro.* This leads to experimental artefacts and difficulties in interpreting functional assays performed *in vitro*.

This same argument can be made against the MSC status of MSCs derived from mesodermal tissue other than bone marrow. Bianco and Robey, define MSCs from these tissues as being 'inducible' rather than 'determined' skeletal progenitors (Bianco and Robey, 2015). In support, it has been demonstrated that just because a cell can undergo tri-lineage differentiation *in vitro* it does not translate to *in vivo* potential. Reinisch and colleagues, compared MSCs derived from human bone marrow, white adipose tissue, umbilical cord, and skin (Reinisch et al., 2015). Whilst the populations have similar phenotypic profile matching the ISCT panel and were differentiated down osteogenic, chondrogenic and adipogenic lineages *in vitro*, only the bone marrow derived MSCs were able to form a haematopoietic microenvironment consisting of bone through a cartilage intermediary structure, *in vivo*.

1.5.2.2. Developmental origins?

In addition to the arguments discussed above, Bianco and Robey strongly dispute that cells from connective tissues other than the skeletal tissues are equivalent stating they are 'developmentally distinct from skeletal lineages'. One must consider however, the developmental ontogeny of bone marrow and all other prospective MSCs is unclear.

Based on knowledge of long bone development, it might be expected that the limb bud, from which the anlagen forms, contains cells capable of both cartilage and bone formation. Mendes et al. (2005) through *in vitro* characterisation aimed to prove this. They performed anatomical mapping and frequency analysis of mesenchymal progenitors by their isolated from different tissues, reporting that cells of the limb bud were pre-chondrogenic but unable to differentiate down osteogenic or adipogenic lineages *in vitro*. This disputed hypothesis, instead suggesting that osteoblast precursors must therefore infiltrate into the anlagen.

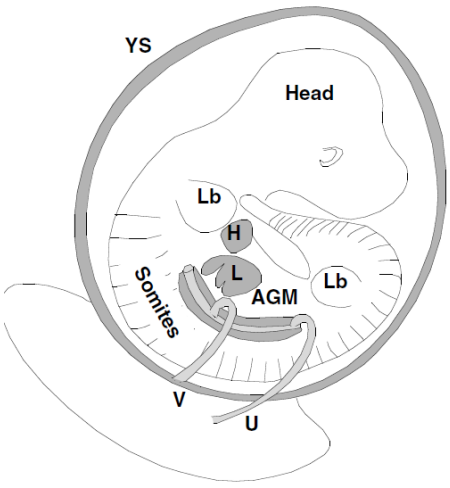

Figure 1-8 – Schematic of a mouse embryo at E11
Schematic to illustrate tissues of a mouse embryo 11 days of age. YS, yolk sac; Lb, limb bud; H, heart; L, liver; AGM, aorta-gonad-mesonephros; U, umbilical artery; vitelline artery (Mendes, Robin and Dzierzak, 2005).

Like the mesenchymal cells that make up the limb bud, osteoblasts are derived from the lateral plate mesoderm as demonstrated by cell tracing using the Hoxb6 gene reporter mouse (Isern et al., 2014). The aorta-gonad-mesonephros (agm) region (see Figure 1-8) is also derived from the lateral plate mesoderm, and it is in this region that Mendes et al. (2005), at the E11 stage of mouse development, solely located cells capable of tri-lineage differentiation indicative of MSCs.

Later developmental time points, on the other hand, located MSCs to primary haematopoietic tissues including the liver and bone marrow. MSCs have been found in the circulation of mouse embryos between E12 and E14 but disappeared by E17 (Mendes, Robin and Dzierzak, 2005) and in human foetal blood, liver and bone marrow during the first trimester (Campagnoli et al., 2001). If MSCs are derived from the same developmental lineage, this could define a potential migratory route for MSCs to reach the multitude of tissues from which they have been isolated and could identify a developmental relationship between these cells.

In support of this, much has been made of the similarities between MSCs and pericytes. Pericytes are found in all tissues but are not a cell lineage – they are defined morphologically based on their location relative to endothelial cells. They are recruited to this location from the surrounding tissue during organ development and growth (Bianco et al., 2013). Additionally, many markers including Nestin (Ferraro et al., 2011), CD146 (Sacchetti et al., 2007), and CXCL12 (in the mouse) (Bianco, 2011) used to identify putative MSCs *in vivo* identify cells localised adjacent to blood vessels. Noteworthy, however, is that not all pericytes have the unique properties of MSCs and most importantly, not all MSCs are located in close proximity to blood vessels (Ma et al., 2014).

In conclusion, the validity of the term ‘mesenchymal’ in MSC remains contentious. Either way, whether MSCs are comparable in adulthood is another question and one that is more important to regenerative repair. Importantly, researchers want to be assured that all cells studied under the term MSC are equivalent. As discussed, to date the main way in which this has been done is by utilisation of the *in vitro* tri-lineage differentiation assay, but this lacks scientific rigour. Nonetheless, this method did receive support in the ISCT position paper that defined this as a method to define ‘multipotent differentiation potential’ (Dominici et al., 2006).

1.5.2.3. True stem cells?

Till and McCulloch (Becker, A. J., McCulloch, E. A. & Till, 1963), were the first to propose the concept of a stem cell; a cell capable of self-renewal and multipotency, through their work on hematopoietic stem cells using the clonal colony formation assay. Functional assays have since become the principle method used to identify all stem cells. True haematopoietic stem cells are now identified by long-term reconstitution assays through serial transplantation. This *in vivo* assay provides evidence that the original cell is capable of generating fully differentiated tissues – in this case mature cells of the blood – and is able to reconstitute cells identical in phenotype and potency to itself. This defines the properties of multi-lineage and self-renewal respectively.

The heterotopic ossicle assay, developed from work by in Tavassoli and Crosby, is considered the equivalent assay for an MSC to demonstrate multipotency - the formation of a miniature bone organ with the correct histology, architecture and skeletal cell/tissue types, driven independently from exogenous, skeletogenic cues. The resulting structure is thought to be the progeny of MSCs alone, forming bone, cartilage, adipocytes, fibroblasts and haematopoiesis supporting stroma. The ability to generate this ectopic ossicle is now considered a more reliable piece of evidence that an MSC is truly a multipotent progenitor. Additionally, Bianco (2008) argued that to truly claim a cell is an MSC, the progeny of a single cell would need to be evaluated for the formation of multiple tissues *in vivo*. This originates in the widely accepted concept that primary MSC cultures are heterogeneous populations, secondary to the heterogeneity observed between tissue sources.

In 2007, Sacchetti, Bianco and colleagues, published the first evidence of self-renewal using this assay (Sacchetti et al., 2007). They took single human bone marrow MSCs identified by their cell surface phenotype and generated a heterotopic ossicle (using a hydroxyapatite carrier). Subsequently, MSCs were harvested from this ossicle, clonally grown *in vitro* and characterised as phenotypically the same as the originally transplanted cell. This data was the first *in vivo* evidence of self-renewal ability of the MSC.

More recent work, by Mendez Ferrer et al. (2010), added further supportive evidence. Ceramic porous cubes have been used by multiple groups to demonstrate multi-lineage differentiation *in vivo* as MSCs can form an ossicle around this pro-osteogenic structure. By transplanting clonal Nestin positive mesenspheres (aggregates of MSCs cultured under non-adherent conditions, which have been shown to be multipotent), the authors, demonstrated that enzymatic digest of the ossicle formed, contained cells which were able to generate ossicles on a second serial transplantation and directly formed osteoblasts (Méndez-Ferrer et al., 2010).

These two studies (Sacchetti et al., 2007; Méndez-Ferrer et al., 2010) provide evidence that MSCs isolated from human bone marrow fulfil the criteria required to claim a cell is a stem cell.

1.5.2.4. The name then is……

To summarise, the 'mesenchymal stem cell' name has some merit but there are concerns in naming all cells that display similar *in vitro* characteristics as the same population. In the ideal world, all MSCs used for experiments on differentiation potential would be characterised by their ability to form heterotopic ossicles or ideally, a phenotypic marker that identifies a cell capable of this function would be identified.

The MSCs used in this thesis for *in vitro* assays are derived from bone marrow. These are a heterogenous population and there are likely to be differences between donors. Nevertheless, the use of standard isolation strategies and the published literature discussed demonstrate that these populations contain multipotent stem cells capable of skeletal lineage differentiation *in vivo*. For these reasons, BMSC is used as an acronym of bone marrow (mesenchymal) stem/stromal cells in the studies presented here.

1.6. Cellular Therapy to Aid Cartilage Repair

Cell therapy is a platform technology available to achieve a regenerative therapy as such it is of clinical utility in the field of cartilage repair and regeneration.

1.6.1. Chondrocytes

Autologous chondrocyte implantation (ACI) is the most well-established cell therapy within the field of articular cartilage repair and was approved for clinical use in the USA in 1997. It requires the isolation of chondrocytes from a non-weight bearing zone, their ex-vivo culture and re-implantation into chondral defects. The technique was first trialled in 23 patients diagnosed with full-thickness articular cartilage defects in 1984, with results indicating a clinical benefit (Brittberg et al., 1994); reduced pain and swelling and similar macroscopic appearance to surrounding cartilage when observed by a second-look arthroscopy.

Since 2017 the use of ACI has been approved by National Institute of Clinical Excellence (NICE) in the UK (NICE, 2017). This suggests the treatment has a positive cost–benefit ratio, previously an area of contention, due to the expense and difficulties associated with harvesting and culturing procedures. Various studies have been conducted to compare the outcomes of ACI versus microfracture. A Cochrane review (Vasiliadis and Wasiak, 2010) concluded that little difference is observed between the two procedures within the first 18 months but ACI repair has better functional results at 3 years. In the UK the treatment is indicated for patients with minimal osteoarthritic damage of the knee and cartilage defects greater than 2 cm^2 in size where symptomatic management has failed, but joint replacement is not indicated.

1.6.2. Stem Cells

Although the use of mature cells such as chondrocytes has proved beneficial in the field of cellular therapy, stem cell research has moved to the forefront of regenerative medicine. Endogenously these cells are vital to the natural turnover and repair of various tissues, and as a result are thought to be a pool of regenerative cells that could be utilised for clinical treatment strategies. Whilst stem cells can differentiate into specific cell types, these cells also secrete a variety of growth factors and cytokines that have the potential to orchestrate tissue repair and regeneration.

In recent years, publications using multiple cell populations including stem cell types have been published in relation to cartilage regeneration and repair. These included peripheral blood mononuclear cells (Hopper et al., 2015), haematopoietic stem cells (Saw et al., 2013) and chondroprogenitors derived from embryonic stem cells (Cheng et al., 2014). MSCs, however, have dominated the research field of cartilage cellular therapy with the evidence of their ability to differentiate into chondrocytes and ease of isolation the initial driving force behind their use. Relative to chondrocytes they have the clear advantages of having a greater *in vitro* proliferation potential and importantly, the ability to be sourced from a choice of different tissues.

1.6.3. MSCs

Many studies, including clinical studies, have looked into the benefit of MSCs as a cell therapy for regenerative therapy of bone and articular cartilage. However, the cell fate and mechanistic action of these cells has been overlooked. As discussed it is well recognised that MSCs have the ability to differentiate into cells that make up bone and cartilage tissue, representing great potential for regenerative medicine. However, in recent years, there is a growing appreciation that MSCs in tissue regeneration and repair may act through a trophic role. This suggests that MSCs are acting as an orchestrator of the tissue regeneration and repair rather than as tissue progenitors. These roles are summaries in Figure 1-9.

1.6.3.1. Do MSCs contribute directly to repair?

The heterotopic ossicle model is a clear demonstration of the ability MSCs have to form cartilage and bone *in vivo*. There is good evidence that bone marrow MSCs are able to recapitulate this in a regenerative environment. They have been administered clinically for the treatment of osteogenesis imperfecta (da Silva Meirelles, Caplan and Nardi, 2008) and fracture repair (Thompson et al., 2002; Huang et al., 2015), where they engraft, differentiate and contribute to newly formed bone. It may be presumptive, however, to assume that they are able to do this in the setting of a synovial joint and the regeneration of articular cartilage where the microenvironment conditions may be unfavourable for chondrogenic differentiation.

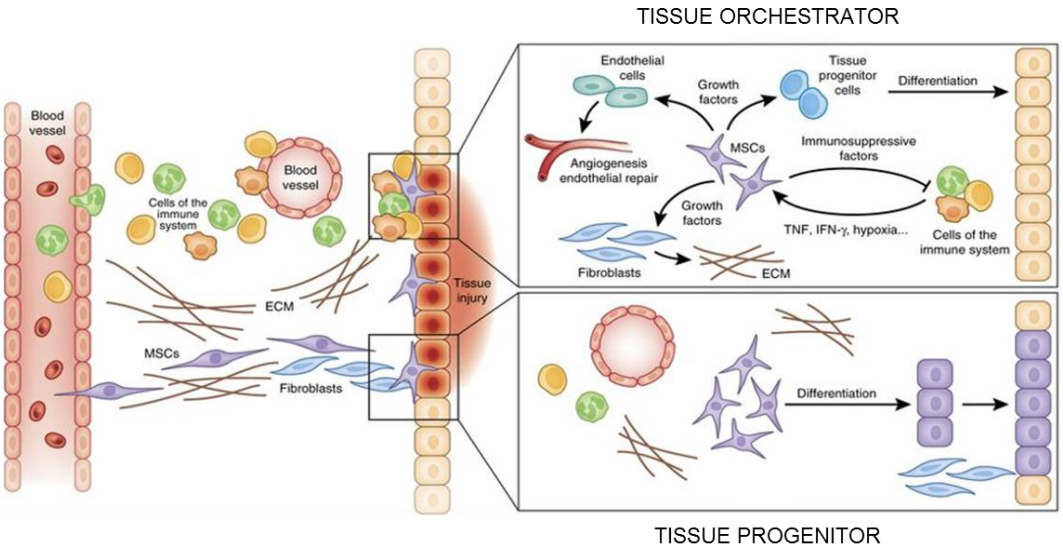

Figure 1-9 – Possible roles of MSCs in tissue repair
When tissue is damaged MSCs are mobilised to the site where they are thought to have two possible roles in tissue repair, acting as a tissue progenitor and differentiating into functional cells of the damaged tissue and/or altering the micronenvironment of the repair as an orchestrator of tissue repair (image adapted from Wang et al., 2014)

1.6.3.2. Do MSCs orchestrate repair?

MSCs are thought to be able to respond to their surrounding microenvironment and consequently that of an injury site. As a result, they secrete reparative site-specific factors such as paracrine growth factors, cytokines, extracellular vesicles as well as directly influencing their neighbouring cells through cell-to-cell interactions. MSCs, therefore, have the potential to influence the viability and proliferation of native cells (including tissue-intrinsic progenitors), induce angiogenesis and reduce apoptosis. Additionally, they are thought to reduce inflammation and alter immune cell responses (Németh et al., 2009). Further, MSCs produce inhibitors of pro-inflammatory cytokines such as interleukin 1 receptor antagonist (Ortiz et al., 2007). In models of OA they have been shown to hinder disease progression (ter Huurne et al., 2012; Diekman et al., 2013). In a clinical pilot study

for OA unresponsive to conservative treatments, injection of MSCs alone improved MRI assessed cartilage quality (Orozco et al., 2013).

Importantly, MSCs have been reported to localise to sites of injury, through specifically broken or inflamed blood vessels (Caplan and Correa, 2011). Furthermore, *in vitro* work has shown they can increase the proliferation and ECM production of the chondrocytes (Wu et al., 2012). Through these mechanisms, MSCs are proposed to establish a specific microenvironment that aids the regeneration of an injured tissue including articular cartilage repair.

1.6.3.3. A third role?

Finally, the issue is further complicated by the role that MSCs are believed to play in haematopoietic cell biology. Some argue that the ability of bone marrow MSCs to support haematopoiesis is their defining feature (Bianco, Robey and Simmons, 2008). In 1977, Dexter et al. showed that cells isolated from mouse bone marrow by plastic adherence could maintain primitive haematopoietic cells (Dexter, Allen and Lajtha, 1977); this was later confirmed in human cell cultures (Gartner and Kaplan, 1980). The interactions of haematopoietic stem and progenitor cells with their local microenvironment in the bone marrow is an area of significant research output documenting the capability of MSCs to be supportive stroma for haematopoietic stem and progenitor cells both *in vitro* and *in vivo*. What role this interaction has in reverse, i.e. the effect of the interaction on the MSCs themselves, has on the other hand, only been minimally explored.

1.7. The Bone Marrow Niche

1.7.1. Stem cell niches

A stem cell niche is a specialised microenvironment that maintains a balance between stem cells in an undifferentiated and self-renewable state, against the promotion of their differentiation. Within a niche, there is a constant dialogue between the stem cells and their surrounding niche cells. Depending on the organism and the stem cell type, these niche cells and the physical structure of the niche can vary greatly. A *C. elegans* hermaphrodite gonad, for example, provides a niche for germline stem cells and is made up of a single cell, the distal tip cell (Byrd and Kimble, 2009). In mammals, there are multiple stem cell niches. For example, paneth cells in the human gut provide essential niche signals for the stem cells of the gut epithelium (Sato and Clevers, 2013). The haematopoietic bone marrow niche, on the other hand, is a significantly more complex highly organised three-dimensional microenvironment, with a plethora of cell types thought to be involved. Based on these examples, one might anticipate that all stem cells require a niche.

1.7.2. MSC niche

As discussed previously (section 1.5), bone marrow MSCs have been found to have stem cell properties of self-renewal and multipotency *in vivo*. It is debatable whether MSCs require a specific niche. MSCs of the bone marrow, and those from other tissues, have been identified in a perivascular location, which perhaps identifies their niche. On the other hand, Sacchetti and colleague's (2007) seminal paper reported that bone marrow MSCs cultured *in vitro* under standard conditions retained their self-renewal and multipotency on subsequent transplant *in vivo*. The maintenance of these properties outside of their native microenvironment would suggest that MSCs are more resilient than other types of stem cells and depend less on extrinsic signals.

1.7.3. Haematopoietic stem cell niche

Haematopoietic stem cells are defined as true stem cells because of their self-renewal capacity and multipotency. The classical model of the haematopoietic system has a hierarchical structure (see Figure 1-10); haematopoietic stem cells (HSCs) at the top which, through an intrinsic network of transcription factors and inputs from the surrounding environment undergo progressive lineage restriction. Through asymmetrical cell division, HSCs ensure a constant supply of all the mature blood cells, in the process defined as haematopoiesis, whilst maintaining their numbers through self-renewal.

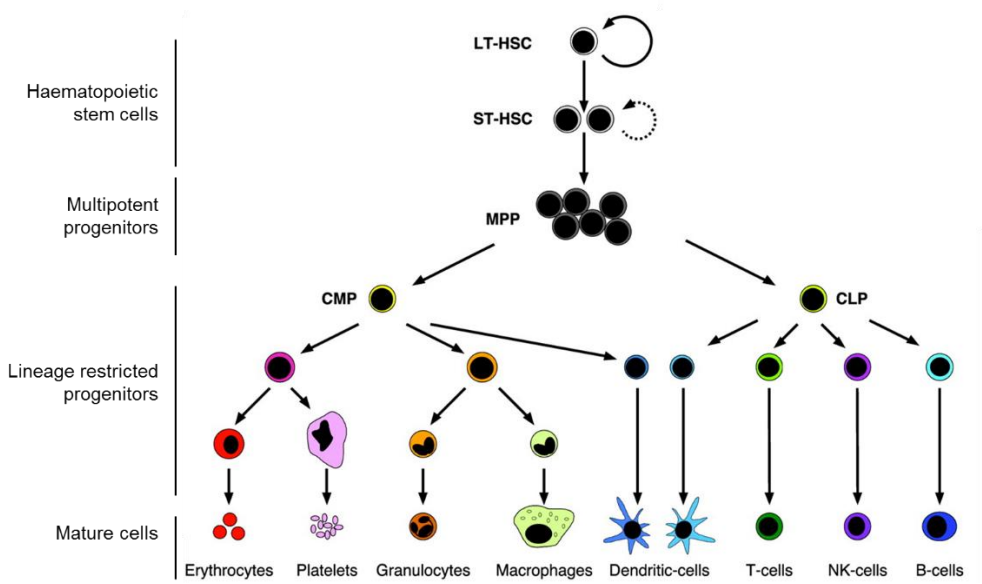

Figure 1-10 – Classical model of haematopoiesis.
Through a series of more committed progenitors, a population of multi-potential haematopoietic stem cells (HSCs) are able to supply all cells of the haematopoietic system. LT-HSC, long term HSC; ST-HSC, short term HSC; MMP, multipotent progenitors, CMP, common myeloid progenitor; CLP, common lymphoid progenitor (image adapted from Passegué et al., 2003)

The bone marrow niche, termed by Schofield in 1978, provides the microenvironment necessary for the survival of haematopoietic stem cells and through intricate signals influences the fate decisions of these haematopoietic precursors; to self-renew, proliferate or differentiate (Ho et al., 2015). Without this environment, it is thought lifelong haematopoiesis would not be possible; all HSCs would commit to lineage differentiation (Schofield, 1978). Whilst it may well be the most widely investigated, the components, location, and functions of the HSC niche remain elusive.

1.7.4. BMSCs and their progeny are a significant component of the Bone Marrow HSC Niche

It has been suggested that a supportive cell of the HSC niche should be rare, in physical proximity to HSCs and be found to express HSC maintenance genes (Frenette et al., 2013). Numerous cell types have been investigated including endothelial cells, haematopoietic, neurones and skeletal cell types.

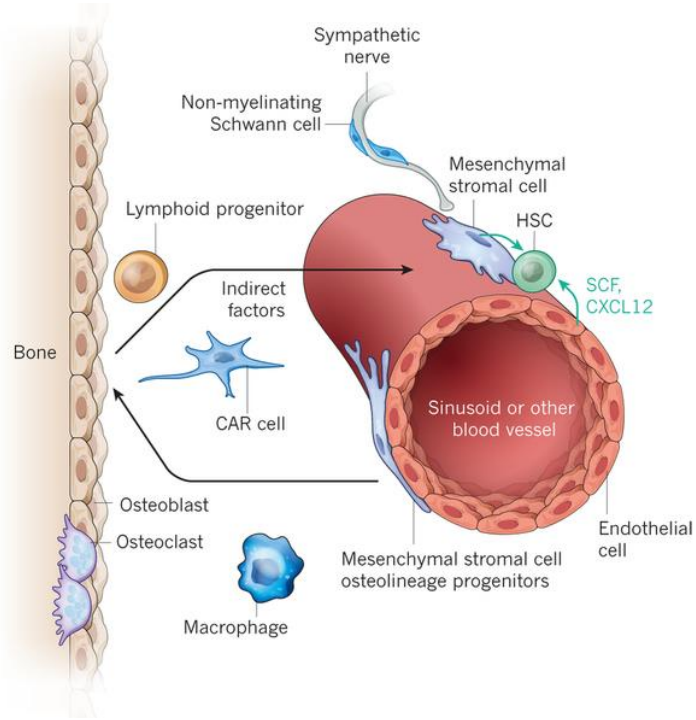

Figure 1-11 – The bone marrow haematopoietic stem cell niche
Haematopoietic stem and progenitors are supported by the microenvironment of the bone marrow niche that is comprised of multiple cell types. MSCs are located close to the vasculature but are also precursors for osteoblasts, another cell type important for HSC maintenance (image from Morrison and Scadden, 2014).

1.7.4.1. Bone marrow stem/stromal cells

The lack of an established single marker to mark all BMSCs, makes investigations into their niche role complex (Panaroni et al., 2014). It is widely accepted, however, that MSCs are located in close proximity to vasculature - associated with the abluminal surface of

sinusoids in both humans and mice. In support of a role for BMSCs in the HSC niche, cells with a perivascular location in the bone marrow are known to express genes involved in the regulation of HSCs such as CXCL12 (Sugiyama et al., 2006) and SCF (Ding et al., 2012). In mice, studies have been conducted ablating the expression of these molecules in cells thought to identify populations of BMSCs. For example, depletion of SCF in Prx1–cre cells leads to the depletion of HSCs (Greenbaum et al., 2013), whilst ablation of CXCL12 expressing cells depleted HSCs as well as impairing the osteogenic and adipogenic potential of bone marrow cells (Omatsu et al., 2010).

Further, transplantation studies into immune-deficient mice of human fluorescently labelled BMSCs demonstrated the ability of these cells to contribute to a functioning haematopoietic microenvironment in the mouse bone marrow (Muguruma et al., 2006). Additionally, human BMSCs are able to generate a haematopoietic environment as shown by the ossicle model, which is infiltrated by host (i.e. mouse) haematopoietic stem and progenitor cells (Sacchetti et al., 2007). This demonstrates both the ability of BMSCs to generate a haematopoietic niche and be part of it; human BMSCs have been re-isolated from this organoid and found by histology to be associated in close proximity to host HSCs.

1.7.4.2. Osteoblasts

A role of osteoblasts specifically in HSC maintenance and differentiation was proposed from evidence demonstrating that these cells could produce cytokines known to play important roles in hematopoietic and myeloid development (Taichman and Emerson, 1994). *In vitro* they are able to support short-term HSC expansion and haematopoiesis (Taichman and Emerson, 1994; Taichman, Reilly and Emerson, 1996) whilst *in vivo* the two cell types are seen to be co-localised at the inner surface of the cavities of trabecular bone (Zhang et al., 2003; Calvi et al., 2003). Furthermore, positive correlation between osteoblast and HSC number has been observed both by increasing numbers (Calvi et al., 2003; Zhang et al., 2003) and in conditional osteoblast ablation studies in mice, where depletion leads to initiation of extra-medullary haematopoiesis outside of the bone marrow (Visnjic et al., 2004). Taken together these results support the notion that committed early stage osteoblasts support haematopoiesis.

1.8. Manipulation of the BM Niche: HSC Mobilising Agents

1.8.1. Haematopoietic stem cells can leave their niche

Under basal conditions, the bone marrow niche is the principal location of HSCs and prevents their differentiation, apoptosis or activation by other stimuli that might be received, to maintain a fixed number of haematopoietic cells in the bone marrow. A small percentage of HSCs can be located in the circulation and their release from the bone

marrow is a normal physiological response (Hoggatt and Pelus, 2011). This peripheral population can increase in the case of infection, injury or inflammation, whereby HSCs are trafficked into the peripheral blood as a response to stress signals. This process is known as mobilisation. Thereafter, through differentiation and self-renewal processes, these cells and their progeny can help to achieve tissue clearance and reconstruction. To drive migration from the niche, interactions between HSCs and their supportive microenvironment must be disrupted. This innate mechanism can be manipulated pharmacologically with the use of cytokines and/or small molecule inhibitors (Lemoli and D'Addio, 2008).

1.8.2. Interactions of HSCs with their niche

As with the identification of cell types of the niche, understanding of the dynamic interactions is yet to be fully established. Direct cell-to-cell interactions have been identified which are thought to be essential in maintaining both HSCs in the niche and their stem cell nature (Jung et al., 2008). Adhesion molecules such as angiopoietin-1, Annexin II and VCAM-1 have been identified and demonstrated to play a role. Additionally, soluble signalling is thought to have a role. One important axis identified is the interaction of the chemokine stromal derived factor-1 (SDF-1/CXCL12) and its receptors CXCR4 and CXCR7 on HSCs (Bendall and Bradstock, 2014).

1.8.3. Therapeutic Use of HSC Mobilising Agents

Autologous or allogenic transplantation of bone marrow cells is the oldest form of anti-cancer immunotherapy. Transplantation can re-establish the haematopoietic system from the top of the hierarchal structure following treatment of haematopoietic malignancies by whole blood irradiation. New agents and those currently under development are aimed at disrupting the interactions of HSCs with their niche pushing their egress into the peripheral blood system. AMD3100 is one such agent that targets the SDF1/CXCR4 interaction by specifically and reversibly binding to CXCR4 (Winkler et al., 2012). By targeting niche interaction molecules, mobilisation can be achieved within hours of administration of this compound. However, whilst this short time span is advantageous the international clinical bone marrow mobilisation standard and agent currently most widely used is G-CSF. This agent requires 4 to 6 days of administration before sufficient numbers of HSCs are present in the periphery harvest (Lowenthal et al., 2007).

In addition to its clinical use for HSC mobilisation, G-CSF is also given to patients with severe neutropenia (low neutrophil numbers) or used for HSC collection and autologous transplantation back into patients who have treatment related bone marrow failure, such as after high dose chemotherapy (Bendall and Bradstock, 2014). Without such a transplantation, a lack of a functioning immune system leaves patients vulnerable to life-threatening infections and irreversible tissue damage.

1.8.4. Granulocyte Colony Stimulating Factor

Granulocyte colony stimulating factor (G-CSF) is an endogenous cytokine, found at low to undetectable levels (below 78pg/mL) in the blood of healthy individuals (de Haas et al., 1994), an observation that is unaffected by age and gender (Kawakami et al., 1990). Levels are known to increase in response to physiologic stimuli and primary infections, returning to normal levels on recovery (Bendall and Bradstock, 2014; Kawakami et al., 1990).

Increased levels of G-CSF results in increased proliferation and activation, whilst inhibiting apoptosis, of the haematopoietic myeloid lineage within the bone morrow and subsequently their release into the peripheral blood (Bendall and Bradstock, 2014). This outcome is a consequence of all cells of this lineage, including committed progenitors, expressing the G-CSF receptor; with G-CSF receptor number per cell increasing with cell maturity. Other mature and immature cells of the blood system are also reported to display the single chain polypeptide receptor, alongside myeloid cells, such as a subset of monocytes, NK cells and B cells (see Figure 1-12) (Singh et al., 2012; Eyles et al., 2006).

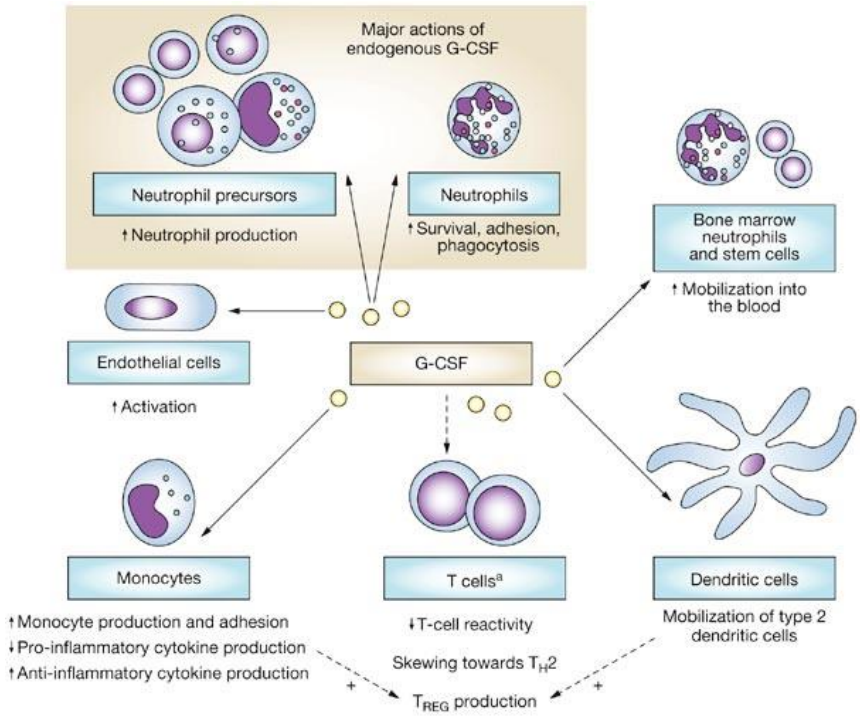

Figure 1-12 - Cellular effects of G-CSF.
This endogenous cytokine effects endothelial cells as well as multiple cells of the immune system either directly or indirectly. TH2, type 2 T-helper cell; TREG, regulatory T cell. (image from Eyles et al. 2006)

1.8.5. G-CSF's Cell Mobilisation Mechanism

Whilst G-CSF has been used for over 30 years, knowledge of its exact mechanisms of action remained unstudied for some time, with consensus being that the cytokine disrupts

the interaction between haematopoietic progenitors and their niche. In the last 20 years, different research groups have looked further into this and slowly information has been added to the field although full understanding of the mechanism remains to be determined. When taken together, results suggest that the mechanism though which G-CSF leads to mobilisation may include multiple pathways.

Importantly, G-CSF does not mobilise haematopoietic stem and progenitor cells (HSPCs) through a direct influence on the cells themselves. This was shown by Liu and colleagues (2000) who demonstrated that in animals lacking the G-CSF receptor on HSPCs (chimeric mouse models), these cells were still mobilised with equivalent efficiency as those expressing the receptor (Liu, Poursine-Laurent and Link, 2000). However, the lack of the G-CSF receptor on all haematopoietic cells prevented G-CSF induced HSC mobilisation.

One candidate for the key haematopoietic cell type that drives HSC mobilisation are cells of the myeloid lineage. These cells can release MMPs which are known to cleave or degrade CXCL12 (Levesque et al., 2003) and VCAM-1 (Levesque et al., 2001) disrupting these signalling axes. As previously discussed, these molecules are vital for the interaction of HSCs and their BM niche.

Cleavage and degradation of critical niche biomolecules is thought to be a likely mechanism linking G-CSF treatment to HSC mobilisation. Genetic animal models however have failed to confirm a role for proteases; mice lacking either individual or combinations of proteases have demonstrated normal mobilisation (Levesque et al., 2004). They may nevertheless be part of a cumulative effect of various mechanisms. CXCL12/CXCR4 dynamics are particularly thought to have a major role in G-CSF mobilisation (Greenbaum and Link, 2011; Semerad et al., 2005); CXCL12 levels decrease rapidly with G-CSF administration and are inversely proportional to mobilisation. Therefore, the ability of MMPs to degrade CXCL12 is noteworthy.

Production of both CXCL12 and VCAM-1 would also be affected by a reduction in the number of cells synthesising this vital HSC niche homing cytokine such as osteo-lineage cells (Singh et al., 2012) which undergo apoptosis with G-CSF administration (Christopher and Link, 2008). The reduction of osteoblasts has recently be shown to be through the G-CSF induced loss of osteoblast supportive monocytes/macrophages (osteomacs), also part of the myeloid lineage (Greenbaum and Link, 2011). The importance of these cells in G-CSF mobilisation is shown in mice expressing the G-CSF receptor exclusively on monocytes, where expected numbers of HSCs are mobilised. Furthermore loss of monocytes results in mobilisation under normal conditions (Winkler et al., 2010).

Finally, the nervous system also has a role in mobilisation, specifically the adrenergic sympathetic nervous system; the administration of a β_2 adrenergic agonist enhances mobilisation (Katayama et al., 2006). However, chimeric BM transplant data demonstrates

that alone adrenergic nerves activity is insufficient to induce effective mobilisation or that a haematopoietic cell type is an intermediary involved in this response pathway, supportive of evidence for a key role for monocytes.

1.9. G-CSF Mobilised Populations for Bone and Cartilage Repair

The mobilisation of HSCs and increasing the number of total haematopoietic cells in the peripheral blood are the most commonly used clinical roles for G-CSF. Most studies using G-CSF in musculoskeletal repair collect these cells as a 'mobilised product' by apheresis and administer it autologously to the site of interest.

In 2009 Saw et al. began a series of studies reporting that bone marrow aspirate injected into the intra-articular space of goats in addition to hyaluronic acid (HA) was able to improve the healing of a cartilage defect generated by subchondral drilling (Saw et al., 2009). Like microfracture, subchondral drilling provides the defect with access to the plethora of bone marrow cells both from the drilling through the subchondral bone and the post-operational injection. Going forward, however, Saw and colleagues moved away from using bone marrow itself, as they translated their findings into the clinical studies, utilising G-CSF mobilised apheresis product as an equivalent. This autologous product required three daily injects of G-CSF before apheresis harvesting, the product was subsequently injected intra-articularly weekly for five weeks from cryopreserved aliquots (Saw et al., 2011). This feasibility study (N=5) demonstrated an improvement in the hyaline nature of cartilage that developed in the defect.

With the success of the feasibility study, a subsequent two-armed randomised trial was conducted with 25 patients in each of two groups comparing treatments with HA alone and HA with autologous mobilised product (Saw et al., 2013). Results indicated improved cartilage repair as assessed by MRI and biopsy histology. These outcomes suggest that a combination of subchondral drilling, G-CSF treatment and intra-articular injection of apheresis product could be a novel treatment strategy for OA repair.

G-CSF administration has also been trialled for clinical feasibility in patients with non-union fractures. Whilst Saw and colleagues utilised the whole apheresis product Kuroda and colleagues in the following studies isolated (i.e. enriched for) $CD34^+$ cells. This is a marker of human haematopoietic stem cells. Initially a case study of an individual patient who had failed bone union at nine months post the initial operative procedure was reported (Kuroda et al., 2011). Following treatment with G-CSF, $CD34^+$ cells were successfully isolated from the apheresis product and added to an atelocollagen gel before administration surgically with an autologous bone graft. This treatment resulted in union after three months with a return to full weight bearing gait for this patient. Subsequently, the authors enrolled a further seven patients into a single arm pilot study (Kuroda et al.,

2014). Five of the patients achieved radiological healing at 12 weeks. Together, these two studies demonstrate the feasibility, safety and the potential of this treatment strategy for fracture repair in patients with failed bone union.

1.10. G-CSF as an adjuvant to musculoskeletal surgical techniques

Saw and Kuroda with their colleagues, utilised G-CSF as a method to enrich the peripheral circulation with cells of the bone marrow before apheresis and direct application of the product to the trauma site. These procedures are classed as a form of cell therapy. In these particular cases, no suggestion was given as to the role of these cells in the regeneration of the tissues. These studies support a role for the mobilised product but one could also ask the question 'what role G-CSF treatment alone would have on repair?'

A number of studies have evaluated the use of G-CSF alone (i.e. no harvest of apheresis product) and shown positive outcomes, as detailed in the table below (see Table 1-1). All except one of these studies have been carried out on animal models. In all cases, the bone defect has been induced including the human trial where an opening-wedge high tibial valgus osteotomy was performed to correct malalignment (Marmotti et al., 2013b). Of note, the majority of studies have utilised G-CSF as an adjuvant for bone repair rather than the repair of cartilage directly. However, the effects of G-CSF could be important for the cartilaginous scaffold that forms during the repair of fractures where endochondral ossification plays an important role. Further, the results from two studies of where osteochondral defects were made in the knees of rats (Okano et al., 2014) and rabbits (Sasaki et al., 2017) have shown improved outcomes at early time points. This may well suggest the benefits of G-CSF in the early healing process.

Another point of interest is the method and dosage regime used for G-CSF administration. Two studies utilised scaffolds to improve repair and incorporated G-CSF within these scaffolds, localising G-CSF administration within the defect itself, here described as peri-operative administration (Ishida et al., 2010; Minagawa et al., 2014). The remaining studies dose subcutaneously but either in the days prior to or after surgery. Depending on the mechanism of action, this difference in the time of administration could have effects on the repair outcome.

Multiple suggestions for the mechanism of action of G-CSF to improve the surgical procedure outcomes have been suggested by these studies but they focus on four main areas; peripheral blood cells (Bozlar et al., 2005; Kaygusuz et al., 2006; Marmotti et al., 2013b), angiogenesis (Bozlar et al., 2005; Ishida et al., 2010), osteogenesis (Ishida et al., 2010; Marmotti et al., 2013b; Minagawa et al., 2014) and MSC proliferation (Marmotti et al., 2013b; Sasaki et al., 2017). To fully understand these mechanisms in the context of bone and cartilage healing of osteochondral repair there is a need for an animal model

through which key cell players can be identified and evaluated. Through this, the value of G-CSF as an adjuvant to surgical treatments such as clinical microfracture can be assessed.

Table 1-1 – Published articles of G-CSF administration alongside surgical procedures

			G-CSF administration			
	Animal or Human	***Injury***	***Pre, Peri or Post Op***	***Delivery***	***Dose number***	***Result***
Bozlar et al., 2005	Rat	Tibial fracture	Post	Sub-cutaneous	7 days continuous	Significant improvement in radiographic and mechanical scores but not bone morphometry
Kaygusuz et al., 2006	Rat	Tibial fracture	Post	Sub-cutaneous	7 days continuous	Improved fracture repair in rats by radiologic and pathology scores
Ishida et al., 2010	Rabbit	Ulnar fracture	Peri	Gelatin hydrogel delivering G-CSF	Single	Improved bone healing at 2, 4 and 8 weeks (new bone bridged the defect gap whereas control had some new bone but also fibrous tissue)
Marmotti et al., 2013	Human	High tibial valgus osteotomy	Pre	Not stated, likely sub-cutaneous	3 days and another dose 4hrs prior to surgery	Improved osteo-integration of a bone graft substitute
Minagawa et al., 2014	Rat	Calvarial defect	Peri	Contained with defect site (applied to osteo-chondructive scaffold)	Single	Enhanced bone regeneration when combined with osteoconductive β-TCP disc
Okano et al., 2014	Rat	Osteo-chondral defect	Pre		4 days prior to surgery	Improved early time-point repair (up to 8 weeks)
Sasaki et al., 2017	Rabbit	Osteo-chondral defect	Pre	Sub-cutaneous	3 days continuous prior to surgery	Improved early time-point repair (at 4 weeks)

1.11. Summary

To summarise, OA is a debilitating condition and a growing healthcare burden, with its incidence predicted to increase with the aging population. Trauma induced cartilage lesions increase the likelihood of a patient to develop OA and therefore intervention to

treat these defects offers an opportunity to delay and possibly prevent the onset of this degenerative disease. Bone marrow stimulation techniques, such as microfracture, are regenerative strategies thought to restore cartilage by delivering bone marrow cells to the defect site. BMSCs are thought to be a key cell type in the repair of bone and cartilage tissue initially damaged by these techniques. Their role however remains unclear with evidence suggesting they act as both tissue progenitors and coordinators of repair. Furthermore, a third role as supportive cells of the bone marrow HSC niche may also have consequences for their role in repair. Understanding the dynamics of these interactions during the repair process provides an opportunity to directly target these endogenous cells with drug and/or biologic therapeutics to improve the quality and quantity of the newly formed tissue.

G-CSF is a biologic that has been proposed for this use. Its administration disrupts the bone marrow niche microenvironment and the interaction between BMSCs and HSCs – knowledge gained from haematology research. However, the impact of this disruption on BMSCs is not well defined nor is the impact of G-CSF directly on these cells. Interestingly, G-CSF has been used in studies of bone and cartilage repair where improved outcomes have been reported. The mechanism by which this occurs however is poorly understood. Before the translation and clinical utility of G-CSF in this setting, further studies are required.

Large animal models, such as sheep, and smaller animals such as rabbits and rats are commonly used for musculoskeletal studies. However mice offer the opportunity to further our understanding of osteochondral repair as they are amenable to genetic manipulation which allows for functional molecular studies. Currently a number of models have been presented in the literature (Fitzgerald et al., 2008; Eltawil et al., 2009; Matsuoka et al., 2015) however further refinement is necessary to improve the accuracy and reproducibility of these models. Using such a model will further understanding of the contribution of different cell populations to osteochondral repair and provide insight into the mechanisms that underlie the structural organisation of the newly formed tissue. Furthermore, this model could then be used as a preclinical model for small molecule and biological agents, such as G-CSF, when designed to improve osteochondral repair outcomes in the context of a surgical therapy.

2. AIMS AND OBJECTIVES

The overall aim of this thesis is to extend the present understanding of haematopoietic and bone marrow stem/stromal cells in osteochondral repair and the impact of G-CSF on the responses of these cells to the injury. To address this overall aim the studies were divided into four specific aims for investigation:

1. **Evaluate the consequences of BMSC and HSPC interactions**

   BMSCs and HSPCs interact in the bone marrow microenvironment that is disrupted during bone marrow stimulation techniques used for cartilage repair. Chapter 4 aims to evaluate the consequences of this interaction for musculoskeletal repair. To address this, the objectives of this chapter are to design and develop and *in vitro* model of these interactions and assess their impact on the differentiation capabilities of BMSCs.

2. **Establish a reproducible osteochondral repair model to investigate key cell players**

   To increase understanding of the cartilage repair process after bone marrow stimulation and identify molecular and cellular mechanisms involved in osteochondral healing a mouse model is required. Chapter 5 aims to develop a mouse osteochondral model by firstly reviewing previously published models, trialling different techniques before choosing an appropriate strategy and using assessment tools for its evaluation. Finally, the model will be used to identify wound healing events and the cells types involved in osteochondral repair.

3. **Evaluate the role of BMSCs and G-CSF in osteochondral repair**

   BMSCs are thought to be vital for the repair of cartilage defects whilst G-CSF has been reported to improve bone and cartilage repair outcomes. Chapter 6 aims to evaluate the role of BMSCs and G-CSF in osteochondral repair using the model developed in the previous chapter. To answer this the objectives are to determine whether BMSCs, marked by nestin in a GFP reporter mouse line, are present in the defect at early healing time points and further assess the impact of G-CSF administration on BMSCs and haematopoietic cells *in vivo*.

4. **Explore the role of G-CSF on BMSCs directly**

   Whilst G-CSF can influence BMSCs cells through changes to the bone marrow microenvironment, the aim of chapter 7 is to explore the ability of BMSCs to respond to G-CSF directly. This will be address by determining if the G-CSF receptor is present and functional in these cells and subsequently the effect of G-CSF exposure on the differentiation of BMSCs.

3. METHODS

3.1. Cell Culture

All work was carried out in a Category 2 certified biological safety cabinet, following standard aseptic technique. Cell cultures were incubated at 37°C, in a humidified atmosphere of 5% CO_2, 20% O_2. Cell expansion was performed in appropriate basal media, as described in Table 3-1, using either Dulbecco's Modified Eagle Medium (DMEM, Thermo Fisher Scientific), alpha Modified Eagle Medium (αMEM, Thermo Fisher Scientific) or RPMI 1640 (Thermo Fisher Scientific). Unless otherwise stated medium was supplemented with 10% (v/v) foetal calf serum (FCS, First Link) and antibiotics at a final concentration of 100 units penicillin and 0.1 mg/mL streptomycin (Thermo Fisher Scientific). BMSCs and sMSCs (see section 3.2.1 for details) were expanded in supplemented αMEM; 25 µg/mL ascorbic acid-2-phosphate (Sigma), 1 ng/mL FGF-2 (PeproTech) (Narcisi et al., 2015). Medium was changed every 2 to 3 days for culture expansion.

Table 3-1 – Cell populations used

Name	*Acquisition*	*Expansion media*	*Used at passage*
Human			
Primary BMSC	Lonza	αMEM (+supp)	<7
Primary BMSC	Patient bone marrow	αMEM (+supp)	<4
Primary sMSCs	Patient bone marrow	αMEM (+supp)	<4
Peripheral blood MNCs	Leukocyte Cone	RPMI	Fresh
Mouse			
Primary BM derived cells	Mice	DMEM	Fresh
D1 ORL UVA cell line	ATCC	DMEM	

Passaging of cells was performed when they reached 70% confluence, using pre-warmed Trypsin-EDTA (0.5 g/L porcine trypsin, 0.2 g/L EDTA-4Na in Hank's Balanced Salt Solution with phenol red) (Sigma) or TrypLE Express (Thermo Fisher Scientific). Primary cells were used within a certain number of passages as indicated in Table 3-1. Adherent cells were plated at a density of 2,300 cells/cm^2 in expansion media after counting. Counting was performed manually using Glasstic Slide 10 with Grids (Kova International). When appropriate, viability was assessed using trypan blue (Thermo Fisher Scientific) (1:1 dilution). All cells were recovered from suspension by centrifugation at 300 x g for between 5 and 10 minutes unless otherwise stated.

For long-term storage cells were cryopreserved and stored in liquid nitrogen vapour. For this, after detachment from plastic, cells were pelleted by centrifugation and re-suspended in cryopreservation medium (FBS, 10% dimethyl sulphoxide (Sigma)). Cryovials were transferred to -70°C in a CoolCell® FTS30 (Biocision) before being transferred to liquid

nitrogen vapour. Cells were revived by thawing cryovials in a 37°C water bath and immediately transferring the contents to a tissue culture flask to which the appropriate media added. Cells were left to attach overnight before the medium was changed and passaging was continued. All haematopoietic cell fractions were used fresh and not cryopreserved before use.

3.2. Primary and cell lines used

3.2.1. Human derived cells

3.2.1.1. Bone marrow mesenchymal stem/stromal cells (BMSCs)

BMSCs used were either purchased from Lonza or isolated from donors at Addenbrooke's Hospital, Cambridge, UK. Pre-characterised Poetics™ human mesenchymal stem cells (Lonza) are confirmed to be positive for BMSC surface antigens by the supplier; CD105, CD166, CD29, CD44 and negative for CD14, CD34 and CD45.

BMSCs were isolated from the femoral or tibial bone marrow of human donors undergoing total or hemi knee or hip joint replacement surgery at Addenbrooke's Hospital, Cambridge, UK. These samples were collected under ethical consent obtained from the Cambridge Local Research Ethics Committee (No. 06/Q0108/213). Written and informed patient consent was obtained for all specimens collected under this ethics.

Immediately after extraction, marrow was placed into a 50 mL tube containing 5 ml of 400 µg/ml heparin sulphate solution (Sigma). Bone marrow was then passed through a 70 µm filter, using a plunger from a 5 mL syringe. Cells were seeded at a density of approximately 50,000 nucleated cells/cm^2 in supplemented αMEM medium (see section 3.1). After 48 hours non-adherent cells were washed off and the adherent cells culture in fresh supplemented αMEM medium. Whilst human BMSCs used in this thesis were not themselves characterised for their phenotypic profile, cells isolated by this method have previously been extensively characterised within the laboratory.

3.2.1.2. Synovial mesenchymal stem/stromal cells (sMSCs)

sMSCs were isolated from the synovial tissue lining the fat pad of human donors undergoing total or hemi knee replacement surgery at Addenbrooke's Hospital, Cambridge, UK. The method of isolation was developed and optimised within the laboratory. Fat pad tissue was removed as much as possible from the fibrous synovial tissue using a scalpel and subsequently digested in 2 mg/mL solution of collagenase A (Sigma) prepared in basic αMEM medium (10% FCS and antibiotics) and incubated overnight at 37°C under constant agitation. Cells were then washed in basic αMEM medium by centrifugation and resuspension, and subsequently plated in supplemented

αMEM medium (see section 3.1). Cells were passaged once colonies of 70% confluency had formed.

3.2.1.3. Leukocyte Cone Peripheral Blood Mononuclear Cells (PB MNCs)

Leukocyte cones were purchased from NHS Blood and Transplant, Addenbrooke's Hospital, in accordance with the Human Tissue Act 2004. Leukocyte cones are a waste product from the isolation of platelets from healthy donors where leukocytes and other mononuclear cells (MNCs) are removed from peripheral blood and remain in the cone. The contents of each leukocyte cone were diluted 1 in 10 with dissociation buffer (PBS with 3% FCS, and 5 mM EDTA) and layered on Lymphoprep™ solution (STEMCELL Technologies) before centrifugation for 20 minutes at 800 x g with a low brake at room temperature. This process separates out MNCs which have a lower buoyant density than the Lymphoprep™ solution and therefore form a sample/medium interface (i.e. "buffy coat") which can be isolated (first described by Böyum 1968). Erythrocytes and polymorphonuclear granulocytes, with a higher density, sediment through the medium to the bottom under centrifugation and are separated from the MNC fraction. The MNC-rich band was removed and re-suspended in dissociation buffer and spin washed twice, 5 minutes each. Mononuclear cells were used directly after isolation in the experiments described in this thesis. When cultured alone these cells were cultured in RPMI expansion medium (10% FCS and antibiotics).

3.2.2. Mouse derived cells

3.2.2.1. Primary bone marrow cells

Primary bone marrow cells used in the first results chapter of this thesis (chapter 4) were derived from 8 to 12-week-old female BALB/c mice housed in the local animal facility, Phenomics. The exception to this, is the use of bone marrow cells derived from the Ubiquitin-GFP reporter mouse line (MGI ID: 3057178) (Schaefer et al., 2001) kindly donated post-mortem by the Clatworthy group, University of Cambridge, aged 16 weeks, male and female.

In all cases skinned hind limbs were dissected and transported in PBS. Cell isolation was subsequently performed under sterile conditions in a tissue culture cabinet. Hind limbs were dissected and as much soft tissue as possible removed to isolate femurs and tibias. Bones were then moved to cold dissociation buffer (PBS with 3% FCS, and 5 mM EDTA) and crushed using a pestle and mortar (Lo Celso and Scadden, 2007). After pipette agitation and washing of bone fragments, the bone marrow suspension was strained through a 30 μm cell strainer and cells pelleted by 5 minutes centrifugation before counting and experimental use in co-culture systems.

3.2.2.2. D1 ORL UVA cell line

D1 ORL UVA (ATCC, CRL-12424) (RRID:CVCL_6495) is a murine stromal cell line that was developed in the 1990's (Patent number US6082364, accepted 04-Jul-2000). The cell line was clonally derived from the BALB/c mouse bone marrow after incubation steps with and then without monocyte-colony stimulating factor. Evidence detailed in the patent filled in 1997 describes that the line is capable of tri-lineage differentiation and when transplanted into the tail vein of mouse recipients, the cells home to the bone marrow. These cells were cultured as described above in DMEM medium (10% FCS and antibiotics).

3.3. Tri-lineage Differentiation and Staining of BMSCs

One of the three main criteria for the identification of MSCs is their ability to undergo tri-lineage differentiation in vitro. Pre-characterised Poetics™ human BMSCs (Lonza) and the cell line D1 ORL UVA were both cultured in differentiation media to stimulate and assess their osteogenesis, chondrogenesis and adipogenesis potential. Differentiation was induced for between 1 and 21 days. Analysis of differentiation was either assessed by gene expression analysis after the harvest of RNA (see section 3.11) or by the assessment of the production of extracellular matrix by histological staining described below. Where differentiation was performed without the exposure of cells to previous experimental conditions and in monolayers, cells were plated at 25,000 cells/cm^2 density and differentiation induced after overnight attachment of cells in the appropriate expansion media.

The effect of G-CSF on the tri-lineage differentiation potential of human BMSCs was assessed by the addition G-CSF (PeproTech) at a final concentration of 100 ng/mL to differentiation media (Furmento et al., 2014).

3.3.1. Osteogenesis

BMSCs can be differentiated into osteoblasts by culturing cells with ascorbic acid, beta-glycerophosphate and dexamethasone. Cells were grown in basic DMEM medium (10% FCS and antibiotics), 50 µg/mL L-ascorbic acid 2-phosphate (Sigma), 10 mM β-glycerol phosphate (Sigma) and 10 nM dexamethasone (Sigma). In some experiments StemPro Osteogenesis medium (Thermo Fisher Scientific) was used in place of this. In both cases medium was changed every 3 to 4 days.

Mineralisation of BMSC monolayers can be visualised by staining with Alizarin Red S (ARS), staining for extracellular calcium-rich deposits produced by osteoblasts during mineralisation. The dye forms a complex with calcium in a chelation process, resulting in a bright red stain (Puchtler, Meloan and Terry, 1969).

After osteogenic differentiation, cultured cells were washed with PBS, fixed with 10% neutral-buffered formalin (Sigma) for 20 to 30 minutes, and again washed with PBS before staining. A 2% Alizarin Red solution pH 4.2 (Alfa Aesar) was added to the cells for 2 to 3 minutes at room temperature and then gently washed with distilled water. Staining was then viewed and imaged using phase contrast microscopy and a macroscopic camera (see section 3.9).

Alizarin red staining was quantified using FIJI from macroscopic images of cell culture wells. Images were cropped to the size of the well and the green channel selected after splitting the channels. An oval was drawn to the shape of the well and the area outside of the well cleared. The image was then inverted and a threshold set from 190 to 255 before converting to black and white (convert to mask). The number of white pixels was then measured as a percentage of the area.

3.3.2. Chondrogenesis

Two different methods were used for chondrogenesis assays. Whilst human BMSCs were cultured in 3D pellets, D1 ORL UVA cells were differentiated in monolayers. Commonly, chondrogenic differentiation is achieved by culturing cells at high density in medium containing Transforming Growth Factor-β (TGF-β) and dexamethasone (Johnstone et al., 1998).

3.3.2.1. D1 ORL UVA chondrogenic induction

Chondrogenesis in the D1 ORL UVA cell line was induced using StemPro Chondrogenesis medium (Thermo Fisher Scientific) made up as directed by the manufacturer's instructions and supplemented with antibiotics at a final concentration of 100 units penicillin and 0.1 mg/mL streptomycin (Thermo Fisher Scientific). Medium was changed every 2 to 4 days. Subsequently the production of glycosaminoglycans, indicative of chondrogenesis, was assessed by histological staining with Alcian blue, a cationic dye (Mowry, 1956) , and their presence in cultured media – dimethyl-methylene blue (DMMB) assay (Farndale, Buttle and Barrett, 1986).

For Alcian blue staining of monolayers, cells were washed with PBS, fixed with 10% neutral-buffered formalin for 20 to 30 minutes and again washed with PBS before staining. A 1% Alcian blue solution (Sigma) diluted in 0.1 M HCl was applied to the cells and left overnight at room temperature. The following day cells were washed three times with 0.1M HCl and finally with distilled water to neutralise the acidity. Staining was then viewed and imaged (see section 3.9).

Cell culture medium was collected from endpoint cultures at 21 days and used to determine the concentration of sulphated glycosaminoglycans present by the DMMB assay. DMMB assay reagent solution (1 L distilled water containing 16 mg 1,9-Dimethyl-

Methylene Blue (Sigma), 2.37 g NaCl, 3.04 g glycine and adjusted to pH3) was prepared and stored at room temperature. 40 µl of each sample was aliquoted into a 96-well plate and 250 µl of the DMMB reagent added to each well. The absorbance was measured immediately on a FLUOstar OPTIMA plate reader (BMG Labtech) at 544nm.

3.3.2.2. Human BMSCs chondrogenic induction

Human BMSCs were induced to undergo chondrogenic differentiation in 3D aggregates/pellets. Chondrogenic medium used for these cultures consisted of DMEM-high-glucose GlutaMAX+ (Thermo Fisher Scientific), ITS+ (Corning) consisting of insulin, transferrin, and selenium diluted 1 in 100, 40 µg/mL L-proline (Sigma), 1 mM sodium pyruvate (Thermo Fisher Scientific), 100 nM dexamethasone (Sigma), 10 ng/mL TGFβ1 (R&D Systems) and antibiotics at a final concentration of 100 units penicillin and 0.1 mg/mL streptomycin (Thermo Fisher Scientific). To form BMSC cell pellets, BMSCs were re-suspended in chondrogenic media at $2.5x10^6$ /mL and 1 mL aliquoted per 15 mL polypropylene tube. Cells were then centrifuged at 300 x g for 8 minutes to form pellets. After 24 hours, the pellets were loosened from the bottom of the tube by gently tapping. Medium was replaced every 2 to 3 days and cultures maintained for up to 21 days.

Chondrogenic pellets were either used for gene expression analysis by qRT-PCR or processed for histological staining. Pellets processed for histology were fixed overnight in 10% neutral-buffered formalin, washed in PBS and subsequently embedded in 3% agarose (Eurogentec) before being processed for paraffin sections (see section 3.13.2.1) and staining (see section 3.13.3). Pellets used for gene expression analysis were lysed as described in (see section 3.11) however prior to RNA isolation pellets were physically dissociated using a cordless motor and disposable pestles (Sigma) in RLT buffer (Qiagen).

3.3.3. Adipogenesis

During adipogenesis cells accumulate lipid rich vacuoles within their cytoplasm which can combine and fill the cytoplasm. (Pittenger et al., 1999) first described an adipogenic differentiation media which contained dexamethasone, insulin, isobutyl methyl xanthine and indomethacin.

In this thesis, StemPro Adipogenesis medium (Thermo Fisher Scientific) was used and made up as per the manufacturer's instructions and supplemented with antibiotics at a final concentration of 100 units penicillin and 0.1 mg/mL streptomycin (Thermo Fisher Scientific). Medium was replaced every 3 to 4 days and cells were then stained with Oil red O. This dye is a lipid-soluble, red lysochrome diazo dye which stains triglycerides and cholesteryl oleate lipids identifying the lipid filled organelles (Ramírez-Zacarías, Castro-Muñozledo and Kuri-Harcuch, 1992).

At 21 days after initiation of adipogenesis, cells were washed with PBS, fixed with 10% neutral-buffered formalin for 20 to 30 minutes and again washed with PBS. The monolayer was then pre-treated with 60% isopropanol to prevent background Oil red O staining. Prior to staining a working staining solution was prepared by 3:2 dilution in distilled water of a 0.3% Oil red O (Sigma) stock solution (in 99% isopropanol) and left to settle. After 10 minutes, the working solution was filtered to remove undissolved Oil red O particles. The 0.18% working solution was then used to stain the cells for 5 minutes before washing with PBS. Staining was then viewed and imaged using phase contrast microscopy (see section 3.9).

Oil red O staining was quantified using FIJI from three phase contrast images per well. The RGB tiff image colour channels were split and the green channel selected for further analysis. The image was then grayscale inverted and a threshold set from 190 to 255 before converting to black and white ("convert to mask"). The number of white pixels was then measured as a percentage of the area.

3.4. Multi-lineage differentiation of haematopoietic progenitors - Colony Forming Cell (CFC) Assay

The Colony Forming Cell assay is the second most rapid method of identifying haematopoietic progenitors, second to phenotypic characterisation, but additionally provides some functional analysis. The assay assesses the ability of a cell to self-renew and differentiate into one or more haematopoietic lineages. The restriction in cellular movement using methylcellulose based medium, allows for the formation of individual colonies. Furthermore, defined colony shapes form based on the haematopoietic lineage and the level of commitment of the original progenitor.

Cells derived from the bone marrow of mouse long bones were suspended in 4 ml of Methocult M3434 (STEMCELL Technologies) at a concentration proportional to 2-3 x 10^5 /mL total bone marrow cells. 1.1 mL of this suspension was then plated in a 6-well plate and incubated for 10 days prior to the imaging (see section 3.9) and analysis of colonies.

3.5. Co-culture of primary mouse haematopoietic cells and D1 ORL UVA cell line

D1 OLR UVA cells were seeded in 12-well plates at a density of 1 x 10^5 cells/well in their appropriate expansion media (see Table 3-1) and grown to 90 to 100% confluency in DMEM expansion media. Haematopoietic cell fractions isolation from the bone marrow of BALB/c mice were then added at concentrations of either 1x10^3, 1x10^4 or 1x10^5 per well, and the co-cultures maintained in DMEM expansion media.

3.6. Protein Functionality of the G-CSF R

To confirm the biological activity of the G-CSF R in human BMSCs, cells were grown to 60 to 70% confluence while PB MNCs were freshly isolated. Cells were then subjected to serum starvation in αMEM with 0.1% bovine serum albumin (BSA) and standard antibiotics to minimise baseline activity. After 24 hours 20 µl of each cytokine was added at final concentrations of 100 ng/mL G-CSF (PeproTech) and 20 ng/mL IL-6 (PeproTech) and cells prepared for protein analysis at 5, 15 and 30 minutes. In some experiments cells were exposed to JAK inhibitors after serum starvation for 1 hour prior to the addition of cytokines at a final concentration of 0.1% dimethyl sulphoxide (DMSO). Controls were exposed to 0.1% DMSO with no inhibitor. JAK inhibitors were either CP 690550 citrate (Tocris) at 1 µM or cucurbitacin I (Tocris) at 10 µM.

3.7. Proliferation Assessment

3.7.1. xCELLigence assay

Real time analysis of adherent cell proliferation was conducted using an xCELLigence System RTCA DP with E-plates (ACEA biosystems). This device measures electrical impedance as cells attach and spread over the E-plate surface covered with a gold microelectrode array. The total area of tissue-culture well covered by cells is displayed as a dimensionless parameter termed cell-index based on the electrical impedance. Hence, the cell-index is directly proportional to the surface of plates covered with cells and can measure cell proliferation over time (Ke et al., 2011).

Plates were blanked on the xCELLigence System with the addition of 50 uL of supplemented αMEM expansion medium to provide a reference impedance value. BMSCs were then seeded at a density of 2,500 cells/well in the same medium. Cells were allowed to settle for 30 minutes at room temperature and then the E-plate was moved to the xCELLigence cradle. After 24 hours the medium was removed from all wells and low serum media (1% FCS in αMEM) used to wash the wells once, before addition of 135 uL per well and the plate replaced in the cradle. After a further 24 hours supplements were added to wells (15 uL) to give 1% FCS, 10% FCS and 100 ng/mL G-CSF final concentration conditions. Each condition was performed in duplicate. Cell-index values were measured at a maximum of every 15 minutes from the addition of cells up to 4 days after the addition of supplements. Cell-index values were normalised to the time at which supplements were added using the xCELLigence RTCA software (v2.0).

3.7.2. CyQuant assay

The CyQUANT Direct Cell Proliferation Assay Kit (Thermo Fisher Scientific) uses a fluorescent cell-permeant DNA-binding dye to measure DNA quantity that correlates with

cell number. This assay was run alongside the xCELLigence assay described above. BMSCs were seeded at a density of 2,500 cells/well (96-well plate) in complete expansion medium and left for 24 hours. Wells were then washed with low serum media (1% FCS in αMEM) and 135 uL added to each well. Supplements were added after 24 hours in 15 uL to generate 1% FCS, 10% FCS and 100 ng/mL G-CSF final concentration conditions. After 4 days the CyQuant assay was performed.

The CyQuant Direct nucleic acid stain and background suppressor were diluted in PBS as per the manufacturer's instructions to prepare a 2X working solution. 150 µL of this working solution was added to each well and the plate incubated at 37°C for 60 minutes. The fluorescence was subsequently measured at a wavelength of excitation of 480 nm and emission of 520 nm using a FluoStar Optima plate reader (BMG Labtech).

3.8. Cell Phenotyping and Phenotype Isolation

Different cell types can be identified by specific cell surface phenotypes. Here, antibodies attached to both magnetic particles and fluorophores have been used to identify and isolate cells based on their cell surface antigens.

3.8.1. Magnetic-activated Cell Sorting

Magnetic-activated cell sorting (MACS) (Miltenyi Biotec) is a widely used method for the separation of cells based on the expression of a cell surface antigens and uses 50 nm superparamagnetic particles that are conjugated to antigen specific antibodies (Miltenyi et al., 1990). Once labelled, the cell fraction is applied to a column matrix made up of ferromagnetic spheres which when placed within a magnetic field amplify the strength of the magnetic field 10,000-fold. Magnetically labelled cells are held in suspension within the column whilst unlabelled cells are able to pass through the column and can be collected as an antigen negative fraction. The labelled cells can be eluted from the column and collected as positive for the antigen of interest. In this thesis, only depletion strategies were used on mouse bone marrow derived cells. The kits used are detailed in Table 3-2.

Table 3-2 - Magnetic-activated cell sorting kits used

Antigen	*Code*	*Species*	*Company*
Lineage depletion kit	130-090-858	anti-mouse	Miltenyi Biotec
CD45 microbeads	130-052-301	anti-mouse	Miltenyi Biotec

Cells were re-suspended at a $1x10^7$/mL and incubated with the antibody cocktail, washed and then incubated with magnetic beads for lineage depletion CD45 antibodies conjugated to magnetic beads. All incubation steps were performed at 4°C in dissociation buffer (PBS with 3% FCS, and 5 mM EDTA). Cells were washed again and re-suspended at $1x10^7$/mL. The cell suspension was filtered through a 30 µm nylon mesh filter (Miltenyi

Biotec) and applied to a pre-wet LS column (Miltenyi Biotec) mounted in a QuadroMacs magnet (Miltenyi Biotec). Columns were rinsed three times with buffer and the elution fraction collected and centrifuged before further use.

3.8.2. Flow Cytometry and Fluorescence-Activated Cell Sorting (FACS)

Flow cytometry can be used to identify and quantify a range of parameters. In addition to fluorescent light emission, flow cytometry uses light scattering properties to determine the size (forward scatter) and internal complexities of cells (side scatter) (Brown and Wittwer, 2000). Fundamentally, a fluidics system it allows each cell to be analysed individually for multiple properties using one or many lasers. This makes flow cytometry a powerful analysis tool for analysis of complex cell populations.

Based on the methods described above for flow cytometry, Fluorescence-activated cell sorting (FACS) sorts heterogeneous cells into two or more fractions based on their individual light scattering and fluorescent characteristics properties.

Table 3-3 details the antibodies used for flow cytometry analysis and sorting. Antibodies were used as per the manufacturer's instructions. Additionally, cells derived from GFP reporter mice were sorted on their GFP fluorescence. The viability dye 7-AAD (Biolegend) was used in all cases by the addition of 5 µl per $1x10^6$ cells and all cell suspensions filtered through a 30 µm nylon mesh filter (Miltenyi Biotec) prior to analysis. Unstained and isotype controls were used to determine auto-fluorescence and non-specific background staining. Laser voltages were set with cells below log 10^{-1}. When multiple staining of cells was required, compensation controls were run using compensation beads (OneComp eBeads, eBioscience) to assess the compensation required for emission spectral overlap.

For flow cytometry analysis a LSR Fortessa (BD Biosciences) was used and for FACS a BD FACSAria III (BD Biosciences) was used, both located at the Cambridge NIHR BRC Cell Phenotyping Hub. The data was assessed with Kaluza Analysis Software (Beckman Coulter).

3.8.2.1. Isolation of mouse bone marrow populations

Primary cells derived from the bone marrow of mice were stained with conjugated antibodies detailed in Table 3-3. After isolation of cells, either directly from tissue or after magnetic-cell sorting, cells were re-suspended in dissociation buffer at $1x10^7$/mL. Antibodies were added and incubated for 30 minutes in the dark at 4°C. Cells were then washed twice in 3 mL dissociation buffer before addition of 7-AAD and then flow cytometry analysis or sorting was performed. Those cells sorted for co-culture were collected into DMEM expansion media before spinning and resuspension into fresh media and addition to 12-well plates containing the D1 ORL UVA cell line.

Table 3-3 - Antibodies used for flow cytometry

Antigen	*Conjugation*	*Clone*	*Species*	*Company*	*Dilution*
Un-conjugated primary antibodies					
CD11b		M1/70	Rat	R&D systems	10 µg/ml
CD45		30-F11	Rat	R&D systems	10 µg/ml
CD29		265917	Rat	R&D systems	10 µg/ml
CD73		496406	Rat	R&D systems	10 µg/ml
CD105		209701	Rat	R&D systems	10 µg/ml
CD106		112734	Rat	R&D systems	10 µg/ml
Sca-1 (Ly-6A/E)		177228	Rat	R&D systems	10 µg/ml
CD44			Sheep	R&D systems	10 µg/ml
Rat IgG2A isotype control		54447		R&D systems	100 µg/ml
Rat IgG2B isotype control		141945		R&D systems	100 µg/ml
Sheep IgG isotype control				R&D systems	100 µg/ml
Conjugated primary antibodies					
c-Kit (CD117)	APC	2B8	Rat	Biolegend	1 in 20
Sca-1 (Ly-6A/E)	BV 605	D7	Rat	Biolegend	1 in 20
CD45	APC/Cy7	30-F11	Mouse	Biolegend	1 in 80
CD31	PE	390	Mouse	Biolegend	1 in 20
Secondary antibodies					
Anti-rat	PE	Poly4054	Goat	Biolegend	2.5 µg/ml
Anti-sheep	PE	HP6017	Mouse	Biolegend	2.5 µg/ml

3.8.2.2. D1 ORL UVA phenotypic analysis

For the phenotypic analysis of the D1 ORL UVA cell line, the cell line was grown to 70% confluency prior to staining. Cells were trypsinised, spin washed in DMEM expansion media and re-suspended in dissociation buffer (PBS with 3% FCS, and 5 mM EDTA); this buffer was used for all the following steps. Cells were then washed a second time and re-suspended at $1x10^7$/mL. Next, cells were stained with primary antibodies from the R&D systems Mouse Mesenchymal Stem Cell Marker Antibody Panel or appropriate isotype controls (antibodies detailed in Table 3-3) for 30 minutes at room temperature, one antibody per tube. Cells were then washed twice before resuspension in 100 µL per tube and addition of either anti-rat or anti-sheep, as appropriate, secondary antibody conjugated to APC. Secondary antibody staining was performed at 4°C for 30 minutes in the dark. Cells were then washed twice and re-suspended in 1 mL before addition of 7-AAD (5 µl per $1x10^6$ cells) and flow cytometry analysis.

3.8.2.3. Separation of co-culture populations

For the separation via FACS of co-cultures containing ubiquintin-GFP reporter mouse cells, cells from 12-well plates were detached by trypsinisation and three replicate wells combined in DMEM expansion media before washing twice in dissociation buffer and stained for viability. Cells were then sorted into DMEM expansion media to isolate GFP negative cells, before lysis for gene expression analysis (see section 3.11).

3.8.3. Immunocytochemistry

Phenotypic analysis of individual human BMSCs was assessed by immunocytochemistry (ICC). This technique visualises proteins using antibodies for specific target antigens and in addition to flow cytometry allows for the analysis of the site of binding within the cell and the cell's morphology.

Cells were grown in 0.7 mm^2 chamber 8-well Millicell® EZ Slides (Millipore). Cells were washed with PBS and fixed with 37°C pre-warmed 4% paraformaldehyde (Sigma), and then incubated with PBS containing 0.1% Tween20 (Sigma) (PBS-T) for 5 minutes to permeabilise the cells. Cells were then blocked in 10% goat serum ((Vector Laboratories)) PBS-T for 30 minutes before the addition of the primary antibody (Table 3-4) diluted in 1% goat serum ((Vector Labs)) in PBS-T and incubation overnight at 4°C. . Antibodies were used as per the manufacturer's instructions and the final incubation concentration optimised.

Table 3-4 – Antibodies used for immunocytochemistry

Antigen	*Code*	*Species*	*Company*	*Dilution*
Primary antibodies				
G-CSF R	ab126167	Rabbit mAb	Abcam	1 in 500
Secondary antibodies				
Anti-rabbit Alexa 488	ab150085	Goat	Abcam	1 in 250

After washing with PBS, cells were then incubated with an Alexa 488 conjugated secondary antibody (Table 3-4) in the dark for 1 hour at room temperature. Additionally Phallodin Alexa 555 (Thermo Fisher Scientific) was added with the secondary antibody for the visualisation of the actin cytoskeleton. After final wash steps with PBS twice and then distilled water, slides were mounted using ProLong Diamond Antifade Mountant with DAPI (Thermo Fisher Scientific). 4',6-diamidino-2-phenylindole (DAPI) (Sigma Aldrich) was used as a nuclear stain, as it binds to AT-rich regions of DNA within the nucleus. Primary and secondary negative wells were prepared alongside to control for non-specificity and background signals. Cells were imaged by confocal microscopy (see section 3.9.2).

3.9. Cell Culture Imaging Techniques and Analysis

3.9.1. Standard Microscopy

Phase contrast imaging used to assess cell morphology, and histological staining of cell culture wells, were both viewed using a Leica DM IRB Inverted Brightfield Microscope and captured using a MicroPublisher 3.3 RTV Camera (QImaging) and Q Capture Pro 7 software. Imaging of co-cultures containing GFP reporter cells was performed using a

Nikon Eclipse Ti Eclipse with an Orca OSG camera (Nikon, Japan) inverted microscope using NIS-Elements Advanced Research.

3.9.2. Confocal Microscopy

Confocal microscopy allows for optical sectioning and the acquisition of high resolution imaging. Additionally, by acquiring multiple planes it allows the construction of 3D images. This technique was used both for immunocytochemistry imaging and the imaging of co-cultures. Images were taken on a Leica Sp5, an ultra-high speed inverted confocal microscope in Cambridge NIHR BRC Cell Phenotyping Hub and analysing using ICY and FIJI (de Chaumont et al., 2012; Schindelin et al., 2012). For immunocytochemistry imaging, z-stacks were taken and the maximum projection displayed.

For the analysis of co-cultures, z-stacks were utilised to assess the interaction of the D1 OLR UVA cell line and bone marrow derived cells from ubiquitin-GFP reporter mice. These co-cultures were fixed for 20 minutes with 37°C pre-warmed 4% paraformaldehyde, and then incubated with PBS containing 0.1% Tween20 (Sigma) (PBS-T) for 5 minutes to permeabilise the cells. Subsequently, Phallodin Alexa 555 (Thermo Fisher Scientific) was applied to cells for 20 minutes for the visualisation of the actin cytoskeleton of D1 ORL UVA cells. Slides were then washed with PBS twice and then distilled water, slides were mounted using ProLong Diamond Antifade Mountant with DAPI (Thermo Fisher Scientific).

3.9.3. Macroscopic Images

Macroscopic images were used to assess Alizarin red histological staining of cell culture wells. These were taken with a Canon EOS 1200D at a distance of approximately 20 cm away from the plate using a camera stand.

3.10. Protein Methods

3.10.1. Protein Isolation

To isolate total cellular protein from cells, they were first washed with PBS and then lysed with protein lysis buffer on ice. This buffer was prepared using RIPA buffer (Millipore) with the addition of cOmplete ULTRA protease inhibitor cocktail (Sigma) and PhosSTOP phosphatase inhibitor tablets (Sigma). Where protein lysis buffer was added to wells of 6 well plates, 100 µl per well was added and cells detached with a cell scraper. Suspension cells such as PB MNCs were washed through centrifugation and lysis buffer added to the cell pellet, 100 µl per $<1x10^7$ cells. Lysates were transferred to low-bind Eppendorf's and rotated at 4°C for 30 minutes. Samples were stored at -70°C and before analysis centrifuged at 14,000 x g for 15 minutes and the supernatant retained for further study.

3.10.2. Protein Concentration

Total cellular protein was concentrated for some samples due to low abundance of the proteins of interest. Protein lysates were transferred to Amicon Ultra-0.5 30KDa centrifugal filter devices (Millipore) and centrifuged for 15 minutes at 14,000 x g. The columns were then inverted in new tubes and centrifuged for 2 minutes at 1,000 x g.

3.10.3. Bicinchoninic (BCA) Assay

The BCA assay, Pierce™ BCA Protein Assay Kit (Thermo Fisher Scientific), was used to quantify total cellular protein. In the presence of peptides comprising of three or more residues copper ions are reduced and detected by bicinchoninic acid (BCA) resulting in the formation of a purple-coloured product (Smith et al., 1985).

Protein lysates were compared to known bovine serum albumin (BSA) (Thermo Fisher Scientific) protein standards prepared at concentrations ranging from 25 to 2000 ng/mL. Protein samples and the BSA standards were diluted 1:8 by the addition of 200 µl of working reagent to 25 µL cell lysate or protein standards in a 96-well plate, each in triplicate. The working reagent was prepared by diluting $CuSO_4$ pentahydride solution (4 %) in BCA 1 in 50. Plates were then incubated for 30 minutes at 37°C. The absorbance for samples and protein standards was subsequently measured at a wavelength of 562 nm using a FluoStar Optima plate reader (BMG Labtech). The protein concentrations of samples were then estimated using the absorbance of the known BSA standards.

3.10.4. Western Blotting

Western blotting is used to detect and analyse proteins based on their molecular weight as well as antibody targeting of antigens (Towbin, Staehelin and Gordon, 1979; Burnette, 1981). Protein lysates were denatured by mixing with 4X NuPAGE sample LDS loading buffer (Thermo Fisher Scientific) supplemented with 10X NuPAGE reducing agent (Thermo Fisher Scientific) and heating to 75°C for 15 minutes. Quantification from the BCA assay was used to ensure consistent amounts of protein were used for each sample.

3.10.4.1. Electrophoresis

Proteins were loaded onto mini-PROTEAN TGX pre-cast gels 10-well 4-20% stain free gels (BioRad) alongside Chameleon Duo Pre-stained protein ladder (Licor). Samples were resolved by electrophoresis in Tris/Glycine/SDS running buffer (BioRad), at 250V for 25 minutes. Proteins were then transferred onto 0.2 µm nitrocellulose or 0.45 µm PVDF membranes using a Trans-Blot Turbo Transfer Pack (BioRad) in a Trans-Blot Turbo semi-dry system, 7 minutes at 25 V.

3.10.4.2. Immuno-Probing and Detection

Membranes were blocked to prevent non-specific binding of the primary antibody by incubation in blocking buffer, prepared by a 1 to 1 dilution of Odyssey blocking solution (Licor) in TBS (Fisher Scientific), for 1.5 hours at room temperature. The membrane was then probed overnight at 4°C with the primary antibody (see Table 3-5) diluted in blocking buffer made using TBS containing 0.1% Tween20 (Sigma) (TBS-T). Antibodies were used as per the manufacturer's instructions and the final incubation concentration optimised.

Membranes were washed three times in TBS-T for 10 minutes per wash to remove excess primary antibody. Subsequently membranes were incubated with secondary antibodies diluted in TBS-T blocking buffer for 1.5 hours at room temperature. Membranes were washed three times in TBS-T for 10 minutes each.

Membranes were then imaged using an Odyssey Fc system (Licor) with an exposure time of 2 minutes or using a ChemiDoc system (BioRad) with automated exposure settings. Both these pieces of equipment detect the fluorescence of the secondary antibody conjugated to a fluorophore.

Table 3-5 – Antibodies used for Western blotting

Antigen	*Code*	*Species*	*Company*	*Dilution*
Primary antibodies				
G-CSF R	ab126167	Rabbit mAb	Abcam	1 in 500
Phospho-p44/42 (Thr202/Tyr204)	9106	Mouse mAb	CST	1 in 2,000
p44/42	4695	Rabbit mAb	CST	1 in 1,000
Phospho-STAT3 (Y705)	ab76315	Rabbit mAb	Abcam	1 in 2,000
STAT3	9139	Mouse mAb	CST	1 in 1,000
Actin-peroxidase	A3854	Mouse mAb	Sigma	1 in 25,000
Secondary antibodies				
IRDye800CW Donkey anti-rabbit	925-32213	Donkey	Licor	1 in 15,000
IRDye680CW Donkey anti-mouse	925-68022	Donkey	Licor	1 in 15,000

When required, membranes were subsequently incubated with actin-peroxidase in TBS-T for 20 minutes at room temperature. After a final two wash steps with TBS-T, 10 minutes each, membranes were developed by chemiluminescence with Amersham ECL Prime Western Blotting Detection Reagent (GE Healthcare). This visualisation technique causes the peroxidase conjugated to the primary antibody to catalyse the oxidation of a chemiluminescent substrate. As the product of this reaction decays from its excited state releasing photons of light at 425nm which are captured. A ChemiDoc system (BioRad) was used to image chemiluminescence.

3.10.4.3. Protein Quantification

Protein bands were quantified by densitometry using Image Studio Lite (Licor) for Odyssey captured images and Image Lab (BioRad) for ChemiDoc captured images.

3.11. Gene Expression

Quantitative real time PCR can be used to assess the gene expression profile of a population of cells by determining genes transcribed to messenger RNA. This analysis therefore requires the isolation of RNA from cells, its transcription to complementary DNA and finally assessment of the quantity of the transcripts of interest.

3.11.1. RNA extraction

Prior to RNA extraction, surfaces and designated RNA pipettes were cleaned with RNaseZAP (Thermo Fisher Scientific) to eliminate any environmental RNase and sterile filter tips used.

RNeasy (QIAGEN) uses a silica-based membrane to which RNA binds after it is released by the lysis of cells. Using a denaturing guanidine-isothiocyanate lysis buffer, RNA is kept intact by the inactivation of RNases. The addition of ethanol provides the appropriate conditions for RNA to bind to a spin column, which can subsequently be washed with various buffers to remove contaminants, before elution of harvested RNA in water.

Cells cultured for gene expression analysis were first washed with PBS before cell lysis by the addition of RLT buffer (QIAGEN) to which 1% β-mercaptoethanol (BME) (Sigma) had been added. Cells isolated from co-cultures and then sorted by FACS were sorted into DMEM expansion media and subsequently spin washed twice with PBS (300 x g for 5 minutes) before the addition of RLT buffer with BME. Cells from the spinal vertebrae of mice on the other hand, were sorted directly into RLT buffer. All samples were stored at -70°C after lysis until required.

The RNeasy protocol was followed as per the manufacturer's instructions described here. Where necessary, for example from 7 day osteogenesis assays, cells were homogenised using a Qiashredder (QIAGEN). For this, samples were added to QIAshredder columns and centrifuged for 2 minutes at 14,000 x g and the flow though retrieved. Cell lysates were combined 1:1 with 70% ethanol, and added to an RNEasy column, which was centrifuged for 20 seconds at 14,000 x g. The flow-through was discarded and 700 µL of RW1 buffer added to the column, before centrifuging again for 20 seconds at 14,000 x g. The column was washed twice with 500 µL of RPE wash buffer under the same centrifugation conditions, and the flow-through discarded. Spin columns were then transferred to clean 2 mL tubes, and centrifuged for 2 minutes at 14,000 x g to remove excess wash buffer and dry the column membrane. The spin columns were then

transferred to clean 1.5 mL Eppendorfs and 30 µL of RNase/DNase-free water added to each column. RNA was eluted by centrifuging for 1 minute at 14,000 x g, and the tubes immediately placed on ice.

RNA concentration and quality was quantified using UV-spectrometry - Nanodrop ND-2000 Spectrophotometer (Thermo Fisher Scientific). Purity was assessed based on 260/280 nm wavelength ratios and a ratio of ~2.0 was accepted as suitable for cDNA synthesis. RNA was stored at -70°C until required.

3.11.2. cDNA Synthesis

Double-stranded complementary DNA (cDNA) is required for qRT-PCR and was synthesised from the extracted RNA using reverse transcriptase. RNA was reverse-transcribed using a QuantiTect Reverse Transcription Kit (QIAGEN), as per the manufacturer's instructions (concentrations of kit contents not provided), alongside reverse transcriptase enzyme negative controls.

RNA was diluted to <1000 ng in 12 µL with RNase/DNase-free water and combined with 2 µL 'gDNase Wipeout Buffer'. This was incubated for 2 minutes at 42°C and then placed on ice. 6 µL of a prepared mastermix solution containing dNTPs, reverse transcriptase and RT buffer was added to each sample and incubated at 42°C for 30 minutes. Subsequently samples were transferred to 95°C for 3 minutes to denature the reverse transcriptase. cDNA was stored at -20°C until required. The total amount of cDNA was considered 1:1 with the quantity of RNA used in the reaction.

3.11.3. Quantitative Real Time PCR

qRT-PCR can determine relative amounts of a specific mRNA transcripts present between two or more samples using the amplification products synthesised by reverse transcription, thus enabling an understanding of gene expression differences between samples. As with traditional PCR, the amplicon is amplified but the addition of a fluorescent dye such as Sybr Green allows for the quantity of an amplicon to be gauged. Sybr Green binds to the double-stranded DNA generated during the amplification step of PCR at which point fluorescence is registered by a detector.

As the amplicon numbers increase with each cycle the fluorescent signal should increase proportionally if the reaction is 100% efficient (Wittwer et al., 1997; Schneeberger et al., 1995). Assessing the efficiency of the reaction is therefore vital before quantification of experimental samples. This was done for all in-house designed primers (see section 3.11.5).

The number of PCR cycles required to detect a real signal exceeding background fluorescence is known as the cycle threshold (C_T). Using a comparative C_T method the

relative gene expression between samples can be calculated (Schmittgen and Livak, 2008). The use of a stable housekeeping gene ensures that varying levels of starting material and quality of RNA is accounted for by subtracting the gene of interest C_T from that of the housekeeping gene. A fold-change is then calculated to determine relative gene expression between samples.

HPRT was validated as a suitable housekeeping gene for the experiments performed in this thesis. This was based on the analysis of several housekeeping genes for both human (HPRT, GAPDH and B2M) and mouse (HPRT and GAPDH) cells and the housekeeping gene selected using the NormFinder Software (Andersen, Jensen and Ørntoft, 2004). HPRT was selected as the best compromise between "stability" and "standard error" for human BMSCs (Appendix 10.2).

3.11.4. qRT-PCR assay

Reaction volumes of 12 uL were used combining 2X QuantiFast SYBR Green PCR Kit (QIAGEN), a final concentration of 10 mM for both forward and reverse primers and 2 uL of 5 ng/ul cDNA. Reactions were run on a StepOnePlus instrument (Applied Biosystems). Thermocycling conditions of 95°C for 5 minutes followed by 40 cycles of 95°C for 10 seconds and 62°C for 30 seconds were used for all primer pairs.

C_T values were quantified in triplicate for each gene and normalised to HPRT housekeeping control. The cDNA template negative controls were run for each primer mix prepared. Analysis of experimental samples was performed by relative quantification using the comparative Ct ($2^{-\Delta\Delta C_T}$) method, normalising to the housekeeping gene HPRT.

The following equations were used for the comparative C_T method:

$\Delta C_T = C_T$ GOI $- C_T$ HK

(where GOI is Gene Of Interest and HK= Housekeeping gene)

$\Delta\Delta C_T = \Delta C_T$ sample $- C_T$ calibrator

Relative quantification $= 2^{-\Delta\Delta_{CT}}$

3.11.5. qRT-PCR primer design

Primers were either purchased pre-designed from Sigma or Qiagen or primer sequences were taken from published literature and checked using NCBI PrimerBlast / NucleotideBlast. Primers were validated for amplification efficiencies between 0.4ng and 100ng of cDNA per reaction above using RNA from appropriate cell types. Primer performance was determined through slope, efficiency and R^2 in StepOne software (Appendix 10.3). Primers with efficiencies between 90 and 110% (with the exception of *Tgfβ* and *Ptprc* mouse primers) and R^2 of greater than 90% were used for experimental

samples. Melt curves were assessed to ensure no primer dimers formed between primer pairs or off target amplification.

3.12. In Vivo Models

3.12.1. Animal Husbandry

All surgery was performed in accordance with the regulations laid out in the Animals (Scientific Procedures) Act 1986. Mice were housed in the Phenomics animal facility, University of Cambridge, according to Home Office requirements under project license 70/8635. All animals were housed in individually ventilated cages under a 12h dark 12h light cycle and fed a standard diet.

3.12.2. Animals Used

Two stains of mice were used for *in vivo* studies in this thesis; wild type C57BL/6 mice, supplied by Charles River and transgenic Nestin-GFP reporter mice (MGI ID: 5523870) (Mignone et al., 2004) kindly donated as a gift from the Mendez-Ferrer group, University of Cambridge. Mice were used between 8 and 12 weeks of age and ear notching conducted for the identification of animals.

3.12.3. Genotyping

Genotyping of transgenic mice was performed to confirm the expression of GFP under the Nestin promotor. Ear biopsies of 2 mm diameter from identification ear notching were collected and genotyped. Biopsies were stored at -20°C until required.

Biopsies were incubated in 100 µL Direct PCR Lysis Regent Ear (Viagen Biotech) containing 0.5 mg/mL Proteinase K (Bioquote) at 55°C overnight. After inactivation at 85°C for 45 minutes, PCR was performed directly on lysate.

PCR reaction mixture (21 µL) consisted of the following components: 2 µl of ear biopsy lysate, 4 µL of 5X Green GoTaq Reaction Buffer (Promega), 0.2 µL of GoTaq G2 DNA Polymerase (Promega), and 2 µL dNTPs (Thermo Scientific) to final concentration of 0.2 µM. Additionally, 0.5 µM of each primer (1 µL each) was added to each reaction; Nestin Primer: 5′ GGAGCTGCACACAACCCATTGCC 3', GFP Primer: 5′ GATCACTCTCGGCATGGACGAGC 3′ (Mignone et al., 2004).

A gradient PCR was run initially to determine the best annealing temperature conditions using a Veriti 96-Well Thermal Cycler (Applied Biosystems). Thermocycling conditions of 94°C for 5 minutes; 30 cycles of 94°C for 30 seconds, an annealing temperature of 67°C for 30 seconds, 72°C for 45 seconds and 72°C for 5 minutes, were subsequently used for genotyping on a Biometra T3 Thermocycler. The PCR-products were run on a 2% agarose

gel prepared in TAE buffer (4.84 mg/mL Tris base, 0.3 mg/mL EDTA made up to pH 8 with glacial acetic acid) containing 0.01% SYBR Safe DNA Gel Stain (Thermo Fisher Scientific) alongside a 100 base pair ladder (New England Biolabs), at 100V, 400mA for 1.5 hours. Gels were imaged under UV light (Syngene inGenius system).

3.12.4. Agent Dose and Delivery

G-CSF is a biologic agent sold for clinical use under the generic name Filgrastim. G-CSF is cross species reactive and therefore clinical grade Filgrastim (Zarzio) was used for animal studies. However, the solution was diluted in 5% glucose (Aqupharm No3, Animalcare) to 10 µg/mL and dosed at 250 µg/kg/day subcutaneously consistent with published literature (Semerad et al., 2005; Christopher and Link, 2008) for 3 days.

3.12.5. Animal Surgery

Mice were acclimatised to the animal facility for a minimum of 7 days and health checked and weighed before surgery. The basic surgical procedure was performed under strict asepsis by a single surgeon. General anaesthesia was induced by exposure to 4% isoflurane and then maintained at 1.5-2%. All mice were given pre-operative analgesia of subcutaneous 1 mg/kg buprenorphine.

The hair over the left knee was clipped, the skin disinfected and the animal placed under a surgical microscope in a dorsal recumbent position on a heat pad. The left leg was bent over a 2.5 mL syringe barrel and the foot taped into place to achieve a right angle at the knee joint. The animal was then draped exposing the knee joint. A small (0.5 to 1 cm) medial para-patellar skin incision was made, the joint capsule opened by blunt dissection and the patella luxated laterally to expose the patella groove articular surface. Osteochondral defects within the patella groove were created using a 26 G needle with 0.6 mm of the tip exposed by the use of a fixed plastic cylinder acting as a depth guard. This instrument was sterilised using ethylene oxide gas sterilisation. Trials with other size needles were performed on euthanised cadavers using the same method of patella groove exposure.

After creation of the osteochondral defect the patella groove was washed with sterile saline and a drop of 0.25% bupivacaine applied to the defect before repositioning the patella. The joint capsule was close with two 7-0 absorbable sutures (Ethicon), one above and one below the patella. Finally, three to four 6-0 sutures (Ethicon) were used to close the skin.

The mice were moved to a clean cage in a warm Incubator to recover, with checks every 15 minutes for the first hour. After this time mice were fully weight bearing and showed no evidence of lameness. Mice were housed in clean, sawdust-lined boxes with mash and

post-operative checks carried out by skilled technical staff every day for the first 7 days post-surgery.

3.12.6. Necropsy

Animals were humanely sacrificed post-operatively by carbon dioxide asphyxiation and tissue samples harvested at various time points between 24 hours and 8 weeks post-surgery. The operated left hind and contralateral right hind limb were both harvested from all animals. Additionally, from transgenic mice, spleens and spinal columns were harvested and peripheral blood samples were taken via cardiac puncture.

3.12.6.1. Hind Limbs

The skin was removed from the hind limbs of mice. On the operated left hind of some animals the patella groove was visualised by luxation of the patella and photographs taken of the osteochondral defect surface using a 20x macro lens. The femur and tibia of all limbs were cut to 0.5 cm away from the knee joint. Samples were then moved to 10% neutral buffered formalin for 24 to 48 hrs at 4°C before preparation for histology (see section 3.13).

3.12.6.2. Peripheral Blood - Cardiac Puncture

Immediately after carbon dioxide asphyxiation, blood was collected by cardiac puncture using a 23G needle and a 2.5 mL syringe. Blood samples were then transfer into 1.3 mL heparin micro tubes. Cells were stained and analysed by flow cytometry as detailed in section 3.8.2.

3.12.6.3. Spleen

Spleens were harvested and transferred to 10% neutral-buffered formalin (Sigma) for 24 hours fixation. Spleens were then processed for paraffin sectioning (see section 3.133.13.2.1).

3.12.6.4. Spinal Vertebrae

The spinal columns were dissected, and soft tissue removed using a scalpel and Kimtech tissue. The spinal column was broken into pieces of approximately 1 cm. Segments were processed for paraffin or cryo-sectioning (see section 3.13) or segments from Nestin-GFP reporter mice were additionally used for the isolation of bone marrow $CD45^{-}GFP^{+}$ cells. Segments used for histology were moved to 10% neutral-buffered formalin for 24 hours fixation at 4°C before further processing.

Where segments were used for isolation of cells, the spinal cord was removed to minimise the contamination of spinal cord derived cells. This was done at dissection by carefully pulling the vertebrae segments along the spinal cord before transfer into cold dissociation

buffer (PBS with 3% FBS, and 5 mM EDTA). Bones were then crushed using a pestle and mortar. After pipette agitation and washing of bone fragments, the bone marrow suspension was strained through a 30 µm cell strainer and cells pelleted at 300 x g. Cells were sorted first by immune-magnetic depletion of $CD45^+$ cells and subsequently re-suspended in dissociation buffer and sorted by FACS (see section 3.8). FACS sorted cells were eluted directly into RLT lysis buffer for the isolation of RNA (see section 3.11).

3.13. Histological Sectioning

Tissue samples were processed for histological analysis. Sections were generated by either paraffin- or cryo- sectioning. In both cases tissues containing bone were de-calcified before embedding (hind limbs and vertebrae samples).

3.13.1. De-Calcification of Bone

By its nature, bone contains a high proportion of mineralised calcium (hydroxyapatite) and the increased density relative to embedding media makes routine histology challenging and causes numerous tissue artefacts. Samples were decalcified by one of two methods; incubation in acid or Ethylenediaminetetraacetic acid (EDTA). Unless stated samples were decalcified with EDTA.

3.13.1.1. EDTA

EDTA is a chelating agent, which captures calcium ions from the surface of apatite crystals, slowly reducing their size. This process is very slow but very gentle maintaining tissue morphology and preserving epitopes for molecular techniques such as immunohistochemistry.

After fixation, samples were washed in distilled water for 30 minutes and then transferred to a decalcification solution of 14% EDTA (Sigma) solution (adjusted to pH 8 using NaOH pellets). Samples were incubated at room temperature, on a rocker and the EDTA solution replaced 2 to 3 times a week. Hind limbs and vertebrae for cyro-sectioning were decalcified for 1 week whereas those for paraffin-sectioning were decalcified for 2 to 3 weeks. The completion of decalcification of samples for paraffin sectioning was confirmed by a lack of resistance on penetration of the tibia with a 27 G needle. In both cases samples were washed in distilled water for 30 minutes before processing and embedding as appropriate.

3.13.1.2. Formic Acid and Hydrochloric Acid Mix

Acid decalcification occurs more quickly than decalcification using EDTA (Skinner et al., 1997). Acid decalcification was used here for the processing of tissues quickly when the surgical technique was being optimised. After fixation, samples were washed in distilled

water for 30 minutes and then transferred to a decalcification solution of 4% formic acid and 4% hydrochloric acid, ensuring the samples were submerged. Samples were left in the acid mix for 4 to 5 hours on a rocker at room temperature.

Samples were then removed and rinsed in distilled water for 5 minutes before the addition of 5 drops of 10% ammonia hydroxide solution (Sigma) to approximately 100 mL of distilled water. Samples were left for 30 minutes to neutralise the acidity before rinsing them in running tap water for 30 minutes before processing and embedding in paraffin.

3.13.2. Embedding and Sectioning

Embedding tissues in different media offers the possibility to analyse different histological characteristics. Paraffin embedding best preserves the structure of the tissue, whilst cryo-sectioning used here preserves the fluorescence present in the GFP transgenic line. All hind limbs were embedded for sagittal sectioning.

3.13.2.1. Paraffin Embedded Sections

Decalcified (bone) and un-decalcified (spleen and chondrogenic cell pellet) samples were transferred to 50% ethanol after washing in distilled water. Samples were then moved to a Leica TP1020 Tissue Processor. This machine moves samples through a series of reagents to allow paraffin infiltration throughout the tissue. First samples are incubated through a series of increasing concentrations of ethanol (50%, 70%, 80%, 95% for 1 hour each and three 100% changes 1 hour each), before immersion in two sequential xylene steps (2 hours each). Finally, samples are moved into 60°C melted paraffin, each bath for 2 hours. All these steps were performed under vacuum. Samples were then orientated as appropriate and embedded in paraffin using Leica HistoCore Arcadia H Embedding Station. Samples were stored at 4°C until required for sectioning.

Samples were sectioned at 5 µm using a Leica BM2255 Microtome and dried onto Superfrost Plus Slides (Thermo Fisher Scientific). Slides were then stored at room temperature or 4°C.

3.13.2.2. Cryo- Embedded Sections

After washing decalcified samples in distilled water, they were then incubated in an increasing gradient of sucrose solutions to equilibrate the tissue to the embedding media; 15% sucrose at 4°C until the tissue sunk (approximately 3 to 4 hrs) and then 30% sucrose overnight. Samples were embedded in OCT compound (Tissue-Tek) in cryo-moulds and placed into liquid nitrogen vapour for 3 to 5 minutes to snap freeze. Samples were kept at -70°C for long-term storage.

Sections were cut in a cryostat (Bright Instruments) using a tungsten carbide tipped knife (Bright Instruments). Before sectioning samples were moved to the cryostat for 1 hour to

acclimatise the tissue. Sections were made at 15 µm either using Kawamoto tape (Kawamoto and Kawamoto, 2014) or direct transfer onto Superfrost Plus Slides (Thermo Fisher Scientific). Slides were then air-dried and transferred to -20°C for storage.

3.13.3. Histological Stains and Counter Stains

Paraffin tissue sections were rehydrated prior to commencing the staining procedures as outlined below. First, sections were warmed on at hot plate at 60°C for 10 minutes before transfer to xylene for 10 minutes, following by a second xylene bath for 10 minutes. Slides were then incubated in decreasing concentrations of ethanol for 5 minutes each (100%, 100%, 95%, 80%, 70%, 50%, 30%), followed by two washes in distilled water for 5 minutes each.

3.13.3.1. DAB Immunohistochemistry of Paraffin Sections

Diaminobenzidine (DAB) is oxidized in the presence of peroxidase and hydrogen peroxide resulting in the deposition of a brown, alcohol-insoluble precipitate at the site of enzymatic activity. By applying antibodies (tagged with horseradish peroxidase) against epitopes of interest, DAB precipitation can be used to identify the location of proteins.

After rehydration to water, samples were treated to unmask antigens through an antigen retrieval procedure. For the identification of collagen proteins, samples were incubated at 37°C in 0.1% hyaluronidase (Sigma) for 50 minutes before washing in PBS for 5 minutes and continuing to the blocking step. Other samples were incubated in 10 mM sodium citrate (Sigma) buffer adjusted to pH 6 containing 0.05% Tween (Sigma). This method was optimised and a final procedure of incubating slides in the buffer at 78°C to 83°C was utilised to help prevent tissue detachment from the slides. After this, slides were left under cold running tap water for 10 min and then blocked.

Slides were blocked for 90 minutes at room temperature in 10% goat serum (Vector Laboratories) diluted in blocking buffer; PBS containing 0.1% Tween20 (Sigma) (PBS-T). Primary antibodies were diluted in blocking buffer at concentrations indicated in Table 3-6 and applied to sections before incubation overnight at 4°C.

The following day slides were washed in PBS four times for 5 minutes each before incubation in 3% hydrogen peroxide (Sigma) for 15 minutes. All incubation steps on the second day were performed at room temperature. Slides were washed three times the host species of the primary antibody used, either an anti-rabbit kit (Rabbit Specific HRP/DAB (ABC) Detection IHC kit, Abcam) was used or an HRP-conjugated secondary antibody (see Table 3-6).

When using the anti-rabbit kit the manufacturer's instructions were followed. Briefly, samples were incubated for 10 minutes with biotinylated goat anti-rabbit, washed four

times in PBS (5 minutes each) and incubated with the streptavidin peroxidase solution for 10 minutes. Otherwise when using an HRP-conjugated secondary, the antibody was diluted in 1% BSA and slides incubated for 1 hour.

After secondary antibody incubation or the streptavidin peroxidase incubation (for the kit samples) slides were washed four times in TBS, 5 minutes each. Samples were then incubated with DAB substrate for the time quoted in Table 3-6 before stopping the enzyme reaction by submersion of the slide in PBS. Finally, samples were counterstained with methyl green (see below).

Table 3-6 – Antibodies used for immunohistochemistry

Antigen	*Code*	*Species*	*Company*	*Dilution*	*DAB incubation*
Primary antibodies					
Type II Collagen	ab34712	Rabbit pAb	Abcam	1 in 100	5 minutes
Type IV Collagen	ab6588	Rabbit pAb	Abcam	1 in 400	3 minutes
NIMP (neutophil)	ab2557	Rat mAb	Abcam	1 in 100	6 minutes
CD68	ab125212	Rabbit pAb	Abcam	1 in 100	3 minutes
Ki67	12202	Rabbit mAb	CST	1 in 400	10 minutes
Secondary antibodies					
HRP-conjugated anti-rat	ab205720	Goat	Abcam	1 in 2,500	

3.13.3.2. Methyl green staining

Methyl green is a nuclear stain that is used as a counterstain to DAB immunohistochemistry staining. After completion of IHC, slides were washed in distilled water for 5 minutes before transfer to preheated (60°C) methyl green (Vector Laboratories) solution for 5 minutes. Slides were then transferred to tap water (three changes) and the slides left for 1 minute in the third tap water change. Slides were then dipped into acetone containing 0.05% acetic acid 6 to 8 times. Sections were then dehydrated through 95% and 100% ethanol (one change, 5 minutes each) and then cleared with xylene (2 changes, 5 minutes each) before mounting in DPX medium.

3.13.3.3. Alcian Blue

Alcian blue stains proteoglycan components of the extracellular matrix. After deparaffinisation and rehydration, sections were stained with a solution of 1% Alcian blue (Sigma) diluted in 0.1 M HCl overnight. Sections were subsequently dehydrated through 95% and 100% ethanol (one change, 5 minutes each) and then cleared with xylene (2 changes, 1 minutes each) before mounting in DPX medium.

3.13.3.4. Haematoxylin / Eosin

Haematoxylin stains basophilic substances such as DNA and RNA in nuclei while eosin colours eosinophilic structures in various shades of red, pink and orange (Schmitz et al., 2010). After deparaffinisation and rehydration, sections were stained with haematoxylin

solution (Cell Signalling Technologies) for 5 minutes and then rinsed in running tap water until clear. Slides were then dipped into 2% acetic acid 10 times, followed by 10 dips into tap water before transfer into a bluing solution of 0.2% ammonium hydroxide in 70% ethanol for 1 minute. Next, slides were dipped 10 times in tap water before incubation in Eosin Y (Sigma) for 30 seconds. Sections were subsequently dehydrated through 95% and 100% ethanol (one change, 5 minutes each) and then cleared with xylene (2 changes, 5 minutes each) before mounting in DPX medium.

3.13.3.5. Safranin O / Fast Green / Weigert's iron haematoxylin

Safranin O staining is a cationic dye that stains acidic proteoglycans orange to red. Fast green acts as a counterstain, staining background tissue and cell cytoplasm green whilst Weigert's iron haematoxylin stains nuclei black (Schmitz et al., 2010).

After deparaffinisation and rehydration, sections were stained with Weigert's iron haematoxylin (Sigma) working solution for 10 minutes, followed by washing under running tap water for 10 minutes. Slides were then transferred to 0.1% Fast Green FCF (Sigma) for 5 minutes, before transferred to 1% acetic acid for 10 to 15 seconds. Subsequently slides were stained in 0.1% Safranin O (Sigma) solution for 5 minutes. Sections were then dehydrated through 100% ethanol (2 changes, 5 minutes), cleared with xylene (2 changes, 5 minutes each) and mounted using DPX mounting medium.

3.13.3.6. Pico-Sirius Red

Pico-Sirius Red stains connective tissue and can be used for the visualisation of type I and III collagen fibres that when viewed under polarised light results in birefringence (Schmitz et al., 2010). After deparaffinisation and rehydration, sections were stained with Pico-Sirius Red solution (Abcam) for 1 hour and then rinsed in 0.5% acetic acid solution. Sections were then dehydrated through 100% ethanol, cleared with xylene (2 changes, 5 minutes each) and mounted using DPX mounting medium.

3.13.3.7. Thionin

Thionin is a metachromatic dye that binds to negatively charged glycosaminoglycans indicative of cartilage matrix (Narcisi et al., 2015). After deparaffinisation and rehydration, sections were stained with 0.5% thionin acetate salt (Sigma) solution for 2 minutes before rinsing with distilled water. Sections were then dehydrated through 100% ethanol, cleared with xylene (2 changes, 5 minutes each) and mounted using DPX mounting medium.

3.13.3.8. Toluidine blue / Fast Green

Toluidine blue, like Safranin O, is a cationic dye that stains proteoglycans and additionally stains acidic nucleic acids (Schmitz et al., 2010). The dye is a metachromatic stain and its staining properties are altered depending upon the pH of the solution. Fast green was used as a counterstain.

After bringing slides to water, they were stained for 10 minutes in 0.04% Toluidine blue (Sigma) made in 0.1 M sodium acetate buffer at pH 4. Slides were then washed in three changes of distilled water (30 seconds each). Counterstaining was carried out in 0.02% Fast Green for 3 minutes before two water washes (30 seconds each). Finally, slides were dehydrated through three changes of 95% ethanol and two changes of 100% ethanol and two changes of xylene before DPX mounting.

3.14. Histological Section Imaging Techniques and Analysis

3.14.1. Standard and Polarised Light Microscopy

Bright field imaging of histological sections was performed using one of two microscopes. Either a Leica DM RXA2 Microscope with images captured using a MicroPublisher 3.3 RTV Camera (QImaging) and Q Capture Pro 7 software or a M8 microscope and scanner (PreciPoint) using ViewPoint software. Polarised light images were taken with the former with the addition of a polarising filter.

3.14.2. Confocal Microscopy

Cryo-sectioned histology images were taken on a Leica Sp5 or Leica SPE ultra-high speed inverted confocal microscopes in Cambridge NIHR BRC Cell Phenotyping Hub. Prior to imaging samples were removed for storage at -20 and washed in distilled water before mounting using ProLong Diamond Antifade Mountant with DAPI (Thermo Fisher Scientific). Z-stacks were taken and analysed using ICY and FIJI (de Chaumont et al., 2012; Schindelin et al., 2012).

3.15. Articular Cartilage Repair Scoring

To assess the level of cartilage repair in the pre-clinical osteochondral imaging model, a modified Pineda scoring system was used (Pineda et al., 1992). Histological sections stained with Safranin O / Fast Green / Weigert's iron haematoxylin were scored blindly by Dr Mark Birch.

Table 3-7 - Histological scoring system based on Pineda et al. (1992)

Filling of defect area (including bone & bone marrow)	
125%	1
100%	0
75%	1
50%	2
25%	3
0%	4
Reconstruction of osteochondral junction	
Yes	0
Almost	1
Not close	2
Matrix staining (bone & cartilage)	
Normal	0
Reduced staining	1
Significantly reduced staining	2
Faint staining	3
No stain	4
Cell morphology	
Normal Reduced staining	0
Most hyaline and fibrocartilage	1
Mostly fibrocartilage	2
Some fibrocartilage, but mostly nonchondrocytic cells	3
Nonchondrocytic cells only	4

3.16. Statistical Analysis

The number of replicates for each experiment are detailed in the figure legends. Points on graphs represent the mean, and error bars show standard deviation unless specified. Analysis was performed using GraphPad Prism 6 to produce graphs/histograms and perform statistical analysis using analysis of variance (ANOVA) or other statistical tests as specified in the figure legends. Tukey and Dunnett's tests were performed as post-hoc analysis to identify differences between experimental groups. Statistical analysis was performed when data from a minimum of three replicates was available.

4. RESULTS: HAEMATOPOIETIC PROGENITORS HAVE A DIRECT EFFECT ON STROMAL CELL FUNCTION

4.1. Background and Rationale

Granulocyte colony stimulating factor (G-CSF) is a commonly used agent in the field of haematological disorders and has a principle action of increasing myeloid lineage cell numbers systemically as well as haematopoietic progenitors and stem cells (HSPCs). The therapeutic use of G-CSF has been reported in several papers to improve the outcomes of a number of surgical approaches for bone and cartilage repair (see section 1.10). However, these reports have lacked comment on the biological mechanism(s) through which this cytokine brings about these effects.

HSPCs commonly reside in the bone marrow of long bones where they are maintained for life long haematopoiesis by the specialised microenvironment of the bone marrow niche. Cells of the bone marrow niche involved in HSPC homeostasis also are of relevance to musculoskeletal repair such as mesenchymal stem/stromal cells (BMSCs). Furthermore, research groups have shown that co-culture of BMSCs and haematopoietic progenitor populations *in vitro* provides a dynamic model in which to study the interactions of these cell types (Jing et al., 2010).

Most of the work studying the interactions of cells within the bone marrow niche has focused on the haematopoietic lineage cells, in an attempt to further understanding of the haematopoietic supportive capacity of the niche microenvironment (Bianco, 2011). There is however evidence of crosstalk between HSPCs and the other cells in the surrounding niche and it is through this action that the HSPCs can regulate the microenvironment itself (Durand, Charbord and Jaffredo, 2018) .

4.2. Aim and objectives

The aim of this chapter is to further understand the influence of HSPC-MSC niche interactions on BMSC fate. To investigate this question, the first objective was to establish a co-culture system that allowed the interaction of murine HSPCs and BMSCs to be studied *in vitro*. This model was then used to characterise specific haematopoietic progenitor subpopulations that influence the differentiation potential of BMSCs. It was hypothesised that BMSC differentiation would be altered by the presence of HSPCs within the surrounding microenvironment.

4.3. The evaluation of D1 ORL UVA cells as murine BMSC model

D1 ORL UVA (ATCC, CRL-12424) (RRID:CVCL_6495) is a murine stromal cell line that was developed in the 1990's and patented in 1997 (Patent number US6082364, accepted 04-Jul-2000). The patent describes evidence that the cell line is capable of tri-lineage differentiation (osteogenesis, chondrogenesis and adipogenesis) and that when transplanted into the tail vein of mouse recipients, the cells home to the bone marrow. The cell line was derived from the non-adherent fraction of BALB/c mouse bone marrow through incubation steps with and then without monocyte-colony stimulating factor. The cell line was subsequently derived clonally from the remaining adherent fraction. Several published papers have utilised the D1 ORL UVA cell line as a model of murine BMSCs (Mussano et al., 2010; Phinney et al., 2006).

Prior to utilising this cell line, multiple attempts had been made to isolate primary murine MSCs by plastic adherence, however expanded cell numbers were not large enough to move forward to co-culture systems (data not shown). For this reason, an established and stable cell line was used in subsequent experiments. After purchase and expansion, the cell line was assessed for its BMSC properties.

4.3.1. Morphological appearance

Morphologically the cell line exhibits characteristics of adherent fibroblastic-like cells, with a stellate form when cultured on plastic (Figure 4-1).

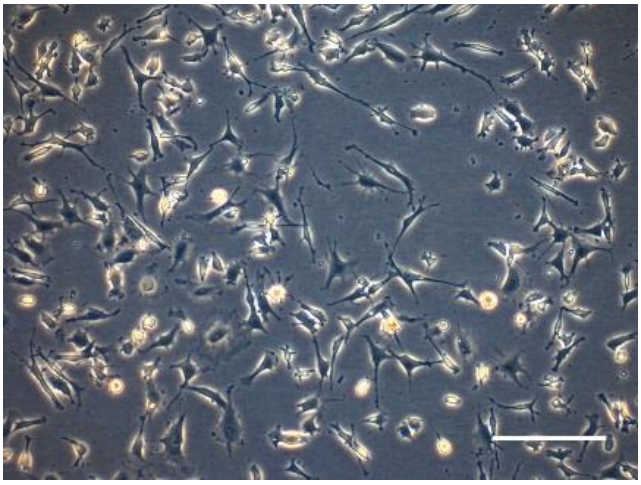

Figure 4-1 – Phase light microscopy image of D1 ORL UVA cell line.
D1 ORL UVA cells were grown on tissue culture plastic and imaged using a 10x objective. Scale bar indicates 200 µm.

4.3.2. Differentiation potential

Differentiation potential is the defining feature of cells described as BMSCs and D1 ORL UVA cells were assessed for their ability to differentiate into osteoblasts, chondrocytes

and adipocytes. Firstly, the cells were evaluated for their ability to form extracellular matrix (ECM) indicative of differentiation down each of these lineages and secondly for the expression of genes related to each lineage over 10 days.

D1 ORL UVA cells were cultured as monolayers for 21 days under osteogenic, adipogenic and chondrogenic conditions. At 7 days morphological changes were seen relative to control media (Figure 4-2). Notably, adipogenic differentiation media led to the formation of phase bright lipid vacuoles within cells (Figure 4-2 C i). After 21 days, tri-lineage differentiation was confirmed by evaluation of biological staining using a light microscope. The matrix staining shown in Figure 4-2 confirmed the potential of these cells to generate the three forms of ECM. Osteogenic differentiation was confirmed by the presence of mineralising matrix and aggregates stained with alizarin red (Figure 4-2 A ii), chondrogenic differentiation by staining for polyanionic matrix with alcian blue (Figure 4-2 A ii), and adipogenic differentiation by the presence of hydrophobic lipid vacuoles stained with oil red O (Figure 4-2 A ii).

Further to the endpoint assessment of the ECM production, gene expression analysis by qRT-PCR was used to elucidate the dynamics of the differentiation process by assessment at multiple timepoints, day 1, 3, 7 and 10 (Figure 4-3). Under osteogenic conditions D1 ORL UVA cells increased the transcription of genes associated with both early and late osteogenic differentiation. For example, between 1 day and 3 days of osteogenic induction the expression of two key transcription factors, *Runx2* and *Sp7* (osterix) both increased over 10-fold at these early time points (Figure 4-3 A). Osterix continued to increase over the timecourse to over 250-fold at 10 days. Between 1 day and 10 days of induction, transcription of key matrix proteins was upregulated. *Bglap* is the gene transcript for osteocalcin, a protein produced soley by osteoblasts, and mRNA levels increased >9,500 fold over this time.

All adipogenic genes assessed showed a rapid increase between day 1 and day 3 (Figure 4-3 C) at which point they remained high and stable up until the final timepoint of day 10. These include the nuclear receptor *Pparγ* gene which is known to activate genes that stimulate lipid uptake and adipogenesis.

Following chondrogenic induction, D1 ORL UVA cells showed a steady increase in abundance of *Sox9*, *Tgfβ* and *Col2a* transcripts up until day 7 (Figure 4-3 B). At day 10 the levels of these chondrogenic genes began to fall in these highly dense monolayer cultures.

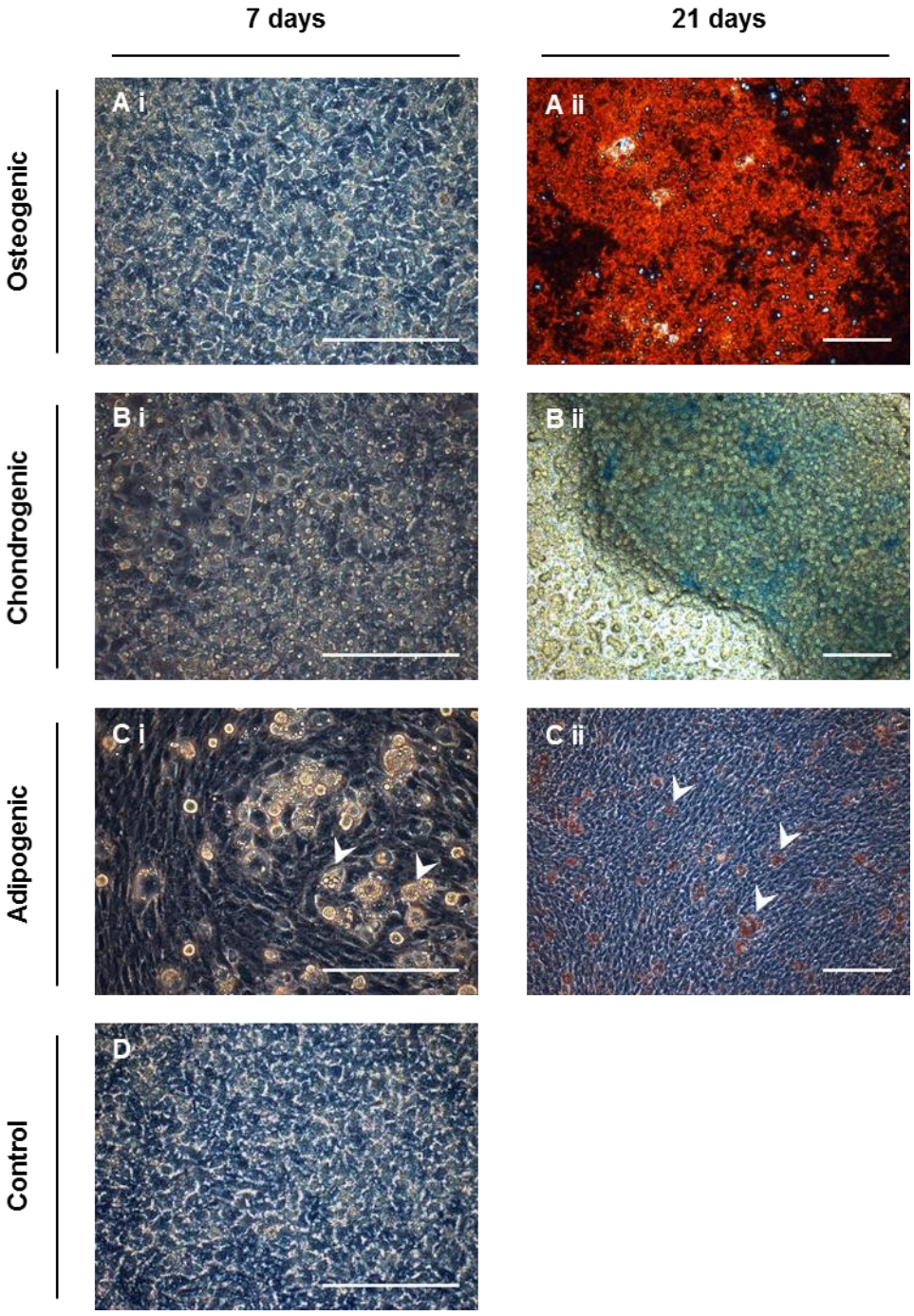

Figure 4-2 - Histological staining of tri-lineage differentiation of the murine cell line D1 ORL UVA.
D1 ORL UVA were differentiated down the osteogenic, chondrogenic and adipogenic lineages (N=3). After 7 days cells were visualised and imaged by light microscopy (20x objective). After 21 days cells were visualised and imaged by light microscopy (10x objective) after histological staining with alizarin red (osteogenesis), alcian blue (chondrogenesis) and oil red O (adipogenesis). Arrowheads indicate lipid vacuoles at 7 days (C i) and at 21 days stained with oil red O (C ii). Scale bars indicate 200 µm.

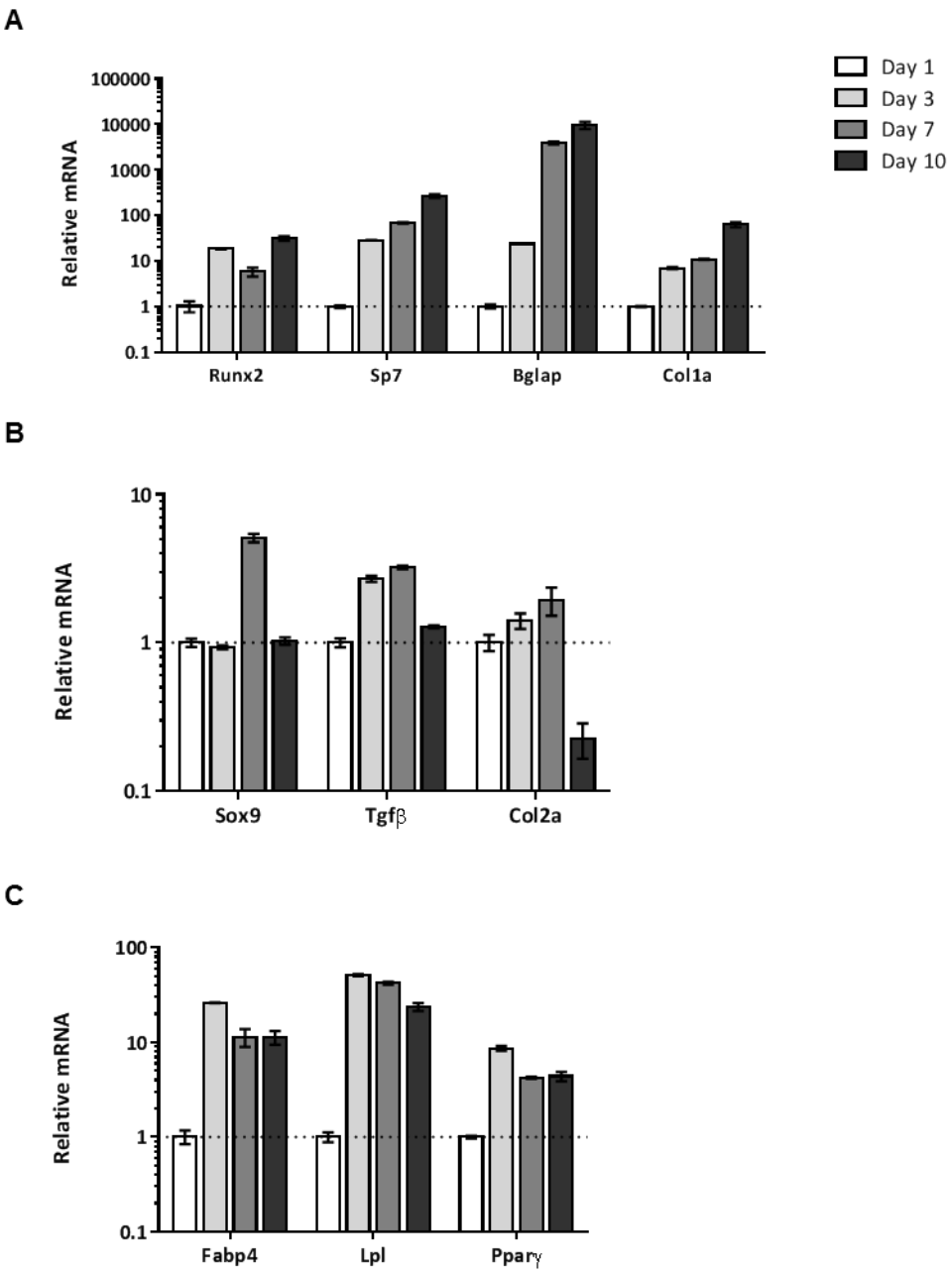

Figure 4-3 – Gene expression analysis of D1 ORL UVA tri-lineage differentiation.
D1 ORL UVA were differentiated down the osteogenic (A), chondrogenic (B) and adipogenic (C) lineages. Cells were harvested at day 1, day 3, day 7 and day 10 and analysed for genes specific for each pathway. Bars indicate the expression of mRNA for each gene normalised to *Hprt*. Error bars indicate the standard deviation of the mean for technical replicates for qRT-PCR run in triplicate (N=1).

4.3.3. Phenotypic Evaluation

Several cell surface antigens have been published as markers of murine MSCs. Using the 'R&D Systems Mouse Mesenchymal Stem Cell Marker Antibody Panel' a selection of these markers were used to assess the phenotypic profile of the D1 ORL UVA cell line by flow cytometry (Figure 4-4).

The cells were grown to 70% confluency in expansion media and stained with one of the eight antibodies or one of three isotype controls (rat IgG_{2A} or IgG_{2B} and sheep IgG). For each sample between 43,000 and 46,000 single cells were recorded and analysed. The appropriate isotype controls were used to set the gates and thus determine the true expression of cell surface markers as a percentage of total single cells.

As expected, the cells demonstrated negativity for haematopoietic markers such as CD45 and CD11b, with less than 2% of cells being positive. With regard to MSC markers, over 90% of cells were positive for CD29, CD44 and CD73 and the majority of cells were positive for CD106 (86.5%), but only 6.3% of cells were positive for CD105. Interestingly, the Sca-1 antigen showed a wide spread in expression indicating its expression is highly variable.

Based on the evidence presented here, confirming the tri-lineage differentiation potential and a phenotypic profile known to represent murine BMSCs, D1 ORL UVA cells were used as a model of murine BMSCs for the co-culture experiments described below.

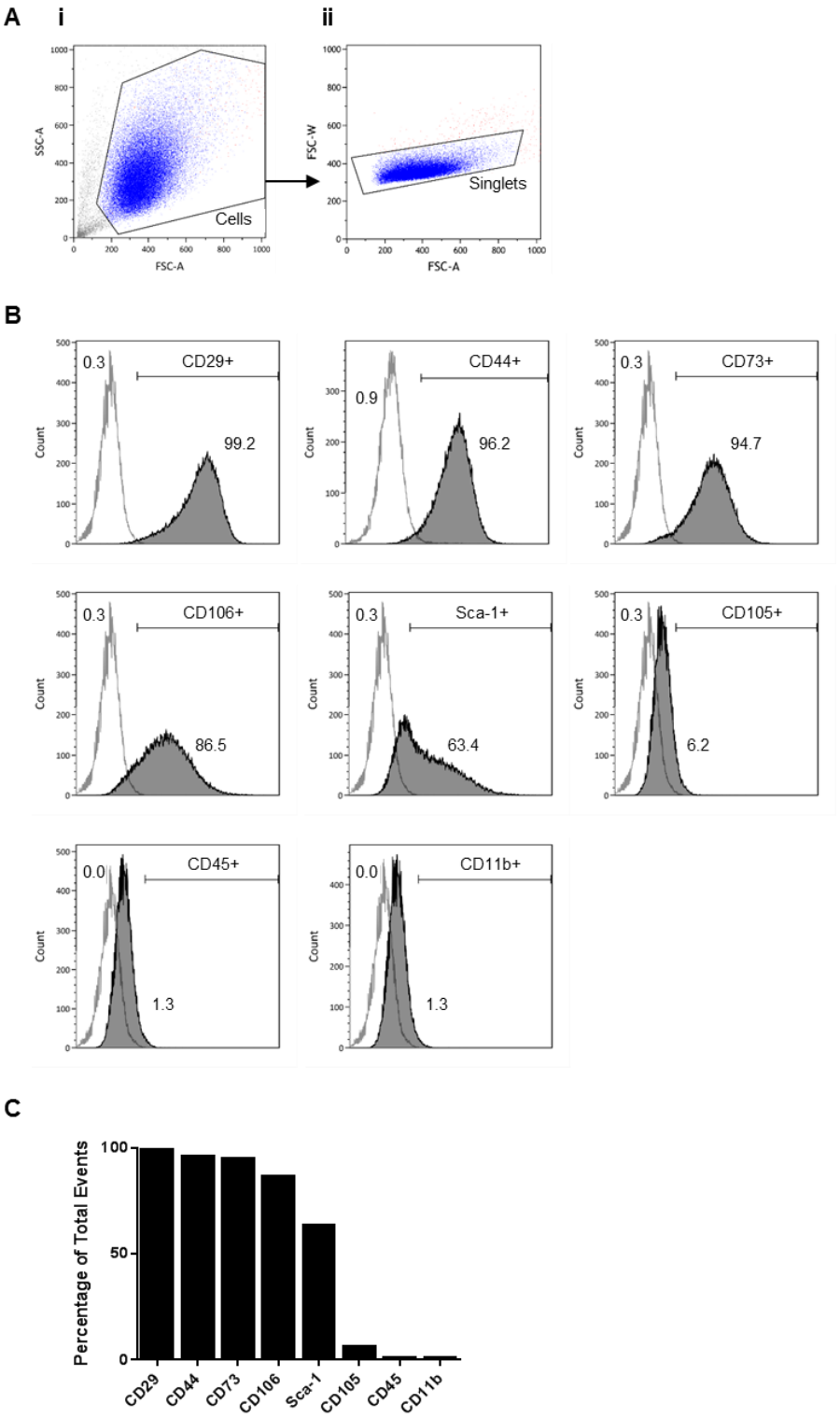

Figure 4-4 – Phenotypic analysis of D1 ORL UVA cells for eight murine MSC markers.

Analysis of the expression of CD29, CD44, CD73, CD106, Sca-1, CD105, CD45 and CD11b on D1 ORL UVA cells by flow cytometry. (A) Scatter plots of (i) forward versus side scatter area used to identify cells and (ii) forward scatter area versus forward scatter width used to eliminate cell doublets. (B) Logarithmic histograms showing the appropriate isotype control (all except CD44 are IgG2A whist CD44 is IgG2B) in white, used to set the gating, with the stained cells overlaid in grey. (C) Graph summarising the percentage of positive cells for each antigen. Secondary antibody was conjugated to APC.

4.4. The lineage negative fraction of primary bone marrow contains haematopoietic stem and progenitor cells

4.4.1. Haematopoietic progenitors

Haematopoietic stem and early progenitors differ phenotypically from more mature cells of the haematopoietic hierarchy as they are negative for mature haematopoietic lineage markers. To isolate a fraction enriched for these early progenitors, bone marrow was harvested from the hind limb long bones of mice by crushing to liberate a single cell suspension and subsequent depletion of mature haematopoietic cells by immune-magnetic separation using a lineage antibody cocktail.

The presence of HSPCs within this population was confirmed by the colony-forming unit cell (CFU-C) assay, Figure 4-5. Culture in methylcellulose restricts the movement of cells and allows for the identification of non-adherent colonies from single progenitors. Based on the morphology of individual cells and the colony itself, the progenitor subtype can be determined. Colonies of the erythroid and macrophage lineage were identified alongside colony forming unit-granulocyte, macrophage, erythroid and megakaryocyte (CFU-GEMM) colonies. The latter is the earliest lineage identifiable by this assay. The results from this assay in Figure 4-5 therefore confirm the ability to isolate primary haematopoietic progenitors from murine bone marrow by lineage depletion.

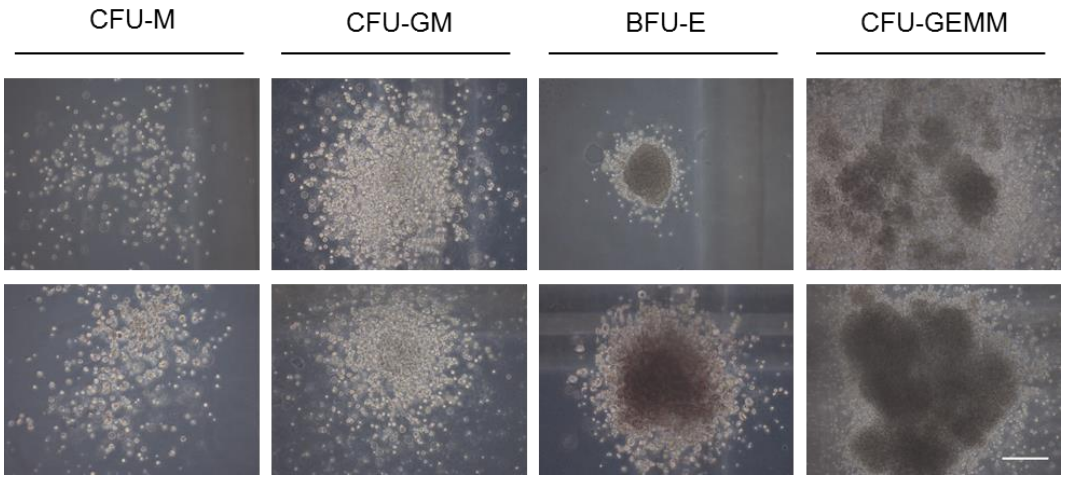

Figure 4-5 – Lineage negative bone marrow cells form haematopoietic colony forming units.
Lineage negative bone marrow cells were cultured in methylcellulose for 14 days cells and then were visualised by light microscopy. Different colony morphologies identify different haematopoietic lineages of the haematopoietic progenitors. (A) CFU-M, a macrophage colony, (B) CFU-E, erythroid based colony, (C) BFU-E, burst forming erythroid colony, (D) CFU-GEMM, granulocyte, macrophage, erythroid and megakaryocyte colony. Images were taken at 10x magnification. Scale bar indicates 100 µm.

4.5. Immuno-depleted bone marrow contains haematopoietic stem cells defined as Lineage negative, Sca-1 and c-Kit positive

Mouse haematopoietic stem cells (HSCs) can be identified more specifically using phenotypic markers. The most basic phenotypic profile for HSCs is positivity for Sca-1 and c-Kit in addition to being negative for mature haematopoietic markers. This is termed the LSK^+ fraction (Peng et al., 2012).

Cells that were isolated from the bone marrow of BALB/c mouse hind limbs and immune-magnetically lineage depleted were subsequently stained with Sca-1 and c-Kit antibodies as well as a viability dye and a lineage marker antibody cocktail. Figure 4-6 illustrates the gating strategy used based on the fluorescence of unstained cells. Firstly, single cells were gated and selected for their negativity for the viability dye 7-AAD, and their negativity for the lineage cocktail. These double negative cells were then analysed for c-Kit and Sca-1 expression (Figure 4-6 D).

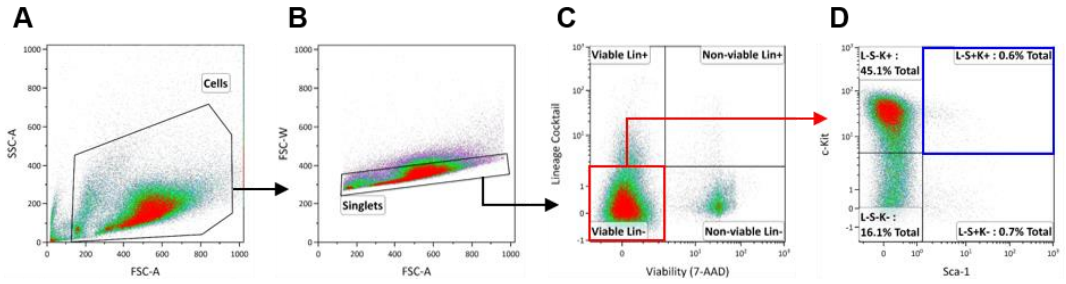

Figure 4-6 – Gating strategy for the identification of LSK^+ cells by flow cytometry. Primary mouse bone marrow cells were isolated and depleted of mature lineage positive haematopoietic cells by immune-magnetic sorting. Enriched lineage negative cells were analysed for the expression of Sca-1 and c-Kit and the absence of lineage markers. (A) Cells were identified based on forward versus side scatter area and (B) single cells by forward scatter area versus forward scatter width. (C) Logarithmic scatter plot used to gate viable lineage negative cells and (D) serial gating for Sca-1 and c-Kit antigens. Gates set against unstained controls.

Figure 4-6 confirms the presence of LSK^+ in the lineage negative fraction. Further, Figure 4-7 shows a comparison between cells of the whole bone marrow isolate against those depleted of mature haematopoietic lineages by immune-magnetic sorting. Cells were stained with 7-AAD, Sca-1 and c-Kit antibodies and a lineage marker antibody cocktail before flow cytometry analysis recording 100,000 events. Figure 4-7 B shows the success of the depletion strategy as the proportion of lineage negative cells increases from 66.7 to 92.5% whilst the number of LSK^+ cells increases by 3.4-fold to 1.2%. Additionally, the proportion of the haematopoietic progenitors defined by their phenotype of lineage negative, Sca-1^- and c-Kit^+ ($L^-S^-K^+$) also increases from 7.06% to 37.4%, an increase of 5.3-fold. The double negative for Sca-1 and c-Kit does not change whilst the Sca-1^+, c-Kit^- cells decreases in proportion by half. In summary, the depletion of lineage positive cells

from mouse bone marrow increases the concentration of haematopoietic stem and progenitors within the total cell fraction.

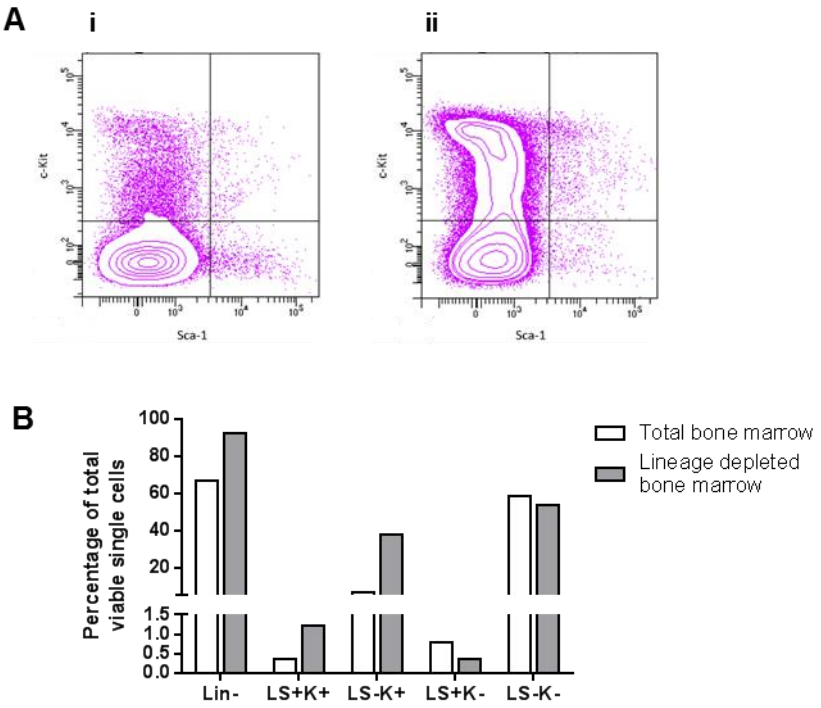

Figure 4-7 – Comparison of lineage negative, Sca-1 and c-kit populations before and after lineage depletion of bone marrow.
Mouse bone marrow cells were analysed by flow cytometry for the expression Sca-1 and c-Kit with and without the previous depletion of mature haematopoietic cells by immune-magnetic cell sorting. (A) Logarithmic scatter plots for Sca-1 and c-Kit after gating for viable lineage negative single cells, (i) total bone marrow, (ii) immuno-magnetic lineage depleted bone marrow. (B) The percentage of each population as a proportion of total viable cells. Gates set against unstained controls. 100,000 total events recorded for each sample.

4.6. Lineage negative Bone Marrow Cells Regulate Stromal Cell Fate

With the confirmation of BMSC properties of the cell line D1 ORL UVA and the ability to isolate a bone marrow fraction enriched for haematopoietic stem and progenitor cells, co-culture experiments of the two populations were set up. The objective of this series of experiments was to determine whether interaction between the adherent cell line D1 ORL UVA and primary haematopoietic stem and progenitor enriched fraction of lineage negative cells had a downstream effect on stromal cell differentiation.

Firstly, the two cells types were co-cultured with either $1x10^4$ or $1x10^5$ lineage negative cells added to 12 well plates in which D1 ORL UVA cells had been grown to 90-100% confluency. Co-cultures were cultured under control media for 3 days before media removal and the addition of differentiation inducing media.

4.6.1. Reduction in matrix production

4.6.1.1. Osteogenesis

After 3 days of co-culture followed by 21 days of osteogenic differentiation, alizarin red staining for mineralised matrix was performed to assess whether differentiation was altered by the presence of lineage negative cells. The addition of $1x10^4$ lineage negative cells showed islands where staining was absent, whilst the osteogenesis of the cell line alone led to complete staining of the wells (Figure 4-8). However, when quantified by FIJI contrast analysis no significant difference was seen. On the other hand, a 10-fold increase in lineage negative cells ($1x10^5$) led to a further reduction in the amount of mineralised matrix and resulted in a significant decrease in alizarin red staining relative to the monoculture of the D1 ORL UVA cell line.

Microscopy analysis using a 10x objective showed that these stain-free regions with a lack of calcium deposits were not devoid of cells but in fact had abundant cells growing but without surrounding calcium deposits. This indicates a lack of matrix production by the cells in these isolated areas and a reduction in osteogenesis.

4.6.1.2. Chondrogenesis

This lack of matrix production was also seen when cells were exposed to chondrogenic stimuli. After 3 days of co-culture with $1x10^5$ lineage negative cells, chondrogenic differentiation led to islands where cells did not form a 3D structure of cells pilling up (Figure 4-9 A). These observations were supported quantitatively by assessment of the production and secretion of proteoglycans in to the media as assessed by the DMMB assay (Figure 4-9 B). This assay showed a significant reduction in proteoglycans not only in the $1x10^5$ co-culture but also in the $1x10^4$ co-culture.

4.6.1.3. Adipogenesis

Whilst matrix production was significantly affected in osteogenic and chondrogenic differentiation assays by the co-culture with HSPC, the effect upon adipogenesis was not clear when assessed by oil red O staining. The images in Figure 4-10 A are representative for each condition, and alongside a further three images from three wells per condition were quantified using FIJI for the percentage of oil red O staining (Figure 4-10 B).

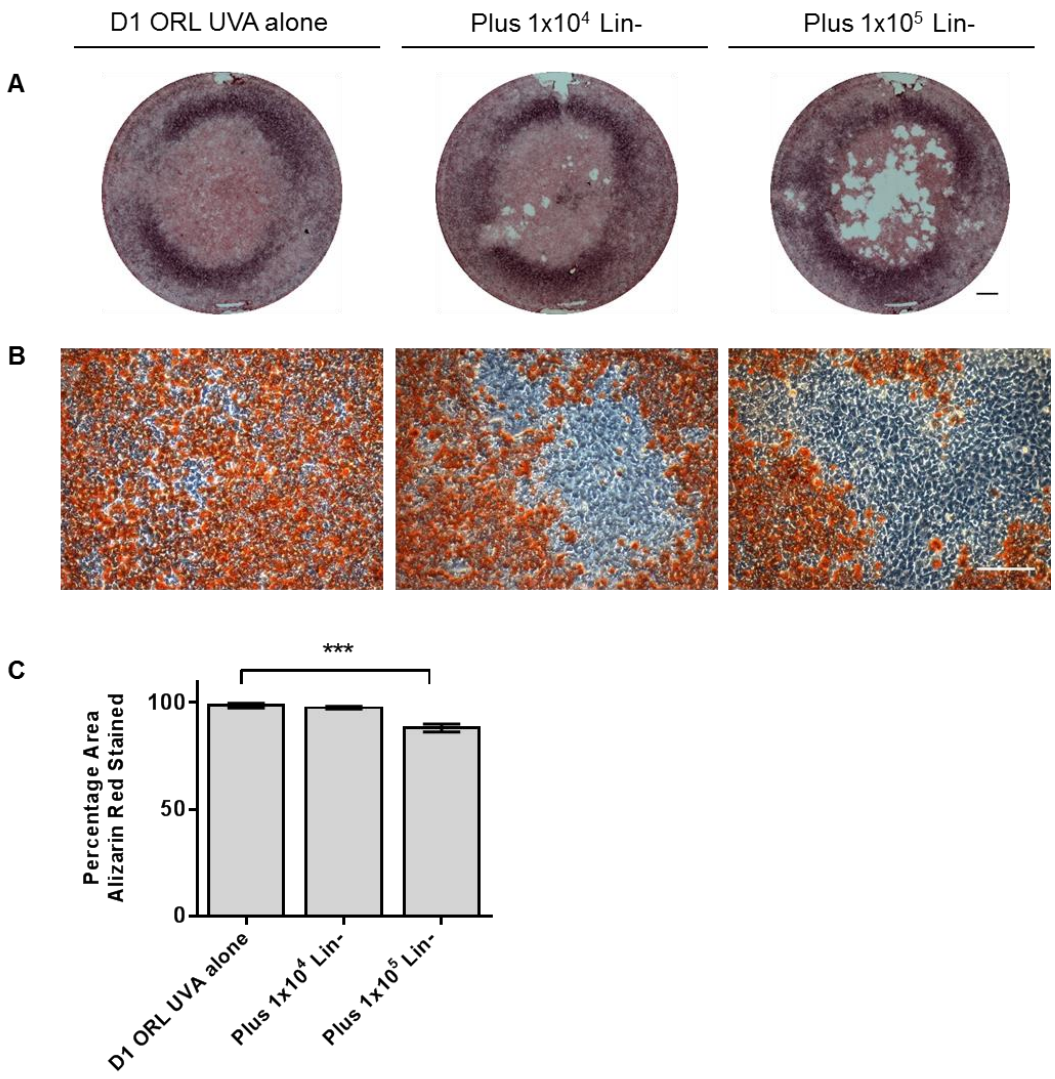

Figure 4-8 - Histological staining and quantification of osteogenic differentiation after co-culture.
D1 ORL UVA cells were grown to confluency in 12-well plates and then cultured either alone or with $1x10^4$ or $1x10^5$ bone marrow lineage negative cells (Lin-) isolated by immuno-magnetic depletion in control media. After 3 days media was replaced with osteo-inductive media. 21 days after osteogenic induction, cells were stained with alizarin red and imaged both macroscopically (A) and microscopically (B). (C) Alizarin red staining was quantified using macroscopic images (N=3). Scale bar indicates 200 µm. Statistical significance was calculated using a one-way ANOVA with Tukey's test for multiple comparisons, with *** indicating a $p<0.001$.

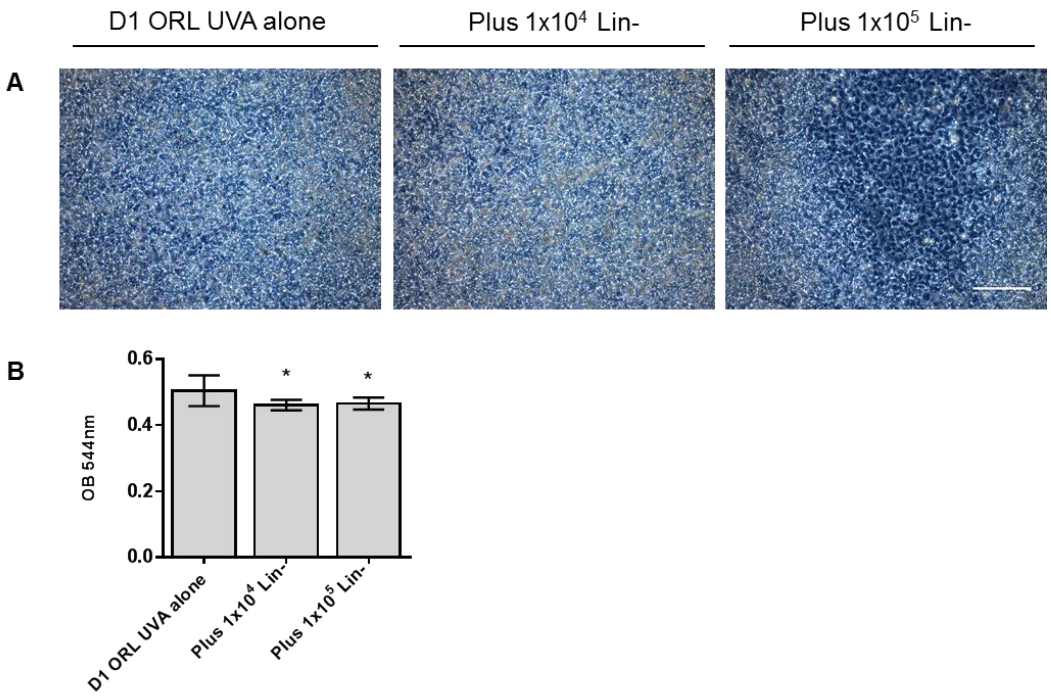

Figure 4-9 - Histological staining and quantification of chondrogenic differentiation after co-culture.
D1 ORL UVA cells were grown to confluency in 12-well plates and then cultured either alone or with $1x10^4$ or $1x10^5$ bone marrow lineage negative (Lin^-) cells isolated by immuno-magnetic depletion in control media. After 3 days media was replaced chondro-inductive media. 21 days after chondrogenic induction, cells were stained with alcian blue and imaged microscopically (A) and media removed for the analysis of proteoglycan content using the DMMB assay (B) (N=3). Scale bar indicates 200 µm. Statistical significance was calculated using a one-way ANOVA with Tukey's test for multiple comparisons, with * indicating a $p<0.1$.

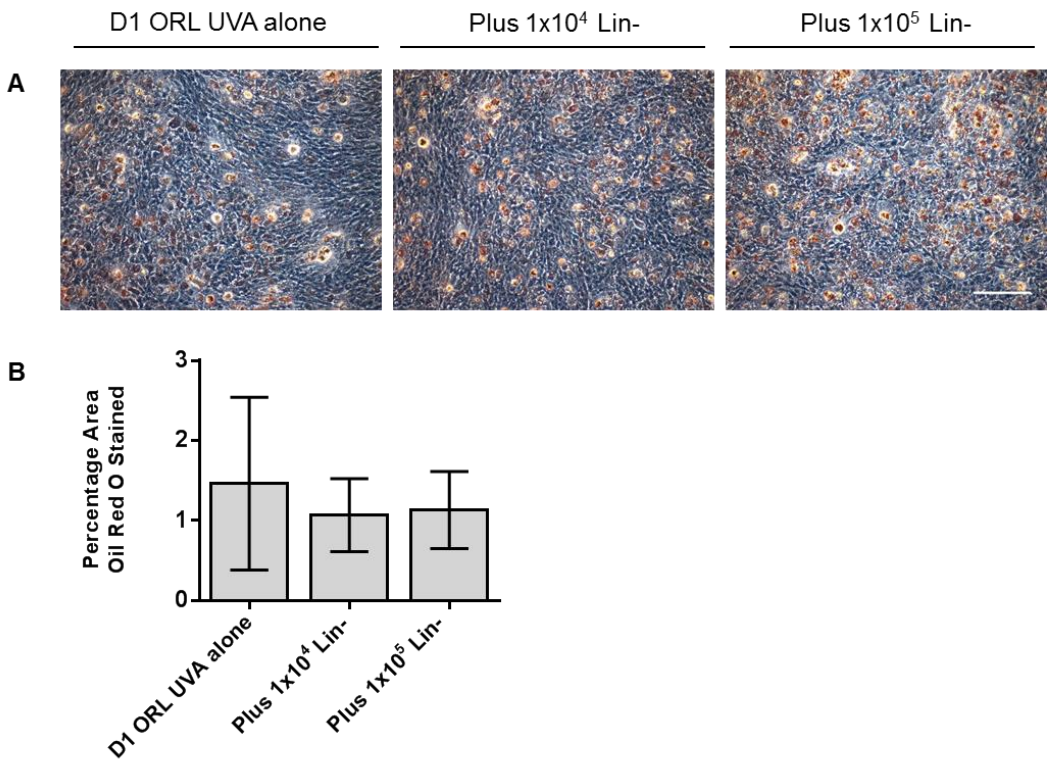

Figure 4-10 - Histological staining and quantification of adipogenic differentiation after co-culture.
D1 ORL UVA cells were grown to confluency in 12-well plates and then cultured either alone or with $1x10^4$ or $1x10^5$ bone marrow lineage negative (Lin^-) cells isolated by immuno-magnetic depletion in control media. After 3 days media was replaced chondro-inductive media. 21 days after osteogenic induction, cells were stained with alizarin red and imaged microscopically (A). (C) Oil red O staining was quantified using microscopic images (N=9). Scale bar indicates 200 µm. Statistical significance was calculated using a one-way ANOVA, no significance.

4.6.2. Change in gene expression at 7 days

As matrix production was seen to be altered in both osteogenesis and chondrogenesis matrix assays when using $1x10^5$ lineage negative cells, gene expression studies were used to support these findings. Rather than allowing differentiation to continue to 21 days, as for matrix assessment, RNA was harvested at 7 days after initiating differentiation of the co-culture. This time point was chosen based on the results from earlier studies (Figure 4-3) where the expression of differentiation genes was induced.

In support of the histological staining results at 21 days, qRT-PCR at 7 days showed no significant change in the expression of adipogenic genes between the two groups (Figure 4-11 C) whilst all osteogenic genes tested decreased (Figure 4-11 B). Chondrogenic gene expression showed a decrease in the transcription factor *Sox9* and the chondrogenic promoting growth factor *Tgfβ*. Type II collagen (*Col2a*), on the other hand was increased by nearly 4-fold (Figure 4-11 C).

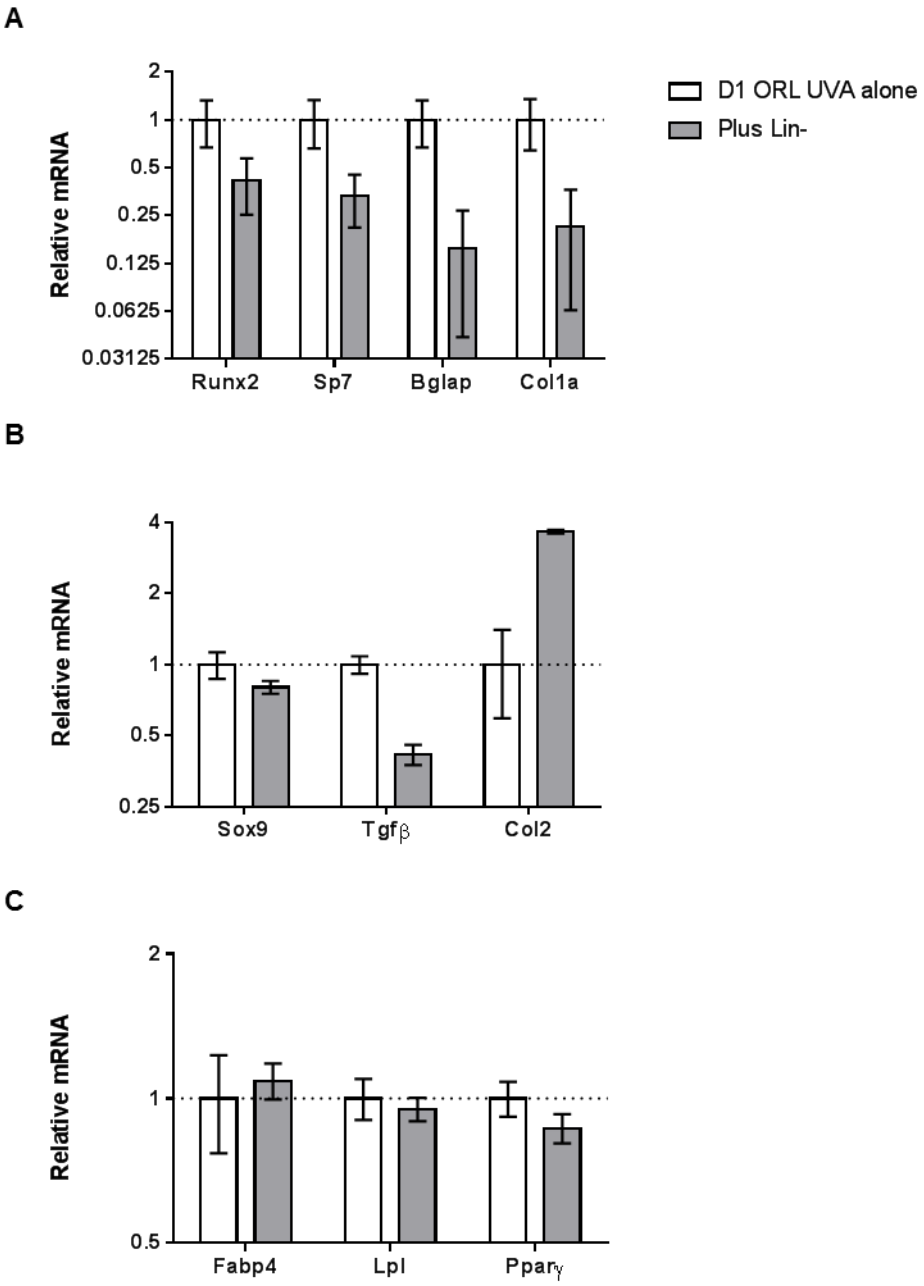

Figure 4-11 - Gene expression analysis of D1 ORL UVA tri-lineage differentiation after co-culture

D1 ORL UVA cells were grown to confluency in 12-well plates and then cultured either alone or with $1x10^4$ or $1x10^5$ bone marrow lineage negative cells isolated by immuno-magnetic depletion in control media. After 3 days media was replaced differentiation inductive media - osteogenic (A), chondrogenic (B) or adipogenic (C). After 7 days in differentiation media cells were harvested and analysed for genes specific for each pathway. Bars indicate the expression of mRNA for each gene normalised to *Hprt*. Error bars indicate the standard deviation of the mean for technical replicates for qRT-PCR run in triplicate (N=1).

4.7. Lineage negative cells integrate into the stromal monolayer and are maintained for 7 days

With the assumption that direct cell-to-cell contact was required for the decrease in D1 ORL UVA osteogenic differentiation after co-culture, confocal microscopy was performed to explore the dynamics of the lineage negative bone marrow cells interaction with the cell line. For this experiment, the haematopoietic fraction was isolated by immune-magnetic depletion from mice expressing GFP under the ubiquitin promoter. The primary cells isolated therefore expressed GFP (Schaefer et al., 2001).

After 3 days of co-culture, cells were fixed and stained with phalloidin, to visualise the actin filaments of the cytoskeleton, and DAPI before confocal imaging. Z-stack projection (Figure 4-12) shows localisation of the GFP positive lineage negative bone marrow cells at both the surface of the D1 ORL UVA stromal layer and beneath. This demonstrates that the two cell populations have a strong interaction with the haematopoietic population incorporating into and beneath the D1 ORL UVA cell layer.

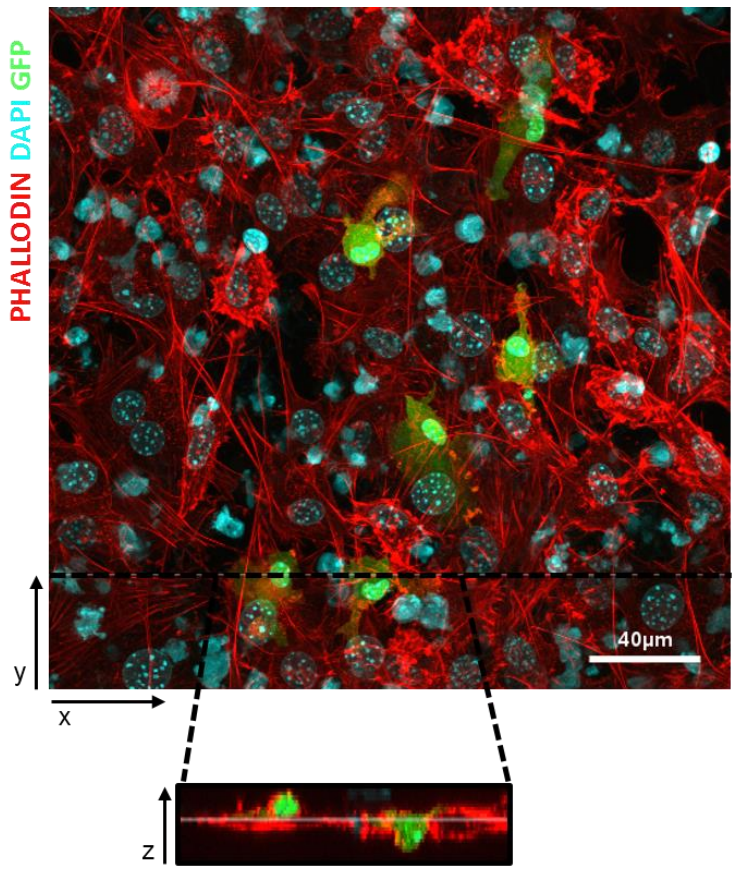

Figure 4-12 – Interaction of bone marrow lineage negative cells and D1 ORL UVA monolayer.
D1 ORL UVA cells were grown to confluency in 0.7 mm^2 wells of glass slide chambers. Bone marrow lineage negative cells isolated by immuno-magnetic depletion from ubiquitin-GFP reported mice were added to the wells in control media. After 3 days media was removed and the cells fixed and imaged by confocal microscopy (A) (63x objective). Actin filaments, red; nucleus, blue; bone marrow lineage negative cells, green. Scale bar indicates 40 µm.

Gene expression analysis at 3 days showed that the cells interacting with the monolayer were haematopoietic lineage cells (Figure 4-13). The expression of *Ptprc* (CD45 protein), a classical marker of haematopoietic cells, and *Cfsr3* (G-CSF receptor) were over 100 times greater in co-cultures than the stromal D1 ORL UVA cells alone. The expression of these genes remained significantly higher than monocultures at 7 days indicating the haematopoietic cells were maintained in the co-culture. Interestingly, genes specific to haematopoietic progenitors, *Flt3* and *Hck* decreased between 3 days and 7 days suggesting a loss of progenitor phenotype.

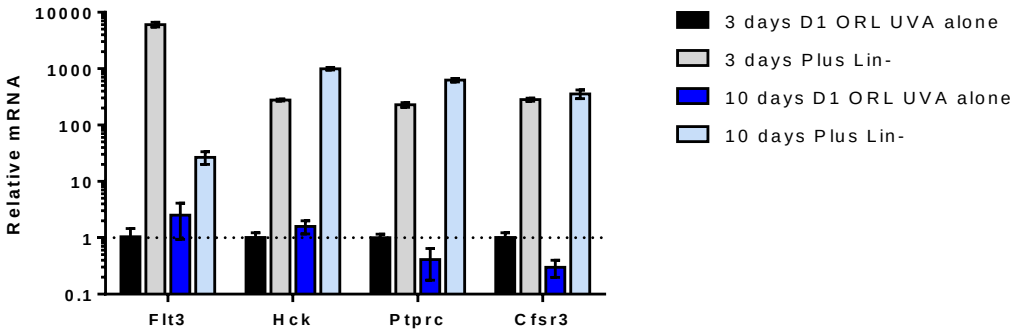

Figure 4-13 – Haematopoietic gene analysis after co-culture.
D1 ORL UVA cells were grown to confluency in 12-well plates and then cultured in control media either alone or with $1x10^5$ bone marrow lineage negative (Lin^-) cells isolated by immuno-magnetic depletion. After 3 days cells were either harvested or media was replaced with fresh control media. After a further 7 days cells were harvested from the remaining wells. All harvested cells were analysed for the expression of haematopoietic genes. Bars indicate the expression of mRNA for each gene normalised to *Hprt*. Error bars indicate the standard deviation of the mean for technical replicates for qRT-PCR run in triplicate (N=1).

4.8. Altered levels of osteogenic gene expression in D1 ORL UVA cells following co-culture with lineage negative cells

Due to the continued presence of lineage negative derived cells at 10 days of co-culture, an assessment was made to determine their specific influence on D1 ORL UVA expression of genes representing osteogenic differentiation. To perform these studies, GFP lineage negative cells from GFP ubiquitin promoter mice were used. After co-culture for 3 days followed by 7 days of osteogenic differentiation, the cells were detached by trypsinisation and separated by fluorescence activated cell sorting. This removed GFP expressing cells and allowed isolation of the GFP negative D1 ORL UVA cells only.

Phase contrast microscopy merged with fluorescent imaging of the GFP channel (Figure 4-14 A), illustrates the presence of GFP cells in the co-culture after 7 days of osteogenic induction. Flow cytometry plots show that as expected in the D1 ORL UVA only culture no GFP cells were detected, whereas in the co-culture, 5.2% of the total cells were GFP positive (Figure 4-14).

Gene expression analysis of unsorted co-cultures showed a decrease in the expression of osteogenic genes, by approximately half, as previously demonstrated in Figure 4-11 (although on this occasion no change in *Runx2* transcript levels were observed). This difference was maintained in GFP- D1 ORL UVA cells isolated by FACS where GFP+ haematopoietic cells had been removed. This confirms that the analysis of osteogenic gene expression in these co-cultures is not skewed by the presence of haematopoietic cell RNA.

4.9. Haematopoietic progenitor fraction ($Lin^-Sca1^-cKit^+$) is predominantly responsible for the reduction in D1 ORL UVA osteogenesis

Having demonstrated that primary lineage negative bone marrow cells reduce the osteogenesis of the stromal cell line D1 ORL UVA, the next step was to investigate which cells of the lineage negative fraction were exerting this effect.

Firstly, the lineage negative population was divided in two based on Sca-1 and c-Kit expression. Figure 4-15 A shows the serial gating strategy used to isolate single viable lineage negative cells and the selection of cells positive for both Sca-1 and c-Kit (LSK^+ fraction). The remaining cells, gated as single viable lineage negative cells, were also collected and named the LSK^- fraction. As previously described for other experiments, these cells were added to confluent layers of D1 ORL UVA cells and cultured for 3 days after which osteogenic induction media was added. However, a limited number of LSK^+ cells were isolated and numbers equivalent to those of lineage negative and LSK^- populations were not available ($1x10^5$/well). Therefore $1x10^3$ LSK^+ cells were added per well.

At 7 days, cells were harvested for mRNA gene expression analysis. In Figure 4-15 the expression of two osteogenic genes, *Bglap* and *Sp7*, is shown for multiple replicates of this experiment. As seen previously the expression of both genes was reduced in all replicates for the co-culture of lineage negative cells with D1 ORL UVA cells (Figure 4-15 B), although this was not significant across all experimental replicates. This trend however was maintained for the co-culture with the LSK^- FACS isolated fraction. The LSK^+ fraction, on the other hand, led to variable results for both genes.

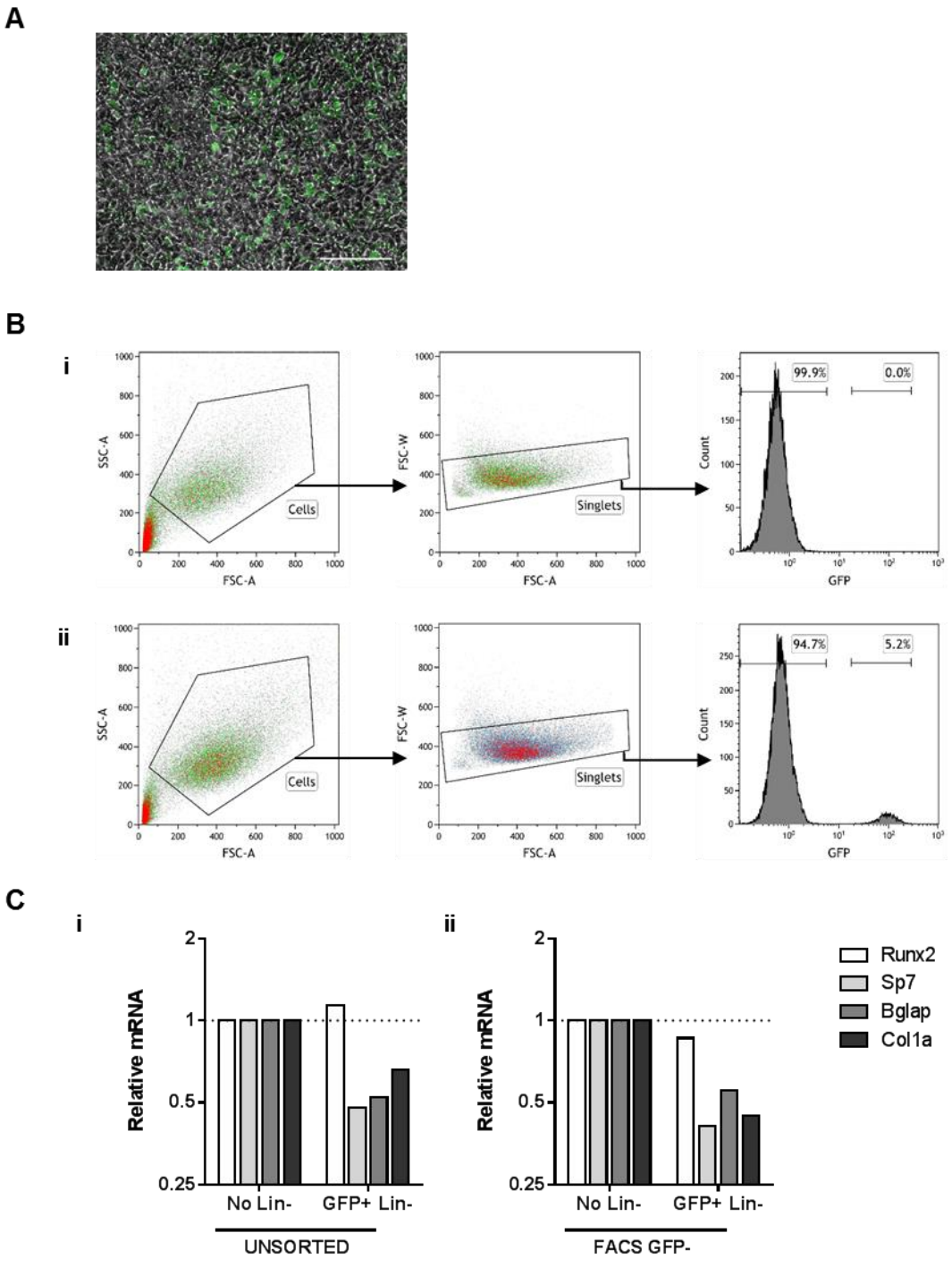

Figure 4-14 - Isolation by FACS and gene expression analysis of D1 ORL UVA GFP$^-$ cells after co-culture.

D1 ORL UVA cells were grown to confluency in 12-well plates. Bone marrow lineage negative (Lin$^-$) cells isolated by immuno-magnetic depletion from ubiquitin-GFP reported mice were added to the wells in control media. After 3 days media was replaced with osteo-inductive media for 7 days and then imaged. (A) Phase contrast with GFP overlay of co-culture. (B) For three wells per condition cells were detached by typsinisation, combined and sorted by FACS for GFP negative cells, (i) D1 ORL UVA alone, (ii) co-culture. Cells were identified based on forward versus side scatter area and then gated for single cells by forward scatter area versus forward scatter width. (C) Subsequently, GFP negative cells were gated and isolated for osteogenic gene expression analysis (i). Gene expression analysis was also conducted for unsorted cultures where RNA was isolated directly from the wells including lineage negative cells (ii). Bars indicate the expression of mRNA for each gene normalised to *Hprt*. (N=1).

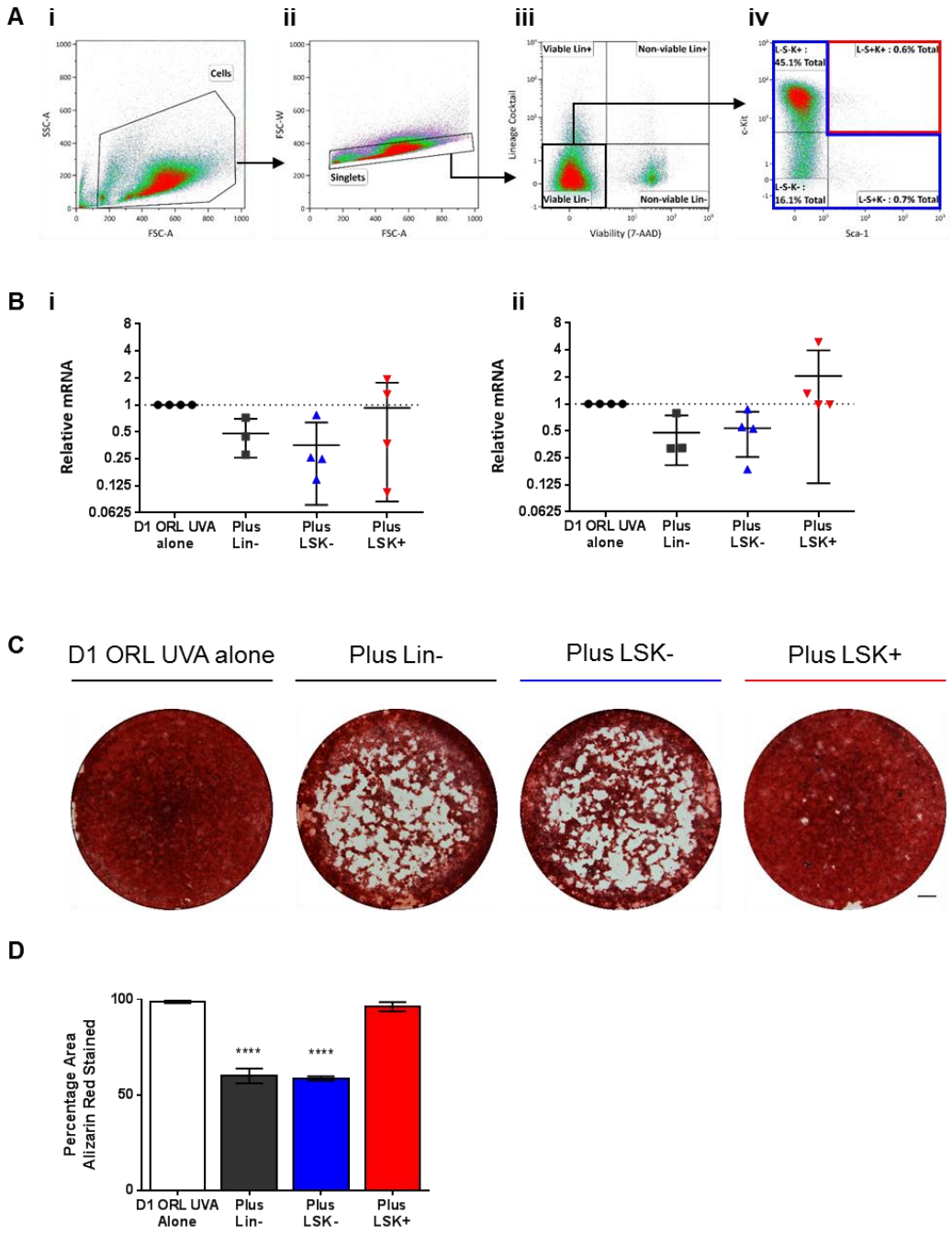

Figure 4-15 –Osteogenic differentiation of D1 ORL UVA after co-culture with lineage negative subpopulations.

Primary mouse bone marrow cells were isolated and depleted of mature lineage positive haematopoietic cells by immune-magnetic sorting. Enriched lineage negative cells were used directly or sub-divided into subpopulations by FACS based on the expression of Sca-1 and c-Kit (A). (i) Cells were identified based on forward versus side scatter area and (ii) single cells by forward scatter area versus forward scatter width. (iii) Logarithmic scatter plot used to gate viable lineage negative cells and (iv) serial gating for Sca-1 and c-Kit antigens. Viable lineage negative cells were sorted into two populations - cells positive for Sca-1 and c-Kit (LSK^+) and those lineage negative cells remaining. Gates set against unstained controls. The primary cell populations were added to D1 ORL UVA cells grown to confluency in 12-well plates. After 3 days media was replaced with osteo-inductive media. After 7 days in differentiation media, cells were harvested and analysed for the expression of two osteogenic genes (B) (i) *Bglap* and (ii) *Sp7*. Bars indicate the expression of mRNA for each gene normalised to *Hprt*. Error bars indicate the standard deviation of the mean for biological replicates across 4 experiments (N=9 or 12). No

significance difference calculated using a one-way ANOVA. In other replicate wells, after 21 days osteo-induction, cells were stained with alizarin red and imaged macroscopically (C). (D) Alizarin red staining was quantified using macroscopic images (N=3, single experiment). Statistical significance was calculated using a one-way ANOVA with a Dunnett test for multiple comparisons, **** p<0.0001. Scale bar indicates 200 µm.

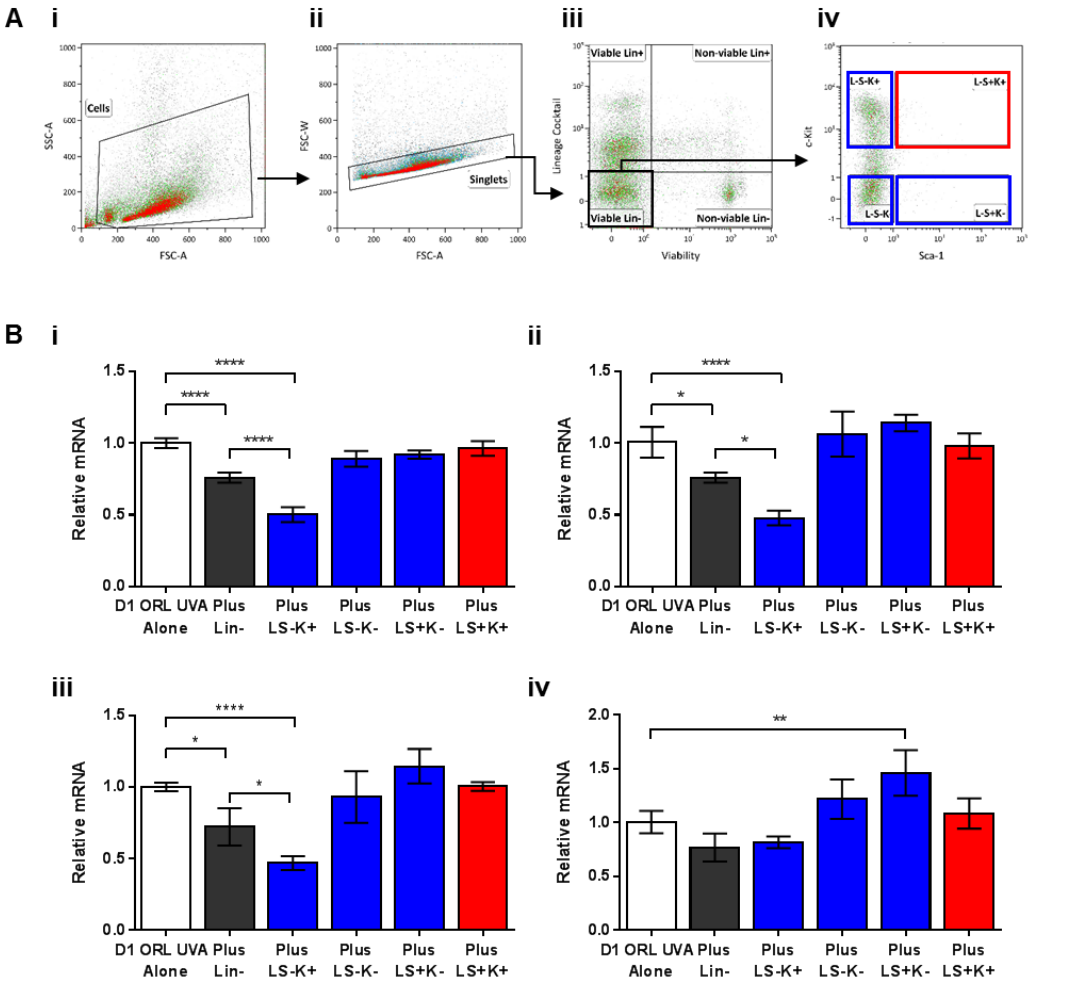

Figure 4-16 - Osteogenic differentiation of D1 ORL UVA after co-culture with lineage negative subpopulations.

Primary mouse bone marrow cells were isolated and depleted of mature lineage positive haematopoietic cells by immune-magnetic sorting. Enriched lineage negative cells were used directly or sub-divided into subpopulations by FACS based on the expression of Sca-1 and c-Kit (A). (i) Cells were identified based on forward versus side scatter area and (ii) single cells by forward scatter area versus forward scatter width. (iii) Logarithmic scatter plot used to gate viable lineage negative cells and (iv) serial gating for Sca-1 and c-Kit antigens. Viable lineage negative cells were sorted into four populations 1. Sca-1$^-$ and c-Kit$^+$ (LS$^-$K$^+$), 2. Sca-1$^-$ and c-Kit$^-$ (LS$^-$K$^-$), 3. Sca-1$^+$ and c-Kit$^-$ (LS$^+$K$^-$) and 4. Sca-1$^+$ and c-Kit$^+$ (LS$^+$K$^+$). Gates set against unstained controls. The primary cell populations were added to D1 ORL UVA cells grown to confluency in 12-well plates. After 3 days media was replaced with osteo-inductive media. After 7 days in differentiation media, cells were harvested and analysed for the expression of osteogenic genes (B). (i) *Runx2*, (ii) *Bglap*, (iii) *Sp7* and (iv) *Col1a*. Bars indicate the expression of mRNA for each gene normalised to *Hprt*. Error bars indicate the standard deviation of the mean for biological replicates of a single experiment (N=3). Statistical significance was calculated using a one-way ANOVA with Tukey's test for multiple comparisons **** p<0.0001, ** p<0.01 and * p<0.1.

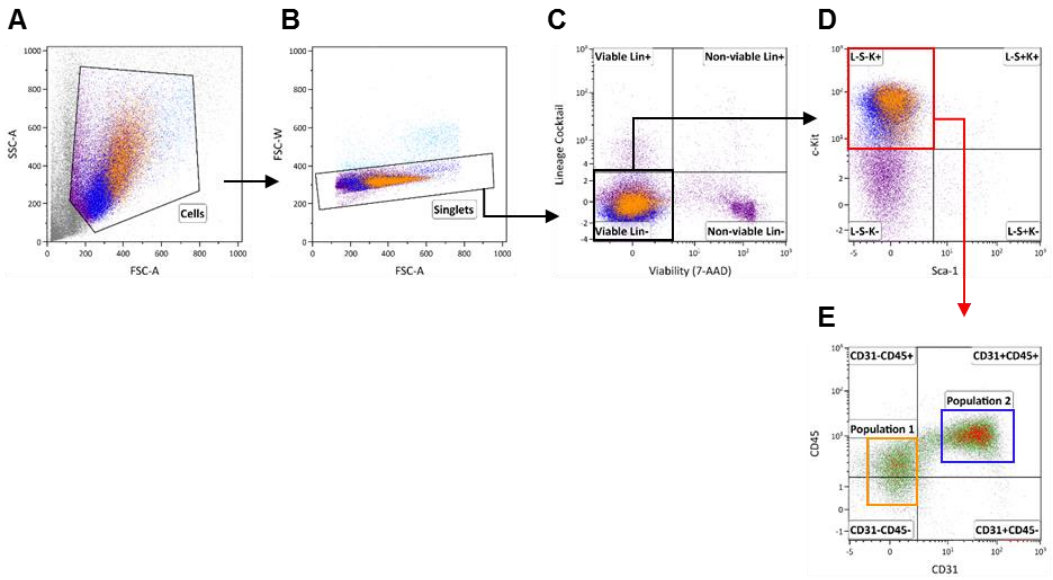

Figure 4-17 – CD45 and CD31 analysis of LS-K$^+$ cells by flow cytometry.
Primary mouse bone marrow cells were isolated and depleted of mature lineage positive haematopoietic cells by immune-magnetic sorting. (A) Cells were identified based on forward versus side scatter area and (B) single cells by forward scatter area versus forward scatter width. (C) Logarithmic scatter plot used to gate viable lineage negative cells and (D) serial gating for Sca-1 and c-Kit antigens. Cells determined to be Sca-1$^-$ and c-Kit$^+$ were analysed for the expression of CD45 and CD31 on a logarithmic scatter plot.

With the potential to reduce D1 ORL UVA osteogenesis predominantly ascribed to the LSK- fraction, this population was further sub-divided as illustrated in the quadrants of the Sca-1 c-Kit flow cytometry plot (Figure 4-16 A iv). The cells were co-cultured as previously described and analysed for osteogenic gene expression. Results for the total lineage negative fraction were consistent with preceding experiments, demonstrating significance, except for *Col1a*. Interesting the only fraction that maintained the reduction in gene expression was the Sca-1 negative, c-Kit positive (LS$^-$K$^+$) fraction of the lineage negative cells. The other two fractions had equivalent transcript levels to D1 ORL UVA cells alone. Furthermore, for the genes *Runx2*, *Bglap* and *Sp7*, the expression was significantly lower than that for the total lineage negative fraction. Noteworthy, *Col1a* did not show a decreased expression in any of the conditions but did increase in co-cultures with the lineage negative, Sca-1, c-Kit negative (LS$^+$K$^-$) cells

4.9.1. The LS$^-$K$^+$ cell fraction contains CD45^{high}CD31$^+$ and CD45^{low}CD31$^-$ subpopulations

To identify what cell types the LS-K$^+$ fraction contains, the cells were additionally stained for CD45 and CD31. In Figure 4-17 E, flow cytometry showed that there were two sub-populations within this fraction, most clearly separated by their expression for CD31. CD45 expression was also different between the two populations with Population 1 having a slightly lower abundance of this antigen relative to Population 2.

4.10. Discussion

The aim of this chapter was to investigate the direct influence of haematopoietic stem and progenitor cells (HSPCs) on the differentiation of bone marrow stem/stromal cells (BMSCs). BMSCs are a key cell type widely studied within the field of musculoskeletal science due to their ability to differentiate into the mesenchymal lineages of bone, cartilage and adipose tissue, as well as a having a trophic role influencing other cell types in the surrounding microenvironment. The BMSC population is thought of as a heterogeneous population within which individual cells have different phenotypes with some cells exhibiting different levels of commitment to particular cell lineages. The ability to drive endogenous BMSC *in vivo* to a particular phenotype could be of benefit in a clinical setting. As HSPC numbers increase after G-CSF treatment, understanding the impact of the interaction between HSPCs and BMSCs in the haematopoietic niche will provide mechanistic insight into the use of G-CSF in skeletal repair strategies.

4.10.1. In vitro co-culture as a model of the BM niche

Monolayers of feeder cells have been used for many years as a method to maintain the multi-potency of HSCs *in vitro* (Dexter, Allen and Lajtha, 1977). By mimicking some of the interplay that occurs *in vivo*, these cultures have allowed researchers to study the role of the microenvironment in controlling the fate of HSCs. Commonly cell lines have been used as the feeder cells and have often been grown out from adherent bone marrow cells. Whilst mostly not defined more specifically than this, these cells are likely to be BMSCs by their most simple definition of plastic adherent bone marrow cells.

In this chapter, the BALB/c mouse bone marrow derived stromal cell line D1 ORL UVA was used to model mouse BMSC activity. To support the use of this cell line the cells were first characterised to confirm their tri-lineage differentiation capability and phenotypic profile of the population. As with human BMSCs, a single marker for mouse BMSCs has not been identified but several markers have been described in the literature (Morikawa et al., 2009; Zhou et al., 2014; Méndez-Ferrer et al., 2010). By using a panel of markers, data presented here shows that the D1 ORL UVA cell line expresses markers such as CD73 and CD44, and lacks haematopoietic markers, supporting previous phenotypic analysis of the cell line (Mussano et al., 2010). It is important to note than unlike primary BMSCs that represent the diversity of BMSC phenotypes, this cell line is likely to represent only an isolated phenotype and therefore a discrete/distinct population of BMSCs. In ideal circumstances primary BMSCs would have been used, however, attempts to reproducibly isolate sufficient numbers of phenotypically similar cell populations were unsuccessful. Further experiments to support the observations made in this chapter could be performed using primary murine cultures, but perhaps more relevantly could be performed using human derived cell populations.

HSPCs and BMSCs reside in close physical association in the bone marrow, making direct co-cultures an important tool in mimicking cell-to-cell niche dynamics and according direct cell-to-cell culture were used here. To begin this series of experiments, the lineage negative fraction of bone marrow enriched for HSPCs was added to the D1 ORL UVA stromal cell line and strong interactions between the two cells populations formed as lineage negative cells integrated into the stromal cell layer. Jing and colleagues (2010) observed similar *in vitro* dynamics between human BMSCs and HSPCs in direct cultures. The authors investigated further and found that BMSCs could act as a physical boundary between distinct compartments of HSPCs – progenitors that are more quiescent were found to migrate below the MSC monolayer, forming a three-dimensional microenvironment (Jing et al., 2010). This supports the conclusion that the co-culture model used in the studies presented here likely represents interactions present in the *in vivo* bone marrow niche.

4.10.2. HSPC enriched fraction reduces osteogenic differentiation

The *in vitro* co-culture model was used first to evaluate the effect of co-culture on the differentiation of the stromal cell line down osteogenic, chondrogenic and adipogenic pathways. Adipogenic differentiation of the stromal cell line was unaffected by co-culture whilst both osteogenic and chondrogenic differentiation were seen to be reduced.

Osteogenic differentiation was assessed by studying early gene expression levels at 7 days after induction of differentiation and matrix deposition of calcium as a late marker of osteoblastic extracellular matrix mineralisation. Since cell populations were not separated following co-culture, gene expression was assessed in RNA isolated from all cells in the co-culture system raising the possibility of lineage negative cell transcripts influencing observations of the stromal cell lines differentiation. *Runx2*, for example, is a gene upregulated early in osteogenic differentiation (Xu et al., 2015) but is also expressed by HSPCs (de Bruijn and Dzierzak, 2017). To try to decipher the contribution of lineage negative cells to the gene expression profile, separation of the two population was performed by FACS prior to analysis. Whilst HPSCs will have contributed to the transcript levels of the housekeeping genes used for normalisation, the evaluation conducted demonstrated that their impact upon relative osteogenic gene transcript levels was minimal. Consequently, further evaluations were made based on total co-culture transcripts.

Through further enrichment steps, the population within the lineage negative bone marrow fraction determined to be responsible for the decreased osteogenesis potential of co-cultures was the lineage negative, Sca-1 negative, c-Kit positive fraction. This phenotype is known to be that of HPCs including multipotent progenitors and common myeloid progenitors that express high levels of c-Kit whilst having low expression of the cell surface the antigen Sca-1. In the C57BL/6 strain of mice the expression of Sca-1 can

differentiate between HSCs and HPCs, unfortunately however, the use of bone marrow fractions derived from BALB/c mice here prevents differentiation between these two populations.

The BALB/c mouse strain was chosen in order to maintain strain species between the two cell populations, as the D1 ORL UVA cell line was original derived from this strain. Unfortunately, the identification of HSCs from Balb/c mice based on LSK^+ expression is not regarded as very effective, as this strain has a lack of Sca-1 expression (Spangrude and Brooks., 1993). This provides an explanation as to why a limited number of LSK^+ cells (HSCs) were isolated from these mice leading to an inability to add equivalent numbers of LSK^+ cells to co-cultures relative to the other populations studied. For this reason the specific effect of HSCs alone on the culture system was not assessed comparably with the other lineage negative fractions and furthermore HSCs were likely to have been sorted into the LS^-K^+ fraction. Therefore, whilst it can be concluded that the HSPC population reduced the subsequent osteogenesis of the stromal cell line, it is not possible to distinguish between the influence of HSCs or HPCs within the HSPC enriched fraction.

Other published studies have used the C57BL/6 strain as a source of LSK^+ and observed a different response after co-culture. Liao et al. (2011) conducted direct co-cultures of LSK populations with primary mouse BMSCs that were pre-conditioned with dexamethasone prior to establishment of co-cultures. The authors' results demonstrated that the addition of LSK^+ cells led to enhanced calcium deposition whereas removal of dexamethasone from the co-culture reduced deposition (Liao et al., 2011). Significantly, the areas where deposition was reduced were where HSPCs were localised, correlating with the data gathered in the work presented here. This data suggests that the interplay between BMSCs and HSPCs in driving BMSC osteogenesis is influenced by the strength of the osteogenic cues. Moreover, a more osteogenic (endosteal-like) niche is generated under culture with dexamethasone. In addition to the strong pro-osteogenic effects of this steroid, it can also act upon HSPCs directly and increase the quiescence of haematopoietic stem cells (Kim et al., 2008). Through this action dexamethasone might drive enhance osteogenesis to BMSC culture alone.

Overall, these observations indicate that the dynamics of the bone marrow niche are complex and that BMSCs and HSPCs have a reciprocal relationship in regulating one another. Additionally, they suggest that BMSC osteogenic differentiation is dependent on both HSPC numbers and osteogenic cues which are likely relevant to G-CSF and bone inducing regenerative therapies.

4.10.3. HSPCs promote and maintain a supporting stromal cell niche

Commonly in musculoskeletal research, the aim is to improve the differentiation potential of BMSCs, for example by adding pro-osteogenic scaffolds (Perez et al., 2018). In

contrast, in these studies HSPCs reduced the deposition of calcium by BMSCs in co-culture. Interestingly, both BMSCs and osteoblasts are known to be key components of the bone marrow niche and therefore the promotion of either phenotype by HSPCs may indicate the potential for dynamic modulation of the niche environment by these haematopoietic cells.

The relationship between HSPCs and BMSCs is believed to be dependent on *in vivo* location within the bone marrow niche, for example the endosteal or vascular regions. As discussed, the co-cultures established here are likely to include higher numbers of HPCs relative to HSCs. The endosteal niche, where osteoblasts are the key cell type, is thought to maintain the quiescence of more primitive HSCs (Lambertsen and Weiss, 1984). The vascular niche, on the other hand, is thought to maintain more mature progenitors, being closer to the vasculature where HPCs are poised to enter the blood stream (Bianco, 2011). BMSCs are considered part of the vascular niche. One might therefore hypothesise that the high numbers of HPCs in the co-culture may lead to the preferential maintenance of BMSCs that make up their vascular stromal compartment rather than promote their differentiation.

Additionally, the experiments conducted in this chapter were performed under normoxic conditions. Although the bone marrow as a whole is considered a hypoxic environment relative to general systemic oxygen levels, within the niche itself there is an oxygen gradient (Parmar et al., 2007). The reduced vasculature of the endosteal niche makes this environment more hypoxic. In the future, it would be worthwhile to assess the effect of oxygen tension on the differentiation of the co-culture. If the decrease in osteogenic differentiation is due to HPSCs and the maintenance of BMSCs in a vascular niche-like culture system, perhaps under hypoxia a more endosteal niche would develop with increased osteogenic differentiation.

4.10.4. Are the trophic/immunomodulatory roles of BMSCs influenced by HSPCs?

Importantly, data collected in the current study demonstrates that $LS^{-}K^{+}$ cells influence stromal cells with BMSC properties. Whilst differentiation has been focused on in this work, the multiple actions of BMSCs mean that other BMSC properties should also be considered e.g. immunomodulatory potential. If interactions between these HSPCs and BMSCs alter the secretome of BMSCs, this may have consequences if BMSCs encounter inflammation or trauma in their surrounding environment. The immunomodulatory ability of the D1 ORL UVA cell line has not been evaluated here nor in published literature, and may worth investigation.

4.10.5. G-CSF and the model

The bone marrow niche is a complex multi-cell environment whereas this co-culture model represents a simplistic version of *in vivo* conditions. Whilst G-CSF treatment of patients increases the number of HSPCs, and other haematopoietic cells, this is only one way G-CSF might affect the activity of BMSC during tissue repair events. This cytokine is seen to cause changes in numerous cell types, from osteoblasts to mature haematopoietic cells, within the bone marrow altering the biology of this complex microenvironment.

To begin to establish the influence of G-CSF within this environment the cytokine could be added to the co-culture model and experimental assessments made as conducted here to understand the cytokines influence on the cross talk between the cell populations. In addition to increasing the number of HSPCs in the bone marrow, G-CSF also alters the transcription profile of these cells (Schuettpelz et al., 2014). When administered *in vivo*, G-CSF can be considered to lead to haematopoietic stress inducing sudden changes in the haematopoietic system.

Jung et al. (2008) isolated HSCs from animals that were haematopoietically stressed either by bleeding to remove 20 to 30% of their blood volume or 5-fluorouracil treatment (another HSC mobilising agent, which is also used as a chemotherapeutic drug). The authors present data showing that in transwell culture HSCs isolated from haematopoietic stressed mice increase osteogenesis of BMSCs through the production of bone morphogenetic proteins (BMP-2 and BMP-6) (Jung et al., 2008). Investigation in to whether G-CSF causes similar changes in HSCs or HSPC populations could add insight into the effect of G-CSF on BMSC function. Furthermore, surgical procedures, such as those used in orthopaedic procedures, that lead to blood loss may additionally exacerbate these effects.

4.10.6. Future directions

Future work could attempt to unpick the cell type responsible for the decrease in osteogenesis of D1 ORL UVA cells. As discussed, the first objective could be to determine whether HSCs or HPCs are responsible but this would require the use of an alternative strain of mice for haematopoietic cell isolation rather than BALB/c mice in order to recover cells based on Sca-1 expression. Additionally, the final experiment conducted in this series of work demonstrated that the lineage negative, Sca-1 negative, c-Kit positive fraction contained two populations identifiable by differences in the expression of CD31 and CD45. CD31 or Platelet Endothelial Cell Adhesion Molecule-1 is commonly used to identify endothelial cells but these cells are negative for CD45. To a lesser extent, CD31 is expressed on myeloid progenitors (Bronte et al., 2000) which as discussed have the $L^-S^-K^+$ phenotype. Initially, the two populations based on CD31 and CD45 of $L^-S^-K^+$ cells

could be evaluated but to define a specific population such as myeloid progenitors a specific isolation strategy would be required such as $CD11b^{+}/Gr\text{-}1^{+}/CD31^{+}$.

Another line of development could be the translation of this model with the use of human derived cells. Initial attempts for this were made here (data not shown) by isolation BMSCs and $CD34^{+}CD38^{-}$ HSCs from human bone marrow. Constraints to the use of this model were a lack of HSC numbers. Perhaps other sources of HSCs could be useful in developing a human model system such as using umbilical cord derived or apheresis product $CD34^{+}CD38^{-}$ cells. The advantage of using primary BMSCs human cells would allow the analysis of different differentiation pathways and immunomodulatory effects of HSCs on the stromal bone marrow component using techniques already established within the laboratory.

Finally, as previously mentioned analysis of the effect of G-CSF on bone marrow niche dynamics may provide insight into the effect of G-CSF upon this microenvironment and whether it primes BMSCs to a particular lineage prior to their exposure to differentiation stimuli.

4.10.7. Summary

This work has identified that HSPCs and BMSCs have a dynamic reciprocal relationship, which influences the differentiation potential of stromal cells when exposed to osteogenic stimulating cues. The influence of G-CSF on these interactions remains to be explored. However, purely on the basis that HSPCs increase in the bone marrow after G-CSF administration, one could hypothesise that osteogenic differentiation is suppressed. If trauma is induced at this time, where osteogenesis is required for repair, it may occur at a lower rate, though cessation of G-CSF treatment has further consequences (see chapter 6 and section 6.6.3). Importantly, it is recognised that the *in vivo* bone marrow niche is a complex microenvironment and G-CSF will have effects on other cells and interactions within the bone marrow, making this perhaps a simplistic view.

5. RESULTS: OSTEOCHONDRAL DEFECT MODEL IN C57BL/6 MICE ILLUSTRATES TEMPORAL AND SPATIAL CELL DYNAMICS DURING REPAIR

5.1. Background and Rationale

Traumatic articular cartilage injuries in adult patients are reported to have limited capacity to repair and consequently predispose affected joints to further cartilage degeneration and increased likelihood of osteoarthritis (OA) (Punzi et al., 2016). Treatments for these defects are limited and commonly patients are required to wait for significant OA progression to warrant surgical intervention such as total joint replacement. Intervening earlier, with treatments such as microfracture and autologous chondrocyte implantation (ACI), has the potential to hinder or halt the progression of joint degeneration as well as treating the acute problem. Unfortunately, the outcomes of these techniques are variable (Fellows et al., 2016).

Whilst articular cartilage is reported to have limited repair potential, spontaneous healing has been described in humans as well as animal models. Importantly, spontaneous healing is particularly associated with full-thickness cartilage defects that penetrate the subchondral bone over cartilage only defects (Lydon, Getgood and Henson, 2017; Dell'accio and Vincent, 2010). This is hypothesised to be due to the access of a full-thickness lesion to the bone marrow below the subchondral bone plate, which contains multiple stem and progenitor cell types. Recapitulation of this using the microfracture technique in human patients has positive outcomes but often leads to the formation of fibrocartilage lacking the properties of the original hyaline cartilage (Caldwell and Wang, 2015). By elucidating the cartilage repair process and understanding the molecular and cellular mechanisms leading to repair tissue, therapeutic targets may be identified to improve these outcomes and encourage intrinsic hyaline cartilage healing.

To both aid understanding of the repair process and to trial potential therapeutics in vivo, an optimised animal model is required. Large animal models are commonly used for cartilage repair studies due to the similarity in structure and mechanical loading relative to humans (Kuyinu et al., 2016). However, for early pre-clinical investigations smaller animals are more useful due to their low cost, ease of maintenance and relatively short regeneration time. Many studies using osteochondral defects have been conducted in rabbits and rats, but mice offer a further advantage, their amenability to genetic manipulation (Eltawil et al., 2009).

5.2. Aim and objectives

This chapter describes the development and evaluation of an osteochondral model in mice. Further insights into the repair process were gained by examining the contribution of different cell types at different stages of repair.

To achieve this, an overview of the currently published models in mice was conducted and an optimised technique established by trialling different methods to generate an osteochondral defect. Once achieved, a time course study was conducted and specimens analysed by histology and immunohistochemistry, firstly to assess the reproducibility and consistency of the defect and secondly to identify different cell types in and around the repair tissue across different time points.

5.3. Literature review of published osteochondral mouse models

Several osteochondral models had previously been described in the literature prior to beginning this work. A summary of the key features from these publications is described in Table 5-1. The published studies had various aims with the earlier published articles looking first to establish a model and then address specific questions using it (Fitzgerald et al., 2008; Eltawil et al., 2009; Martinez et al., 2015). Later articles then reference the Eltawil et al. (2009) paper for its methodology (Matsuoka et al., 2015; Mak et al., 2015). Whilst some insight has been made into the cell dynamics within these models limited time points have left scope for an in depth analysis of defect healing over time.

Based on the information gathered by analysis of the published literature, decisions were made for experimental parameters. Firstly, across all studies detailed in Table 5-1 the C57BL/6 strain of mice was used (excluding Martinez et al., 2015). This strain is well characterised to have a poor healing ability and is reported in all cases to fail to fully heal the cartilage injury by 8 weeks. This provides an opportunity to analyse the process by which the defect attempts to repair with the potential to adapt the process and quantify any improved repair that occurs through intervention. Importantly, C57BL/6 mice are the most popular strain of genetically manipulated mice and therefore it is worthwhile establishing a repair model in these mice in the first instance.

Secondly, the age of the mice is a key feature. Eltawil et al. (2009) and Matsuoka et al. (2015) aimed to assess the differences in the repair between mice of different ages, finding that younger mice showed improved repair. Importantly, all the studies documented used skeletally mature animals of 8 weeks of age as a standard reference (excluding Martinez et al., 2015, where 15 weeks was used).

Finally, the method of inducing a defect is detailed in Table 5-1. All studies made the defect in the distal femur within the patella (or trochlear) groove and, barring Mak et al.,

the patella was dislocated laterally before the defect was made using a needle between 25G and 27G. The type of the defect, on the other hand, falls into one of two types; either a cylindrical defect made by rotation of the needle, or a scratch produced by passing the needle along the length of the patella groove.

The papers all claim to form osteochondral defects and in the simplest of cases this was confirmed during surgery by the appearance of blood to confirm penetration of the subchondral bone. Eltawil et al. (2009), Matsuoka et al. (2015) and Mak et al. (2015) all attempted to control the depth of the defect by modifying the needle, with either a glass bead or a 21G needle sheathing the smaller needle to prevent deeper penetration of the defect into the marrow cavity.

Table 5-1 – Review of published patella groove osteochondral defect studies

	Fitzgerald et al., 2008	***Eltawil et al., 2009***	***Martinez et al., 2015***	***Matsuoka et al., 2015***	***Mak et al., 2015***
Age of mice:	8 weeks	8 weeks or 8 months	15 weeks	3 weeks, 4 weeks and 8 weeks	4 to 6 weeks
Sex:	Male and female	Male	Female	Not defined	Not defined
Strain:	C57BL/6 and MRL/MpJ	C57BL/6 and DBA/1	BKS	C57BL/6	C57BL/6 and MRL/MpJ
Defect location:	Patella (trochlear) groove	Patellar groove	Patella (trochlear) groove	Patellar groove	'Needle was inserted under the patella tendon from the medial side and aimed towards the femur'
Defect made with:	27G needle – circular motion	26G needle with bead (200um of tip exposed)	25G needle	21G over 27G needle	26G with bead (1.45mm of tip exposed)
Defect width/length:	Cylindrical – measured to be 0.6-0.8mm diameter	Longitudinal along length of groove. Width defined by the needle	Cylindrical – measured to be 0.5mm diameter	Longitudinal along length of groove. Width defined by the needle	Cylindrical – diameter defined by needle
Defect depth:	'Penetration of subchondral bone confirmed by appearance of blood'	200um (glass bead on to tip)	'penetrating into the subchondral bone'	300um 'Penetration of subchondral bone was confirmed by bleeding from the cartilage injury site'	1.45mm

5.4. Model development

Using the key features from the published studies discussed above, certain parameters were defined before beginning model optimisation. Female, C57BL/6 strain mice were chosen between 8-10 weeks of age with the aim to generate a cylindrical osteochondral defect within the patella groove of the distal femur. A cylindrical defect was chosen to ensure production of an osteochondral defect by a more controllable pushing motion rather than a sweeping scratch. Firstly, experimental trials were conducted on *ex vivo* cadavers of mice to gain practice and insight into the practicalities of the technique.

Once a method was established to access the joint by lateral displacement of the patella, different needle sizes were compared. Needles were selected of sizes similar to those used in the published studies discussed above (section 5.3). The largest needle trialled was 21G. This was found to be large relative to the patella groove, which led to difficulties in needle placement and regularly led to breakage of the ridge of the femoral condyles. Similar difficulties were found with the 23G needle. The smallest size trial was 27G. These were found to be fragile and susceptible to bending when pushed against the surface of the joint. Optimal needle size to maintain the needle integrity and generate a defect with minimal damage to the surrounding joint structure was as a result determined to be 26G.

Histological sections were generated from these trials and can be seen in Figure 5-1 and highlight the need to consider further the needle placement. Whilst establishing that the defect should be located centrally within the patella grove, the length of the groove meant optimal placement for a cylindrical defect needed to be determined. As shown in Figure 5-1 (21G, 23G, 25G and 27G), histological analysis revealed that in initial attempts defects were made relatively posteriorly/low in the groove, a location which has limited articular cartilage as this site is non-loading bearing and encounters minimal friction. This meant the defect needed to be positioned more superiorly in the patella groove. However, the depth must be limited as the presence of an open growth plate in mice means the top of the patella groove is a vulnerable location to breakage of the epiphysis. Furthermore, as shown in Figure 5-1 (26G) the defect can also penetrate through the epiphyseal growth plate of the femur. A compromise is therefore required and the defect must be positioned centrally along the length of the patella groove.

In line with three of the published protocols, a method with which to establish a controlled depth was investigated. Whilst the methodology of Matsuoka and colleagues' (2015) using a larger needle to sheath a smaller one sounded promising, fabrication of the sheathed needle and its use for defect generation encountered difficulties. Firstly, cutting of larger 21G needles with which to sheath the 26G needle led to compression of the metal and meant the hollow cylinder was regularly no longer fully open so that the smaller needle could not be inserted. Further, on trial of metal sheath needles on mouse cadavers, the edge of the sheath caused damage to the ridge of the femoral condyles due to its

sharp nature. This was a cause for concern as the aim was to make a defect with sharp intact cartilage borders.

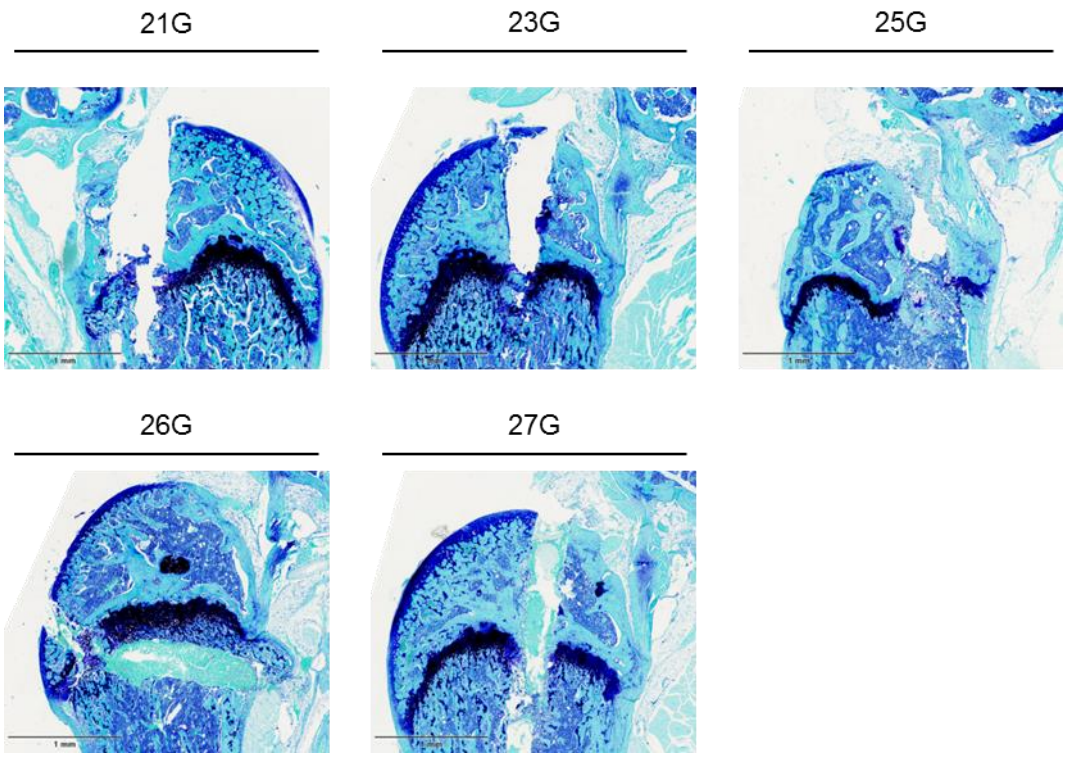

Figure 5-1 – Trial of different gauge needles to generate an osteochondral defect
Mice cadavers were used for the trial of needles ranging from 21G to 27G to determine the optimal size for use going forward. The placement of the defect was observed relative to the articular cartilage and femoral epiphyseal growth plate highlighted in dark blue. Sagittal sections stained with Toluidine blue / Fast Green. Sections decalcified under acid conditions. Scale bar indicates 1 mm.

Subsequently, this led to trial of other sheathing materials. Whilst, Eltawil et al. (2009) and Mak et al. (2015) utilised beads attached with resin glue, it was decided to adopt the idea of sheathing the needle to help ensure that the needle entered at a perpendicular angle. A method using small green plastic collars was developed. This had the advantage of controlling the depth whilst avoiding damage to the femoral condyles on rotation of the needle.

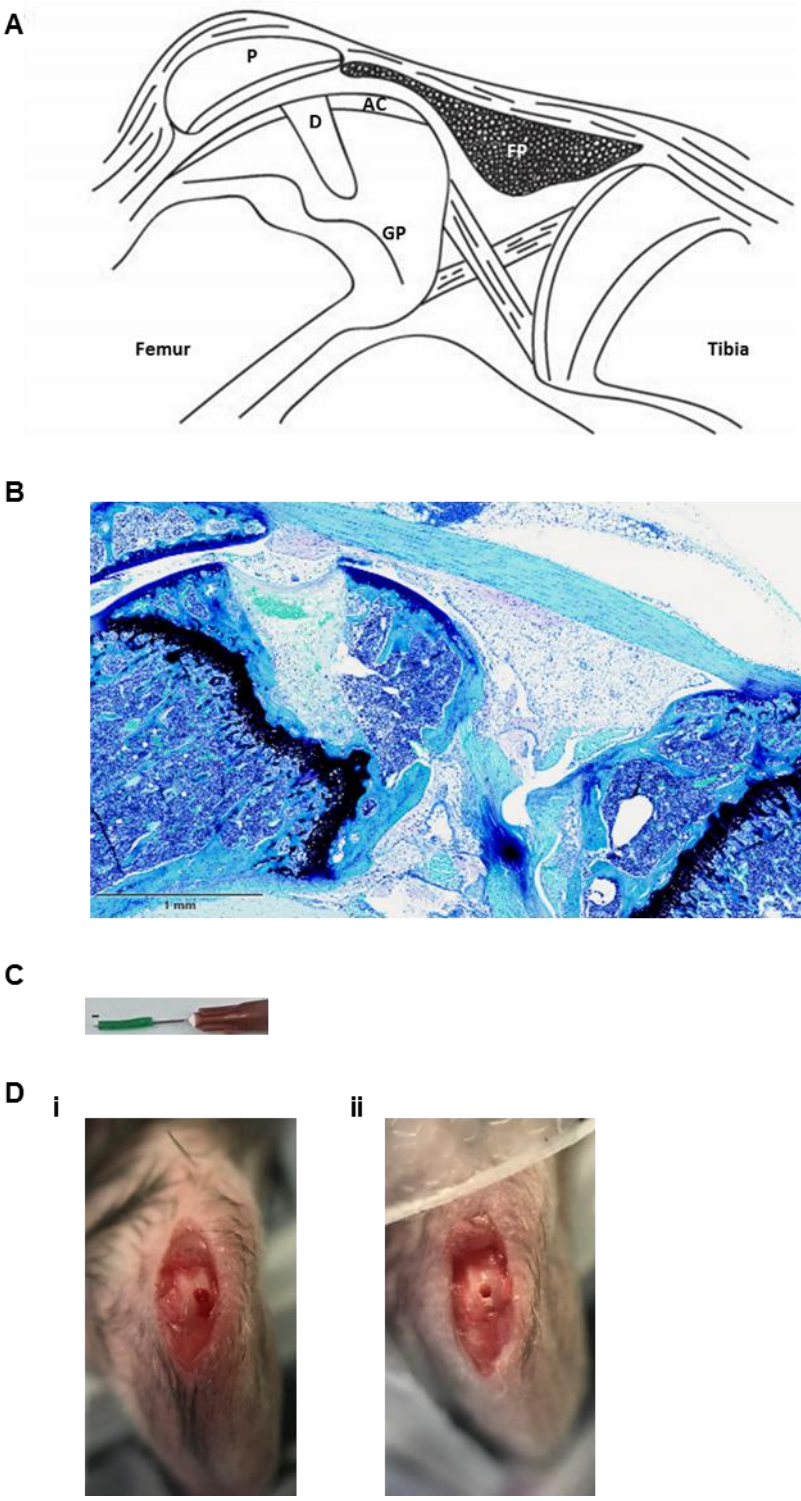

Figure 5-2 – Generation of an osteochondral defect in the patella groove
(A) Schematic representation of the sagittal cross-sectional view of the middle of the patella groove after generation of an osteochondral defect within the articular cartilage. (B) Toluidine blue / Fast Green staining of a sagittal histological section from a mouse 24 hours after generation of the defect. (C) The devise used to generate the defect - a 26G needle with 0.06 mm of its tip exposed, denoted by 0.6 mm line. (D) The left hind of two mice during surgery. A 1 cm skin incision was made over the left knee joint, and the patella groove exposed by lateral dislocation of the patella, and an osteochondral defect made by pressure and rotation of the device. Some defects bleed after penetration (i) whilst others remained hollow (ii). The patella was replaced and sutured in place before skin suturing. P, patella; AC, articular cartilage; D, osteochondral defect; GP, growth plate; FP, fat pad. Scale bar indicates 1 mm.

5.5. Generation of an osteochondral defect

Figure 5-2 A shows a schematic of the cross-sectional view across the centre of the patella groove and the optimal positioning of the osteochondral defect under the patella within the articulating cartilage, penetrating the bone. Figure 5-2 B shows the histology of an animal at 24 hours post-surgery and an osteochondral defect positioned as intended. Figure 5-2 C shows the device used to produce this defect – a 26G needle with 0.6mm of the tip expose by the positioning of a green plastic collar. A full description of the final surgical procedure can be found in the methods section (see section 3.12.5). Figure 5-2 D shows images of two mice during the surgical procedure before realignment of the patella. This demonstrates that not all osteochondral defects bled during surgery.

5.6. Reproducibility and consistency of creating the model osteochondral defect

At 24 hours post-surgery, animals were sacrificed and the patella groove re-exposed for photography and macroscopic assessment of the defect. Figure 5-3 A shows the defect for 8 mice at this time point. In all animals the defect had infilled with tissue. In some animals this tissue was bloodier in appearance (Figure 5-3 A i to iii) whereas in others the boundaries were more difficult to assess (vi to viii). Black dotted lines denote the femoral condyles and demonstrate that the defect was located centrally within the patella groove. Figure 5-3 B shows the ratio of the defect relative to the width of the femoral condyles. This data indicates that the defect expands across 43% of the groove (N=8).

To further assess the reproducibility and consistency of the osteochondral defect generated across different individual mice, histomorphometric measurements were made from sagittal histological sections of these mice. Figure 5-3 C shows sections from a single mouse at 150 μm intervals moving from the medial to lateral side stained with Safranin O / Fast Green which were used for these measurements. Firstly, the histology sections demonstrate the change in morphology of the joint across the patella groove. On the first section (Figure 5-3 C i), the distal femur is at it's largest, articulating directly against the proximal tibia with mensci visible in the joint space. The femoral growth plate, stained red by the Safranin O stain, has a wave morphology. 150 μm further (Figure 5-3 C ii) the morphology is similar, but the wave of the femoral growth plate is slightly flatter. At this point the edge of the osteochondral defect can also be identified. The next section (Figure 5-3 C iii) is from within the patella groove. This can be identified by several anatomical features aside from the presence of the osteochondral defect. Firstly, the femoral growth plate is now almost flat and secondly the joint space is wider as the femoral and tibial surface no longer directly articulate, instead, the cruciate ligaments can be seen in this space.

Using serial sections from three mice, measurements were taken for the cross-sectional width, depth and area of the defect. Figure 5-3 D presents values for the width of the defect at intervals of a maximum of 50 µm. With the maximum width centred on 0 µm, the shape of the defect was cylindrical and similar across the three animals shown. Furthermore, the maximum width, depth and area were consistent and highly reproducible (Figure 5-3 E) with the coefficient of variation of these measurements and the defect to patella groove width ratio all between 4.5 and 6.5% (Table 5-2).

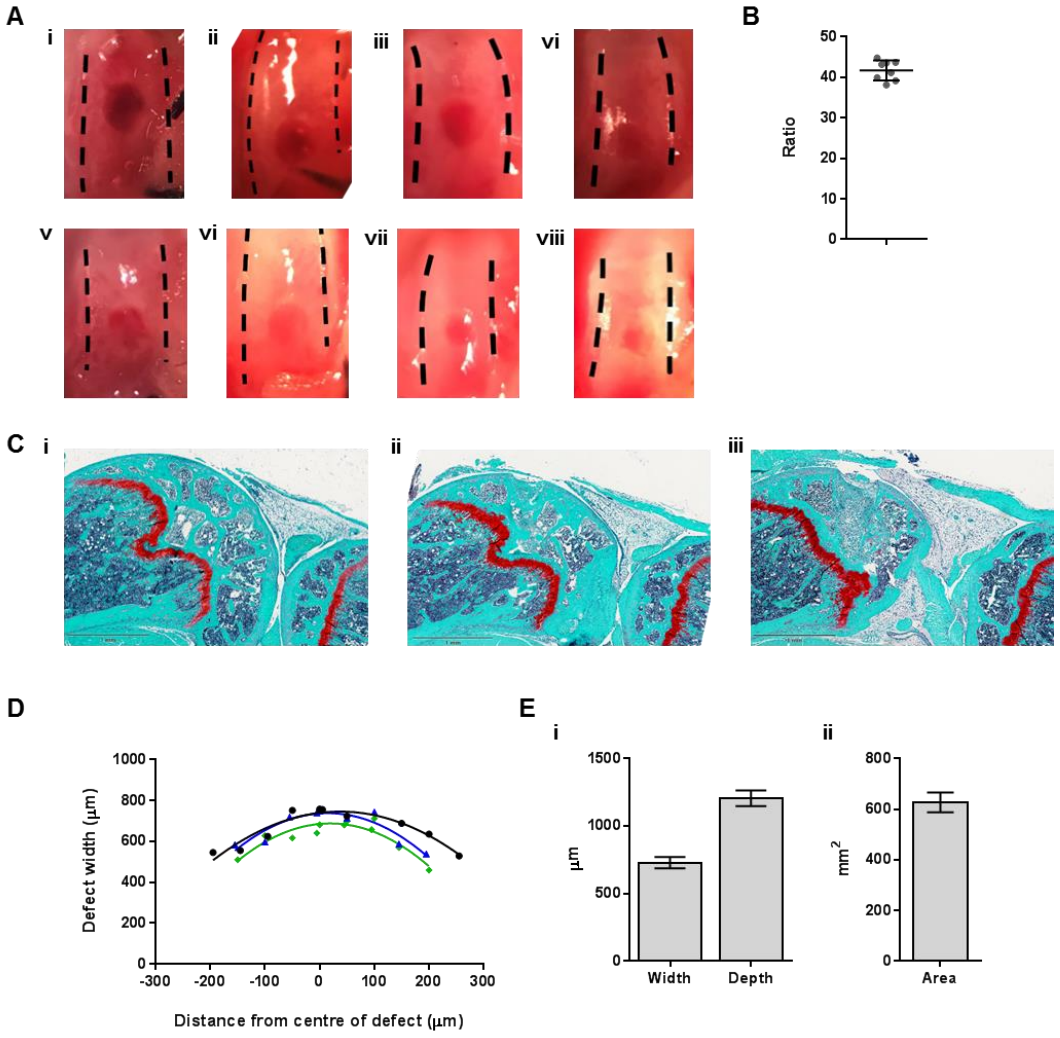

Figure 5-3 – Reproducibility and consistency of the osteochondral defect
Osteochondral defects were generated in eight mice and after animal euthanasia at 24 hours the defect imaged (A). (B) Graph shows the ratio of measurements taken for the width of the defect to the width of the patella groove (N=8). Joints were prepared and sagittal sections prepared. Safranin O (red) staining of the femoral growth plate provides a landmark for histology preparation (C). Counterstained with Fast Green and haematoxylin. Scale bar indicates 1 mm. Measurements for histomorphometric analysis of the defect (width, depth and area) were taken from these sections. (D) Width of the defect across serial sections, maximum 50 µm apart. 0 represent the centre of the defect – the largest width. Polynomial regression, r squared value between 0.84 and 0.90 for each animal. The maximum measurement for (i) width, depth and (ii) area. All the values are expressed as mean ± standard deviation (N=3).

Table 5-2 – The mean, the standard deviation (SD) and coefficient of variation (CV) of histomorphometric measurements

	Groove to Defect Ratio *(N=8)*	***Width*** *(N=3)*	***Depth*** *(N=3)*	***Area*** *(N=3)*
Mean	41.64	729.0 µm	1205 µm	626.3 mm^2
SD	±2.48	±41.62	±58.58	±39.50
CV	5.88%	5.71%	4.87%	6.31%

5.7. Analysis of osteochondral repair over 8 weeks

A time course analysis was conducted over 8 weeks post-surgery, eight mice per group. Mice were scarified at 24 hours, 1 week, 2 weeks, 4 weeks and 8 weeks post-surgery. All operations were performed without incident. All animals recovered and were weight bearing within the 30 minutes of removal from anaesthesia. Due to time constraints, only three or four animals from each group were sectioned and used for further analysis.

5.7.1. Early healing osteochondral defects have distinct repair regions

Figure 5-4, Figure 5-5, and Figure 5-6, show Toluidine Blue / Fast Green staining of the distal femur of mice at 24 hours, 1 week and 2 weeks respectively after generation of the osteochondral defect. Toluidine blue is a basic dye and stains nuclei and denotes areas of acidic proteoglycans such as the articular cartilage and femoral growth plate whilst Fast Green is used here as a counterstain.

At all of the time points, a clear boundary between the intact articular cartilage and the borders of the defect is clearly seen (except for one mouse at 2 weeks where articular cartilage crosses over the defect). However, the deeper margins of the defect become less clear over time. Whilst clear at 24 hours, and definable at 1 week, by 2 weeks the repair of the tissue makes it difficult to determine the borders of the defect.

Cellular organization was observed by higher 40x magnification of the defects. For the purposes of description, the defect can be considered in three regions: top middle and bottom. At 24 hours, the patella-articulating surface of the defect shows the presence of an overlying cap of fibres orientated across the defect. Beneath this a less dense fibrous network is seen in which cells are widely dispersed. One animal (Figure 5-4 B I top) had a large cluster of red blood cells in this tissue whilst the other two animals had red blood cell clusters and nucleated cells distributed throughout the top and middle regions. By 1 week, the top of the defect has become significantly denser in structure with lateral fibrous structures continuing to cap the articular surface. Red blood cells are still present but in smaller in clusters below this fibrous cap. At 2 weeks on the other hand, these cells are no longer present and the matrix structure of this top section of the defect has significantly changed. Most obvious is the overall increase in positive staining with toluidine blue and

specifically its strong staining of lacunae within which cells sit. This is suggestive of the presence of chondrocytes that are depositing a proteoglycan rich matrix. Interestingly these cells are not at the level of the articulating surface but 50 μm below, extending down to 300 μm and within the centre of the defect rather than at the side edges. In one animal at 1 week, these histological observations of chondrogenesis are also seen deeper, in the middle region of the defect.

In the defects at 24 hours and 1 week, blue/purple stained material is identifiable in all animals, although there is variability. Furthermore, in one animal per time point there was clear disruption of the distal femoral growth plate. Debris from the growth plate was not significant in the 2-week animals, except two animals where there was a chondrogenic island at the very base of the defect.

Most notable at 2 weeks was the re-establishment of bone marrow architecture at the base of the defect. Additionally, bone structures appear to be re-forming with Fast Green staining intensity similar to the undamaged surrounding bone. This differs from the earlier time points where the Fast Green staining was less intense and bone appeared more fragmented. Furthermore, at 2 weeks cell nuclei were also visible in the bone tissue within the defect identifying osteocytes whilst absent at earlier time points and osteoblasts are visible on the surface of bone fragments.

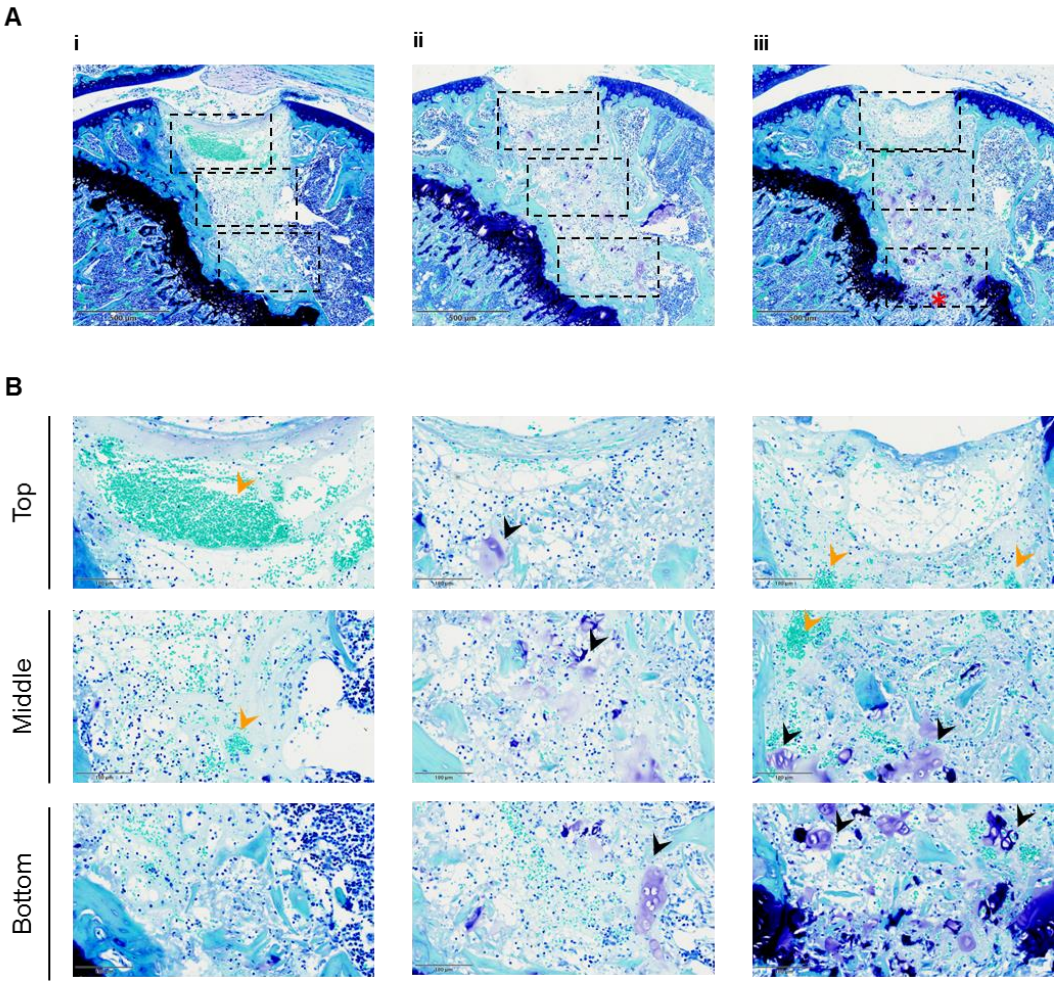

Figure 5-4 – Osteochondral defect histology at 24 hours post-surgery.
Toluidine blue / Fast Green staining of sagittal sections of the patella groove 24 hours after the generation of an osteochondral defect. 8.5x images (A) and 40x images (B) of three mice (i, ii and iii) showing the top, middle and bottom regions of the defects. Red star indicates damage to the femoral growth plate. Black arrowheads indicate toluidine blue stained tissue within the defect. Orange arrowheads indicate red blood cell clusters. Scale bars indicate 500 µm (A) and 100 µm (B).

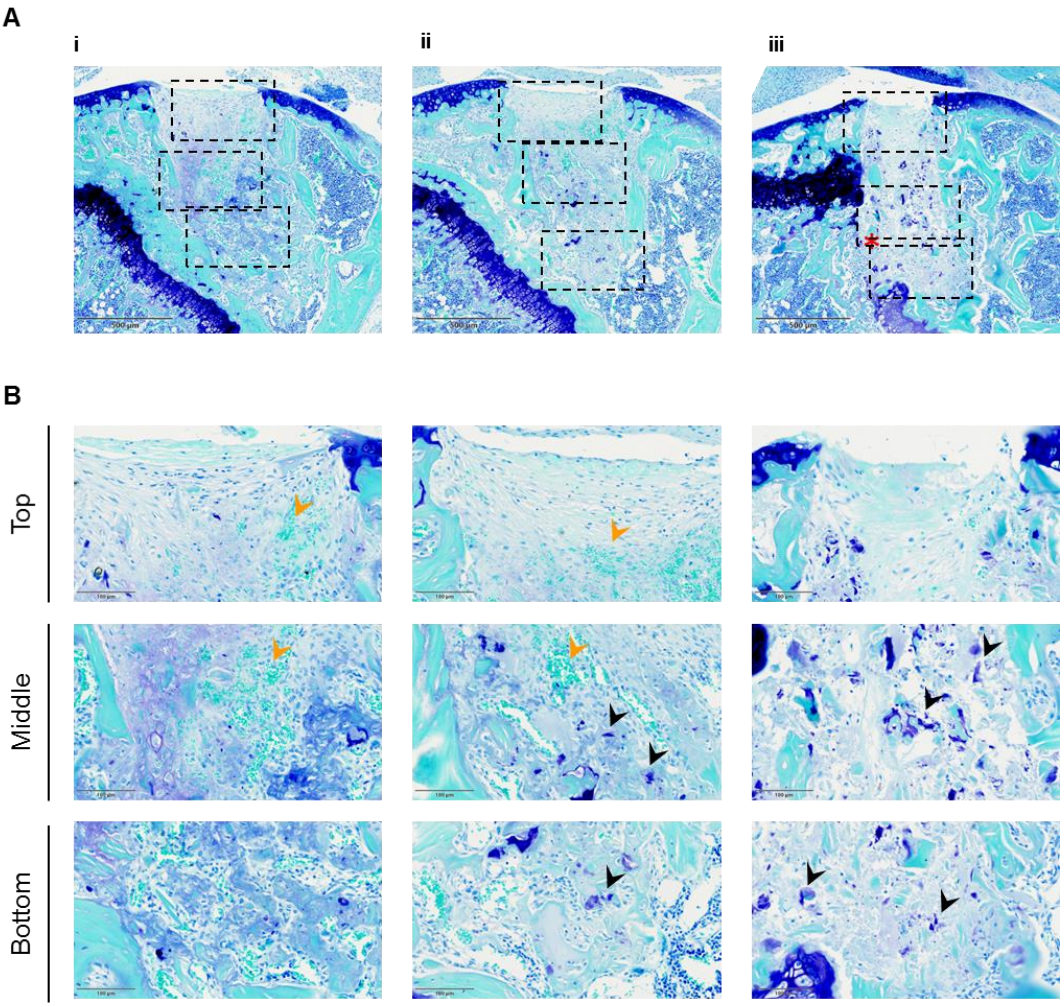

Figure 5-5 – Osteochondral defect histology at 1 week post-surgery.
Toluidine blue / Fast Green staining of sagittal sections of the patella groove 1 week after the generation of an osteochondral defect. 8.5x images (A) and 40x images (B) of three mice (i, ii and iii) showing the top, middle and bottom regions of the defects. Red star indicates damage to the femoral growth plate. Black arrowheads indicate toluidine blue stained tissue within the defect. Orange arrowheads indicate red blood cell clusters. Scale bars indicate 500 µm (A) and 100 µm (B).

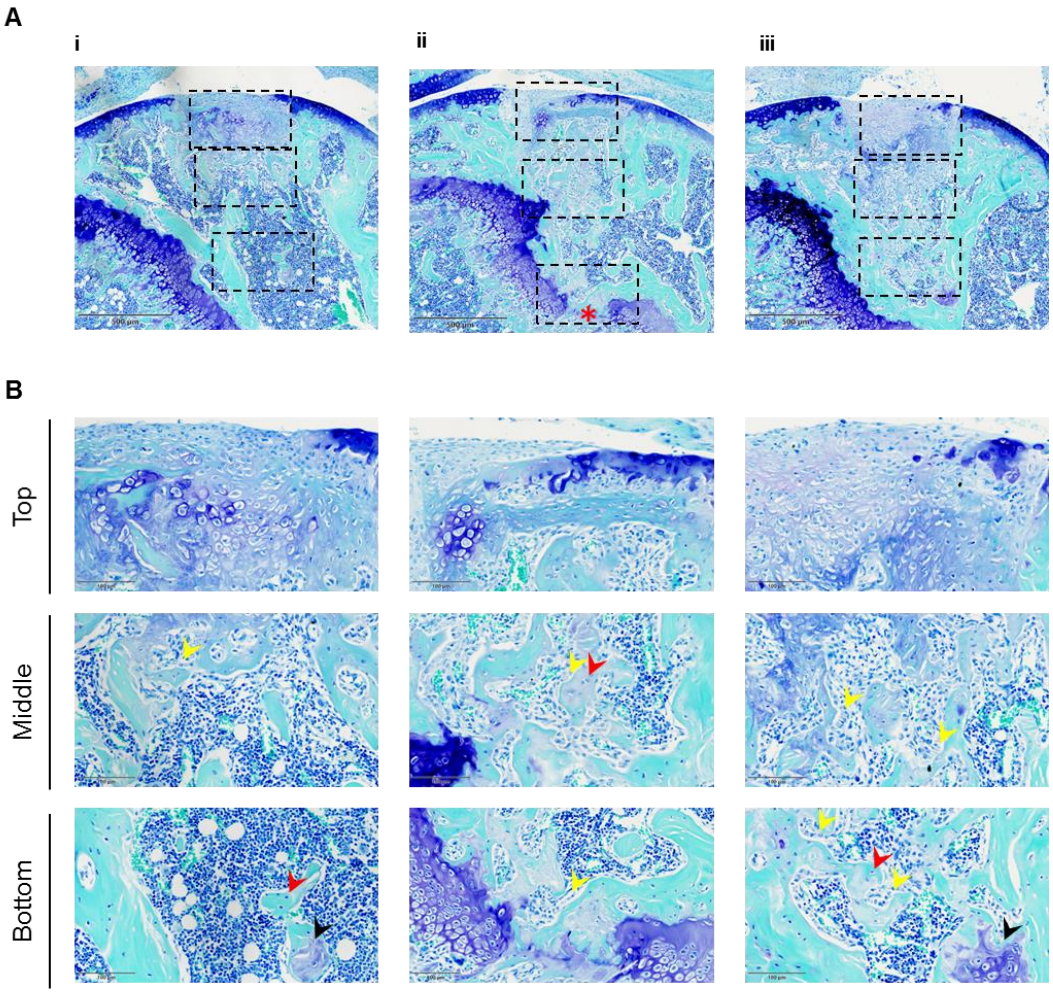

Figure 5-6 – Osteochondral defect histology at 2 weeks post-surgery.
Toluidine blue / Fast Green staining of sagittal sections of the patella groove 2 weeks after the generation of an osteochondral defect. 8.5x images (A) and 40x images (B) of three mice (i, ii and iii) showing the top, middle and bottom regions of the defects. Red star indicates damage to the femoral growth plate. Black arrowheads indicate toluidine blue stained tissue within the defect. Yellow arrowheads indicate osteoblasts on, and red arrowheads osteocytes in, bone fragments within the defect site. Scale bars indicate 500 µm (A) and 100 µm (B).

5.7.2. C57BL/6 osteochondral defects can regenerate articular cartilage

By 4 weeks after injury (Figure 5-7) there was evidence, by toluidine staining, of proteoglycan content across the entire defect at the articular surface in two of the three animals. However, the margin of the original defect with the surrounding articular cartilage was still identifiable. This was mostly apparent because of the increased thickness of cartilage at these locations and overgrowth of the repair tissue above the level of the surrounding articular cartilage. Interestingly, in the animal with the poorest level of healing (Figure 5-7 iii), there was an absence of any chondrogenesis, relative to that observed in the 2-week animals. The defect surface in this animal was highly cellular and more fibrous in appearance. In comparison, the base of the defect was well healed with bone and bone marrow tissue like the other animals in the group. This is most notable in the Safranin O / Fast Green / Haematoxylin stained sections. Like Toluidine Blue, Safranin O stains proteoglycans red and nuclei are counterstained with haematoxylin.

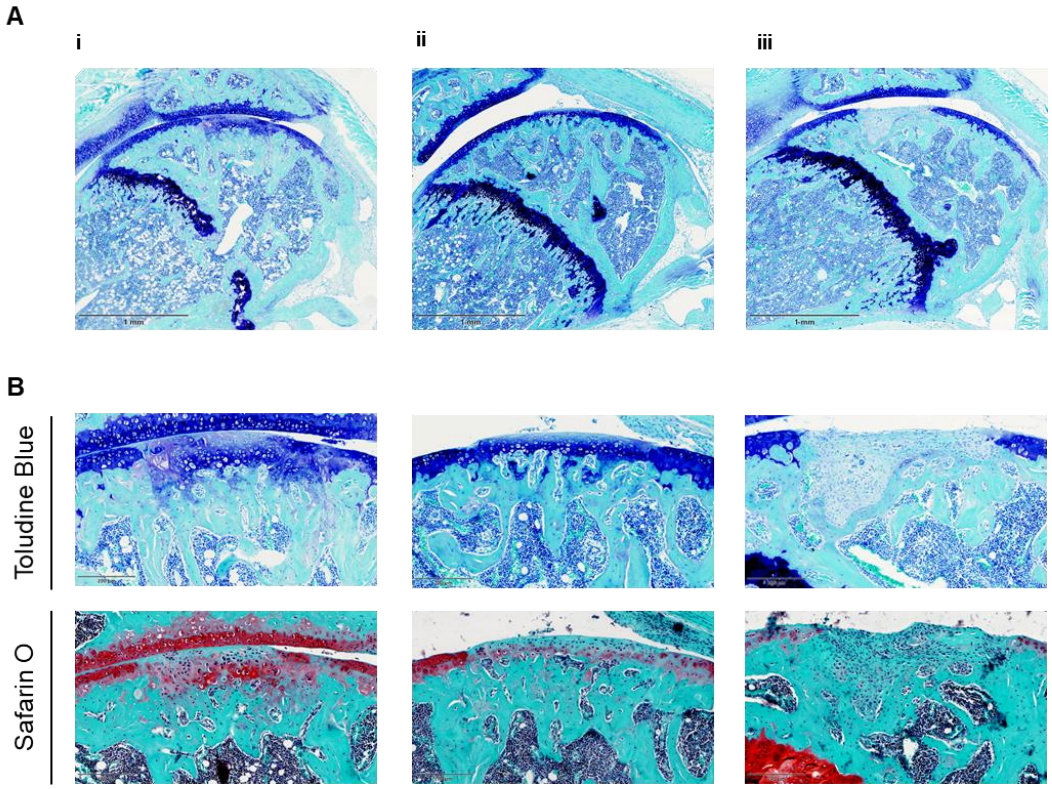

Figure 5-7 – Osteochondral defect histology at 4 weeks post-surgery.
Sagittal sections of the patella groove 4 weeks after the generation of an osteochondral defect. 8.5x images Toluidine blue / Fast Green (A). 40x images Toluidine blue / Fast Green and Safranin O /Fast Green staining (B) showing the top regions of the defects. Scale bars indicate 1 mm (A) and 100 µm (B).

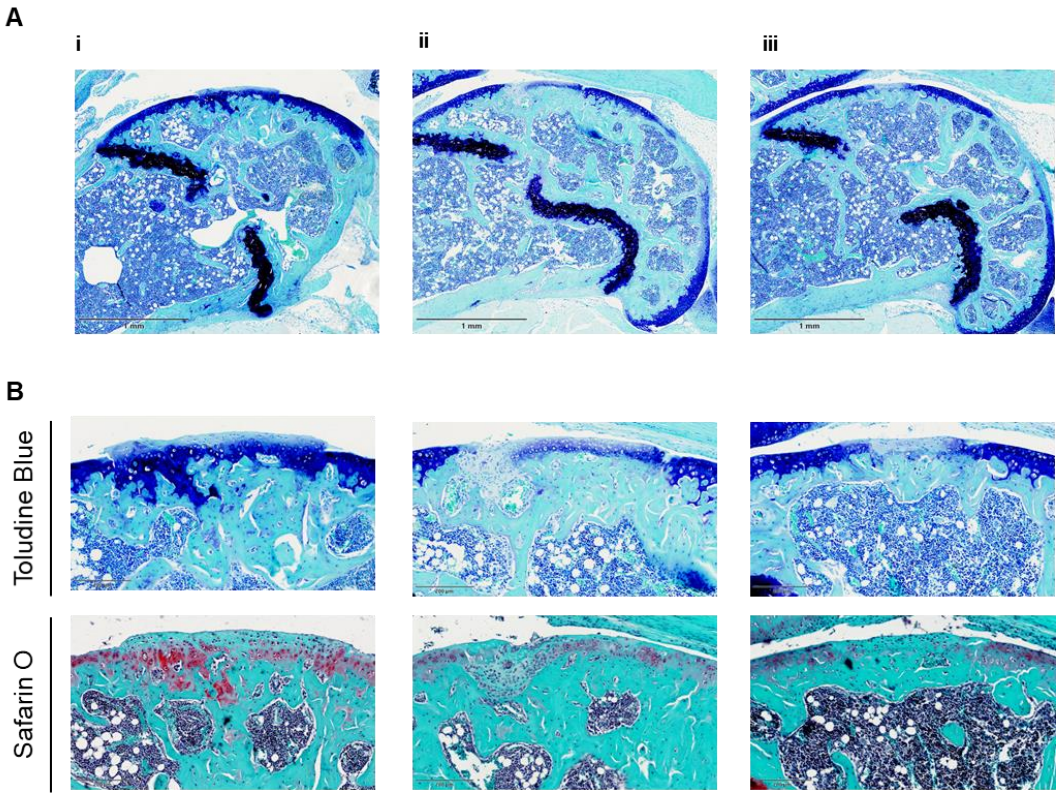

Figure 5-8 – Osteochondral defect histology at 8 weeks **post-surgery.**
Sagittal sections of the patella groove 8 weeks after the generation of an osteochondral defect. 8.5x images Toluidine blue / Fast Green (A). 40x images Toluidine blue / Fast Green and Safranin O /Fast Green staining (B) showing the top regions of the defects. Scale bars indicate 500 µm (A) and 100 µm (B).

In Figure 5-8 the 8-week animals are shown. The histological observations between the different animals were contrasting. The animal with the best level of healing (Figure 5-8 i) exhibited histological morphology similar to that seen in two animals at 4 weeks with toluidine blue staining across the defect with overgrowth of proteoglycan negative tissue above the intact articular cartilage level. The second animal (Figure 5-8 ii) had a proteoglycan rich matrix partially covering the injury starting from the distal side of the defect. On the proximal side, a dense highly nucleated area of tissue is observed. The third animal at this time point (Figure 5-8 iii) had toluidine positive matrix at the distal and proximal edges of the defect but minimal staining at the centre. The haematoxylin staining showed cells present in this central region but they do not have the appearance of chondrocytes as they lack the defining lacunae.

5.7.3. Quality and variability of repair

A modified Pineda scoring system was used to quantify articular cartilage repair. This system is composed of four parameters: (1) filling of the defect, (2) reconstitution of the osteochondral junction, (3) matrix staining, and (4) cell morphology. Together these scores result in an overall score that ranges from 0 (complete regeneration) to 14 points

(no repair) while maximum point values for single parameters range between 2 and 4. Scoring of Safranin O / Fast Green / haematoxylin stained sections is shown in Figure 5-9. All animals scored the maximum of 14 points at 24 hours and at 1 week all defects improved to a score of 10. At 2 weeks there was a variation in the repair scores with the standard deviation increasing from ±0 to ±3.11 (Table 5-3), although as seen in Figure 5-9 a single outlier animal skewed the score with a lower level healing. This variation however remained in the 4 week animals with Pineda scores ranging from 3 for the best healed animal to 9. These observations illustrate the increased variability between animals at later time points.

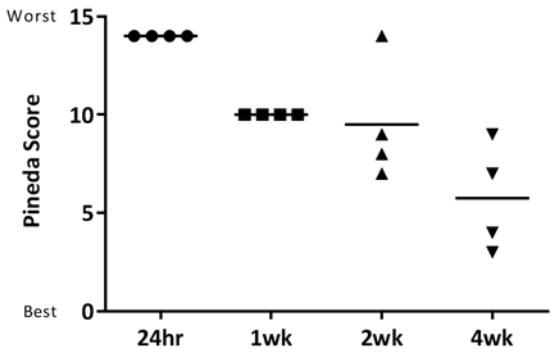

Figure 5-9 – Articular cartilage repair scores across time after generation of an osteochondral defect.
Mice were sacrificed at various time points post-surgery. Safranin O / Fast Green / haematoxylin stained representative sections from the centre of the defect were scored using the Pineda scoring system (N=4).

Table 5-3 – Scores for individual parameters of the Pineda score

	Filling of the defect	*Reconstruction of osteochondral junction*	*Matrix staining*	*Cell morphology*	*Total*
24 hours	4 (±0)	2 (±0)	4 (±0)	4 (±0)	14 (±0)
1 week	0 (±0)	2 (±0)	4 (±0)	4 (±0)	10 (±0)
2 weeks	1 (±2)	1.75 (±0.5)	3.75 (±0.5)	3 (±0.82)	9.5 (±3.11)
4 weeks	0.5 (±0.58)	1 (±0.82)	2.25 (±1.5)	2 (±1.15)	5.75 (±2.75)

5.7.4. Matrix remodelling

To further assess the healing at each time point histological sections were immunostained for type II collagen and type VI collagen. Type II collagen is an important structural component of healthy articular cartilage and was seen to increase overtime within the defect region. At 1 week staining was present and strong in discrete areas consistent with the toluidine staining seen in Figure 5-5. By 2 weeks positive staining was seen centrally within the defect just below the articular cartilage level whilst at 4 weeks the staining had

moved up to the articular surface. There is a lack of any real difference in the type and organisation of repair tissue between the 4 and 8 weeks time-points. In the better healed animals, the intensity of staining matched the staining of the undamaged surrounding cartilage.

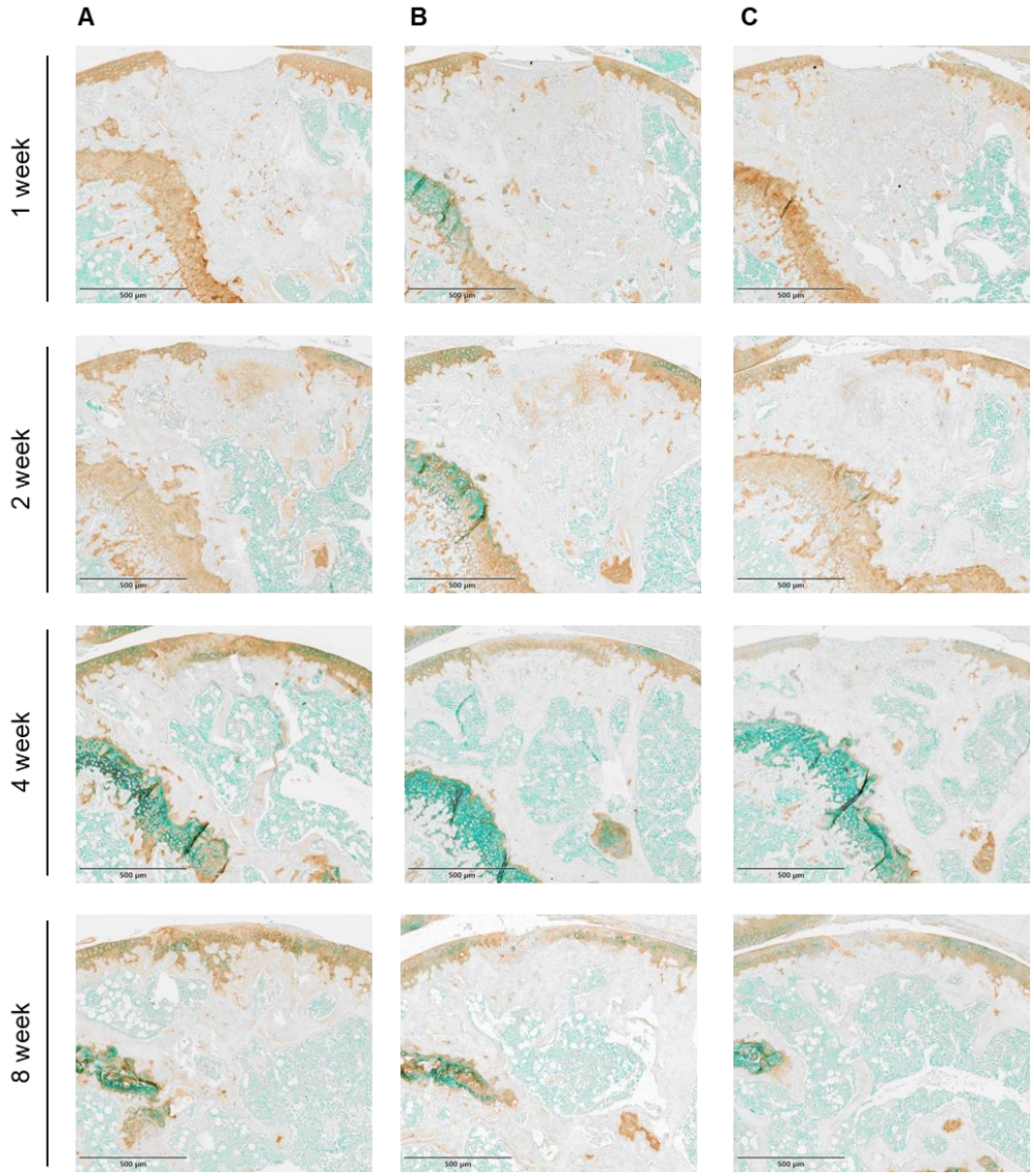

Figure 5-10 – Type II collagen staining of osteochondral defects
Sagittal sections of the patella groove at 1 week, 2 week, 4 weeks and 8 weeks after the generation of an osteochondral defect stained by immunohistochemistry for type II collagen (brown). Nuclei are counterstained with methyl green. Scale bars indicate 500 µm.

Type VI collagen is another extracellular protein present in healthy articular cartilage, although in contrast to collagen type II, the staining is mainly concentrated in the pericellular matrix. Additionally, the staining had a higher intensity in the superficial layer of articular cartilage relative to deeper layers. At 1 week, this protein was localised to the

top half of the defect clearly marking the boundary between defect and surrounding bone. At later time points the staining continued to be localised to the top of the defect and remained stronger than the surrounding undamaged cartilage. In the most well healed animals the staining was localised to the superficial area of repaired articular cartilage extending over the level of the defect neighbouring undamaged cartilage.

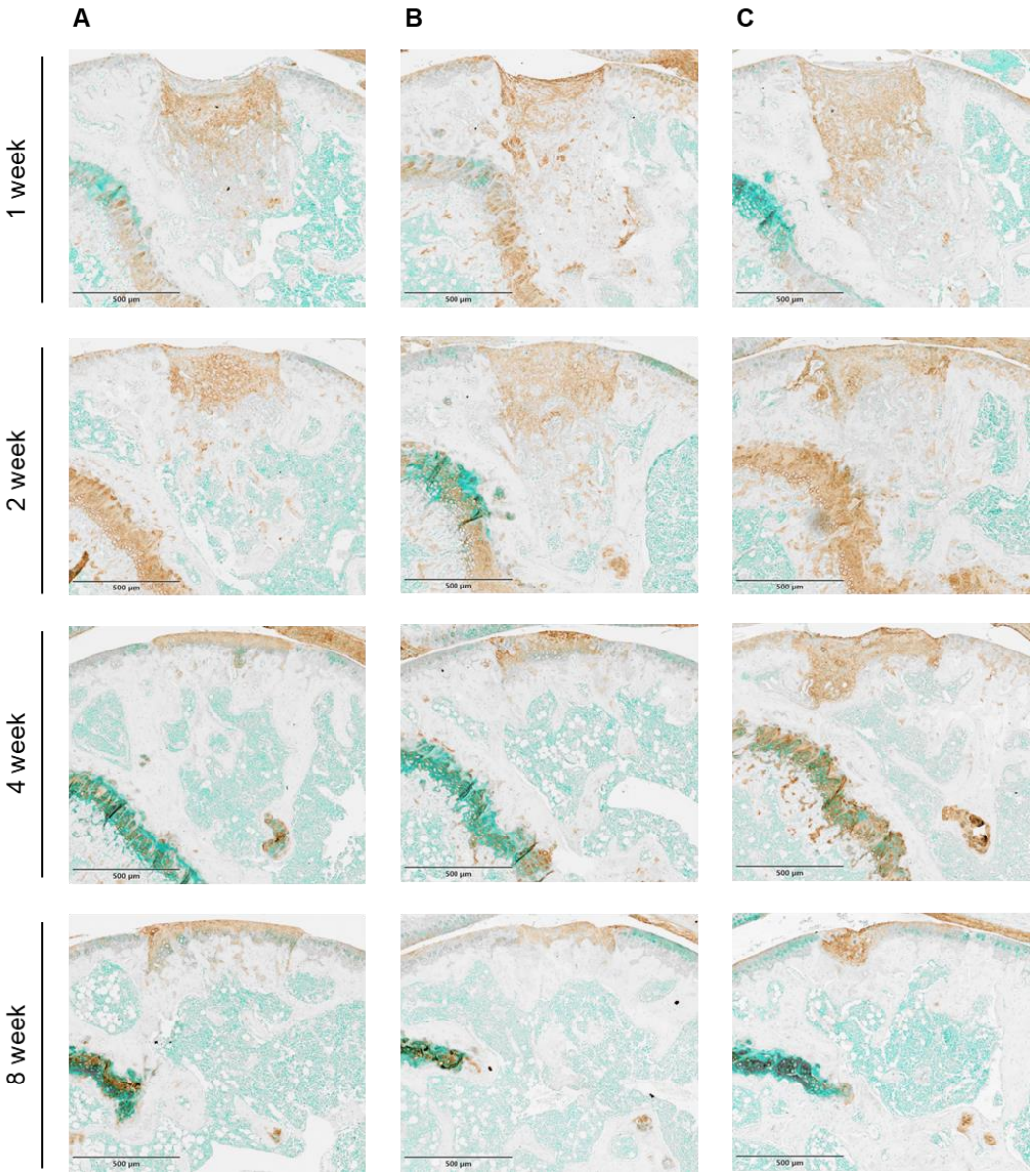

Figure 5-11 – Type VI collagen staining of osteochondral defects
Sagittal sections of the patella groove at 1 week, 2 week, 4 weeks and 8 weeks after the generation of an osteochondral defect stained by immunohistochemistry for type VI collagen (brown). Nuclei are counterstained with methyl green. Scale bars indicate 500 µm.

Picrosirius red stained histological sections were imaged under polarised light resulting in enhancement of the natural birefringence of the collagen fibres. This allowed comparison across the time points of the cartilage and bone tissue organisation as well as the assessment of bone remodelling.

At 24 hours within the defect there was a lack of birefringent material (Figure 5-12). However, broken fragments of bone were identifiable at the boundary of the defect. Additionally, the upper edge of the defect was clear due to the strong birefringence of the neighbouring undamaged cartilage and bone. This clear boundary remained at 1 week whilst at 2 weeks the border was less clear as collagen fibres were synthesised and laid down within the repair material. Furthermore, at 2 weeks there was evidence of bone remodelling within the repair tissue as lamellar bone was found within the lower portion of the defect site. At 4 weeks parallel bundles of collagen perpendicular to the articular surface were identifiable as well as superficial fibres, similar to undamaged cartilage, in line with the surface. In the 8 weeks sample there was some evidence of integration with the neighbouring tissue as fibres curved and crossed the wound interface.

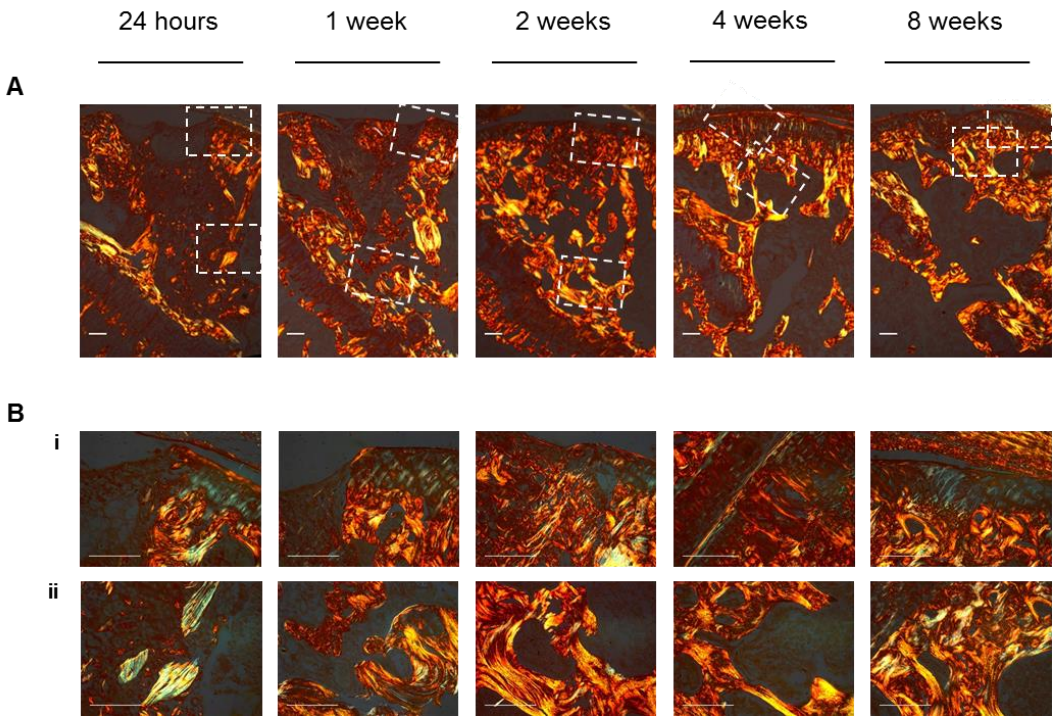

Figure 5-12 – Polarised light imaging of osteochondral defects stained with Picrosirius red.
Sagittal sections of the patella groove at 1 week, 2 week, 4 weeks and 8 weeks after the generation of an osteochondral defect were stained with Picrosirius red and imaged under polarised light. 5x images (A) and 40x images (B); (i) at the articular surface and (ii) relatively deeper as indicated by the white boxes in (A). Scale bars indicate 100 µm.

5.7.5. Cell Dynamics during osteochondral injury repair

5.7.5.1. Proliferation of cells

Ki67 is present during all active phases of the cell cycle (G_1, S, G_2, and mitosis), but is absent from resting cells (G_0). At 24 hours there is limited positive staining within the defect region (Figure 5-13). By 1 week post-surgery a number of Ki67 positive cells are present within the defect site, indicated by black arrowheads in Figure 5-14 B. Interestingly, there is a large increase in proliferating cells in the bone marrow cavities in the surrounding bone marrow relative to the 24 hour animals. At 2 weeks there is still positive staining in the neighbouring bone marrow, however, less proliferation is identified in the defect area relative to 1 week samples (Figure 5-15). Noteworthy, no positive staining is seen in the articular cartilage boarding the defect at any time point.

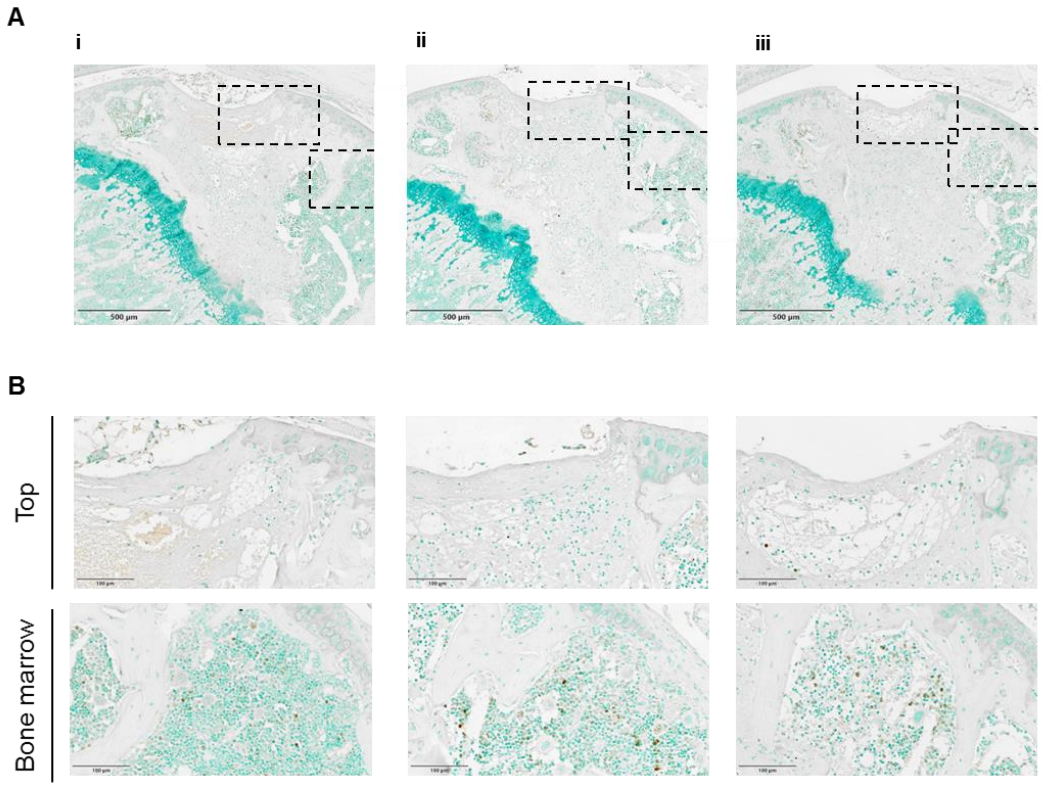

Figure 5-13 – Ki67 staining of osteochondral defects at 24 hours
Sagittal sections of the patella groove at 24 hours after the generation of an osteochondral defect stained by immunohistochemistry for Ki67. 5x images (A) and 40x images (B) of three mice (i, ii and iii) showing the top region of the defect and an area of neighbouring bone marrow cavity. Brown DAB staining identifies positively stained cells. Nuclei are counterstained with methyl green. Black arrowheads indicate positive staining in the top region. Scale bars indicate 500 µm (A) and 100 µm (B).

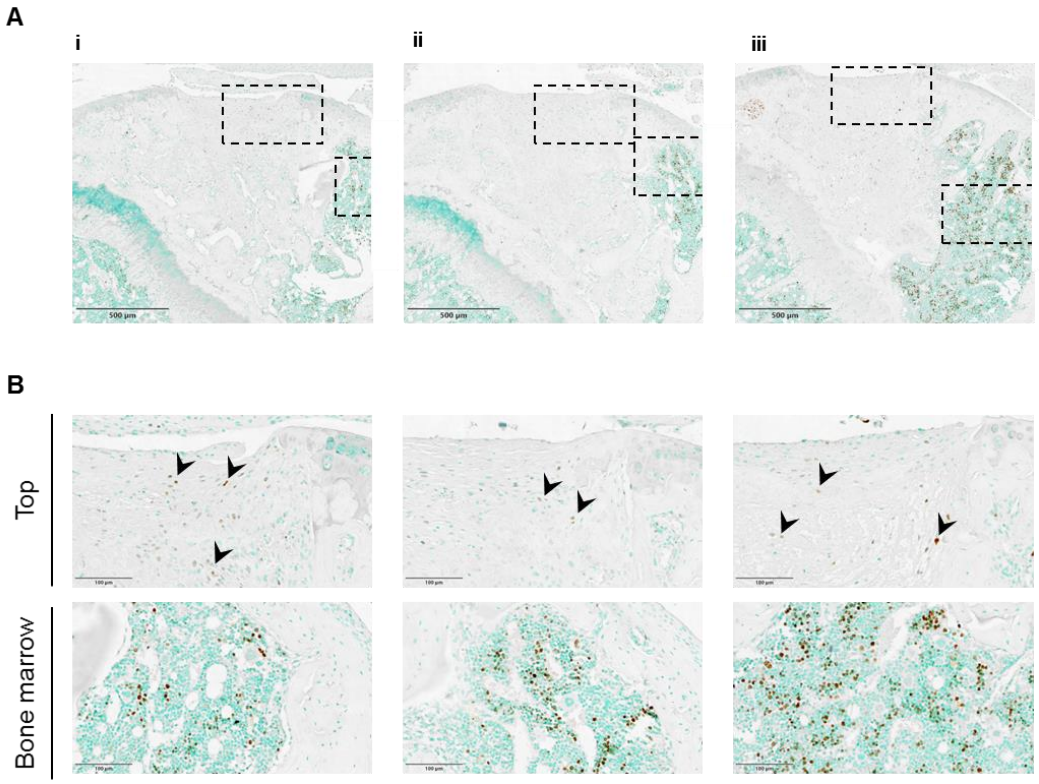

Figure 5-14 – Ki67 staining of osteochondral defects at 1 week
Sagittal sections of the patella groove at 1 week after the generation of an osteochondral defect stained by immunohistochemistry for Ki67. 5x images (A) and 40x images (B) of three mice (i, ii and iii) showing the top region of the defect and an area of neighbouring bone marrow cavity. Brown DAB staining identifies positively stained cells. Nuclei are counterstained with methyl green. Black arrowheads indicate positive staining (B Top). Scale bars indicate 500 µm (A) and 100 µm (B).

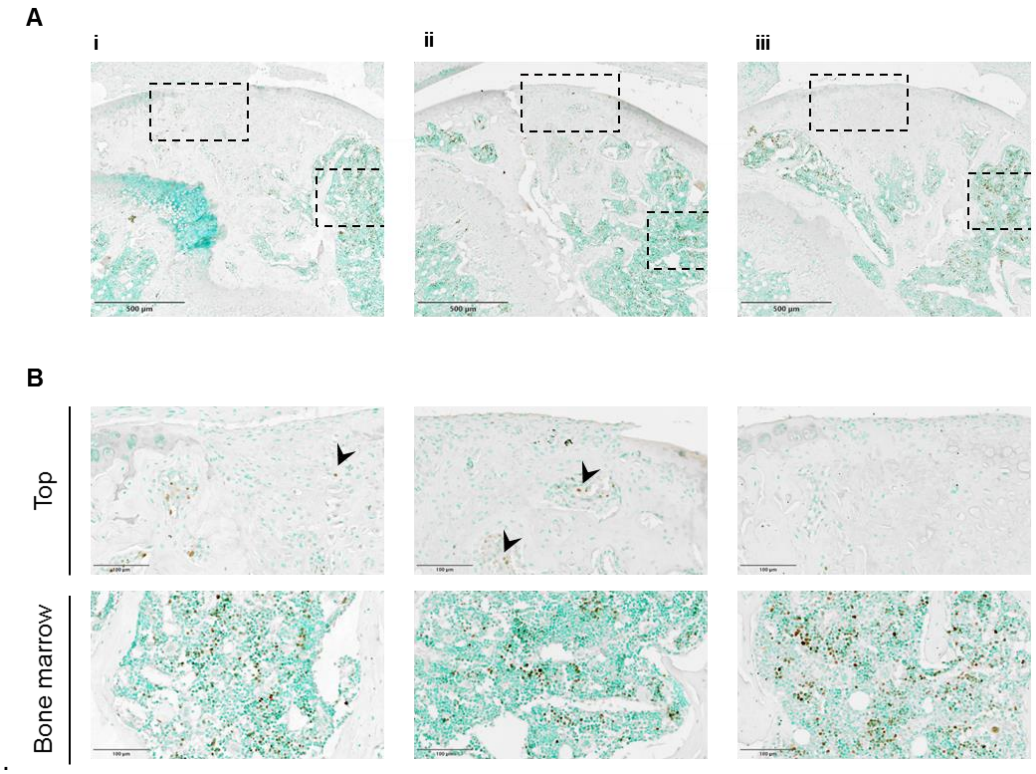

Figure 5-15 – Ki67 staining of osteochondral defects at 2 weeks
Sagittal sections of the patella groove at 2 weeks after the generation of an osteochondral defect stained by immunohistochemistry for Ki67. 5x images (A) and 40x images (B) of three mice (i, ii and iii) showing the top region of the defect and an area of neighbouring bone marrow cavity. Brown DAB staining identifies positively stained cells. Nuclei are counterstained with methyl green. Black arrowheads indicate positive staining (B Top). Scale bars indicate 500 µm (A) and 100 µm (B).

5.7.5.2. Identification of neutrophils and monocytes

Neutrophils were identified using a NIMP antibody that is highly specific for murine Ly-6G and Ly-6C proteins. These cells were observed within the defect at 24 hours after surgery but were not present in 1 and 2 week specimens (Figure 5-16).

The protein CD68 is highly expressed by cells in the monocyte lineage. Using an antibody against CD68, monocytes were identified in the repair tissue of the osteochondral defects at 1 week and 2 weeks throughout the defect tissue (Figure 5-17. Minimal staining however was detected at 24 hours after surgery.

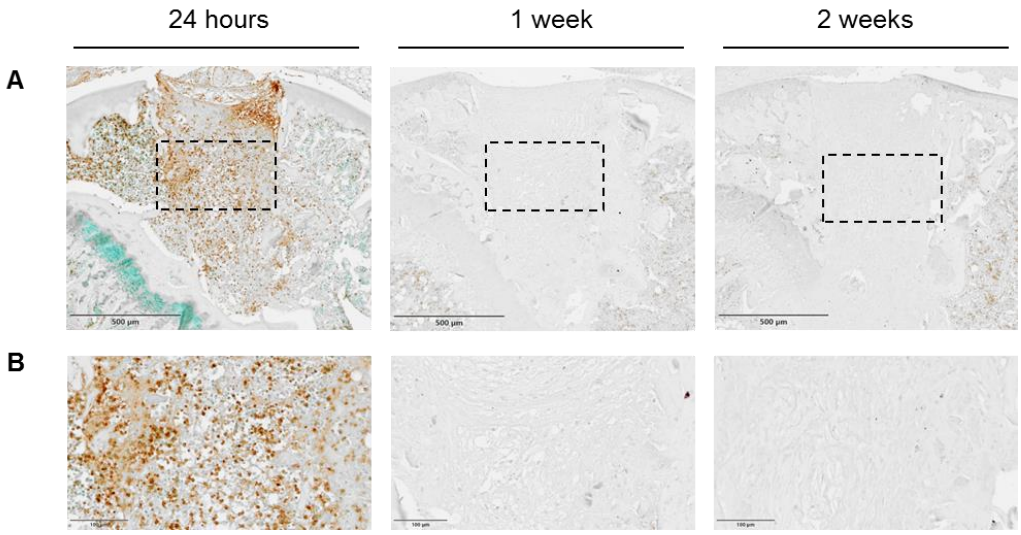

Figure 5-16 – NIMP staining of osteochondral defects for the identification of neutrophils
Sagittal sections of the patella groove at 24 hours, 1 week and 2 weeks after the generation of an osteochondral defect stained by immunohistochemistry for NIMP. Representative image shown from three mice per time point. Brown DAB staining identifies positively stained cells. Nuclei are counterstained with methyl green. Scale bars indicate 500 µm (A) and 100 µm (B).

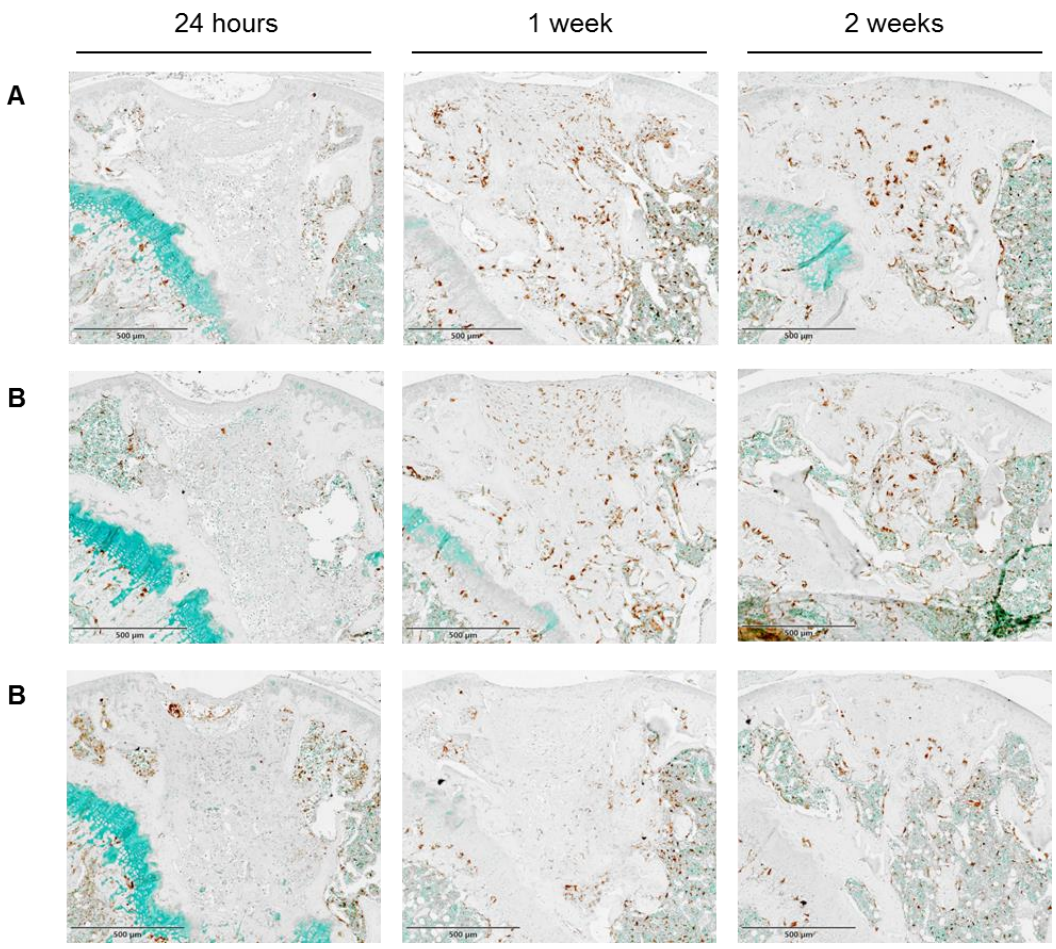

Figure 5-17 – CD68 staining of osteochondral defects for the identification of monocytes
Sagittal sections of the patella groove at 24 hours, 1 week and 2 weeks after the generation of an osteochondral defect stained by immunohistochemistry for CD68. Brown DAB staining identifies positively stained cells. Nuclei are counterstained with methyl green. Images of three mice per time point (A, B and C). Scale bars indicate 500 µm.

5.8. Discussion

Traumatic articular cartilage lesions can lead to pain and the development of osteoarthritis (OA). Bone marrow stimulation techniques such as microfracture are used clinically in an attempt to repair cartilage damage and delay the onset of OA. This technique however does not have consistent outcomes and commonly forms a repair tissue lacking the properties of the original hyaline cartilage. The therapeutic development of microfracture to improve the quality and quantity of repair tissue is currently hindered by a lack of robust models for the analysis of the molecular pathways involved. Furthermore, the mechanism and key cells types involved in osteochondral repair are not well understood.

5.8.1. Development of an osteochondral surgical defect model

Pre-clinical animal models are an important stage in the testing of novel therapeutics and treatment strategies. Whilst larger animals are more comparable to humans regarding joint size and articular cartilage thickness, smaller animals offer the advantage of more reproducible changes though higher throughput. Mice in particular offer the opportunity for detailed molecular and mechanistic studies, through the use of genetically manipulated animals.

The model developed here was designed to be a full thickness osteochondral defect penetrating into the bone marrow of the distal femur. By developing a reliable device to create the surgical defect with a stopper to control the depth, a consistent size of defect was generated as seen by analysis of specimens at the 24 hour time point. Serial histological sections were quantified for the cross-sectional width, depth and area of the defect and the maximum value for each parameter recorded. These values showed consistency with coefficients of variation (CVs) all less than 7%.

The defects occupied on average 43% of the patella groove and by routine observation of the articular cartilage surface appeared to be located centrally within the groove. However, whilst centrally located, the angulation of the defect was not initially controllable. An additional confounding factor was the technical difficulty encountered to orientate samples at an angle so that they were cut on exactly the vertical sagittal plane. In one animal at 24 hours and another at 1 week it can be observed that the growth plate is not flat, an anatomical feature which is seen at the midline of the patella groove suggesting true vertical sectioning was not achieved. These challenges were acknowledged during sample processing and although they may have influenced measurements of the defect size, by measuring across serial sections this should have been limited.

A histological scoring system, the modified Pineda score, was used to quantify the repair of the defect and demonstrated the formation of new tissue over time. Improvements in the repair score were seen up to 4 weeks although variation between animals was

apparent. Previously, Fitzgerald et al. (2008) noted a decrease in cartilage repair scores between 6 and 12 week after creation of an osteochondral defect in female MRL/MpJ mice. Interestingly, this might suggest that whilst repair is achieved initially, the cartilage is not maintained long term. This lack of long-term integrity is a feature seen in human patients after microfracture surgery (Bark et al., 2014). Studies following mouse osteochondral defects to a later time point are required to confirm whether osteochondral repair tissue in this model significantly deteriorates as the mice age further. Nonetheless, the model may provide an opportunity to understand why human microfracture fails to generate articular cartilage with long-term durability and further aid the development of therapeutics to improve outcomes.

The Pineda scoring system also highlights the increase in variability in repair at later time points. Whilst the bone and bone marrow repair appears consistent across animals, articular cartilage repair varies. One feature that could lead to variation in healing between animals is the level of defect bleeding that occurred during surgery, as some defects visibly bleed whilst others did not. The clinical microfracture technique uses an awl to push down into the subchondral bone, and like the needle used here, this results in the compaction of bone. Unlike drilling, the use of an awl, or needle here, leads to the compaction of bone lining the defect potentially limiting or blocking the supply of blood and access to the bone marrow compartments, as seen by Chen et al. (2009) in a rabbit model. When it is considered that cells of the bone marrow are thought to be the key to successful repair, the blocking off of this tissue may be a contributing factor to some defects healing better than others.

A depth of 0.6 mm was chosen during model development for the defect depth. This depth was deemed suitably deep to penetrate through the articular cartilage, through the subchondral bone plate and into the bone marrow cavity. However, measurements of defect depth demonstrate that in fact defects were over 1 mm deep. This highlights a potential discrepancy in the needle stopper design. Either the stopper was place too high on the needles exposing a large proportion than intended or the stopper may have slipped during the curing of the glue after fixation to the needle. Whilst deeper than intended the coefficient of variation between the three animals measured at 24 hours was less than 5% indicating consistency in the depth.

Even though consistent, the increase in depth from that intended led to the disruption of the femoral ephyseal growth plate in several animals. It should also be noted that this might have been exacerbated by the inability to control the angle at which the needle entered the patella groove. The growth plate contains proliferative and hypertrophic chondrocytes and is vital for bone growth during development. By disrupting this structure it is possible that cells from the growth plate were liberated and played a role in the repair tissue. Interestingly, looking at the specimens regeneration of the broken growth plate

was not observed, an observation seen in patients who suffer growth plate fractures whilst children (Chung and Xian, 2014). This results in the diaphysis and ephyseal bone marrow compartments remaining linked and, as well as the cells of the growth plate, this could alter the repair mechanism and most importantly its success. One should note however that in the patient population who acquire a cartilage lesion the growth plate is already closed and replaced with bone.

Further, a number of factors mean that the osteochondral defect generated here is not a directly comparable model of the microfracture technique. Firstly, a cartilage lesion through traumatic injury will likely induce a level of inflammation in the joint (Lieberthal, Sambamurthy and Scanzello, 2015). Here, defects were generated in wild type mice with previously healthy joints and no underlying level of inflammation. Secondly, whilst the patella groove offers a location of relatively easy access and uniform thickness to induce an osteochondral defect, this location is not the classical location at which osteochondral defects can usually be found in patients. Commonly they occur in the femoral condyles an anatomical area too small in mice for the creation of a defect using this method. There is a clear difference between these two anatomical locations in terms of the loading forces that they are exposed to. Mechanical load and shear forces are thought to be significant contributing factors to the repair potential of clinical defects. For example in joint distraction, where articulating surfaces are separated removing direct mechanical loading, cartilage repair is reported to improve (van der Woude et al., 2017). For these reasons, the repair of the osteochondral defects generated here are not absolutely equivalent to microfracture treatment in a clinical setting. Nonetheless, the model may provide insights into the key cellular players and biological mechanisms in the repair process.

5.8.2. Wound healing pattern

By understanding the healing of osteochondral defects and the cells involved in the repair process, it is hoped that insight into potential therapeutic targets can be obtained. The healing of wounds is known to follow a series of coordinated biological events and the sequence is best characterised in the repair of the skin. The process of osteochondral healing is less well defined but it is probable that it follows a series of defined steps. The first stage of wound repair irrespective of the tissue is the formation of a blood clot following the damage of local blood vessels. This results in a haematoma composed of a fibrin plug that traps proteins and cells and acts as a temporary scaffold to allow migratory cells to move in and around the wound.

5.8.2.1. Inflammatory cells

At 24 hours the osteochondral defect in this study is seen to have the open fibrous structure, indicative of a haematoma, through which cells are spatially distributed and clusters of red blood cells are seen trapped. Through immunohistochemistry staining,

neutrophils were confirmed to be a predominant cell type. These cells are known to arrive at sites of damage within the first hour where they phagocytose debris and secrete proteases to break down damaged tissue. Subsequently neutrophils die via apoptosis at around 2 days and consistent with this there is a loss of neutrophil staining at 1 week, at which time macrophages are observed to become a predominant cell type. These early stages follow the sequence of events previously described in other tissues (Shah et al., 2012).

Damaged tissue within the defect created in this study included fragments of bone and cartilage, which were seen clearly at 24 hours and 1 week. The pieces of proteoglycan rich matrix within the defect are likely to originate from the articular surface or the broken growth plate. These fragments were absent however in the 2 week samples. This could indicate the clearance of tissue debris by phagocytic cells such as macrophages.

In addition to this role, macrophages are thought to have a vital role in wound healing by inducing other reparative processes such as the induction of angiogenesis and the laying down of new ECM. Furthermore, these cells are highly plastic and can change phenotype influencing the inflammatory status of their surrounding microenvironment depending on exogenous or endogenous stimuli to which they are exposed. A more reparative phenotype, commonly referred to as M2 macrophages, is thought to facilitate proliferation and angiogenesis within tissues where as a more inflammatory phenotype, M1, is thought to exacerbate inflammation and classically have a role in the response to pathogens. Whilst the results here demonstrate that macrophages are present in osteochondral repair tissue, the inflammatory status has not been investigated. It is likely that there is a temporal change in the phenotypes of macrophages, a hypothesis supported by observations in the analysis of fracture repair in long bones. Schlundt and co-workers. (2015) demonstrated that inflammatory M1 macrophages are present during the initial healing but that they are replaced by M2 macrophages when repair tissue is formed (Schlundt et al., 2018). This switch is important as prolonged inflammation and unsuccessful healing are associated with prolonged presence of pro-inflammatory macrophages (Claes, Recknagel and Ignatius, 2012).

Previous studies of osteochondral repair models in mice have compared super-healing strains, such as MRL/MpJ mice to the poor healing strain used here, C57BL/6 (Fitzgerald et al., 2008; Mak et al., 2015). These studies have shown that the super-healing strain has better outcomes and these has been partly explained by an impaired inflammatory response in this strain. Whether this correlates to the balance of M1 and M2 macrophages during the repair process and the relative levels of pro- and anti-inflammatory factors released by these cells is yet to be explored. Therefore, the mouse model described in this chapter provides the opportunity for investigation in this area and the potential of therapeutics to drive specific macrophage phenotypes.

5.8.2.2. Proliferation

Classically the next stage of wound repair after the inflammatory phase is defined as the proliferative stage. During the proliferative stage endothelial cells are attracted to the wound site by chemotaxis in response to the release of angiogenic factors by other cells. This leads to the tissue being interspersed with small blood vessels. From morphological analysis of toluidine blue / fast green staining, at 1 week red blood cells can be identified within the repair tissue at the defect site but whether these are remnants of the haematoma or the formation of new blood vessels would require endothelial localisation by immunohistochemistry. Attempts were made to stain for blood vessels using antibodies against CD34 and CD31 (data not shown), however further optimisation of the staining process using other antibodies is required.

Surprisingly, high levels of proliferation did not appear at any of the time points assessed within the defect site, as assessed by Ki67 staining which marks all cells except those in resting G0 phase. This may suggest that within the defect there is minimal expansion of cell populations and rather that cells migrate into the defect from the surrounding area. This is supported by positive staining for increased proliferation in the bone marrow cavities surrounding the defect at 1 and 2 weeks, suggesting that the immune cells neighbouring the defect proliferate in response to the neighbouring trauma.

There is evidence from published *in vitro* and *in vivo* studies that demonstrates that chondro-progenitors in the superficial cartilage zone can rapidly proliferate and migrate over an injured cartilage surface (Seol et al., 2012). In this study some animals did show extension of neighbouring articular cartilage across the defect. On the other hand, another explanation could be that this cartilage is actually the original articular cartilage that was not sufficiently removed during surgery. The relatively blunt needle used to generate the defect here may have been insufficient in making a clean cut at the cartilage boundary in some animals. Furthermore, no proliferation (marked by Ki67 staining) was identified in chondrocytes of the intact articular cartilage neighbouring the defect created in this study. This discrepancy with previous literature where activation of chondrocytes proliferation was observed could be due to differences in the type and extent of cartilage trauma. For example, Seol et al., 2012 saw the proliferation and migration of chondrocytes after impaction damage to cartilage whereas bone marrow stimulation trauma, leads to a lack in response by neighbouring chondrocytes as seen here or in other studies (Shapiro, Koide and Glimcher, 1993; Eltawil et al., 2009).

A further argument against the hypothesis of chondrocytes initiating the repair of articular cartilage from the intact boundaries is the lack of integration seen in the defects. This is regarded as one of the biggest limitations of therapies such as microfracture. It is thought that defects fail as the lack of a smooth and seamless integration between the two articular cartilage interfaces is lacking and collagen fibres do not cross the boundary. Polarised

light imaging in the work presented here identifies collagen fibres perpendicular to the surface within the defect region at 4 weeks. As only one animal was analysed by this method, further work is required to examine if collagen fibres cross the boundary.

5.8.2.3. Changes in the extracellular matrix

The extracellular matrix of the defect changes overtime as cells remodel the defect site. As discussed, a fibrin scaffold is initially formed as blood and bone marrow clot within the defect. Collagen is subsequently deposited forming a fibrous network around which new tissue formation occurs. To this end, it has been proposed that the quality of the initial clot formed, may define how successfully the process progresses (Paletta, Arnoczky and Warren, 1992). In this study, a significant amount of matrix remodelling took place within the first 4 weeks of osteochondral defect repair.

One extracellular protein that is laid down early in wound repair is type VI collagen (Oono et al., 1993). In the osteochondral defect generated here, this form of collagen is already present at 1 week (not assessed at 24 hours). Type VI collagen is a non-fibrillar collagen which encourages the attachment of osteoblasts (Izu et al., 2016) and proliferation, integrity and attachment of chondrocytes (Smeriglio et al., 2015). This collagen protein therefore has an important role in the normal homeostasis of osteochondral tissues as well as their repair. The deletion of this protein in mice has been shown to lead to an accelerated development of age-related osteoarthritic joint degeneration, reduced bone mineral density and altered mechanical properties of the chondrocyte pericellular matrix (Alexopoulos et al., 2009). The cells responsible for laying down this protein have not been identified, however, the importance of this protein would make them a target for therapeutic intervention to improve repair outcomes.

Later in the healing of osteochondral defects, collagens specific to bone and cartilage tissue, type I collagen and type II collagen respectively, are laid down. Here, collagen type II was assessed by immunohistochemistry. Commonly this assessment is used to define the quality of the repair tissue as 90% of articular cartilage is made up of this protein. Interestingly, at 2 weeks type II collagen was identified in the central portion of the defect below the articular surface. Alongside the observation of cells isolated in lacunae, this suggests the presence of active chondrocytes secreting ECM proteins. Future investigations into the origin of these cells could potential answer a longstanding question within the field of whether bone marrow stromal/stem cells (BMSCs) differentiate to repair bone and cartilage or if another cell population is responsible such as cells derived from the synovium, as proposed by De Bari and colleagues (Roelofs et al., 2017). Furthermore, whether this population of chondrocytes arises from a single cell or multiple cells undergoing differentiation in parallel could be addressed.

Intriguingly, whilst type II collagen was identified in the central and upper regions of the defect during repair, at no time points was this protein identified in the lower portion of the defect. Furthermore, this deeper region appears to reform its original architecture of bone and bone marrow more quickly than the tissue closer to the articular surface. Either this could indicate that chondrocytes at this location were missed between time points or it could suggest a different pattern of repair takes place at this location.

5.8.3. Endochondral or Intramembranous Ossification

As described in the introduction to this thesis (section 1.4), bone forms through two different ossification processes during development, either in the presence or the absence of a cartilaginous scaffold. Although the long bones of the limbs form by endochondral ossification through a cartilage anlage, it has been demonstrated that intramembranous ossification plays a role in the fracture repair of long bones (Marsell and Einhorn, 2011). Evidence gathered in this series of work suggests that both processes may also take place in the repair of osteochondral defects, an observation previously made by Shapiro et al. in 1993 using a rabbit model.

Here, it is observed that the top area of the defect, closer to the articular surface, shows hallmarks of endochondral ossification. Chondrocytes are present below the level of surrounding articular cartilage at 2 weeks and later are replaced with bone marrow and bone by 4 weeks, indicating a transition of the ECM as seen in the long bone development. These observations correlate with those reported in fracture repair where cartilage ‘islands’ are observed within the fibrous tissue of the fracture callas and mark sites of endochondral ossification (Marsell and Einhorn, 2011). Chondrocytes would then transition to hypertrophic chondrocytes and begin to mineralise their surrounding microenvironment. Going forward, to confirm endochondral ossification is the process of bone repair in the model developed here, staining for markers of this transition could be performed such as type X collagen. Additional time points may also be required, between 2 and 4 weeks, to capture the processes that transform a type II collagen rich ECM to that of bone and bone marrow.

In contrast, observations in a sheep model of a 7 mm osteochondral defect by Lydon et al. (2017) reported a lack of chondrocyte islands within the centre of the defect. The evidence shown in this publication indicates that the formation of new cartilage begins at the upper margins of the defect site moving down along the damaged bone that lines the defect before endochondral ossification takes place. The authors suggest that the increased load at the interface with bone relative to elsewhere within the defect results in chondrogenesis of BMSCs at this location rather than in islands dispersed throughout the defect. This therefore perhaps highlights the difference in loading forces within the mouse

osteochondral defect generated here in the patella groove relative to the sheep femoral condyle.

In addition to endochondral ossification, the results from the mouse osteochondral defect technique developed here also showed signs of intramembranous ossification occurring within the defect site. More specifically, within the lower region of the defect cuboidal osteoblasts that secrete bone matrix were identified. Additionally, by 2 weeks nuclei are observed within bone at the base of the defect whereas they are not present at 1 week. This indicates that osteoblasts have become embedded within the bone matrix they secrete and are now trapped becoming osteocytes. Further supporting the hypothesis that intramembranous ossification rather than endochondral ossification is the key process occurring within the lower portion of the defect is a lack of chondrocytes observed at this location unlike in the more superficial regions. Several differences may account for why intramembranous or endochondral ossification occurs within the different regions. For example, mechanical forces (Szarko and Xia, 2012) and oxygen levels (Zhou, Cui and Urban, 2004) will change with depth, and are known to alter repair processes.

The observation of intramembranous ossification correlates with observations made by Shapiro and colleagues (1993) in a rabbit model. The sheep model by Lydon et al. (2017) on the other hand leads the authors to comment that no intramembranous ossification was seen in their model. One possible explanation for this is the variation in the depth of the defect. Whilst not comparable directly, as mice and sheep have different sized joints and articular cartilage thickness, the defect generated here was significantly deeper relative to the cartilage thickness. This might suggest that a deeper defect in sheep may induce intramembranous ossification in the repair of spongy bone located away from the articular surface of the distal femur.

5.8.4. C57BL/6 mice can repair osteochondral defects

The healing potential of mice is known to differ among strains with C57BL/6 mice being widely regarded as poor healers. Commonly the healing of ear notches have been used to assess the healing ability of different mouse strains but studies have observed that the poor capacity of C57BL/6 mice to heal is also present in the healing of osteochondral defects.

Several studies have reported an inability of the articular cartilage of C57BL/6 mice to heal (Fitzgerald et al., 2008; Eltawil et al., 2009). However, in the results shown here we see the regeneration of matrix positive for proteoglycan and type II collagen, both key proteins of articular cartilage. Published studies have demonstrated a lack of these proteins in mice of a similar age and at similar time points after generation of an osteochondral defect similarly located in the patella groove.

One clear difference between the model described here and these other models is the depth of the defect (Eltawil et al., 2009; Fitzgerald et al., 2008). Whilst all studies classified their defects to be osteochondral, from the histology shown in these papers some only minimally enter the subchondral bone. Research has previously demonstrated that good quality bone is needed for good cartilage repair (Gomoll et al., 2010) and as described above deeper defects are hypothesised to repair bone by both endochondral and intramembranous ossification. The increased depth may be the key to improved repair in the C57BL/6 strain although a direct comparative study would be required to conclude this.

At 4 and 8 weeks the animals with the best level of repair also showed over growth above the level of the neighbouring cartilage. The very superficial layer of this repair tissue stained more weakly for proteoglycan but had a high type VI collagen content than the cartilage below it, suggesting it is more fibrous. It would be interesting to use later time points to assess if this fibrous superficial layer is remodelled back to the joint surface over time. Further, whilst cartilage overgrowth is not reported in microfracture patients, there is evidence of subchondral bone overgrowth during the first 12 months post-surgery (Mithoefer, Venugopal and Manaqibwala, 2016). One might speculate that the time points used here are too early to show this, but that with continued endochondral ossficiation the subchondral bone may impede into the articular cartilage zone.

5.8.5. Summary and future directions

Here, a reproducible osteochondral model in C57BL/6 mice has been developed, refining previously published methods (see Table 5-1). This model shows the influx of different cell populations into the repair tissue in a temporal manner and the ability of this strain of mice to regenerate cartilage matrix at the articular surface as observed by restoration of tissue structure, an observation previously not demonstrated (Figure 5-18). Further, it may allude to the benefit of generating defects that penetrate further into the bone and bone marrow.

Going forward this model provides an opportunity to study the mechanism and contribution of cells to osteochondral repair. To date the molecular mechanisms regulating osteochondral repair have been poorly understood due to an inability to identify key cell types in larger animal models. An understanding of how articular cartilage repairs after osteochondral damage is important in order to develop and improve the outcomes of treatments such as microfracture. Importantly the model developed here was generated using the C57BL/6 strain of mice, the background strain for many genetic mouse models. As well as inducible and conditional knock out strains, reporter strains will in the future allow for the role of specific proteins and different cell populations to be elucidated including BMSCs.

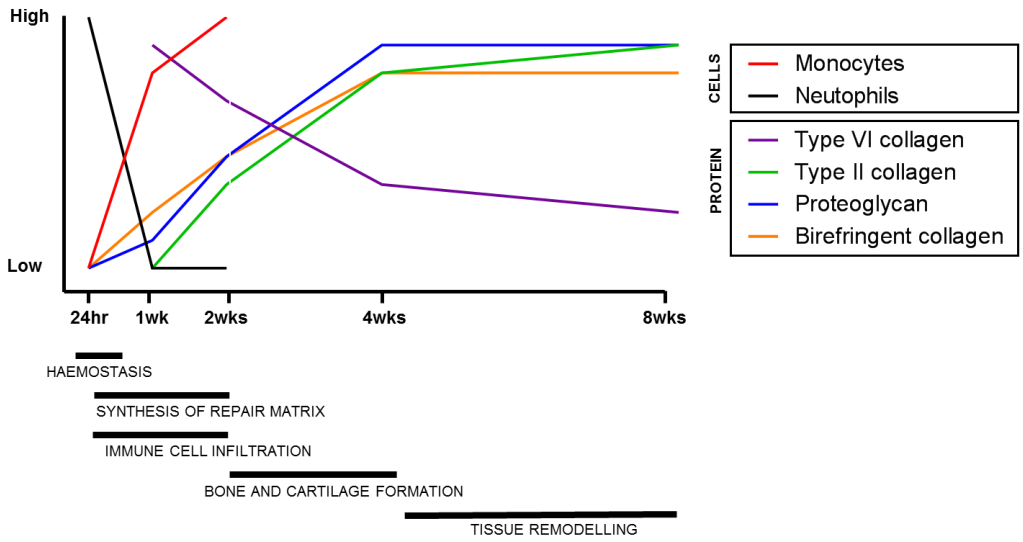

Figure 5-18 – Temporal changes of cell populations and protein abundance in a mouse osteochondral defect
Timeline of changes that occur in cell populations (CD68+ monocytes and NIMP+ neutrophils) and the protein abundance of a surgically induced osteochondral defect in the distal femur of mice.

In the context of this thesis, the model also provides the opportunity to study the effect of G-CSF treatment on repair outcomes. Furthermore, cells that respond to G-CSF are now known to be present in the osteochondral repair tissues, including neutrophils and macrophages. This may in the future allow further insight into the mechanism by which G-CSF aids the repair of bone and cartilage.

6. RESULTS: G-CSF TREATMENT POST SURGICAL TRAUMA INFLUENCES OSTEOCHONDRAL HEALING IN THE MOUSE

6.1. Background and Rationale

Bone marrow mesenchymal stem/stromal cells (BMSCs) are thought to be involved in the repair of surgically induced osteochondral defects. Their exact function, however, is yet to be fully elucidated. Possible roles involve both progenitor and/or a trophic function (Wang et al., 2014). The lack of an ability to identify these cells using a single marker has hindered the clear assessment of their location and function *in vivo*. As a result, few studies have looked at the fate of endogenous BMSCs in contrast to the numerous experiments that trace BMSCs after implantation.

In recent years, the class VI intermediate filament protein nestin has become one of the more commonly used markers to identify BMSCs *in vivo* (Xie et al., 2015). A Nestin-GFP reporter mouse was developed by Migone and colleagues in 2004 allowing the identification of these cells in situ and their isolation ex vivo (Mignone et al., 2004). Nestin positive cells have been validated as a population of BMSCs in both mice and humans capable of both tri-lineage differentiation and the formation of a haematopoietic supportive environment *in vivo* (Isern et al., 2014; Méndez-Ferrer et al., 2010).

Granulocyte colony stimulating factor (G-CSF) has been proposed as a therapeutic agent to aid bone and cartilage repair and has previously shown improved repair outcomes (see section 1.10). However, the mechanism through which this agent acts lack understanding. Currently it is known to influence haematopoietic lineage cells directly and there is evidence that it influences cells of the bone marrow microenvironment indirectly such as osteoblasts and BMSCs (Greenbaum and Link, 2011).

6.2. Aim and objectives

The aim of this chapter is to investigate the role Nestin-GFP labelled cells play during osteochondral repair in the defect model described in the previous chapter and to assess the influence of G-CSF on their response. The primary objective of this chapter was to identify BMSCs *in situ* utilising Nestin-GFP reporter mice. Secondly, the impact of G-CSF on these cells was investigated by analysis of peripheral blood and bone marrow of the spinal vertebrae. It was hypothesised that Nestin-GFP cells are involved in the repair of an osteochondral defect and also respond to systemically administered G-CSF.

6.3. Identification of Nestin-GFP reporter mice

Nine Nestin-GFP reporter mice were genotyped to confirm their expression of GFP under the Nestin promoter. Figure 6-1 A depicts the design of the cassette developed by Migone et al. (2004). Using primer sequences from Migone et al. (2004), GFP expression was confirmed in all mice by using PCR analysis of ear biopsies (Figure 6-1 B). A single mouse had a significant lower abundance of PCR product possibly due to technical reason such as lack of starting material or possibly the animal was heterozygous rather than homozygous - it is not possible to delineate between the two. Further, confocal images of cryo-sectioned spinal cord and femoral bone marrow cavity of a Nestin-GFP mouse, Figure 6-1 C, demonstrated the presence of, and the ability to image, GFP positive cells within both tissues.

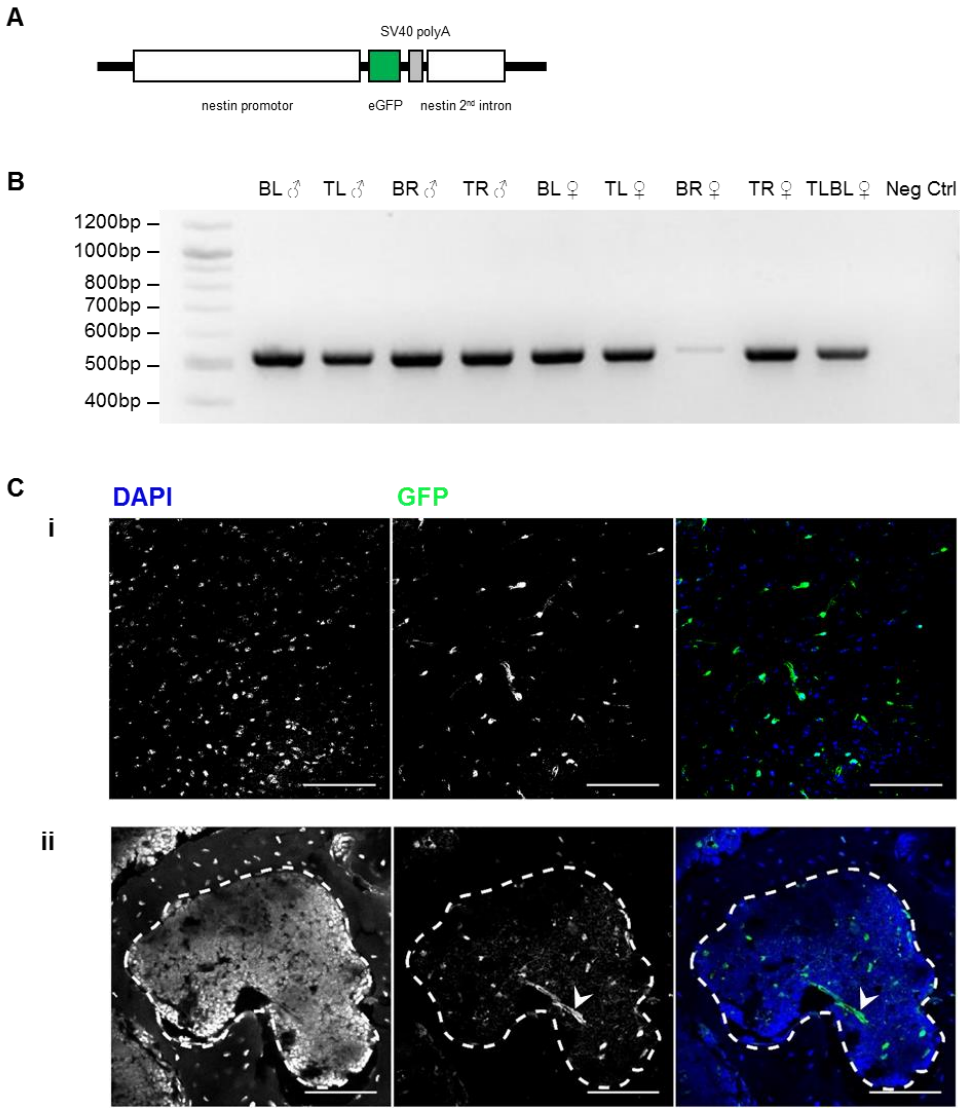

Figure 6-1 – Genotyping and assessment of GFP expression in Nestin-GFP reporter mice.
Mice were assessed for the confirmation of GFP construct insertion and the presence of detectable GFP cells within tissues. (A) Schematic of the Nestin-GFP construct where the enhanced version of GFP (eGFP) has been placed under control of the Nestin promoter and the second intron of the Nestin gene. (B) Image of agarose gel run with the genomic

DNA PCR product to confirm the presence of the GFP insertion, expected fragment of 510 bp. (C) Confocal imaging of cryosections, DAPI nuclear staining (blue) and reporter GFP (green) merged. (i) Spinal cord (ii) femoral bone marrow cavity. Arrowhead highlights a bone marrow Nestin-GFP positive cell. Dashed line indicates bone contours. Scale bars indicate 100 µm.

6.4. Experimental design

The second objective of this chapter was to use the Nestin-GFP reporter mice to assess the effect of G-CSF on BMSCs. Figure 6-2 describes the experimental design used. The nine genotyped mice were divided into three groups of three. All mice underwent osteochondral defect surgery as in Chapter 5. Mice in Group 1 were sacrificed 24 hours after surgery with no G-CSF administration whilst mice in Group 2 and Group 3 were given G-CSF for three days. Group 2 mice were sacrificed 24 hours after the final dose whilst Group 3 mice were sacrificed at 7 days post-surgery.

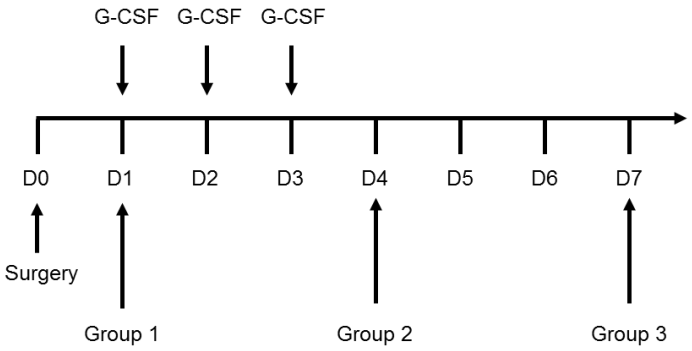

Figure 6-2 - Schematic of experimental approach
Nine Nestin-GFP reporter mice underwent surgery to create a osteochondral defect in their distal femur under the patella groove. Three mice were sacrificed 24 hours (D1) after surgery, Group 1. The remaining six mice (Groups 2 and 3) were given administered G-CSF for three days. Three mice were sacrificed 24 hours after the final injection (Group 2) (D4) and the remaining three mice were sacrificed after a further 3 days, 7 days (D7) post-surgery (Group 3).

6.5. GFP signal is present in the osteochondral defect

Nestin-GFP mice that had undergone osteochondral surgery were sacrificed at 24 hours or 4 days after the procedure and their operated limb prepared for cyro-sectioning.

In Figure 6-3 sagittal sections are shown for the defects are shown. At 24 hours (D1) (Figure 6-3 A) and 4 days ((Figure 6-3 B) after surgery GFP signal was detected within the defect. At both time points spindle-like nestin-GFP cells are observed in the bone marrow cavity (marked by *). However, the appearance of GFP fluorescence in the defect differed as it was more punctate (indicated by white arrowheads) and less associated with discrete cell structure.

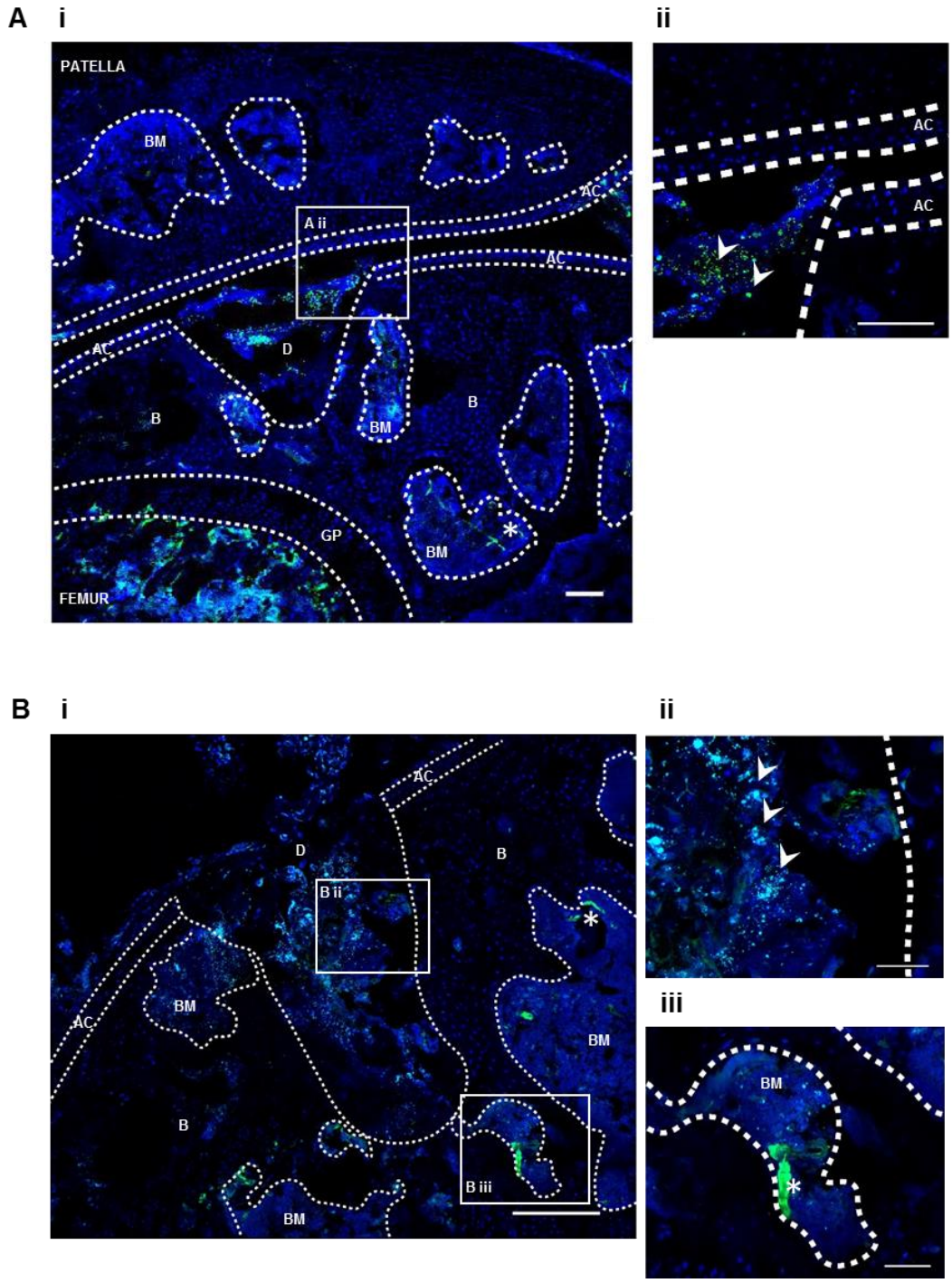

Figure 6-3 – Confocal imaging of an osteochondral defect in Nestin-GFP mice.
Saggital cryo-sections of osteochondral defects at 24 hours (A) and 4 days (B) after surgery were imaged by confocal microscopy. DAPI nuclear staining (blue) and reporter GFP (green) merged. Arrowheads highlight punctate GFP fluorescence within the defect and * indicate spindle-like cells positive for GFP. Dashed line indicates bone and cartilage contours; AC, articular cartilage, B, bone; BM, bone marrow; D, defect. Scale bars indicate (A i and ii) 100 µm, (B i) 50 µm, (B ii and iii) 200 µm.

6.5.1. Change in peripheral blood cell populations following surgery and G-CSF treatment

The most explored action of G-CSF is its ability to mobilise hematopoietic stem and progenitor cells (HSPCs) into the peripheral circulation. Blood samples from sacrificed mice were taken by cardiac puncture and analysed by flow cytometry for the presence of HSPCs using the lineage negative, Sca-1 positive and c-Kit marker panel as previously used in result chapter 1. The results are shown in Figure 6-4 show changes in the proportions of different haematopoietic cell fractions. Firstly, analysis of lineage markers (Figure 6-4 A i) demonstrate a change in the cellular composition of the peripheral blood. Interestingly the lineage positive cells are seen as a single cluster in group 1 and 2 whereas group 3 show sub-populations, this was consistent across the three mice at each time point. Furthermore, the number of lineage negative cells changed but whilst the mean percentage of these cells relative to the total population reduced, there was large variation between the animals in groups 2 and 3, i.e. those post-surgery and G-CSF treatment.

The lineage negative fraction of cells from blood were further assessed for the number of haematopoietic stem and progenitors marker by Sca-1^+ and c-Kit^+ (LSK^+) staining and Sca-1^- and c-Kit^+ ($L^-S^-K^+$) staining respectively. No significant changes were identified but the number of LSK^+ cells was observed to decrease after treatment whilst $L^-S^-K^+$ numbers remained at 8.5 to 11.8%.

6.5.2. Bone marrow cells proliferate following surgery and G-CSF treatment

Ki67 was used to identify cell proliferation in the bone marrow cavities of the distal femoral epiphysis of the right hind leg that had no surgical intervention (contralateral limb) (Figure 6-5 A). A lack of staining was observed in the three animals in group 1 and group 2. However, in group 3 positively stained cells were observed indicative of proliferating cells. Ki67 staining was also performed on the contralateral limb of animals sacrificed at 24 hours and 1 week in the previous chapter (chapter 5). Similarly, this animals show an increase in positively stained cells from 24 hours post-surgery to 1 week (Figure 6-5 B).

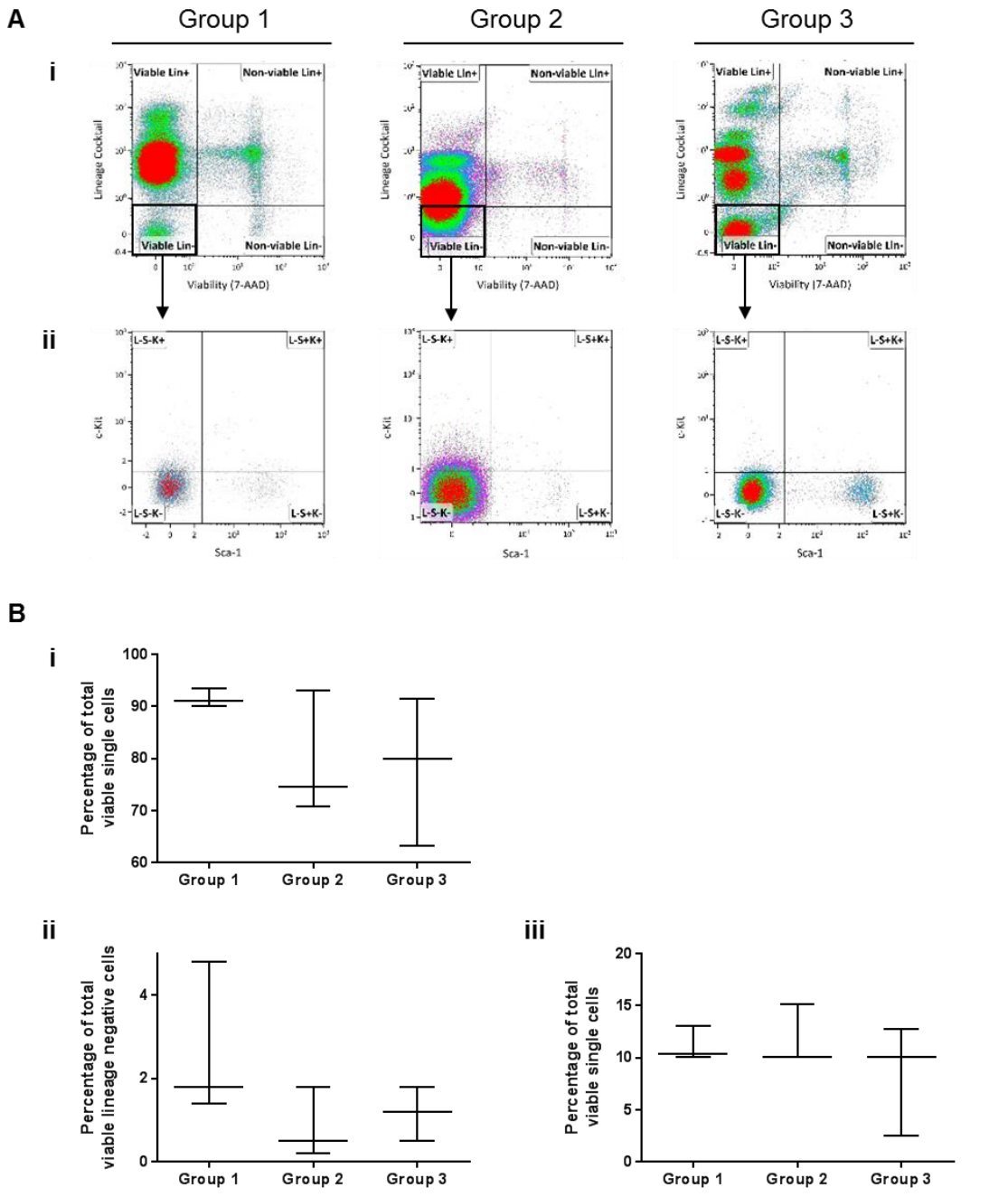

Figure 6-4 – Analysis of peripheral blood cell populations after G-CSF administration

Cardiac puncture peripheral blood samples were analysed by flow cytometry for the expression of mature haematopoietic lineage markers and Sca-1 and c-Kit expression. (A) Cells were identified based on forward versus side scatter area (not shown) and gated (i) on a logarithmic scatter plot for viable lineage positive or negative cells. (ii) Lineage negative cells were serially gated for Sca-1$^-$ and c-Kit$^+$ expression. (B) Graph of the percentage of each population (i) Lineage positive cells as a percentage of total cells, (ii) lineage negative, Sca-1$^+$ and c-Kit$^+$ and (iii) lineage negative, Sca-1$^-$ and c-Kit$^+$. Gates set against unstained controls.

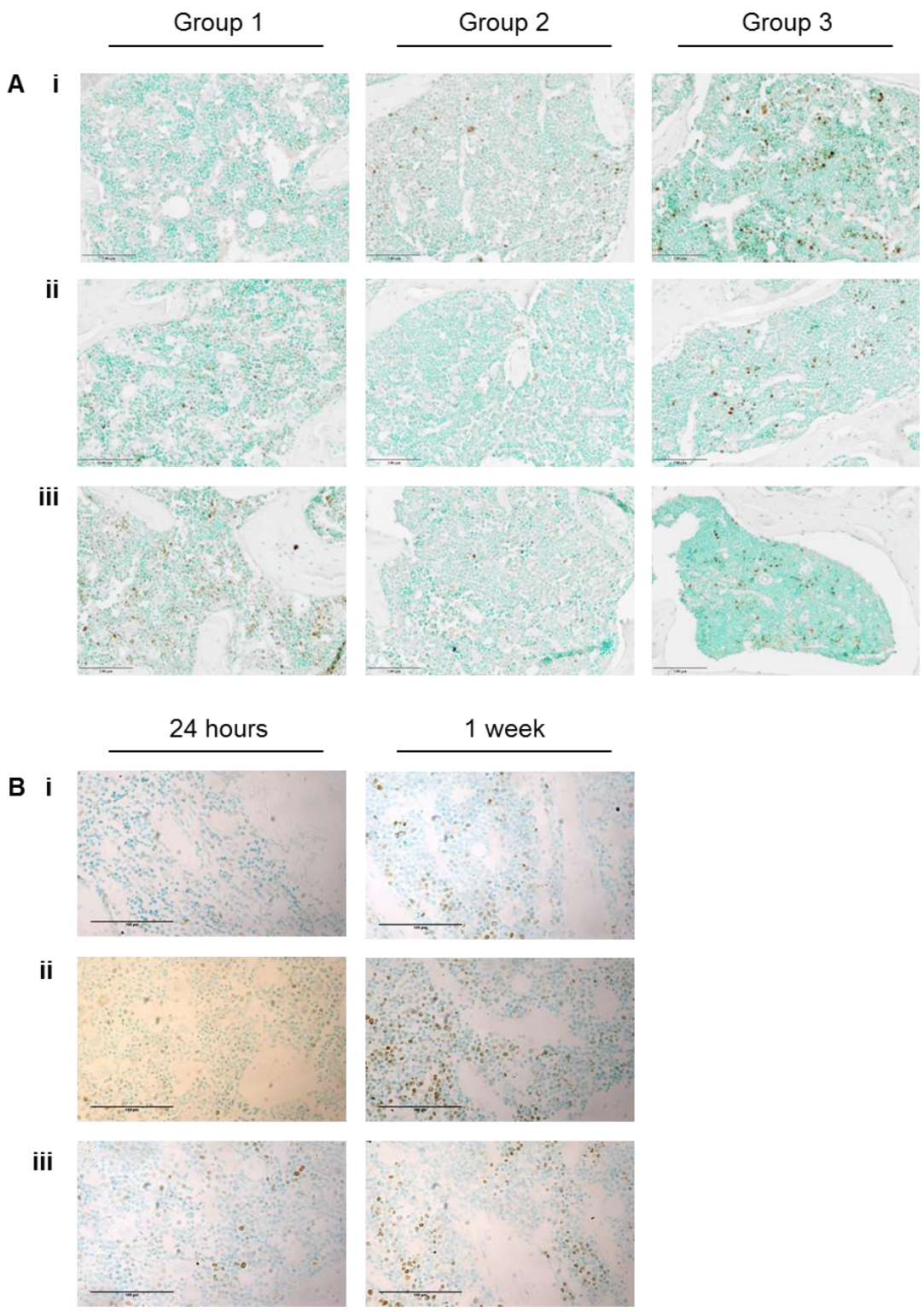

Figure 6-5 – Analysis of cell proliferation in the bone marrow cavity of the contralateral limb
Sagittal sections of the contralateral limb (non-surgical) from each of the three treatment groups were stained by immunohistochemistry for Ki67 (A). This was repeated for the contralateral limbs of the mice sacrificed in chapter 5 at 24 hours and 1 week. Images were taken from the bone marrow cavities in the femoral epiphysis of three animals per group (i, ii and iii). Brown DAB staining identifies positively stained cells. Nuclei are counterstained with methyl green. Scale bars indicate 100 µm.

6.5.3. The number of peripheral blood and spleen GFP$^+$ cells increases following surgery and G-CSF treatment

Peripheral blood samples for all mice were collected by cardiac puncture and analysed by flow cytometry for the presence of GFP$^+$ cells. As shown in Figure 6-1, the spinal cord contains a large number of GFP$^+$ cells and therefore this tissue was used as a positive control showing 12% of cells were GFP$^+$. A significant increase in the number of GFP$^+$ cells was observed in the peripheral blood samples increasing by over 5-fold between groups 1 or 2 and group 3.

GFP staining of spleens demonstrated the presence of GFP in the spleen of animals. Interesting GFP$^+$ spindle-like cells increased in number in the spleen of group 3 animals, whilst only a minimal number of these cells were present in animals in groups 1 and 2 (indicated by black arrowheads in Figure 6-7)

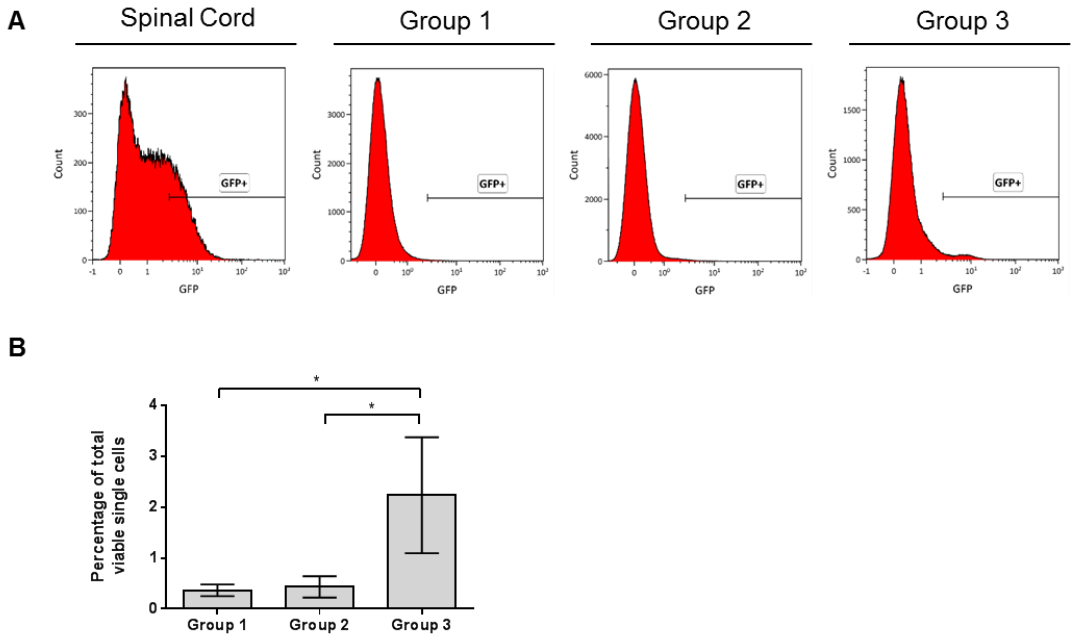

Figure 6-6 – Analysis of Nestin-GFP positive cells in the peripheral blood.
Cardiac puncture peripheral blood samples were analysed by flow cytometry for the expression of GFP. (A) Cells were identified based on forward versus side scatter area (not shown) and gated for the expression of GFP. Cells from the spinal cord were also analysed as a positive control. (B) Graph of the percentage GFP positive cells as a percentage of total cells. Statistical significance was calculated using a one-way ANOVA with Tukey's test for multiple comparisons, with * indicating a $p<0.1$.

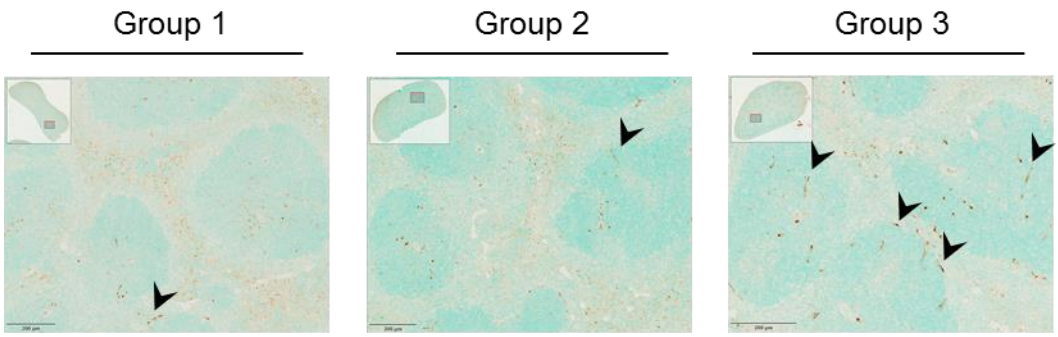

Figure 6-7 – Analysis of Nestin-GFP positive cells in the spleen
Spleens were harvested from all sacrificed mice, processed for paraffin sections and immunohistochemically stained for the GFP. Brown DAB staining identifies positively stained cells. Nuclei are counterstained with methyl green. Black arrowheads indicate positive staining of spindle-like cells. Scale bars indicate 200 µm.

6.5.4. Gene expression changes in GFP$^+$ cells

Bone marrow was isolated from the spinal vertebrae of all mice after the removal of the spinal cord. CD45$^-$ cells were enriched by immunomagnetic depletion of CD45$^+$ cells before FACS isolation of GFP$^+$ cells (Figure 6-8 B). The number of GFP$^+$ cells as a percentage of the total single cells ranged from 0.2 to 3% however, no difference was observed between the groups (Table 6-1). Interestingly, the animal with the ID BR ♀ that showed a weaker band for the presence of the nestin-GFP construct (Figure 6-1) also showed the lowest percentage of GFP$^+$ cells.

Table 6-1 – GFP cells isolated from spinal vertebrae bone marrow

	Animal ID	***% of GFP$^+$ singlets***	***Number of CD45$^-$ GFP$^+$ cells isolated***
Group 1	TR ♂	1.00	13,000
	BL ♀	1.40	33,851
	TLBL ♀	1.70	33,464
Group 2	BR ♂	3.40	19,068
	TR ♀	1.00	92,000
	BR ♀	0.20	31,000
Group 3	TL ♀	0.60	34,000
	TL ♂	3.00	46,000
	BL ♂	1.30	38,000

The CD45$^-$GFP$^+$ cells were analysed by qRT-PCR for the expression of *Runx2, Bglap, Sp7*, and *AdipoQ* (Figure 6-8 C). Large variation was observed between animals in each group and no significant difference in the expression was calculated for *Bglap, Sp7*, and *AdipoQ* transcripts. The expression of *Runx2* however did show an increase in expression with time and a significant difference between groups 1 and 3.

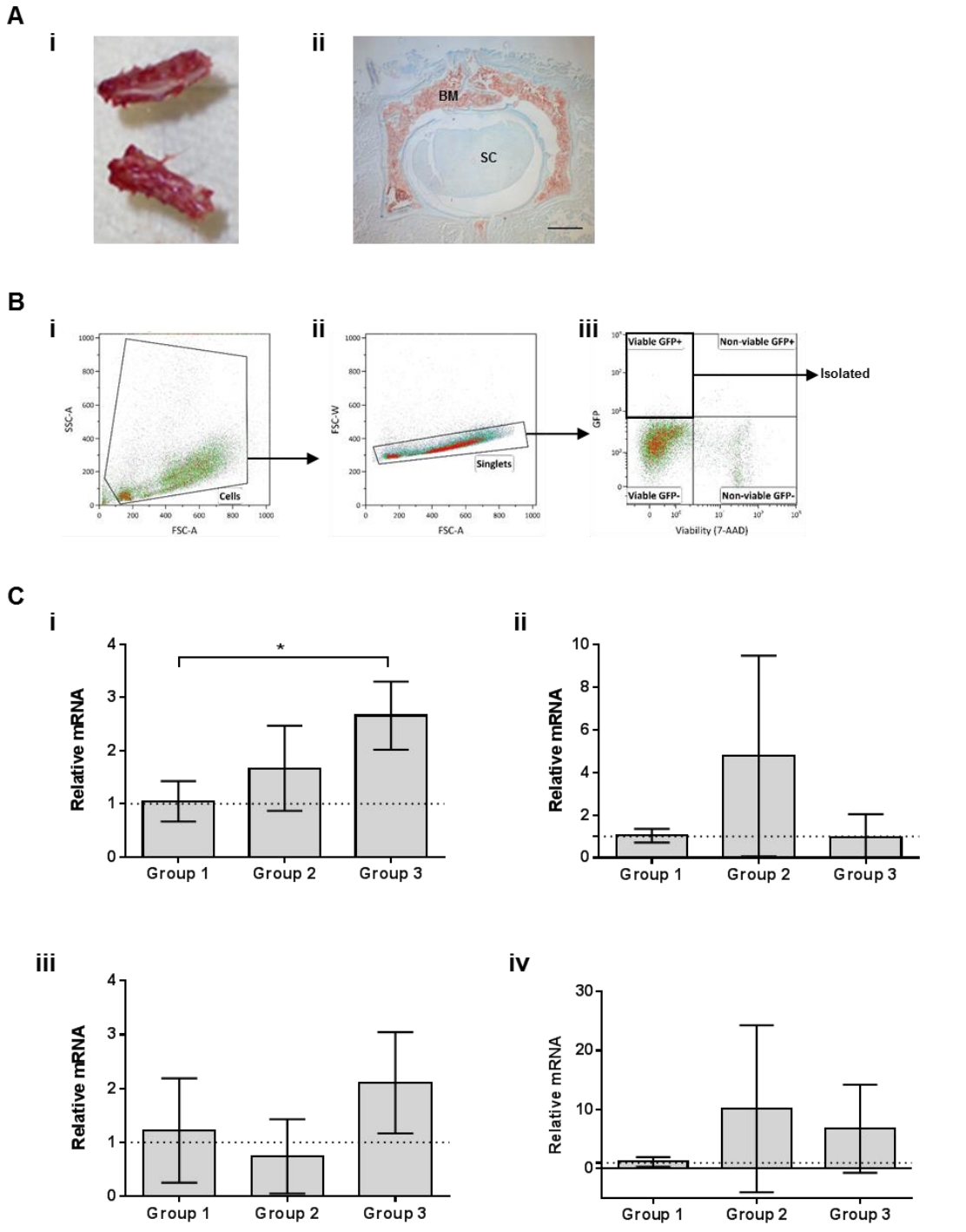

Figure 6-8 – Gene expression analysis of spine bone marrow Nestin-GFP cells.
Bone marrow from spinal vertebrae was isolated and analysed by qRT-PCR. (A) Vertebrae were harvested, and the spinal cord removed. (i) vertebrae pieces, (ii) transverse histological section of a vertebrae stained (Safranin O / Fast green). SC, spinal cord; BM, bone marrow. Scale bar indicates 200 µm (B) CD45- cells were enriched by immunomagnetic depletion and subsequently GFP^+ cells isolated by FACS. (i) Cells were identified based on forward versus side scatter area and (ii) single cells by forward scatter area versus forward scatter width. (iii) Viable GFP^+ cells were isolated. (C) Gene expression analysis for (i) *Runx2*, (ii) *Bglap*, (iii) *Sp7,* (iv) *AdipoQ* normalised to *Hprt*. Error bars indicate the standard deviation of the mean for three animals per group (N=3). Statistical significance was calculated using a one-way ANOVA with Tukey's test for multiple comparisons, with * indicating a $p<0.1$.

6.6. Discussion

The aim of experiments presented in this chapter was to produce preliminary data assessing the role of BMSCs and G-CSF in osteochondral repair. There are two main hypotheses that address the role of BMSCs in the repair of bone and cartilage tissue. Firstly their function as tissue progenitors, which has long been thought of as their primary role. Secondly, the more recently described role in the orchestration and immune-modulation of repair processes through the secretion of trophic factors.

Nestin is an intermediate filament protein that is known as a neural stem/progenitor cell marker and the nestin-GFP mouse model has become widely utilised as a method to identify BMSCs *in vivo* (Xie et al., 2015). In these preliminary studies, a nestin-reporter mouse line was used to elucidate the fate of BMSCs after trauma-induced osteochondral repair.

6.6.1. Are nestin positive cells present in osteochondral repair tissue?

The first question to be addressed was whether nestin positive cells were present in the defect site. Mice were sacrificed at 1 day and 4 days post-surgery and histological sections analysed to identify the presence of nestin positive BMSCs. However, whilst these cells were present in the bone marrow cavities of the distal femur, their identification within the osteochondral defect was inconclusive. The majority of GFP signal appeared very bright and punctate and not in clear cell-associated aggregations as seen in the bone marrow cavities. Importantly, this signal was deemed not to be the autofluorescence of red blood cells commonly seen in fluorescence imaging of vascular tissues, as the vessels within the bone marrow cavities themselves did not reproduce this bright staining. Furthermore, the advantage of using a reporter line removes the possibility of non-specific antibody staining. Therefore, it is concluded that the green fluorescence observed was derived from nestin positive cells but this raises the question of what this punctate fluorescence represents.

6.6.1.1. Cell death

In the early stages after trauma many cells die as a result of the injury, either by necrosis or apoptosis, and either of these processes could be responsible for the fluorescence observed in these experiments. Firstly, the induction of the necrotic pathway in BMSCs would result in the release of the cell's contents into the local environment, including GFP. Secondly, controlled cell death by apoptosis would also likely show punctate green staining as the cell forms and releases apoptotic bodies. Importantly, necrosis might be viewed as detrimental to wound repair by increasing the inflammatory status of the area but is likely a key initial response that triggers the innate immune system to the site of tissue damage. Apoptosis is a regulated cell response and is an important part of the

spatial and temporal coordination of cell events that are responsible for effective wound repair.

Apoptotic cells release membrane-bound extracellular vesicles termed, apoptotic bodies, in a highly regulated process that accompanies the disassembly of the cell cytoskeleton. In addition, apoptotic cells have been reported to release smaller extracellular vesicles that contain 'find-me' signals to attract phagocytes for the clearance of apoptotic cells (Caruso and Poon, 2018). Phagocytes are an important cell type in the early stages of wound repair and the recruitment of these cells is thought to be a key factor in preventing apoptotic cells from undergoing secondary necrosis where they can release potentially damaging pro-inflammatory contents. Investigation into the release of extracellular vesicles by BMSCs has become a key area of research in the understanding of the BMSCs trophic action in recent years (Vonk et al., 2018) but little research has been conducted into the effects of dying BMSCs on cell and tissue specific processes.

As well as the release of 'find-me' signals, other downstream events could be induced by phagocytosis itself. As discussed in the previous chapter macrophages are important phagocytic cells in the osteochondral defect being a predominant cell type at 1 week after their migration into the defect. Phagocytic cells have the ability to make a critical decision as to whether or not initiate an immune response depending upon the molecules released by and/or exposed on the dying cells. Phagocytes can ultimately either actively suppress or elicite inflammation (Arandjelovic and Ravichandran, 2015). Macrophages are well accepted to have pro-inflammatory and anti-inflammatory phenotypes but whether this is a transient state, or distinct subtypes remains unclear. *In vitro* co-cultures have shown the ability of BMSCs to down-regulate pro-inflammatory responses in macrophages (Németh et al., 2009; Chiossone et al., 2016) and extracellular vesicles play a part in this (Hyvärinen et al., 2018). One can hypothesise that the phagocytosis of apoptotic BMSC fragments could induce a more immune-suppressive response thought to be of benefit to wound repair. For example, early apoptotic leukocytes have similarly been reported to deliver immunosuppressive signals to dendritic cells (Morelli, 2006). Moreover, in an animal model of graft-verus-host-disease, Galleu and colleagues (2017) demonstrated that the engulfment of apoptopic BMSCs by phagocytes led to the production of indoleamine 2,3-dioxygenase, a marker of immunosuppression (Galleu et al., 2017). Therefore, nestin BMSCs could modulate the early wound microenvironment by undergoing apoptosis.

There is evidence in the published literature that exogenous BMSCs aid the repair of osteochondral defects however, they disappear over time from the wound site. The mechanism of this cell loss, whether through cell death or migration remains unknown. For example, de Windt and colleagues (2017) published a first in man trial where autologous chondrons (chondrocytes isolated with their pericellular matrix) were

transplanted with allogenic BMSCs. The clinical trial reported that, whilst 80 to 90% of the cell transplanted were allogenic BMSCs, they were not detectable in the repair tissue at 1 year, as assessed by DNA analysis (de Windt et al., 2017). Similarly, in an osteochondral model by Mak and colleagues (2016), synovial mesenchymal stem cells (sMSCs) were transfected with GFP using lentivirus and injected intra-articularly. This study showed GFP^+ cells were detectable in the defect at two weeks but not at four weeks. The authors suggest the "loss" of the sMSCs is suggestive that the cells may differentiate (silencing the GFP) but also that they migrate away from the defect area or die. Overall, both Mak and Windt with their respective colleagues' present results that could be suggestive that implanted BMSCs die within the repair tissue and do not contribute directly to repair. The data presented in this chapter may represent this response in the endogenous BMSCs marked by nestin-GFP.

6.6.2. Increase in BMSCs in the peripheral circulation

One confounding factor about the design of this study is the delineation between effects of the surgical procedure and the exogenous administration of G-CSF. Data presented here demonstrates an increase in the number of GFP positive cells in the systemic circulation as assessed by flow cytometry analysis of peripheral blood. Nestin positive cells have previously been reported to increase in number systemically as a response to trauma (Yang et al., 2015) but BMSCs are also known to increase in the peripheral circulation in response to G-CSF (Lund, Baso and Orchard, 2006).

6.6.2.1. Nestin-GFP cell response to trauma

BMSCs marked by nestin positivity have been reported to respond to trauma by an increase in their number in the peripheral circulation and bone marrow (Yang et al., 2015), supporting the hypothesis that creation of an osteochondral defect leads to the increase seen here. Furthermore, BMSC are recruited to sites of injury (Rustad and Gurtner, 2012; Yang et al., 2015). Due to limited animal numbers, GFP signal was only analysed at 1 and 4 days post-surgery and at these time points, only bright punctate staining was observed within the defect. Going forward, it would be of interest to use later time points to assess if GFP signal similar to that seen in the bone marrow, which is more cell associated, is observed within the defect site. If observed this would suggest that nestin-BMSCs can move through the extracellular matirx scaffold into the wound during the repair process as observed for other cell types e.g. monocytes, as described in the previous chapter and synovial MSCs in Mak and colleagues' (2016) study.

It is important to note that nestin positive cells are not confined to the bone marrow and have been located in many tissues including the central nervous system where nestin marks neural stem cells (Xie et al., 2015). It is not possible to say if the GFP positive cells identified in the peripheral blood in this study are derived solely from haematopoietic

tissues or the multiple tissues where these cells reside. For example, an increase in GFP positive cells was seen in the spleen in the present study. Results from Yang et al. (2015) indicate that nestin positive cells increase in the bone marrow after skin injury and using a chimeric mouse model they show that at least a proportion of these cells are derived from the bone marrow. This therefore supports a hypothesis that the increase in peripheral blood GFP signal here at least partly is derived from the mobilisation of bone marrow nestin positive cells.

6.6.2.2. Nestin-GFP cell response to G-CSF

The bone marrow microenvironment is known to respond to the systemic administration of G-CSF. It leads to both increased hematopoietic stem cells (HSCs) numbers and importantly their mobilisation from the bone marrow into the bloodstream. The mechanism of action of this cytokine is not well understood but it is known to disrupt the interactions between haematopoietic stem and progenitor cells (HSPCs) and cells of their bone marrow microenvironment. BMSCs are known to have a role within this microenvironment but the action of G-CSF on these cells has not been thoroughly explored except that it is known to cause an increase in their number in the peripheral circulation (Lund, Baso and Orchard, 2006).

Nestin positive BMSCs specifically are components of HSC niches and G-CSF treatment selectively downregulates the HSCs maintenance gene CXCL12 in these cells (Mendez-Ferrer et al., 2010). However, whilst this suggests that G-CSF affects nestin positive BMSCs, their mobilisation is not seen (Yang et al., 2015) unlike the global BMSC population (Lund, Baso and Orchard, 2006). This can be explained by the heterogeneity of the BMSCs as nestin positive cells only represent a fraction of the total BMSC population. Pdgfrα and Sca-1 (Morikawa et al., 2009), and Leptin receptor (Zhou et al., 2014), are other mouse *in vivo* markers associated with distinct subgroups of BMSCs.

In summary, whilst both trauma and G-CSF treatment could be responsible for the increase in numbers of GFP^+ cells in the peripheral blood, data from the literature suggest that the effect of systemic signals from the injured osteochondral environment may predominate. In the future, analysis of GFP^+ cell numbers within the bone marrow in animals with only one of the variables, osteochondral defect surgery or G-CSF treatment, would allow a clearer understanding of nestin positive cell dynamics in this context.

6.6.3. G-CSF and the expression of osteogenic differentiation genes in nestin positive cells

Whilst the cause of an increase in GFP signal in the peripheral circulation requires further exploration, in 2010 Mendez-Ferrer and colleagues (in supplementary material), presented results which showed a change in the gene expression profile of bone marrow nestin positive cells after G-CSF treatment. The authors showed a significant decrease in

the expression of differentiation genes by these cells following G-CSF treatment (Méndez-Ferrer et al., 2010). In data presented here, cells of the same phenotype were isolated from the bone marrow of the spinal vertebrae and expression of differentiation associated genes investigated. Assessment of *AdipoQ* expression was performed both here and in the aforementioned published work. Whilst Mendez-Ferrer and colleagues showed a decrease in expression of this gene, the expression changes showed large variation between animals in the data described here. Increased transcripts of this gene are indicative of adipogenic differentiation.

There is strong evidence of a relationship between bone and G-CSF treatment and therefore osteogenic genes were also investigated. In both mice and humans, sustained G-CSF administration is known to cause osteopenia – the loss of bone matrix (Sekhar et al., 2001; Kokai et al., 2002). A significant reduction in the number of bone lining osteoblasts in mice, caused by apoptosis, has been observed within 1 day of G-CSF administration (Christopher and Link, 2008; Winkler et al., 2010). Further, gene expression analysis of whole bone marrow by Christopher and Link (2008) showed a dramatic reduction in the expression of late osteogenic genes. Most interestingly, evidence from Winkler and colleagues (2010), shows that whilst bone lining osteoblasts are significantly reduced during G-CSF treatment, after treatment is complete there is a resurgence in these cells to 2-fold higher than before treatment began. This rebound has been associated with the recruitment of new osteoblasts rather than the recovery of quiescent osteoblasts (Christopher and Link, 2008). Consequently, a hypothesis can be put forward suggesting that G-CSF administration leads to an inhibition of progenitor maturation to fully differentiated osteoblasts, and when treatment ends progenitors held at this bottleneck are able to differentiate leading to a dramatic resurgence in osteoblast numbers.

In this chapter, analysis of osteogenic genes from CD45 negative, nestin-GFP positive spinal vertebrae bone marrow cells did not follow this hypothesis. Only the transcription factor *Runx2* showed a significant difference between untreated and G-CSF treated mice, with transcript levels increasing from day 0 to day 7 where animals had osteochondral surgery and 3 days G-CSF treatment followed by 3 days of no G-CSF treatment. Whilst not reaching statistical significance the transcription factor *Sp7* did follow a trend in line with the hypothesis described. Here, after G-CSF treatment a small decrease in expression was seen which increased above baseline levels at 3 days after ending treatment. The data gathered in this study are not going to be conclusive due to the lack of animal numbers but this work does show the feasibility of this analysis strategy, however before moving forward to a larger study some of the limitations should be considered.

The CD45 negative, nestin-GFP cells analysed by Mendez-Ferrer et al. (2010) used a similar isolation strategy to that employed in the experiments presented here, although bone marrow from long bones was used in the original study in contrast to marrow from spinal vertebrae in this work. A factor that may contribute to a difference in the results between this published study and that reported in this chapter, is the possibility of spinal cord contamination. Neural stem cells within the central nervous system express nestin and whilst removal by careful dissection should have reduced their influence, some carry over is likely. Furthermore, a comparison between the effect of G-CSF on long bone and spinal vertebrae has not been conducted. Here, this tissue was used as a method to gain as much data as possible from the nine mice available.

6.6.4. Future directions

As discussed the main limitation of this chapter was the study design and the use of nine mice to try to gain insight into multiple hypotheses. The role of trauma and G-CSF were assessed in the same animals and therefore the independent effects of these two variables cannot be truly deconstructed. With hindsight, perhaps it would have been more effective to answer a single question. On the other hand, the preliminary data gathered does aid in the design of a more detailed study or studies on the role of G-CSF and nestin positive BMSCs in osteochondral repair. Some of the limitations of this work and how they can be addressed are discussed further:

6.6.4.1. Confirmation of G-CSF functionality

This piece of work was the first time G-CSF was studied within our research group in mice, and it was therefore thought important to confirm the bioactivity of the product and compare response to that reported in the literature. Firstly, analysis of haematopoietic populations in the peripheral circulation was assessed by flow cytometry analysis but whilst differences were observed between the three treatment groups, the quantification strategy was flawed. The relative number of HSCs by LSK^+ staining and HSPCs by $L^-S^-K^+$ were expected to increase. However, the influence of G-CSF on mature populations within the haematopoietic system is likely to have obscured any increases in these cells. For this reason, in the future the number of LSK^+ cells per mL of blood would be a more accurate way to assess this effect of G-CSF rather than quantification as percentage of total cells.

Secondly, proliferation in the bone marrow compartment of the right hind distal femur (the contralateral limb to surgery) of mice was assessed. G-CSF's principle role is to increase the number of myeloid cells by the activation of proliferative pathways through binding to the G-CSF receptor. As expected, an increase in proliferation marker Ki67 was seen after the administration of G-CSF. However, the analysis of the bone marrow from a similar location in mice described in the previous chapter also showed an increase in cell

proliferation. This suggests that creation of the osteochondral defect leads to a systemic bone marrow response and therefore this is not a usable method to determine the functionality of the G-CSF administered.

Consequently, as the functionality of the G-CSF was not confirmed in this study (although this was demonstrated for the same batch in an *in vivo* sheep study (Lydon et al., unpublished) a second preliminary study is required before further work using this cytokine is conducted. This assessment does not require the use of reporter mice and could be performed in wild type animals. Importantly this should be done in a model where no surgical injury is performed unlike the study described here.

6.6.4.2. G-CSF and osteochondral repair

Investigation into the effect of G-CSF on osteochondral repair could also be carried out in wild type mice with output measures such as those developed and discussed in the previous chapter 5. In the introduction to this thesis studies that demonstrate an improvement in musculoskeletal repair with G-CSF are discussed (see section 1.10). It would be worthwhile to explore if these findings can be reproduced using the osteochondral defect model developed in this thesis. If the results demonstrate improved outcomes, investigations into the cell and molecular mechanisms could subsequently be carried out. For example, to assess the role of G-CSF on nestin positive BMSCs and the influence of this on osteochondral repair, larger group sizes would be required than those used here and vitally control animals where no G-CSF is administered at parallel time points would be required.

6.6.4.3. Role of nestin positive BMSCs in osteochondral repair – tissue progenitor

Whether nestin positive cells are able to contribute to osteochondral repair tissues as tissue progenitors will require the use of animals that have been allowed to heal over a longer period of time. 1 and 4 days after defect creation, as used here, only represent the very early stages of repair, as demonstrated in chapter 5. In addition to using just nestin-GFP mice a ROSA26 mouse where tdtomato is expressed (a red fluorescent reporter) for the remaining lifespan of the cell, would be advantageous in identifying the cells even after the nestin promoter is switched off. In this way if the cells differentiate and remain in the repair tissue, they will be identifiable.

6.6.4.4. Role of nestin positive BMSCs in osteochondral repair – tissue orchestrator

In the early time points where nestin-GFP expression was assessed here, only punctate staining was observed. As discussed previously this may be suggestive of apoptosis and an immunomodulatory action or even the ability to promote survival or a tissue regenerative response of other cells as previously reported (Wu et al., 2011, 2012; Vonk et al., 2018; Bekkers et al., 2013).

The small numbers of animals used in these studies presented here meant that there was a low abundance of RNA isolated for each experimental group and therefore only a limited number of genes could be analysed. Based on the data of published work (Christopher and Link, 2008; Winkler et al., 2010; Méndez-Ferrer et al., 2010), it was decided to analyse the expression of genes that represented differentiation. In the future, analysis of genes related to the immunomodulatory properties of cells may elucidate if G-CSF exposure changes these properties of the cells, with and without surgery. *In vitro* work using nestin positive cells may be worthwhile starting points as immuno-regulatory properties of this population is yet to be explored in the literature.

6.6.5. Summary

In summary, the work described in this chapter has produced preliminary data analysing the role of nestin positive cells and G-CSF in osteochondral repair. Initial results suggest that in the early phases of osteochondral healing nestin positive cells die and evidence from the literature suggests that this might be part of the immunomodulatory function of BMSCs. Additionally data shows that nestin positive cells react to trauma and/or G-CSF treatment by increasing their numbers in the peripheral circulation. To determine whether G-CSF improves the outcomes of osteochondral repair through the response on nestin positive cells further work is required.

7. RESULTS: NON-HAEMATOPOIETIC CELLS ARE TARGETED BY G-CSF IN MUSCULOSKELETAL REPAIR

7.1. Background and Rationale

Granulocyte colony stimulating factor is well established to have a significant biological effect on cells of the haematopoietic system. It has an important role in the regulation of neutrophils under basal conditions but is also important in disease and injury, for example in response to infection (Cebon et al., 1994). It is able to increase the proliferation and survival of multiple haematopoietic cell lineages. In addition to its role in haematopoietic system, G-CSF is also thought to have actions upon non-haematopoietic cells that display its transmembrane receptor including cardiomyocytes, neuronal precursors, endothelial cells (Touw and van de Geijn, 2007). Additionally, there is some evidence that bone marrow stem/stromal cells (BMSCs) display the receptor.

G-CSF treatment has been reported to lead to mobilisation of BMSCs into the peripheral circulation in response to G-CSF treatment (Lund, Baso and Orchard, 2006). However, it is unknown if this is a reaction to G-CSF binding directly to BMSCs or due to changes in the bone marrow microenvironment as a whole where interactions between haematopoietic stem and progenitor cells (HSPCs) and their niche are disrupted. Furthermore, little investigation into the downstream effects of potential ligand binding to the G-CSF receptor (G-CSF R) in BMSCs has been conducted. Importantly, if this binding does occur it may have consequences for BMSC fate. What's more, this may have consequences for the response of BMSCs in bone and cartilage repair such as osteochondral repair.

7.2. Aim and objectives

The work in this chapter aims to elucidate this and the consequences of this binding for BMSC fate. Firstly, analysis of the G-CSF R expression in BMSCs was analysed and the downstream signalling pathways known to be induced in other cell lineages on G-CSF binding assessed. Secondly, the impact of G-CSF on the proliferation and differentiation of BMSCs was investigated using *in vitro* assays. It was hypothesised that the G-CSF R can be found on BMSCs and G-CSF binding activates downstream intracellular signals.

7.3. Bone marrow MSCs express the G-CSF R

BMSCs isolated at orthopaedic joint replacement surgery and BMSCs purchased from Lonza (UK) were analysed for the presence of the G-CSF R by Western blot analysis of cell lysates. In parallel, peripheral blood mononuclear cells (MNC) were used as a positive control for expression of the receptor as well as recombinant G-CSF R originally isolated

from a mouse myeloma cell line. G-CSF R has four isoforms with the predicted molecular weight varying between 85 kDa and 95 kDa (UniProt, 2018). The recombinant G-CSF R used in the work presented here has a strong band at this molecular weight range (Figure 7-1). When quantified by densitometry the two Lonza purchased BMSC populations also have a quantifiable band at this molecular weight, whilst the patient derived BMSCs do not. The patient samples however do have a band at a molecular weight of 68 kDa. When normalised to β-actin the Lonza purchased BMSCs have a higher abundance of this protein.

To investigate the presence of the receptor further Lonza BMSCs were examined by immunocytochemistry (Figure 7-2 and Figure 7-3). Confocal microscopy evaluation shows positive staining in cell populations from both Lonza patients. Immunocytochemistry evaluation indicates the presence of G-CSF R localised to the cell membrane as Alexa 488 green fluorescence is seen across the cell surface. Additionally the G-CSF R is also localised in intracellular organelles

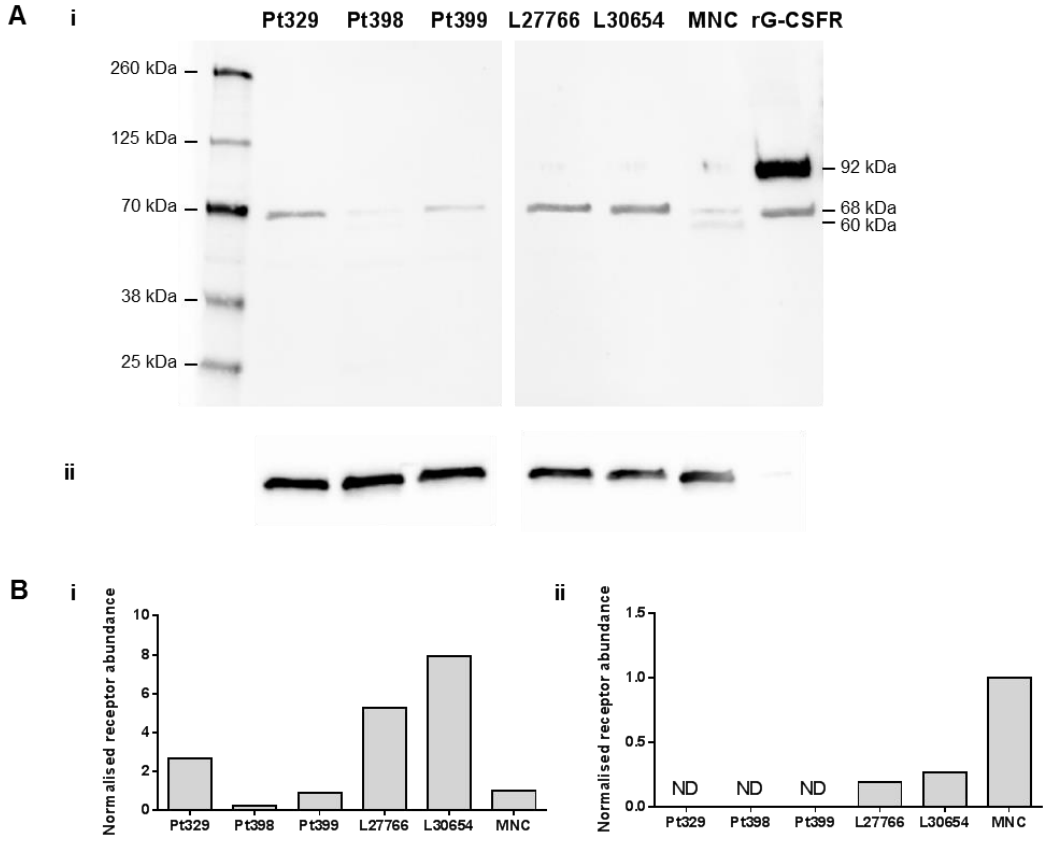

Figure 7-1 – G-CSF R detection in BMSCs by Western blotting
BMSCs derived from patients (Pt-) and purchased from Lonza (L-) were analysed for the presence of G-CSF R protein by Western blotting. (A) Cell lysates were run on a single gel. (i) The blot was probed for G-CSF R, then an 800nm secondary antibody, antibody predicted molecular weight 92 kDa. MNC protein lysate and recombinant G-CSF R is included for reference alongside the molecular weight marker. (ii) The blot was probed for β-Actin as a loading control, chemiluminescence detection. (B) Graphs of densitometry values normalised to β-actin. (i) 68kDa molecular weight bands, (ii) 92 kDa molecular weight bands.

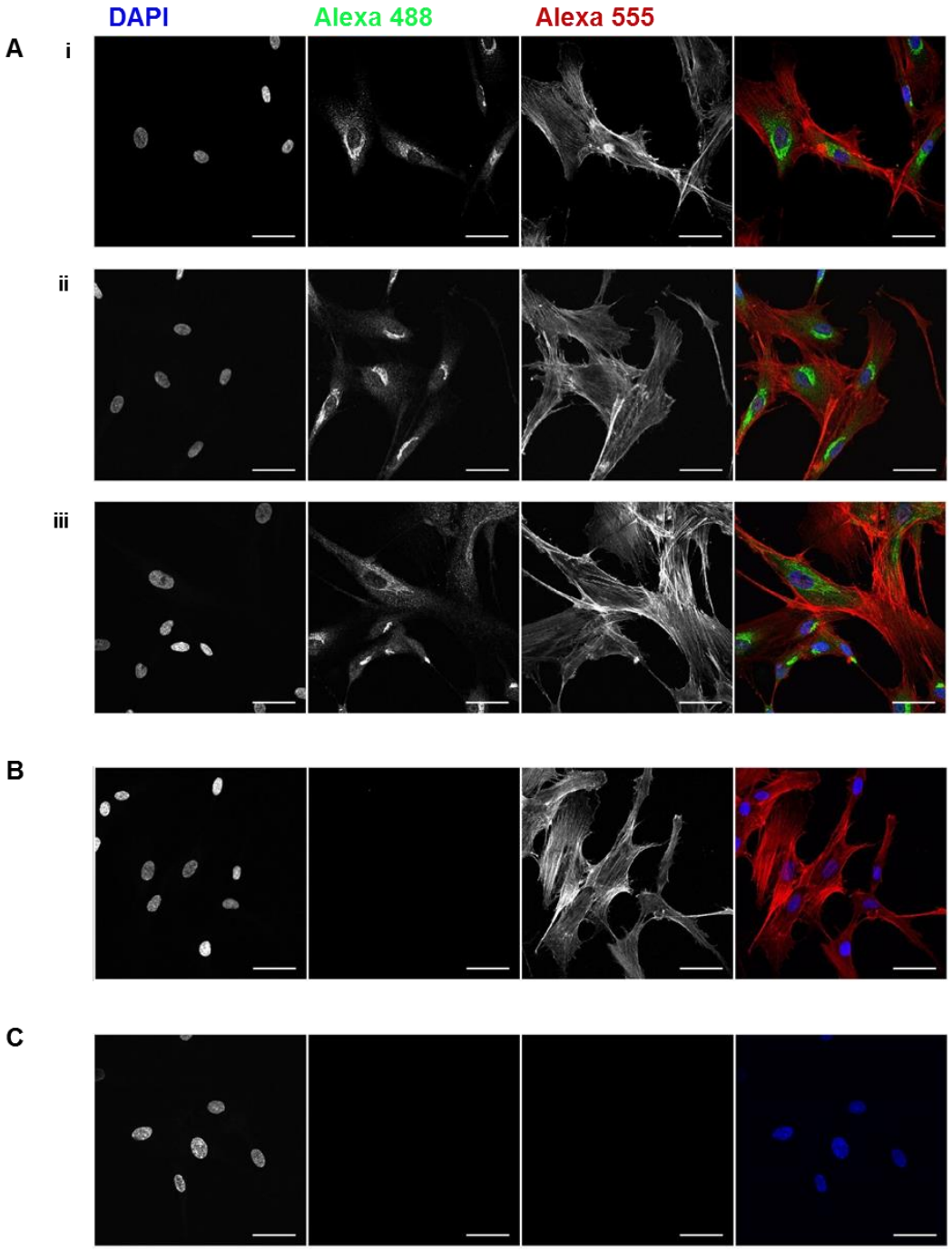

Figure 7-2 – G-CSF R detection in BMSCs by immunocytochemistry (L27766)
L2777 BMSCs purchased from Lonza were analysed for the presence of G-CSF R protein. Cells were grown in 0.7 mm^2 wells of glass slides and fixed before immunocytochemistry staining for G-CSF R (Alexa 488 secondary antibody) (A). Nuclei were counterstained with DAPI and the actin cytoskeleton with phalloidin (Alexa 555). (B) G-CSF R primary antibody negative control, (C) secondary antibody and phalloidin negative control. Imaged by confocal microscopy (63x objective), maximum projection shown. G-CSF R, green; actin filaments, red; nucleus, blue. Scale bar indicates 50 µm.

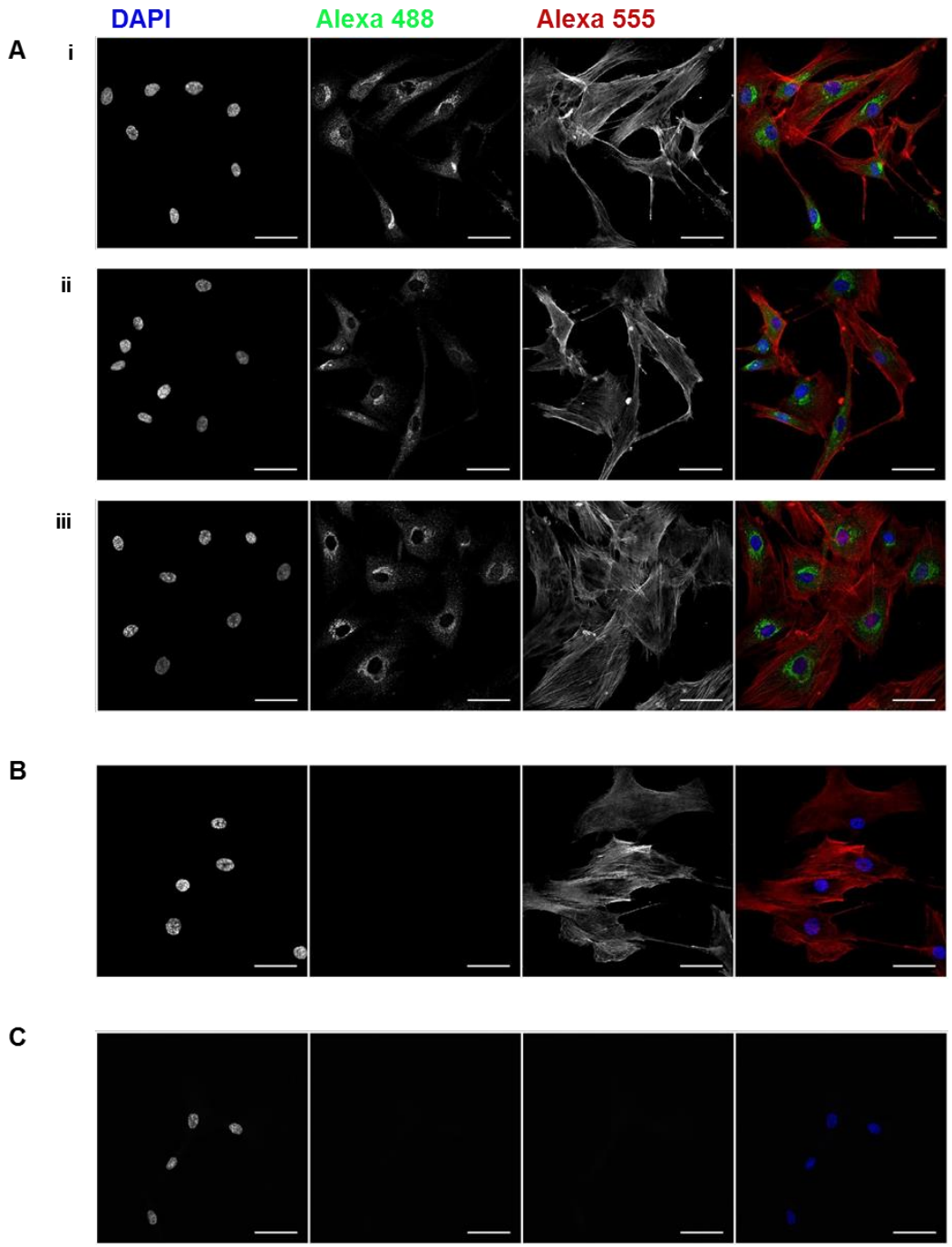

Figure 7-3 – G-CSF R detection in BMSCs by immunocytochemistry (L30654)
L2777 BMSCs purchased from Lonza were analysed for the presence of G-CSF R protein. Cells were grown in 0.7 mm^2 wells of glass slides and fixed before immunocytochemistry staining for G-CSF R (Alexa 488 secondary antibody) (A). Nuclei were counterstained with DAPI and the actin cytoskeleton with phalloidin (Alexa 555). (B) G-CSF R primary antibody negative control, (C) secondary antibody and phalloidin negative control. Imaged by confocal microscopy (63x objective), maximum projection shown. G-CSF R, green; actin filaments, red; nucleus, blue. Scale bar indicates 50 µm.

7.4. Functional G-CSF R on BMSCs is activated through JAK2/STAT3 and MAPK/ERK pathways

To determine whether the G-CSF R is functional in BMSCs, the phosphorylation kinetics of the JAK2/STAT3 and MAPK/ERK pathways were examined. Cells were serum starved and then exposed to G-CSF (100 ng/mL) for specific time periods and protein lysates were submitted to Western blotting. Quantification by densitometry shows an increase in the phosphorylation of the STAT3 transcription factor in both BMSC populations over time when normalised to total STAT3 (Figure 7-4). Interestingly, the cells derived from patient L30654 had apparent increased phosphorylation compared to patient L27766 cells. This difference was further highlighted for the phosphorylation of the MAPK/ERK signalling proteins p42 and p44 where only L30654 showed a marked increase in phosphorylation. For L30654 BMSCs phosphorylation was highest at 15 minutes after stimulation with G-CSF and remained elevated at 30 minutes. In contrast, p42 and p44 phosphorylation was unchanged for L27766 cells whilst STAT3 phosphorylation peaked 30 minutes after stimulation.

Whilst G-CSF R protein of 92 kDa was identified by Western blot analysis for three orthopaedic patient derived BMSCs, the cells were subjected to the same phosphorylation kinetics evaluation of the STAT3 pathway. Densitometry analysis revealed that the phosphorylation of STAT3 increased by over 1.5 times. Together these results identify the presence of functional G-CSF receptors on the cell surface of BMSCs.

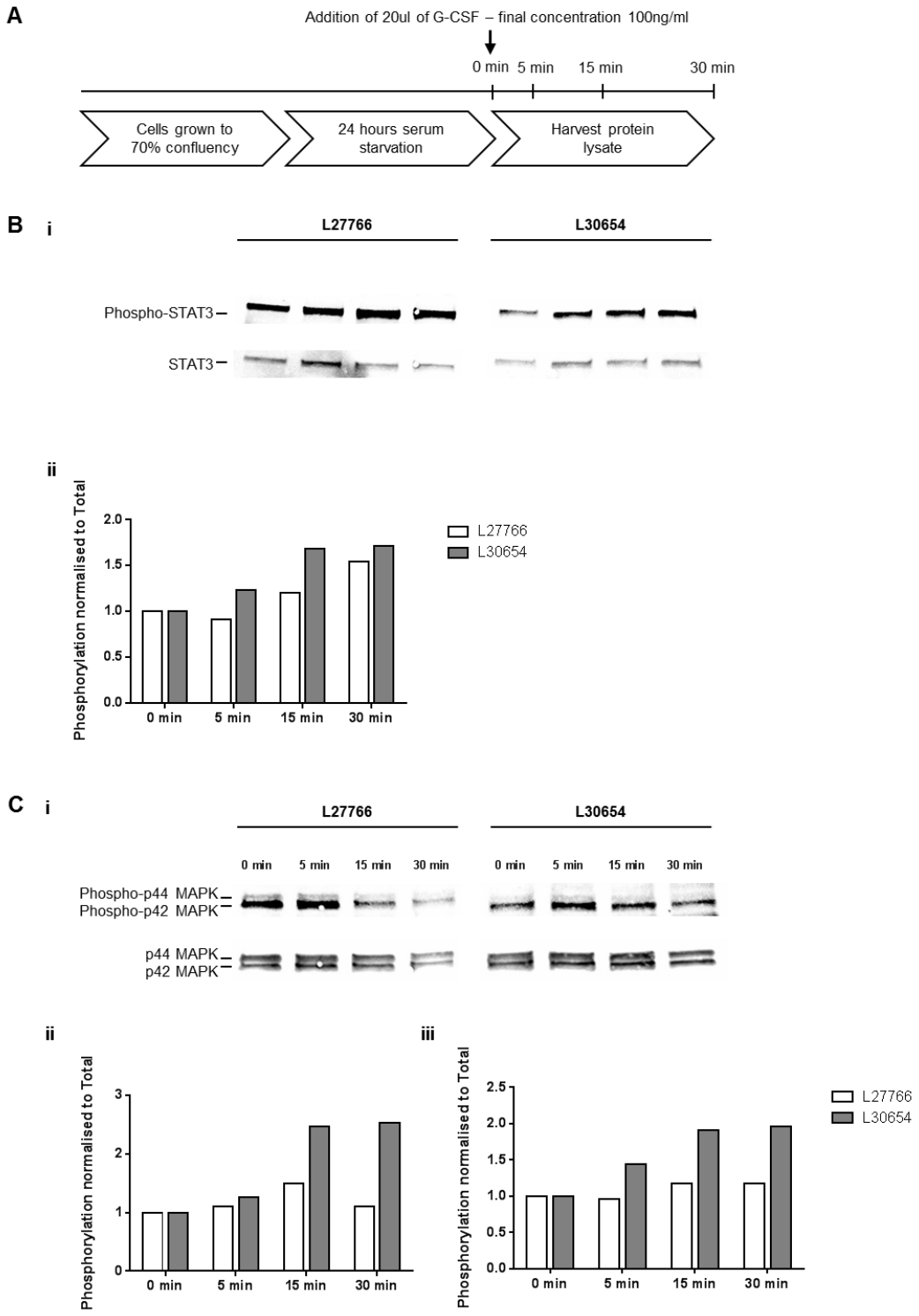

Figure 7-4 – Analysis of Lonza BMSC G-CSF R functionality
BMSCs purchased from Lonza (L27766 an L30654) were analysed for the activation of the JAK2/STAT3 and MAPK/ERK pathways by the detection of STAT3 and p42/p44 phosphorylation respectively. (A) A schematic describes the treatment of BMSCs prior to the exposure to G-CSF for the two patients. Cell lysates were analysed by Western blotting. (B) (i) The blot was probed for phosphorylated STAT3 (88 kDa) and total STAT3 (86 kDa) on the same membrane using 800nm and 680nm secondary antibodies respectively. (ii) Graphs of densitometry values of phosphorylated STAT3 normalised to total STAT3. (C) (i) The blot was then probed for phosphorylated p42/p44 (42 and 44 kDa) and total p42/p44 (42 and 44 kDa) on the same membrane using 680nm and 800nm secondary antibodies respectively. Graphs of densitometry values of (ii) phosphorylated p42 normalised to total p42 and (iii) phosphorylated p44 normalised to total p44.

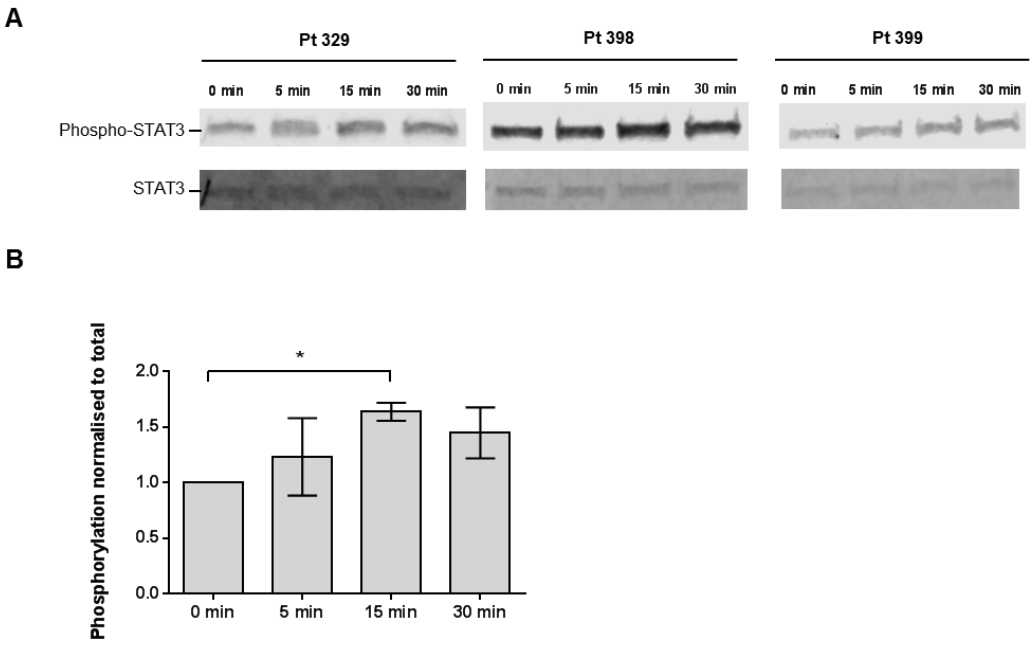

Figure 7-5 – Analysis of orthopaedic patient BMSC G-CSF R functionality
BMSCs derived from three patients (Pt-) were analysed for the activation of the JAK2/STAT3 pathway by the detection of STAT3 phosphorylation. (A) The blot was probed for phosphorylated STAT3 (88 kDa) and total STAT3 (86 kDa) on the same membrane using 800nm and 680nm secondary antibodies respectively. (B) Graphs of densitometry values of phosphorylated STAT3 normalised to total STAT3. One-way ANOVA, Tukey Test, * $p<0.05$, all others non-significant.

7.5. Synovial derived MSCs have increased response to G-CSF compared to BMSCs

As well as from bone marrow, mesenchymal stem/stromal cells have been isolated from other tissues of the knee joint including the synovium lining the fat pad. These cells have also been reported to be involved in the repair of articular cartilage defects. To evaluate whether these cell populations may also respond to G-CSF treatment, the presence of the receptor and its activation were assessed in BMSCs and synovial mesenchymal stem/stromal cells (sMSCs) from the same orthopaedic patient. As observed for other patient derived samples, no band was seen for the G-CSF R with molecular weight between 85 kDa to 95 kDa, whilst a band of 68 kDa was detected. When normalised to a loading control, β-actin, the sMSCs had a 36-fold increased abundance of this protein. Although it is likely that this molecular weight corresponds to intracellular located G--CSF R, increased levels of the 68 kDa protein does correlate with increased phosphorylation of the STAT3 pathway in the Lonza derived BMSCs. In terms of STAT3 phosphorylation sMSCs showed a 2.7-fold increase compared to a 1.5-fold in the BMSCs from the same patient.

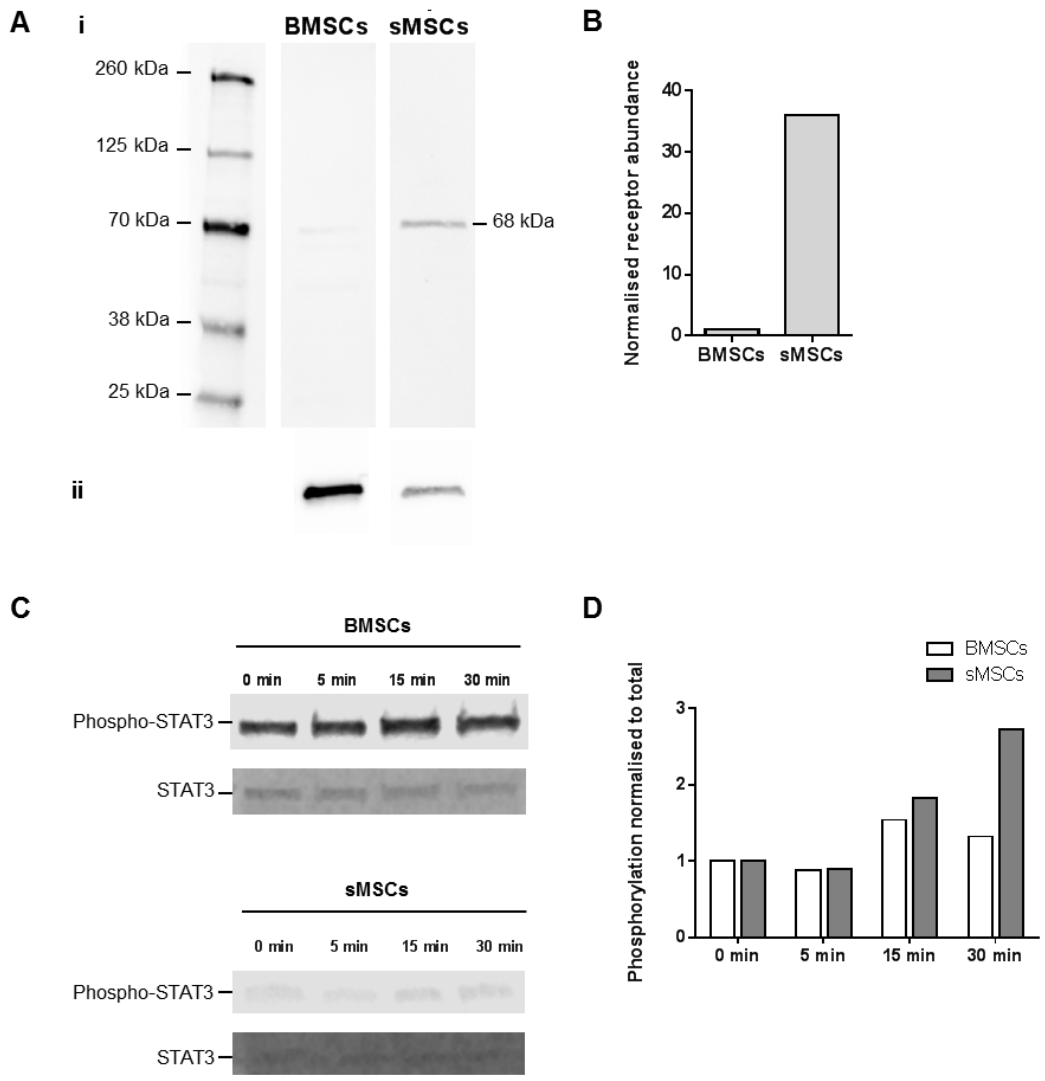

Figure 7-6 – Comparison between BMSCs and synovial derived MSCs from the same patient for G-CSF R presence and functionality

BMSCs and sMSCs derived from the same patient were analysed for the presence of G-CSF R protein by Western blotting. (A) (i) Cell lysates were run on a single gel alongside a molecular weight marker. The blot was probed for G-CSF R (predicted molecular weight 92 kDa), then with an 800nm secondary antibody. (ii) The blot was probed for β-Actin as a loading control, chemiluminescence detection. (B) Graphs of densitometry values normalised to β-actin for 68 kDa protein. (C) BMSCs and sMSCs were exposed to G-CSF after 24 hours serum starvation for various lengths of time as indicated. Cell lysates were analysed by Western blot. Blots were probed for phosphorylated STAT3 (88 kDa) and total STAT3 (86 kDa) on the same membrane using 800nm and 680nm secondary antibodies respectively. (D) Graphs of densitometry values of phosphorylated STAT3 normalised to total STAT3.

7.6. Further characterisation of STAT signalling in response to G-CSF using small molecular weight pathway inhibitors

To verify the significance of the JAK2/STAT3 pathway in BMSCs the JAK inhibitor CP 690550 citrate (CP69) and the JAK2 specific inhibitor Cucurbitacin I (Cucu) were used. Protein lysates were prepared from cells exposed to one of the inhibitors for 1 hour before cytokine stimulation. CP69 is a potent JAK inhibitor and under control conditions reduced endogenous phosphorylation dramatically whilst Cucu caused a minimal decrease (Figure 7-7). Peripheral blood mononuclear cells (PB MNCs) were used as a control alongside IL-6 stimulation, a cytokine widely described to induce downstream signalling in both BMSCs and PB MNCs.

Figure 7-7 C shows that both inhibitors effectively blocked STAT3 phosphorylation stimulated by IL-6 in BMSCs and MNCs at 15 and 30 minutes; CP69 reduced the response by 10 times, from a 22-fold increase to 2-fold and Cucu by over half to a 10-fold increase relative to baseline levels at 15 minutes. No clear stimulation of PB MNCs was seen by stimulation with G-CSF and therefore responses to G-CSF in the presence of inhibitors were equivalent to the phosphorylation without the addition of G-CSF. This was also seen for the response to G-CSF in BMSCs.

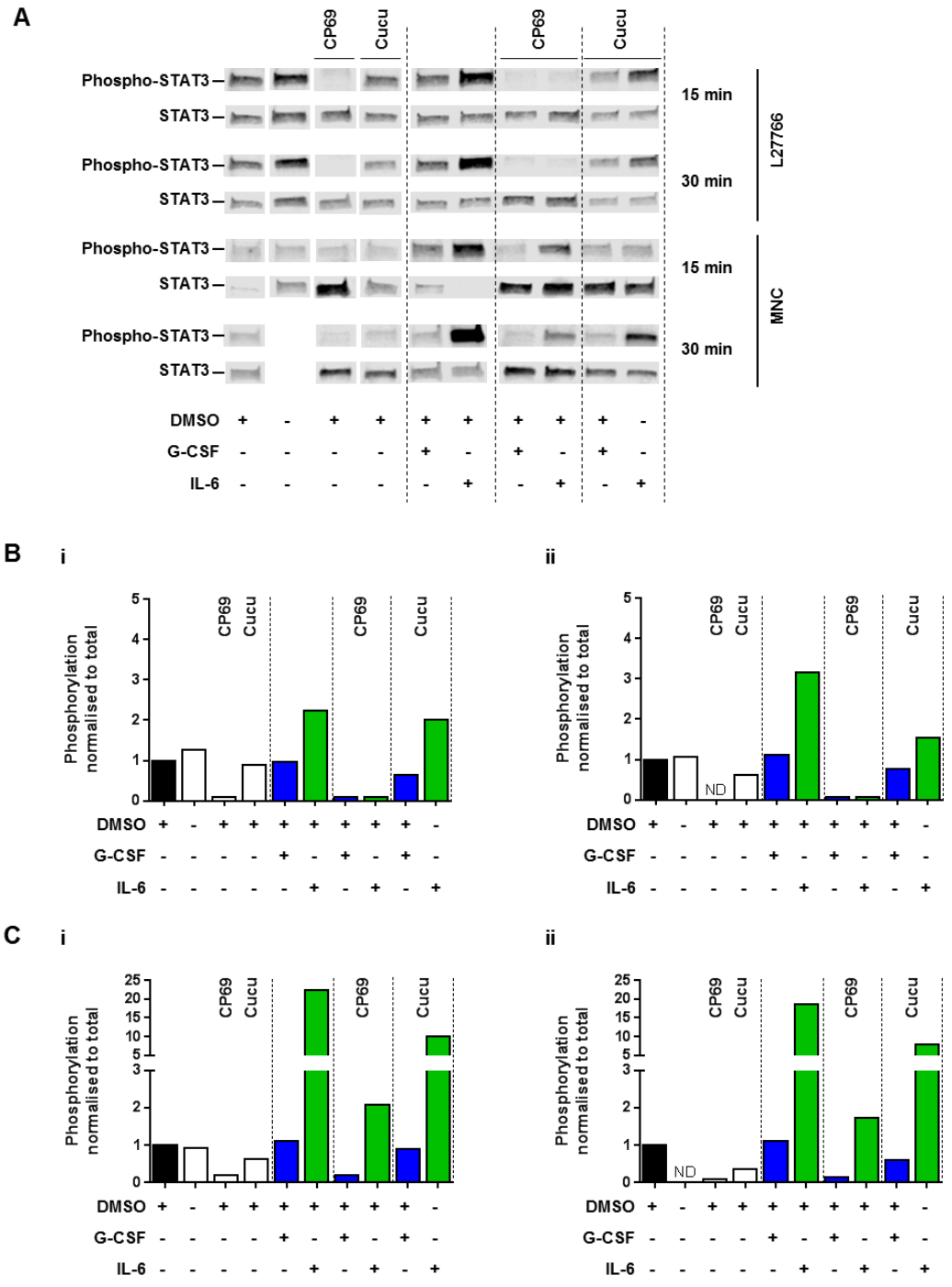

Figure 7-7 – Assessment of the integrity of G-CSF induced JAK2/STAT3 signalling using small molecular weight pathway inhibitors

BMSCs purchased from Lonza (L27766) were analysed for the inhibition of the JAK2/STAT3 pathway by two JAK inhibitors after its induction by G-CSF exposure. BMSCs were grown to 70% confluency and then serum starved for 24 hours. Peripheral blood (PB) MNCs were isolated and cultured in serum starvation media for 24 hours. Selected cells were then exposed to either CP 690550 citrate (CP69) or Cucurbitacin I (Cucu) (prepared in DMSO) for 1 hour. Controls were either left in starvation media or the equivalent amount of DMSO added. G-CSF at 100 ng/mL or IL-6 at 20 ng/mL was then added for 15 or 30 minutes. (A) (i) Cell lysates were run across four gels alongside a molecular weight marker. Blots were probed for phosphorylated STAT3 (88 kDa) and total STAT3 (86 kDa) on the same membrane using 800nm and 680nm secondary antibodies respectively. (B and C) Graphs of densitometry values of phosphorylated STAT3

normalised to total STAT3. (B) BMSCs, (i) 15 minutes or (ii) 30 minutes exposure to cytokines (C) PB MNCs, (i) 15 minutes or (ii) 30 minutes exposure to cytokines.

7.7. Activation of the G-CSF R does not increase human BMSC proliferation

G-CSF is known to be a mitogen for cells expressing its receptor such as neutrophils. To investigate whether G-CSF is able to induce proliferation in BMSCs, cells were cultured in xCELLigence E-plates under reduced serum conditions (1% v/v FCS) for 24 hours before stimulation with 10 ng/mL G-CSF or 10% (v/v) FCS. The addition of FCS to BMSCs induced proliferation as seen in Figure 7-8 A, whilst the addition of G-CSF resulted in no increase in impedance values, rather a small decrease over 4 days. Cells were run in parallel in 96-well plates and after 4 days the amount of DNA quantified. This study supported the xCELLigence data showing a significant DNA increase in wells treated with 10% FCS whilst no difference was seen in G-CSF treated wells.

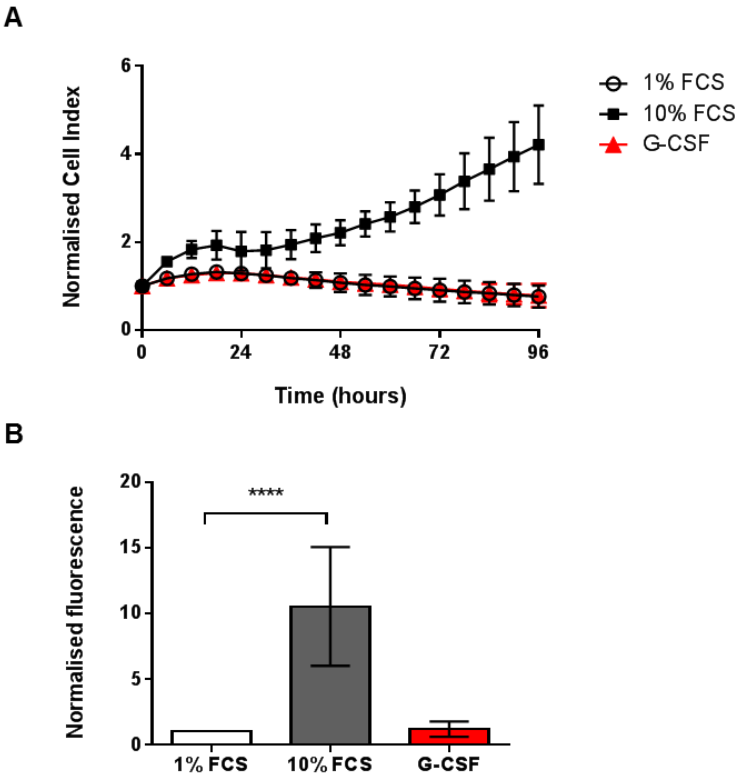

Figure 7-8 – Analysis of BMSC proliferation induction by G-CSF
BMSCs purchased from Lonza were analysed for proliferation by (A) real time analysis using xCELLigence E-plates and (B) assessment of DNA quantity. Cells were grown in either 1% FCS, 10% FCS or 1% FCS supplemented with 100 ng/mL G-CSF. xCELLigence cell index values were normalised to the time at which the cytokines were added. Data shown for values at every 6 hours. DNA quantity at 4 days was determined using the CyQuant assay. One-way ANOVA, Dunnett's Test, * $p<0.0001$.

7.8. No significant change in expression of STAT-3 responsive genes in response to G-CSF in human MSCs

The expression of STAT3-responsive genes were then examined by qRT–PCR, alongside genes associated with immunomodulatory properties, in G-CSF treated BMSCs. Figure 7-9 shows that no significant difference was detected for any of the transcripts studied between wells where G-CSF was added relative to wells where it was not.

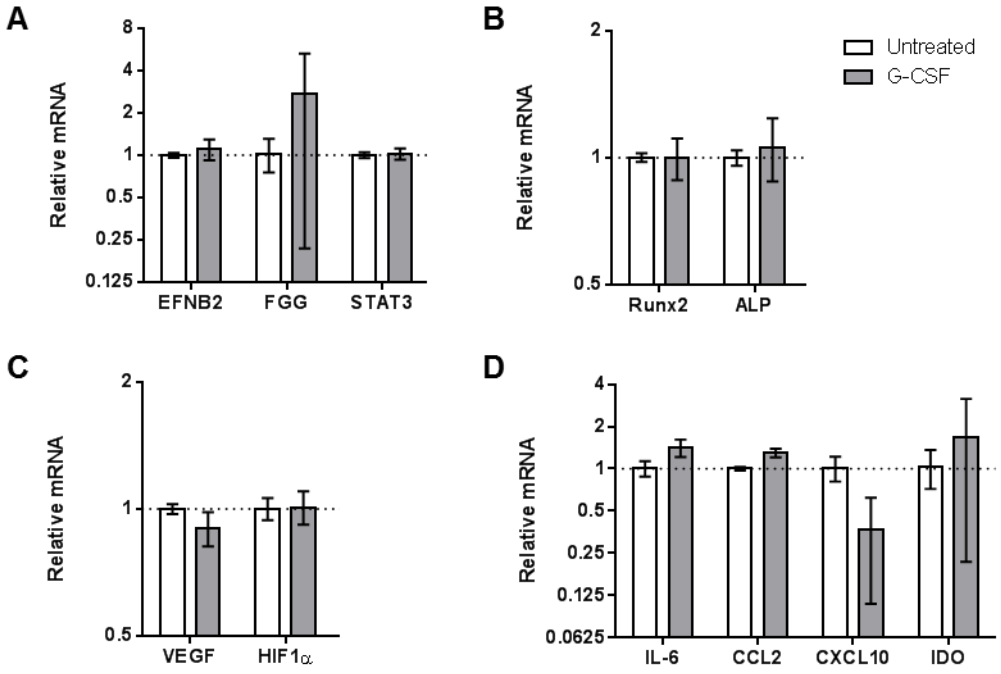

Figure 7-9 – Gene expression analysis of BMSCs after G-CSF exposure
BMSCs purchased from Lonza (L27766) were analysed for gene expression. Cells were grown to 70% confluency and then serum starved overnight before the addition of 100 ng/mL G-CSF. After 24 hours cells were lysed and analysed by qRT-PCR. Gene are shown subdivided into four categories (A) genes downstream of STAT3, (B) early markers of osteogenesis, (C) genes indicative of angiogenesis and (D) genes related to immunomodulatory properties. Bars indicate the expression of mRNA for each gene normalised to HPRT. Error bars indicate the standard deviation of the mean for biological replicates of a single experiment (N=3).

7.9. G-CSF and BMSC differentiation

Next, the effect of G-CSF on the differentiation of BMSCs towards osteogenic, chondrogenic and adipogenic lineages was assessed. BMSCs purchased from Lonza (UK) were grown in 12-well plates and osteogenic or adipogenic inductive medium added. For the assessment of chondrogenic differentiation cells were cultured in high-density pellets with chondro-inductive medium. In treated wells 100 ng/mL G-CSF was added to the differentiation media. Each differentiation pathway was assessed in BMSCs isolated from two patients.

Figure 7-10 shows representative images of Alizarin red staining for calcium in osteogenic differentiated wells. Calcium deposition, representative of osteogenic differentiation, was unaffected by the addition of G-CSF within the culture medium. Likewise, representative images of Oil Red O staining in Figure 7-11 demonstrate the ability of BMSCs to accumulate lipid-filled vesicles in response to adipogenic inductive medium. Further the level of adipogenic differentiation was unaffected by the presence of G-CSF.

Chondrogenic differentiation of BMSCs was determined by histological thionin staining of cell pellets after 21 days of differentiation. Whilst osteogenic and chondrogenic differentiation of BMSCs was unaffected by the presence of G-CSF in the culture medium, the production of proteoglycan was seen to be lower in cell pellets of both patients exposed to G-CSF. This was illustrated by weaker purple thionin staining (Fig 1-12). Additionally, variation in response was observed between control samples of the two patients. Interestingly, BMSCs from patient L30654 deposited more calcium than L27766 during osteogenesis but cells from this second patient showed a better chondrogenic potential with stronger proteoglycan staining.

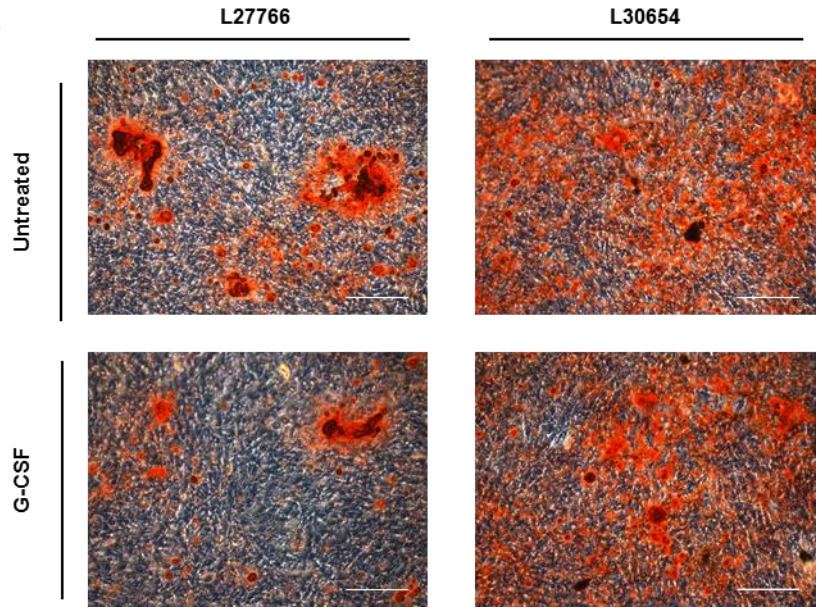

Figure 7-10 – Analysis of the influence of G-CSF on the osteogenesis of BMSCs
BMSCs purchased from Lonza (L27766 and L30654) were exposed to osteo-inductive media with and without the addition of 100 ng/mL G-CSF. After 21 days cells were stained with Alizarin red and imaged microscopically. Respresentative images shown. Scale bar 200 µm.

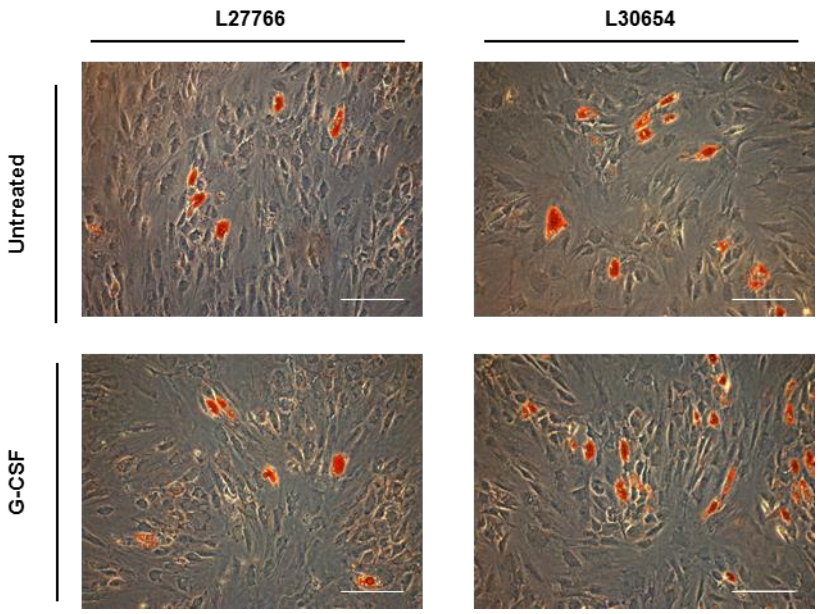

Figure 7-11 – Analysis of the influence of G-CSF on the adipogenesis of BMSCs
BMSCs purchased from Lonza (L27766 and L30654) were exposed to adipogenesis inductive media with and without the addition of 100 ng/mL G-CSF. After 21 days cells were stained with Oil Red O and imaged microscopically. Respresentative images shown. Scale bar 200 µm.

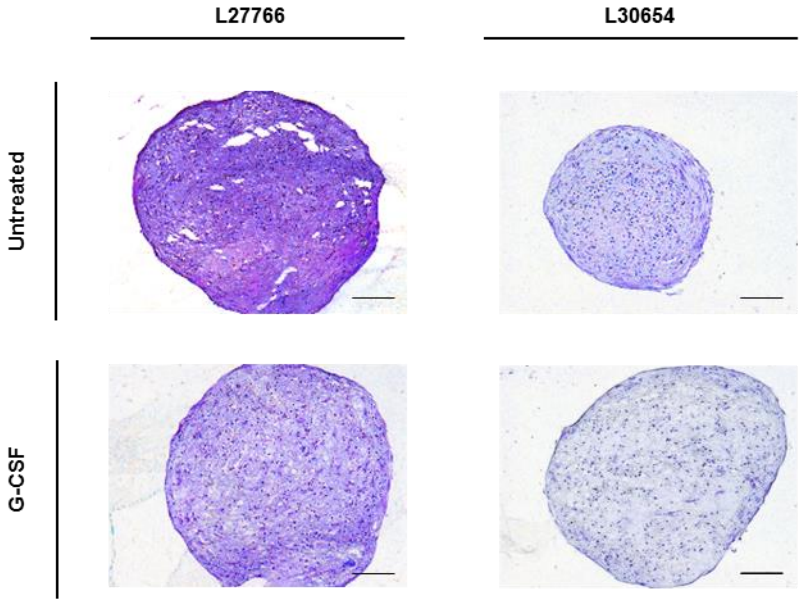

Figure 7-12 – Analysis of the influence of G-CSF on the chondrogenesis of BMSCs (L27766 and L30654) by histological evaluation
BMSCs purchased from Lonza (L27766 and L30654) were cultured in high-density cell pellets and exposed to chondrogenic inductive media with and without the addition of 100 ng/mL G-CSF. After 21 days cells were processed for paraffin sectioning and 5µm sections cut prior to staining with thionin. All sections were stained at the same time. Scale bar 100 µm.

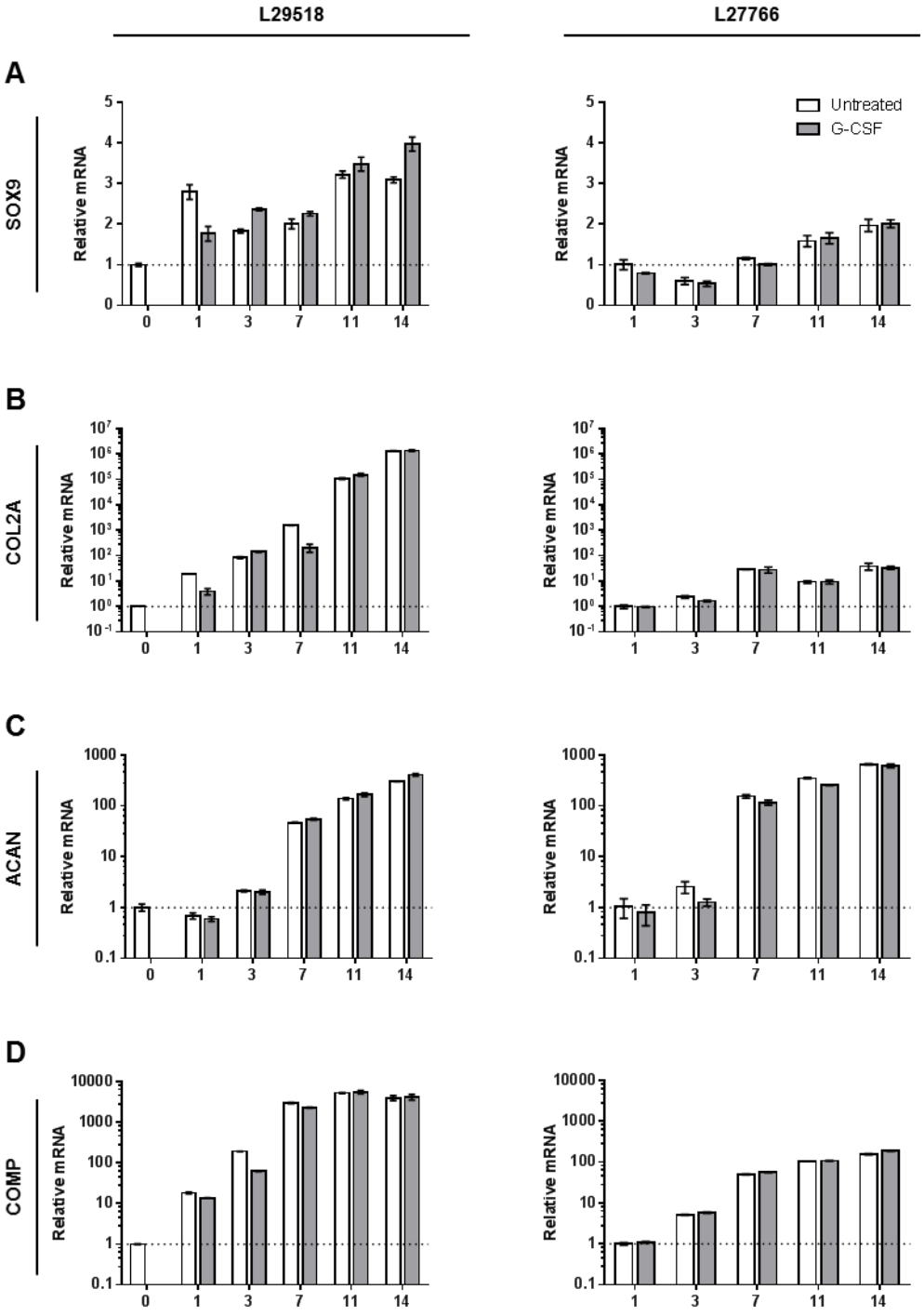

Figure 7-13 – Analysis of the influence of G-CSF on the chondrogenesis of BMSCs by gene expression over time
BMSCs purchased from Lonza (L27766 and L29518) were cultured in high-density cell pellets and exposed to chondrogenic inductive media with and without the addition of 100 ng/mL G-CSF. At the time points indicated cells were lysed for RNA isolation and qRT-PCR conducted for chondrogenic genes; (A) *SOX9*, (B) *COL2A*, (C) *ACAN* and (D) *COMP*. Bars indicate the expression of mRNA for each gene normalised to HPRT. Error bars indicate the standard deviation of the mean for technical replicates for qRT-PCR run in triplicate. A minimum of three pellets were combined for each condition (N=>3).

To investigate further the reduction in chondrogenesis by BMSCs caused by the presence of G-CSF, gene expression analysis was conducted at different time points. BMSCs (Lonza, UK) were used from two different patients, one of which was used for the assessment in Figure 7-12 (L27766) and a second patient (L29518). The cells were grown in high-density pellets with and without the addition of 100 ng/mL G-CSF to chondrogenic inductive medium. Figure 7-13 demonstrates that for both patients there was no significant difference in the number of transcripts for the transcription factor *SOX9* or the chondrogenic specific proteins type II collagen (*COL2A*), aggrecan (*ACAN*) and cartilage oligomeric matrix protein (*COMP*). The lack of difference in these two culture conditions was also seen by proteoglycan staining for L27766 using thionin, Figure 7-14, where pellets for histological assessment were produced alongside the gene expression samples. These results differ from those shown in Figure 7-12 for the same patient.

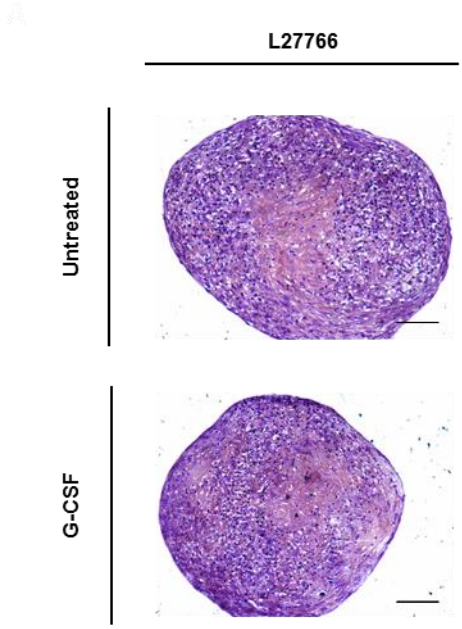

Figure 7-14 – Analysis of the influence of G-CSF on the chondrogenesis of BMSCs (L27766 repeat) by histological evaluation
BMSCs purchased from Lonza (L27766) were cultured in high-density cell pellets and exposed to chondrogenic inductive media with and without the addition of 100 ng/mL G-CSF. After 21 days cells were processed for paraffin sectioning and 5µm sections cut prior to staining with thionin. All sections were stained at the same time. Scale bar 100 µm.

7.10. Discussion

The G-CSF receptor is well documented to be expressed by a range of haematopoietic cells including myeloid progenitors, neutrophils, monocytes and lymphocytes (Singh et al., 2012). Additionally, the expression of the receptor has been reported in cells of non-haematopoietic tissues such as cardiomyocytes, neuronal precursors, endothelial cells and placental tissue (Touw and van de Geijn, 2007). As discussed previously, G-CSF administration to patients and experimental animal models causes the mobilisation of haematopoietic stem and progenitor cells as well as the proliferation of cells from the haematopoietic myeloid lineage in the bone marrow.

The mechanism by which G-CSF leads to the mobilisation of HSPCs from the bone marrow is not well established. However, the interruption of interactions between the cells and their microenvironment is known to be part of the response. BMSCs are one component of the haematopoietic stem cell niche and have been reported in some studies to respond to G-CSF. To understand how G-CSF influences osteochondral repair it is important to investigate the action of this cytokine on BMSCs as they are thought to be a key cell type in the regeneration of bone and cartilage.

7.10.1. G-CSF receptor

Firstly, to confirm the potential of BMSCs to respond to this cytokine, analysis was conducted to confirm the presence of the G-CSF receptor in these cells. Previously other authors have reported the presence of the receptor in both human and mouse BMSCs (Ponte et al., 2012; Hokari et al., 2009) and here Western blot and immunocytochemistry analysis confirmed the presence of the receptor in human BMSCs.

The G-CSF R is a transmembrane protein consisting of 813 amino acids to which G-CSF binds on the cell surface. However, the localisation of the receptor here was not solely associated with the membrane. Firstly, Western blot analysis identified the G-CSF R to be of a lower molecular weight (68 kDa) than the predicted molecular weight (92 kDa) for this protein. Secondly, immunocytochemistry imaging showed the receptor to be located within an intracellular organelle.

Previous studies (Ponte et al., 2012) investigated the G-CSF R by Western blot using membrane fractions from BMSCs as the authors found G-CSF R protein levels too low for detection in total cell extracts. Consequently, no comment was made on intracellular localised G-CSF R. In the data presented here, studying orthopaedic patient isolated BMSCs, detection of the higher molecular weight (92 kDa) G-CSF R was unsuccessful. It may therefore be worthwhile in the future to isolate enriched fractions of membrane proteins to confirm the presence of the full length receptor at the cell surface.

Several hypotheses can be made to account for the presence of the 68 kDa form of G-CSF R in BMSCs. One suggestion is that a significant proportion of the G-CSF R within BMSCs is accumulated in an un-glycosylated form within the endoplasmic reticulum awaiting post-translational modification. The G-CSF R has multiple N-glycosylation sites and glycosylation of the receptor has been shown necessary for the transport of the receptor to the cell surface (Li and Sartorelli, 1994). A second hypothesis is that there may be a soluble form of the receptor contained within the cells. Fukunaga et al. (1990) demonstrated the presence of a human G-CSF R mRNA transcript encoding a receptor with an 88 base pair deletion corresponding to the transmembrane domain, and so a lower molecular weight protein than the membrane receptor (Fukunaga et al., 1990). Either way, these results raised the question of whether BMSCs are able to respond to extracellular G-CSF.

7.10.2. Intracellular signalling pathways activated by G-CSF

The binding of G-CSF to its receptor is known to induce a conformational change and subsequently the transduction of several intracellular signalling cascades including the JAK2/STAT3 and PI3K/AKT, and MAPK/ERK pathways (Dwivedi and Greis, 2017). To study if the G-CSF receptor found in BMSCs is functional, the activation of these pathways following G-CSF treatment was assessed using phospho-specific antibodies. Results demonstrated the induction of both JAK2/STAT3 and MAPK/ERK pathways in BMSCs but showed patient variability. Additionally, the JAK2/STAT3 pathway was activated in BMSCs from older orthopaedic patients to a similar level even though the presence of the higher molecular weight receptor species, predicted to be glycosylated, G-CSF receptor was undetected by Western blot analysis in these patients.

Following the observation that L27766 and L30654 showed activation of the JAK2/STAT3 pathway after G-CSF exposure, the significance of the pathway was assessed using inhibitors of Janus kinase (JAK). JAKs are enzymes which associate with the cytosolic domain of cytokine receptors and on binding of a cytokine to its receptor JAKs are brought into apposition resulting in trans-phosphorylation and the initiation of downstream signalling events through the recruitment and phosphorylation of signal transducers and activators of transcription (STATs). By inhibition of the JAK enzymatic function STAT protein phosphorylation is prevented.

Unfortunately, whilst positive controls using IL-6 confirmed the suitability and functionality of the assay and inhibitors used here, the activation of the JAK2/STAT3 pathway by G-CSF was not successful both in BMSCs and in peripheral blood mononuclear cells (PB MNCs) on the single occasion this assay was conducted. L27766 was used due to availability of low passage cells whilst use of L30654, which showed a stronger response to G-CSF, may have been more appropriate for this analysis. However, the failure to

activate the signalling pathway in PB MNCs suggests the G-CSF used for this assay was non-functional. For this reason, the ability of the inhibitors to decrease the G-CSF induced phosphorylation of STAT3 was not observed and these studies need to be repeated to confirm the activation of the JAK2/STAT3 pathway by G-CSF in BMSCs. Of note, one way to confirm the functionality of G-CSF in the future could be the use of the cell line NFS-60 which is dependent on G-CSF for survival (Weinstein et al., 1986).

7.10.3. Downstream effects of G-CSF treatment of BMSCs

The observation of increased phosphorylation of STAT3 in BMSCs following treatment with G-CSF led to experimentation into the downstream consequences of this interaction. Activation of the JAK2/STAT3 signalling pathway is known to lead to transcriptional changes in cells, which can ultimately influence cell survival, proliferation and differentiation each of which is relevant to the potential of BMSCs to aid osteochondral repair.

7.10.3.1. Proliferation

G-CSF is well established to increase the proliferation of myeloid lineage cells (Touw and van de Geijn, 2007). In 2017, Sasaki and colleagues reported that G-CSF increases the proliferation of rabbit BMSCs, as assessed by cell counting. In the current work, both DNA assessment and real time analysis of the cell surface coverage of human BMSCs contradicted the findings of Sasaki and colleagues. This could potentially be due to a species difference. Rabbits are known to have stronger spontaneous healing capabilities than humans although whether this correlates to the ability of BMSCs to response to G-CSF is unexplored. Furthermore, Sasaki et al. used BMSCs isolated from juvenile rabbits at 12 weeks of age which are likely more responsive to proliferation induction signals that could be induced by G-CSF exposure than cells isolated from adult humans.

There is evidence from *in vivo* studies that G-CSF administration in humans leads to an increase in the number of BMSCs present in the peripheral circulation (Lund, Baso and Orchard, 2006). However, whether this is the result of movement of BMSCs from the bone marrow or an increase in the number of BMSCs is unknown. The results acquired from this *in vitro* study suggest that BMSC proliferation does not occur through the direct action of G-CSF on these cells although this does not rule out the possibility that BMSCs proliferate through changes within the overall bone marrow microenvironment.

7.10.3.2. Differentiation

G-CSF is known to drive haematopoietic progenitors to differentiate towards the granulocytic lineage and therefore the ability of G-CSF to influence the differentiation of BMSCs was assessed. Foremost, these experiments demonstrated that the exposure of BMSCs to G-CSF during differentiation does not prevent their differentiation down

osteogenic, chondrogenic and adipogenic lineages. Evaluation of matrix production after osteogenic and adipogenic differentiation showed the production of calcium enriched matrix and lipid vacuoles for each lineage respectively with no observed differences between the untreated and G-CSF treated cells. Chondrogenic differentiation on the other hand did demonstrate a difference in the ECM content when G-CSF was added to the culture media and was therefore this observation was investigated further. The expression of chondrogenic genes in BMSC pellets was assessed over the first 14 days of differentiation but this showed no change when G-CSF was included in the media. The histology of chondrogenic pellets from this individual experiment prepared at the same time as the expression analysis did not show such pronounced differences in matrix staining, in contrast to the earlier data.

On both occasions when chondrogenic differentiation was assessed, BMSCs from more than a single patient were assessed in parallel and importantly altered matrix staining observed in chondrogenic cultures across patients. Furthermore, the cells from a single patient (L27766) were used both for the initial assessment and the second experiment where gene expression was determined. Interestingly, BMSCs from this patient showed a difference in the matrix composition when cultured with G-CSF on the first occasion but not the second. One likely reason for this difference ties with the previously mentioned non-functionality of G-CSF suggested in experiments studying STAT3 phosphorylation and its inhibition by JAK inhibitors. For this reason, more studies are required to better understand how G-CSF treatment alters the ECM of chondrogenic pellets, by reducing proteoglycan content.

This finding is perhaps somewhat unexpected given that G-CSF has been shown to improve cartilage repair in some animal models (Okano et al., 2014; Sasaki et al., 2017). However, there are important key differences. Firstly, G-CSF acts on a multitude of cells and therefore the signals received by BMSCs and other progenitors undergoing chondrogenesis is considerably more complex than the direct effect of G-CSF modelled in the *in vitro* studies presented here. Secondly, the G-CSF administered in these studies was used for a short period of time only. From studies investigating G-CSF and bone that this is known to be an important factor (Christopher and Link, 2008; Winkler et al., 2012, 2010). Whilst here G-CSF had no significant influence on the ability of BMSCs to differentiate into cells that deposit a calcium rich matrix, possibly due to the simplicity of the assay, *in vivo* long-term G-CSF administration causes osteopenia through osteoblast apoptosis. On the other hand, short term G-CSF is seen to increase the number of osteoblasts (Winkler et al., 2012, 2010). It is therefore important going forward to analyse the difference between the transient exposure to G-CSF and its presence in culture medium throughout chondrogenic differentiation.

An important point of note here is also that it cannot be said if chondrogenesis is impeded or whether the matrix produced by differentiating BMSCs is degraded by another molecule produced by these cells, for example matrix metalloproteinases (MMPs). These enzymes are vital during developmental processes and in wound repair allowing the turnover of tissue and the migration of cells through the wound matrix (Caley, Martins and O'Toole, 2015). Lopez Ponte and colleagues' (2012) showed that G-CSF treatment causing an increase in the expression of the inactive pro-MMP2. This might suggest an increase in the MMP2 activity in a microenvironment where BMSCs are exposed to G-CSF. This may be of relevance as MMP2 knock out mice have delayed fracture repair and bone remodelling (Lieu et al., 2011) and therefore by increasing MMP2 levels G-CSF may improve bone and cartilage repair outcomes after long bone fracture and in osteochondral defects.

7.10.3.3. Immunomodulation

The immunomodulatory function of BMSCs after G-CSF exposure was not evaluated here. However, there is evidence in the literature to suggest this might be worth investigation. This cytokine has anti-inflammatory actions on monocytes (Boneberg and Hartung, 2002), suppresses the proliferation of T cells after mitogen-stimulation (Reyes et al., 1999), and systemic administration of G-CSF reduces prostaglandin E2 production by *ex vivo* BMSCs (Ok Bozkaya et al., 2015). With the knowledge that G-CSF can act directly on BMSCs as presented here, one can hypothesis that G-CSF might induce an immunomodulatory trophic phenotype in these cells.

7.10.4. Summary

In summary, this chapter has shown that the G-CSF receptor is present in BMSC and that these cells are able to respond directly to G-CSF through the JAK2/STAT3 signalling pathway. Data present here suggest that one of the biological effects of this could be an altered extracellular matrix when cells are differentiated under chondrogenic condition whilst adipogenic and osteogenic lineages were unaffected. Additionally, whilst G-CSF induces the proliferation of myeloid lineage cells, this was not observed in BMSCs.

8. OVERALL DISCUSSION

The aim of this thesis was to extend the understanding of haematopoietic and bone marrow stem/stromal cells in osteochondral repair as well as the impact of G-CSF on the response of these cells to the surgical injury. Bone marrow stimulation techniques have been used for many years to treat focal articular cartilage defects however the outcomes are often suboptimal (Fellows et al., 2016). The ability to repair articular cartilage, and also bone in osteochondral repair, have focused on the differentiation of bone marrow stem/stromal cell (BMSC) although their trophic role is becoming better understood. The use of G-CSF as an adjuvant to bone and cartilage healing strategies has demonstrated positive outcomes in previously published work (Table 1-1) (Marmotti et al., 2013b; Sasaki et al., 2008; Okano et al., 2014). However, the mechanism by which G-CSF is able to bring about an improved response still lacks understanding but it could be through altering the differentiation and trophic properties of BMSCs.

8.1. Generation of a mouse osteochondral repair model

One of the key objectives of this thesis was to develop a model in which the mechanisms and key therapeutic targets of osteochondral repair could be established. This was successfully achieved and the establishment of this consistent and reliable model is described in the second results chapter of this thesis (chapter 5). One surprising outcome of this work was the ability of the poor healing C57BL/6 strain to heal osteochondral surgical defects, as this contradicts previously published work (Fitzgerald et al., 2008; Eltawil et al., 2009). It is hypothesised that this is due to the increased depth of the defect made in this study, which allows for greater access to the underlying bone marrow and results in both intramembranous and endochondral ossification zones within the defect. The time points analysed in the data presented here were similar to those previously conducted, but it is possible that the integrity and quality of repair could deteriorate overtime and therefore longer time points will be required.

8.2. BMSCs as tissue progenitors

Whilst the trophic potential of BMSCs has been shown to be a significant part of the *in vivo* function of these cells, their contribution as tissue progenitors is an essential component of BMSCs as cell therapy for some diseases (Huang et al., 2015; Thompson et al., 2002; da Silva Meirelles, Caplan and Nardi, 2008). Recent studies however have questioned whether these cells are able to act in this way in the context of cartilage repair (Mak et al., 2015; de Windt et al., 2017). Histological analysis of the osteochondral model developed in the work presented here, identified isolated chondrocyte clusters deep within the repair tissue at 2 weeks. This observation is suggestive of endochondral ossification

and supports a conclusion that chondrocyte precursors such as BMSCs, independently differentiate at spatially distinct sites away from the surrounding cartilage and bone that neighbours the defect. It is therefore argued that further investigation into factors that drive the temporal and regional differentiation of endogenous BMSCs in the context of surgically induced osteochondral trauma is warranted.

8.2.1. Haematopoietic stem and progenitor cells influence the differentiation of BMSCs

G-CSF is known to increase the number of haematopoietic stem and progenitor cells (HSPCs) within the bone marrow. HSPCs and BMSCs interact directly with each other *in vivo* in the bone marrow niche, a microenvironment specialised to maintain the survival and quiescence of haematopoietic stem cells (HSCs). Therefore, chapter 4 investigated the influence of this interaction on the differentiation and cell fate of BMSCs as this could be of relevance to the understanding of G-CSF's role in the repair of bone and cartilage tissues. The study conducted here describes the ability of HSPCs to reduce the matrix deposition of calcium and thus inhibit the osteogenic differentiation of the BMSC cell line D1 ORL UVA. This demonstrates that HSPCs can influence the make-up of their surrounding microenvironment that *in vivo* consists of both BMSCs and osteoblasts (Durand, Charbord and Jaffredo, 2018). Additionally, this series of work adds to mechanistic insight into the use of G-CSF by illustrating how one of its target cell types, HSPCs directly influence osteogenesis.

8.2.2. BMSCs can respond directly to G-CSF altering their differentiation progression

The bone marrow is a complex microenvironment and the most dramatic and well characterised effect of G-CSF is on the components of the haematopoietic system. However, there is also evidence that G-CSF acts directly on BMSCs. Results presented in chapter 7 of this thesis support this with demonstration that human BMSCs express the receptor for this cytokine and intracellular signalling pathways can be activated upon G-CSF treatment of these cells. Whilst one paper indicates that G-CSF is able to induce rabbit BMSC proliferation *in vitro* (Sasaki et al., 2017), data presented here does not support this for human BMSCs. However, experiments in chapter 6 perhaps suggest that these cells do increase their number when G-CSF is administered *in vivo* as the number of nestin positive cells do increase in both the spleen and the systemic circulation, although it cannot be ruled out that the trauma induced in these mice may have contributed to this observation.

The effect of G-CSF on BMSC differentiation status was assessed in the nestin-GFP reporter mice by assessing GFP positive cells in the spinal vertebrae. Unfortunately, the inconsistency of the data and limited animal numbers prevented any conclusions from

being drawn from this study. However, earlier data from Mendez-Ferrer et al. (2010) has shown a decrease in differentiation genes in these mice. In light of this, the influence of G-CSF on the *in vitro* differentiation of human BMSCs was evaluated (chapter 7). Whilst adipogenesis and osteogenesis were unaffected, the production of proteoglycan by BMSCs was reduced under chondrogenesis inductive culture. This is perhaps contrary to what one might expect as G-CSF has been shown to improve articular cartilage repair in animal models (Sasaki et al., 2008; Okano et al., 2014).

Although osteogenesis was unaffected by G-CSF in the *in vitro* assay performed here (chapter 7), it is well accepted that *in vivo* administration of G-CSF leads to the apoptosis of osteoblasts (Christopher and Link, 2008) and osteopenia in both mice and human patients (Kokai et al., 2002; Sekhar et al., 2001). However, short-term administration has been shown in mice to lead to a resurgence in the number of osteoblasts once treatment has ended (Winkler et al., 2012, 2010). This short-term exposure might be the key and therefore it would be worthwhile to repeat the *in vitro* experiments with G-CSF included in the media for only a proportion of the differentiation assay. One might hypothesise that the reduction in proteoglycan production by chondro-induced BMSCs is a result of continued exposure throughout the culture period and results might be altered if G-CSF were only present for the initial period of the assay.

8.3. BMSCs and their trophic/immunomodulatory response

Within the repair tissue of the surgically induced osteochondral defect in mice in chapter 5, both neutrophils and monocytes were identified. These cell types have a major role in wound healing as part of the granulation tissue, clearing potential pathogens and wound debris. Additionally, they are thought to help regulate inflammation and produce mediators that activate other cells involved in the repair process (Wilgus, Roy and McDaniel, 2013). Interestingly, both G-CSF (Martins, Han and Kim, 2010; Boneberg and Hartung, 2002) and BMSCs (Chiossone et al., 2016; Németh et al., 2009) are thought to enhance this ability of monocyte lineage cells, whilst G-CSF also increases the number of neutrophils and monocytes within the circulation.

8.3.1. Cell death is an immunomodulatory function of BMSCs

The trophic and immunomodulatory role of BMSCs is reflected in their ability to respond and migrate to injury sites where they secrete reparative factors such as paracrine growth factors, cytokines and extracellular vesicles. Through this action they influence the viability and proliferation of neighbouring cells, induce angiogenesis, reduce inflammation and alter immune cell responses (Wang et al., 2014). Here it is proposed that another potential mechanism through which BMSCs carry out this action that is cell death. Analysis of nestin positive cells within the osteochondral defect (chapter 6) suggests that

nestin positive BMSCs die within the first few days of repair. The death of these cells may be a mechanism through which these cells release signals to the surrounding microenvironment, such as through the release of apoptotic bodies and other extracellular vesicles or the phagocytosis of cell debris by cells such as neutrophils and monocytes. Importantly macrophages are progeny for the monocytic-lineage and are able to influence repair by either exhibiting a pro-inflammatory or a reparative phenotype. The mechanisms by which BMSCs drive the more reparative macrophage phenotype through their death is worthy of future investigation.

8.3.2. G-CSF and trophic/immunomodulatory properties

G-CSF is known to both increase the proliferation and prevent the apoptosis of neutrophils as well increase the number of monocytes in the circulation. For this reason, in addition to G-CSF's clinical use as a method to increase and mobilise HSCs into the periphery, it is also used to treat neutropenia where white blood cell counts are reduced. In this way, G-CSF treatment may influence the haematopoietic composition of the initial haematoma and the granulation tissue. Moreover, rather than just increasing the numbers of haematopoietic cells, G-CSF has also been shown to alter the phenotype and milieu secreted by haematopoietic cells. For example, it induces monocytes to produce anti-inflammatory mediators and attenuates their capacity to release pro-inflammatory cytokines (Boneberg and Hartung, 2002).

The ability of G-CSF to alter the trophic and immunomodulatory properties of BMSCs has not directly been investigated in this thesis. However, preliminary gene expression data from human BMSCs cultured *in vitro* with G-CSF does show changes, although not statistically significant, in genes associated with these properties. Furthermore, as previously mentioned, G-CSF is shown to reduce the expression of differentiation genes in nestin positive BMSCs (Mendez-Ferrer et al., 2010) and therefore a different phenotype, such as an immunomodulatory phenotype, may be driven by G-CSF exposure. Finally, in chapter 4, the co-culture of HSPCs, known to increase with G-CSF administration, with a BMSC cell line demonstrates the reduction of an osteoblastic phenotype of these stromal cells and therefore this could suggest a shift to either the maintenance of the original phenotype, a more niche supportive phenotype and/or a more trophic phenotype.

8.4. Overall conclusions

Overall, this thesis has added to understanding of the role of BMSCs and haematopoietic cells in the repair of bone and cartilage in the context of osteochondral repair. Evidence presented here further supports a role for BMSCs as both tissue progenitors and orchestrators of the repair environment. Furthermore, data gathered demonstrate that this

environment is complex with cross talk of multiple bone marrow cells influencing the cell fate of BMSC and immune cells. Moreover, this is additionally influenced by the exogenous administration of G-CSF, a cytokine that can exert direct effects on a diverse range of cell types involved in the repair process including BMSCs. Finally, this thesis reports the development of a refined osteochondral model in mice. This model will be used in the future to elucidate the role of many of the cell types involved in osteochondral wound repair, with feasibility demonstrated here with the BMSC Nestin-GFP reporter mouse line. Going forward, this will aid a better understanding of BMSC as a cellular therapy and G-CSFs mechanism of action, allowing greater precision, translation and clinical utility.

9. REFERENCES

Abramson, S.B. and Attur, M., 2009. Developments in the scientific understanding of osteoarthritis. *Arthritis research & therapy*, 11(3), p.227.

Alexopoulos, L.G., Youn, I., Bonaldo, P. and Guilak, F., 2009. Developmental and osteoarthritic changes in *Col6a1* -knockout mice: Biomechanics of type VI collagen in the cartilage pericellular matrix. *Arthritis & Rheumatism*, 60(3), pp.771–779.

Andersen, C.L., Jensen, J.L. and Ørntoft, T.F., 2004. Normalization of Real-Time Quantitative Reverse Transcription-PCR Data: A Model-Based Variance Estimation Approach to Identify Genes Suited for Normalization, Applied to Bladder and Colon Cancer Data Sets. *Cancer Research*, 64(15), pp.5245–5250.

Anderson, D.D., Chubinskaya, S., Guilak, F., Martin, J.A., Oegema, T.R., Olson, S.A. and Buckwalter, J.A., 2011. Post-traumatic osteoarthritis: Improved understanding and opportunities for early intervention. *Journal of Orthopaedic Research*, 29(6), pp.802–809.

Arandjelovic, S. and Ravichandran, K.S., 2015. Phagocytosis of apoptotic cells in homeostasis. *Nature immunology*, 16(9), pp.907–17.

Archer, C.W., Dowthwaite, G.P. and Francis-West, P., 2003. Development of synovial joints. *Birth Defects Research Part C: Embryo Today: Reviews*, 69(2), pp.144–155.

ARUK, 2013. *Osteoarthritis in General Practice*. [online] Available at: <https://healthinnovationnetwork.com/resources/osteoarthritis-in-general-practice-arthritis-research-uk-2013/> [Accessed 26 Sep. 2018].

De Bari, C., Kurth, T.B. and Augello, A., 2010. Mesenchymal stem cells from development to postnatal joint homeostasis, aging, and disease. *Birth Defects Research Part C: Embryo Today: Reviews*, 90(4), pp.257–271.

Bark, S., Piontek, T., Behrens, P., Mkalaluh, S., Varoga, D. and Gille, J., 2014. Enhanced microfracture techniques in cartilage knee surgery: Fact or fiction? *World journal of orthopedics*, 5(4), pp.444–9.

Baron, R. and Kneissel, M., 2013. WNT signaling in bone homeostasis and disease: from human mutations to treatments. *Nature Medicine*, 19(2), pp.179–192.

Bayliss, L.E., Culliford, D., Monk, A.P., Glyn-Jones, S., Prieto-Alhambra, D., Judge, A., Cooper, C., Carr, A.J., Arden, N.K., Beard, D.J. and Price, A.J., 2017. The effect of patient age at intervention on risk of implant revision after total replacement of the hip or knee: a population-based cohort study. *The Lancet*, 389(10077), pp.1424–1430.

Becker, A. J., McCulloch, E. A. & Till, J.E., 1963. Cytological demonstration of the clonal nature

of spleen colonies derived from transplanted mouse marrow cells. *Nature*, 197, pp.452–4.

Bekkers, J.E.J., Tsuchida, A.I., van Rijen, M.H.P., Vonk, L.A., Dhert, W.J.A., Creemers, L.B. and Saris, D.B.F., 2013. Single-Stage Cell-Based Cartilage Regeneration Using a Combination of Chondrons and Mesenchymal Stromal Cells. *The American Journal of Sports Medicine*, 41(9), pp.2158–2166.

Bendall, L.J. and Bradstock, K.F., 2014. G-CSF: From granulopoietic stimulant to bone marrow stem cell mobilizing agent. *Cytokine & Growth Factor Reviews*, 25(4), pp.355–367.

Bianco, P., 2011. Bone and the hematopoietic niche : a tale of two stem cells. 117(20), pp.5281–5289.

Bianco, P., Cao, X., Frenette, P.S., Mao, J.J., Robey, P.G., Simmons, P.J. and Wang, C.-Y., 2013. The meaning, the sense and the significance: translating the science of mesenchymal stem cells into medicine. *Nature medicine*, 19(1), pp.35–42.

Bianco, P. and Robey, P.G., 2015. Skeletal stem cells. *Development (Cambridge, England)*, 142(6), pp.1023–7.

Bianco, P., Robey, P.G. and Simmons, P.J., 2008. Mesenchymal Stem Cells: Revisiting History, Concepts, and Assays. *Cell Stem Cell*, 2(4), pp.313–319.

Bijlsma, J.W.J., Berenbaum, F. and Lafeber, F.P.J.G., 2011. Osteoarthritis: An update with relevance for clinical practice. *The Lancet*, 377(9783), pp.2115–2126.

Boneberg, E.M. and Hartung, T., 2002. Molecular aspects of anti-inflammatory action of G-CSF. *Inflammation research*, 51(3), pp.119–28.

Böyum, A., 1968. Isolation of mononuclear cells and granulocytes from human blood. Isolation of monuclear cells by one centrifugation, and of granulocytes by combining centrifugation and sedimentation at 1 g. *Scandinavian journal of clinical and laboratory investigation. Supplementum*, 97, pp.77–89.

Bozlar, M., Aslan, B., Kalaci, A., Baktiroglu, L., Yanat, A.N. and Tasci, A., 2005. Effects of human granulocyte-colony stimulating factor on fracture healing in rats. *Saudi medical journal*, 26(8), pp.1250–4.

Brittberg, M., Lindahl, A., Nilsson, A., Ohlsson, C., Isaksson, O. and Peterson, L., 1994. Treatment of deep cartilage defects in the knee with autologous chondrocyte transplantation. *The New England journal of medicine*, 331(14), pp.889–895.

Brown, M. and Wittwer, C., 2000. Flow cytometry: principles and clinical applications in hematology. *Clinical chemistry*, 46(8 Pt 2), pp.1221–9.

de Bruijn, M. and Dzierzak, E., 2017. Runx transcription factors in the development and

function of the definitive hematopoietic system. *Blood*, 129(15), pp.2061–2069.

Buckwalter, J.A., 2003. Sports, Joint Injury, and Posttraumatic Osteoarthritis. *Journal of Orthopaedic & Sports Physical Therapy*, 33(10), pp.578–588.

Burnette, W.N., 1981. "Western blotting": electrophoretic transfer of proteins from sodium dodecyl sulfate--polyacrylamide gels to unmodified nitrocellulose and radiographic detection with antibody and radioiodinated protein A. *Analytical biochemistry*, 112(2), pp.195–203.

Byrd, D.T. and Kimble, J., 2009. Scratching the niche that controls Caenorhabditis elegans germline stem cells. *Seminars in Cell & Developmental Biology*, 20(9), pp.1107–1113.

Caldwell, K.L. and Wang, J., 2015. Cell-based articular cartilage repair: the link between development and regeneration. *Osteoarthritis and Cartilage*, 23(3), pp.351–362.

Caley, M.P., Martins, V.L.C. and O'Toole, E.A., 2015. Metalloproteinases and Wound Healing. *Advances in wound care*, 4(4), pp.225–234.

Calvi, L.M., Adams, G.B., Weibrecht, K.W., Weber, J.M., Olson, D.P., Knight, M.C., Martin, R.P., Schipani, E., Divieti, P., Bringhurst, F.R., Milner, L. a, Kronenberg, H.M. and Scadden, D.T., 2003. Osteoblastic cells regulate the haematopoietic stem cell niche. *Nature*, 425(6960), pp.841–846.

Campagnoli, C., Roberts, I.A., Kumar, S., Bennett, P.R., Bellantuono, I. and Fisk, N.M., 2001. Identification of mesenchymal stem/progenitor cells in human first-trimester fetal blood, liver, and bone marrow. *Blood*, 98(8), pp.2396–402.

Caplan, A.I., 1991. Mesenchymal stem cells. *Journal of orthopaedic research : official publication of the Orthopaedic Research Society*, 9(5), pp.641–650.

Caplan, A.I. and Correa, D., 2011. The MSC: An Injury Drugstore. *Cell Stem Cell*, 9(1), pp.11–15.

Caruso, S. and Poon, I.K.H., 2018. Apoptotic Cell-Derived Extracellular Vesicles: More Than Just Debris. *Frontiers in Immunology*, 9, p.1486.

Cebon, J., Layton, J.E., Maher, D. and Morstyn, G., 1994. Endogenous haemopoietic growth factors in neutropenia and infection. *British journal of haematology*, 86(2), pp.265–74.

Lo Celso, C. and Scadden, D., 2007. Isolation and transplantation of hematopoietic stem cells (HSCs). *Journal of visualized experiments : JoVE*, (2), p.157.

Charnley, J., 1961. Arthroplasty of the hip. A New Operation. *The Lancet*, 277(7187), pp.1129–1132.

de Chaumont, F., Dallongeville, S., Chenouard, N., Hervé, N., Pop, S., Provoost, T., Meas-Yedid, V., Pankajakshan, P., Lecomte, T., Le Montagner, Y., Lagache, T., Dufour, A. and Olivo-Marin, J.-C., 2012. Icy: an open bioimage informatics platform for extended reproducible research. *Nature Methods*, 9(7), pp.690–696.

Chen, D., Shen, J., Zhao, W., Wang, T., Han, L., Hamilton, J.L. and Im, H.-J., 2017. Osteoarthritis: toward a comprehensive understanding of pathological mechanism. *Bone Research*, 5, p.16044.

Cheng, A., Kapacee, Z., Peng, J., Lu, S., Lucas, R.J., Hardingham, T.E. and Kimber, S.J., 2014. Cartilage Repair Using Human Embryonic Stem Cell-Derived Chondroprogenitors. *STEM CELLS Translational Medicine*, 3(11), pp.1287–1294.

Chiossone, L., Conte, R., Spaggiari, G.M., Serra, M., Romei, C., Bellora, F., Becchetti, F., Andaloro, A., Moretta, L. and Bottino, C., 2016. Mesenchymal Stromal Cells Induce Peculiar Alternatively Activated Macrophages Capable of Dampening Both Innate and Adaptive Immune Responses. *STEM CELLS*, 34(7), pp.1909–1921.

Christopher, M.J. and Link, D.C., 2008. Granulocyte colony-stimulating factor induces osteoblast apoptosis and inhibits osteoblast differentiation. *Journal of bone and mineral research : the official journal of the American Society for Bone and Mineral Research*, 23(11), pp.1765–1774.

Chung, R. and Xian, C.J., 2014. RECENT RESEARCH ON THE GROWTH PLATE: Mechanisms for growth plate injury repair and potential cell-based therapies for regeneration. *Journal of Molecular Endocrinology*, 53(1), pp.T45–T61.

Cibrián Uhalte, E., Wilkinson, J.M., Southam, L. and Zeggini, E., 2017. Pathways to understanding the genomic aetiology of osteoarthritis. *Human molecular genetics*, 26(R2), pp.R193–R201.

Claes, L., Recknagel, S. and Ignatius, A., 2012. Fracture healing under healthy and inflammatory conditions. *Nature Reviews Rheumatology*, 8(3), pp.133–143.

Dell'accio, F. and Vincent, T.L., 2010. Joint surface defects: clinical course and cellular response in spontaneous and experimental lesions. *European cells & materials*, 20, pp.210–7.

Dexter, T.M., Allen, T.D. and Lajtha, L.G., 1977. Conditions controlling the proliferation of haemopoietic stem cells in vitro. *Journal of Cellular Physiology*, 91(3), pp.335–344.

Diekman, B.O., Wu, C.-L., Louer, C.R., Furman, B.D., Huebner, J.L., Kraus, V.B., Olson, S.A. and Guilak, F., 2013. Intra-articular delivery of purified mesenchymal stem cells from C57BL/6 or MRL/MpJ superhealer mice prevents posttraumatic arthritis. *Cell transplantation*, 22(8), pp.1395–408.

Ding, L., Saunders, T.L., Enikolopov, G. and Morrison, S.J., 2012. Endothelial and perivascular cells maintain haematopoietic stem cells. *Nature*, 481(7382), pp.457–462.

Dominici, M., Le Blanc, K., Mueller, I., Slaper-Cortenbach, I., Marini, F., Krause, D., Deans, R., Keating, A., Prockop, D. and Horwitz, E., 2006. Minimal criteria for defining multipotent mesenchymal stromal cells. The International Society for Cellular Therapy position statement. *Cytotherapy*, 8(4), pp.315–317.

Dowthwaite, G.P., Bishop, J.C., Redman, S.N., Khan, I.M., Rooney, P., Evans, D.J.R., Haughton, L., Bayram, Z., Boyer, S., Thomson, B., Wolfe, M.S. and Archer, C.W., 2004. The surface of articular cartilage contains a progenitor cell population. *Journal of Cell Science*, 117(6), pp.889–897.

Driban, J.B., Sitler, M.R., Barbe, M.F. and Balasubramanian, E., 2010. Is osteoarthritis a heterogeneous disease that can be stratified into subsets? *Clinical Rheumatology*, 29(2), pp.123–131.

Drost, A.C., Weng, S., Feil, G., Schäfer, J., Baumann, S., Kanz, L., Sievert, K.-D., Stenzl, A. and Möhle, R., 2009. In vitro Myogenic Differentiation of Human Bone Marrow-Derived Mesenchymal Stem Cells as a Potential Treatment for Urethral Sphincter Muscle Repair. *Annals of the New York Academy of Sciences*, 1176(1), pp.135–143.

Durand, C., Charbord, P. and Jaffredo, T., 2018. The crosstalk between hematopoietic stem cells and their niches. *Current Opinion in Hematology*, 25(4), pp.285–289.

Dwivedi, P. and Greis, K.D., 2017. Granulocyte colony-stimulating factor receptor signaling in severe congenital neutropenia, chronic neutrophilic leukemia, and related malignancies. *Experimental Hematology*, 46, pp.9–20.

Eltawil, N.M., De Bari, C., Achan, P., Pitzalis, C. and Dell'Accio, F., 2009. A novel in vivo murine model of cartilage regeneration. Age and strain-dependent outcome after joint surface injury. *Osteoarthritis and Cartilage*, 17(6), pp.695–704.

Eyles, J.L., Roberts, A.W., Metcalf, D. and Wicks, I.P., 2006. Granulocyte colony-stimulating factor and neutrophils--forgotten mediators of inflammatory disease. *Nature clinical practice. Rheumatology*, 2(9), pp.500–510.

Farndale, R.W., Buttle, D.J. and Barrett, A.J., 1986. Improved quantitation and discrimination of sulphated glycosaminoglycans by use of dimethylmethylene blue. *Biochimica et biophysica acta*, 883(2), pp.173–7.

Fellows, C.R., Matta, C., Zakany, R., Khan, I.M. and Mobasheri, A., 2016. Adipose, Bone Marrow and Synovial Joint-Derived Mesenchymal Stem Cells for Cartilage Repair. *Frontiers in genetics*, 7, p.213.

Ferraro, F., Lymperi, S., Mendez-Ferrer, S., Saez, B., Spencer, J. a., Yeap, B.Y., Masselli, E., Graiani, G., Prezioso, L., Rizzini, E.L., Mangoni, M., Rizzoli, V., Sykes, S.M., Lin, C.P., Frenette, P.S., Quaini, F. and Scadden, D.T., 2011. Diabetes Impairs Hematopoietic Stem Cell Mobilization by Altering Niche Function. *Science Translational Medicine*, 3(104), p.104ra101-104ra101.

Fitzgerald, J., Rich, C., Burkhardt, D., Allen, J., Herzka, a. S. and Little, C.B., 2008. Evidence for articular cartilage regeneration in MRL/MpJ mice. *Osteoarthritis and Cartilage*, 16(11), pp.1319–1326.

Fox, A.J.S., Bedi, A. and Rodeo, S.A., 2009. The Basic Science of Articular Cartilage: Structure, Composition, and Function.

Frenette, P.S., Pinho, S., Lucas, D. and Scheiermann, C., 2013. *Mesenchymal stem cell: keystone of the hematopoietic stem cell niche and a stepping-stone for regenerative medicine. Annual review of immunology*, .

Friedenstein, A.J., Chailakhyan, R.K. and Gerasimov, U. V, 1987. Bone marrow osteogenic stem cells: in vitro cultivation and transplantation in diffusion chambers. *Cell and tissue kinetics*, 20(3), pp.263–72.

Friedenstein, A.J., Petrakova, K. V, Kurolesova, A.I. and Frolova, G.P., 1968. Heterotopic of bone marrow. Analysis of precursor cells for osteogenic and hematopoietic tissues. *Transplantation*, 6(2), pp.230–247.

Fukunaga, R., Seto, Y., Mizushima, S. and Nagata, S., 1990. Three different mRNAs encoding human granulocyte colony-stimulating factor receptor. *Proceedings of the National Academy of Sciences of the United States of America*, 87(22), pp.8702–6.

Furmento, V.A., Marino, J., Blank, V.C. and Roguin, L.P., 2014. The granulocyte colony-stimulating factor (G-CSF) upregulates metalloproteinase-2 and VEGF through PI3K/Akt and Erk1/2 activation in human trophoblast Swan 71 cells. *Placenta*, 35(11), pp.937–946.

Galleu, A., Riffo-Vasquez, Y., Trento, C., Lomas, C., Dolcetti, L., Cheung, T.S., von Bonin, M., Barbieri, L., Halai, K., Ward, S., Weng, L., Chakraverty, R., Lombardi, G., Watt, F.M., Orchard, K., Marks, D.I., Apperley, J., Bornhauser, M., Walczak, H., Bennett, C. and Dazzi, F., 2017. Apoptosis in mesenchymal stromal cells induces in vivo recipient-mediated immunomodulation. *Science translational medicine*, 9(416), p.eaam7828.

Gartner, S. and Kaplan, H.S., 1980. Long-term culture of human bone marrow cells. *Proceedings of the National Academy of Sciences of the United States of America*, 77(8), pp.4756–9.

Gelber, A.C., Hochberg, M.C., Mead, L.A., Wang, N.Y., Wigley, F.M. and Klag, M.J., 2000. Joint injury in young adults and risk for subsequent knee and hip osteoarthritis. *Annals of*

internal medicine, 133(5), pp.321–8.

Goldring, M.B. and Marcu, K.B., 2009. Cartilage homeostasis in health and rheumatic diseases. *Arthritis Research & Therapy*, 11(3), p.224.

Gomoll, A.H., Madry, H., Knutsen, G., van Dijk, N., Seil, R., Brittberg, M. and Kon, E., 2010. The subchondral bone in articular cartilage repair: current problems in the surgical management. *Knee surgery, sports traumatology, arthroscopy : official journal of the ESSKA*, 18(4), pp.434–47.

Gosset, M., Berenbaum, F., Thirion, S. and Jacques, C., 2008. Primary culture and phenotyping of murine chondrocytes. *Nature Protocols*, 3(8), pp.1253–1260.

Greenbaum, A., Hsu, Y.-M.S., Day, R.B., Schuettpelz, L.G., Christopher, M.J., Borgerding, J.N., Nagasawa, T. and Link, D.C., 2013. CXCL12 in early mesenchymal progenitors is required for haematopoietic stem-cell maintenance. *Nature*, 495(7440), pp.227–230.

Greenbaum, A.M. and Link, D.C., 2011. Mechanisms of G-CSF-mediated hematopoietic stem and progenitor mobilization. *Leukemia*, 25(2), pp.211–217.

de Haas, M., Kerst, J.M., van der Schoot, C.E., Calafat, J., Hack, C.E., Nuijens, J.H., Roos, D., van Oers, R.H. and von dem Borne, A.E., 1994. Granulocyte colony-stimulating factor administration to healthy volunteers: analysis of the immediate activating effects on circulating neutrophils. *Blood*, 84(11), pp.3885–3894.

Hattori, S., Oxford, C. and Reddi, A.H., 2007. Identification of superficial zone articular chondrocyte stem/progenitor cells. *Biochemical and biophysical research communications*, 358(1), pp.99–103.

Ho, M.S.H., Medcalf, R.L., Livesey, S. a. and Traianedes, K., 2015. The dynamics of adult haematopoiesis in the bone and bone marrow environment. *British Journal of Haematology*, 170(4), pp.472–486.

Hoggatt, J. and Pelus, L.M., 2011. Mobilization of hematopoietic stem cells from the bone marrow niche to the blood compartment. *Stem cell research & therapy*, 2(2), p.13.

Hokari, M., Kuroda, S., Chiba, Y., Maruichi, K. and Iwasaki, Y., 2009. Synergistic effects of granulocyte-colony stimulating factor on bone marrow stromal cell transplantation for mice cerebral infarct. *Cytokine*, 46(2), pp.260–266.

Hopper, N., Wardale, J., Brooks, R., Power, J., Rushton, N. and Henson, F., 2015. Peripheral Blood Mononuclear Cells Enhance Cartilage Repair in in vivo Osteochondral Defect Model. *PLOS ONE*, 10(8), p.e0133937.

Huang, S., Xu, L., Zhang, Y., Sun, Y. and Li, G., 2015. Systemic and Local Administration of Allogeneic Bone Marrow-Derived Mesenchymal Stem Cells Promotes Fracture Healing in

Rats. *Cell Transplantation*, 24(12), pp.2643–2655.

ter Huurne, M., Schelbergen, R., Blattes, R., Blom, A., de Munter, W., Grevers, L.C., Jeanson, J., Noël, D., Casteilla, L., Jorgensen, C., van den Berg, W. and van Lent, P.L.E.M., 2012. Antiinflammatory and chondroprotective effects of intraarticular injection of adipose-derived stem cells in experimental osteoarthritis. *Arthritis & Rheumatism*, 64(11), pp.3604–3613.

Hyvärinen, K., Holopainen, M., Skirdenko, V., Ruhanen, H., Lehenkari, P., Korhonen, M., Käkelä, R., Laitinen, S. and Kerkelä, E., 2018. Mesenchymal Stromal Cells and Their Extracellular Vesicles Enhance the Anti-Inflammatory Phenotype of Regulatory Macrophages by Downregulating the Production of Interleukin (IL)-23 and IL-22. *Frontiers in immunology*, 9, p.771.

Isern, J., García-García, A., Martín, A.M., Arranz, L., Martín-Pérez, D., Torroja, C., Sánchez-Cabo, F. and Méndez-Ferrer, S., 2014. The neural crest is a source of mesenchymal stem cells with specialized hematopoietic stem cell niche function. *eLife*, 3, p.e03696.

Ishida, K., Matsumoto, T., Sasaki, K., Mifune, Y., Tei, K., Kubo, S., Matsushita, T., Takayama, K., Akisue, T., Tabata, Y., Kurosaka, M. and Kuroda, R., 2010. Bone regeneration properties of granulocyte colony-stimulating factor via neovascularization and osteogenesis. *Tissue engineering. Part A*, 16(10), pp.3271–3284.

Izu, Y., Ezura, Y., Koch, M., Birk, D.E. and Noda, M., 2016. Collagens VI and XII form complexes mediating osteoblast interactions during osteogenesis. *Cell and tissue research*, 364(3), pp.623–35.

Jiang, Y. and Tuan, R.S., 2015. Origin and function of cartilage stem/progenitor cells in osteoarthritis. *Nature Reviews Rheumatology*, 11(4), pp.206–212.

Jing, D., Fonseca, A.V., Alakel, N., Fierro, F. a., Muller, K., Bornhauser, M., Ehninger, G., Corbeil, D. and Ordemann, R., 2010. Hematopoietic stem cells in co-culture with mesenchymal stromal cells -modeling the niche compartments in vitro. *Haematologica*, 95(4), pp.542–550.

Johnstone, B., Hering, T.M., Caplan, A.I., Goldberg, V.M. and Yoo, J.U., 1998. In VitroChondrogenesis of Bone Marrow-Derived Mesenchymal Progenitor Cells. *Experimental Cell Research*, 238(1), pp.265–272.

Jung, Y., Song, J., Shiozawa, Y., Wang, J., Wang, Z., Williams, B., Havens, A., Schneider, A., Ge, C., Franceschi, R.T., McCauley, L.K., Krebsbach, P.H. and Taichman, R.S., 2008. Hematopoietic stem cells regulate mesenchymal stromal cell induction into osteoblasts thereby participating in the formation of the stem cell niche. *Stem cells*, 26(8), pp.2042–2051.

Katayama, Y., Battista, M., Kao, W.M., Hidalgo, A., Peired, A.J., Thomas, S. a. and Frenette, P.S., 2006. Signals from the sympathetic nervous system regulate hematopoietic stem cell egress from bone marrow. *Cell*, 124(2), pp.407–421.

Kawakami, M., Tsutsumi, H., Kumakawa, T., Abe, H., Hirai, M., Kurosawa, S., Mori, M. and Fukushima, M., 1990. Levels of serum granulocyte colony-stimulating factor in patients with infections. *Blood*, 76(10), pp.1962–1964.

Kawamoto, T. and Kawamoto, K., 2014. Preparation of Thin Frozen Sections from Nonfixed and Undecalcified Hard Tissues Using Kawamot's Film Method (2012). In: *Methods in molecular biology (Clifton, N.J.)*. pp.149–164.

Kaygusuz, M.A., Turan, C.C., Aydın, N.E., Temel, İ., Fırat, S., Bulut, T. and Kuku, İ., 2006. The effects of G-CSF and naproxen sodium on the serum TGF-β1 level and fracture healing in rat tibias. *Life Sciences*, 80(1), pp.67–73.

Ke, N., Wang, X., Xu, X. and Abassi, Y.A., 2011. The xCELLigence System for Real-Time and Label-Free Monitoring of Cell Viability. In: *Methods in molecular biology (Clifton, N.J.)*. pp.33–43.

Kim, H., Choi, J.-Y., Lee, J.M., Park, Y.S., Suh, H., Song, H.-R., Jo, S.A. and Jo, I., 2008. Dexamethasone increases angiopoietin-1 and quiescent hematopoietic stem cells: A novel mechanism of dexamethasone-induced hematoprotection. *FEBS Letters*, 582(23–24), pp.3509–3514.

Kohn, M.D., Sassoon, A.A. and Fernando, N.D., 2016. Classifications in Brief: Kellgren-Lawrence Classification of Osteoarthritis. *Clinical orthopaedics and related research*, 474(8), pp.1886–93.

Kokai, Y., Wada, T., Oda, T., Kuwabara, H., Hara, K., Akiyama, Y., Ishii, S. and Sawada, N., 2002. Overexpression of granulocyte colony-stimulating factor induces severe osteopenia in developing mice that is partially prevented by a diet containing vitamin K2 (menatetrenone). *Bone*, 30(6), pp.880–885.

Koyama, E., Shibukawa, Y., Nagayama, M., Sugito, H., Young, B., Yuasa, T., Okabe, T., Ochiai, T., Kamiya, N., Rountree, R.B., Kingsley, D.M., Iwamoto, M., Enomoto-Iwamoto, M. and Pacifici, M., 2008. A distinct cohort of progenitor cells participates in synovial joint and articular cartilage formation during mouse limb skeletogenesis. *Developmental Biology*, 316(1), pp.62–73.

Kraus, V.B., Blanco, F.J., Englund, M., Karsdal, M.A. and Lohmander, L.S., 2015. Call for standardized definitions of osteoarthritis and risk stratification for clinical trials and clinical use. *Osteoarthritis and Cartilage*, 23(8), pp.1233–1241.

Kuroda, R., Matsumoto, T., Miwa, M., Kawamoto, A., Mifune, Y., Fukui, T., Kawakami, Y., Niikura, T., Lee, S.Y., Oe, K., Shoji, T., Kuroda, T., Horii, M., Yokoyama, A., Ono, T., Koibuchi, Y., Kawamata, S., Fukushima, M., Kurosaka, M. and Asahara, T., 2011. Local transplantation of G-CSF-mobilized CD34 + cells in a patient with tibial nonunion: A case report. *Cell Transplantation*, 20(9), pp.1491–1496.

Kuroda, R., Matsumoto, T., Niikura, T., Kawakami, Y., Fukui, T., Lee, S.Y., Mifune, Y., Kawamata, S., Fukushima, M., Asahara, T., Kawamoto, A. and Kurosaka, M., 2014. Local transplantation of granulocyte colony stimulating factor-mobilized CD34+ cells for patients with femoral and tibial nonunion: pilot clinical trial. *Stem cells translational medicine*, 3(1), pp.128–134.

Kuyinu, E.L., Narayanan, G., Nair, L.S. and Laurencin, C.T., 2016. Animal models of osteoarthritis: classification, update, and measurement of outcomes. *Journal of orthopaedic surgery and research*, 11, p.19.

Kwoh, C.K., 2013. Clinical relevance of bone marrow lesions in OA. *Nature Reviews Rheumatology*, 9(1), pp.7–8.

Lambertsen, R.H. and Weiss, L., 1984. A model of intramedullary hematopoietic microenvironments based on stereologic study of the distribution of endocloned marrow colonies. *Blood*, 63(2), pp.287–297.

Lemoli, R.M. and D'Addio, A., 2008. Hematopoietic stem cell mobilization. *Haematologica*, 93(3), pp.321–4.

Levesque, J.-P., Hendy, J., Takamatsu, Y., Simmons, P.J. and Bendall, L.J., 2003. Disruption of the CXCR4/CXCL12 chemotactic interaction during hematopoietic stem cell mobilization induced by GCSF or cyclophosphamide. *The Journal of clinical investigation*, 111(2), pp.187–196.

Levesque, J.-P., Liu, F., Simmons, P.J., Betsuyaku, T., Senior, R.M., Pham, C. and Link, D.C., 2004. Characterization of hematopoietic progenitor mobilization in protease-deficient mice. *Blood*, 104(1), pp.65–72.

Levesque, J.P., Takamatsu, Y., Nilsson, S.K., Haylock, D.N. and Simmons, P.J., 2001. Vascular cell adhesion molecule-1 (CD106) is cleaved by neutrophil proteases in the bone marrow following hematopoietic progenitor cell mobilization by granulocyte colony-stimulating factor. *Blood*, 98(5), pp.1289–1297.

Li, G., Yin, J., Gao, J., Cheng, T.S., Pavlos, N.J., Zhang, C. and Zheng, M.H., 2013. Subchondral bone in osteoarthritis: insight into risk factors and microstructural changes. *Arthritis Research & Therapy*, 15(6), p.223.

Li, J. and Sartorelli, A.C., 1994. Evidence for the glycosylation of the granulocyte colony-stimulating factor receptor. *Biochemical and biophysical research communications*, 205(1), pp.238–44.

Liao, J., Hammerick, K.E., Challen, G. a., Goodell, M. a., Kasper, F.K. and Mikos, A.G., 2011. Investigating the role of hematopoietic stem and progenitor cells in regulating the osteogenic differentiation of mesenchymal stem cells in vitro. *Journal of Orthopaedic Research*, 29(10),

pp.1544–1553.

Lieberthal, J., Sambamurthy, N. and Scanzello, C.R., 2015. Inflammation in joint injury and post-traumatic osteoarthritis. *Osteoarthritis and cartilage*, 23(11), pp.1825–34.

Lieu, S., Hansen, E., Dedini, R., Behonick, D., Werb, Z., Miclau, T., Marcucio, R. and Colnot, C., 2011. Impaired remodeling phase of fracture repair in the absence of matrix metalloproteinase-2. *Disease Models & Mechanisms*, 4(2), pp.203–211.

Liu, F., Poursine-Laurent, J. and Link, D.C., 2000. Expression of the G-CSF receptor on hematopoietic progenitor cells is not required for their mobilization by G-CSF. *Blood*, 95(10), pp.3025–3031.

Lotz, M.K., Otsuki, S., Grogan, S.P., Sah, R., Terkeltaub, R. and D'Lima, D., 2010. Cartilage cell clusters. *Arthritis and rheumatism*, 62(8), pp.2206–18.

Lowenthal, R., Ragg, S., Anderson, J., Nicholson, L., Harrup, R. and Tuck, D., 2007. A randomized controlled clinical trial to determine the optimum duration of G-CSF priming prior to BM stem cell harvesting. *Cytotherapy*, 9(2), pp.158–164.

Lund, T.C., Baso, L. and Orchard, P.J., 2006. G-CSF Mobilized Human Mesenchymal Stem Cells Are Found in the Peripheral Blood and Have Telomere Limited Growth Potential. *Blood*, 108(11).

Lydon, H., Getgood, A. and Henson, F.M.D., 2017. Healing of Osteochondral Defects via Endochondral Ossification in an Ovine Model. *CARTILAGE*, p.194760351771381.

Ma, S., Xie, N., Li, W., Yuan, B., Shi, Y. and Wang, Y., 2014. Immunobiology of mesenchymal stem cells. *Cell Death & Differentiation*, 21(2), pp.216–225.

MacKay, J.W., Kapoor, G., Driban, J.B., Lo, G.H., McAlindon, T.E., Toms, A.P., McCaskie, A.W. and Gilbert, F.J., 2018. Association of subchondral bone texture on magnetic resonance imaging with radiographic knee osteoarthritis progression: data from the Osteoarthritis Initiative Bone Ancillary Study. *European Radiology*.

Mackie, E.J., Ahmed, Y.A., Tatarczuch, L., Chen, K.-S. and Mirams, M., 2008. Endochondral ossification: How cartilage is converted into bone in the developing skeleton. *The International Journal of Biochemistry & Cell Biology*, 40(1), pp.46–62.

Mackie, E.J., Tatarczuch, L. and Mirams, M., 2011. The skeleton: a multi-functional complex organ. The growth plate chondrocyte and endochondral ossification. *Journal of Endocrinology*, 211(2), pp.109–121.

Madry, H., van Dijk, C.N. and Mueller-Gerbl, M., 2010. The basic science of the subchondral bone. *Knee Surgery, Sports Traumatology, Arthroscopy*, 18(4), pp.419–433.

Mak, J., Leonard, C., Foniok, T., Rushforth, D., Dunn, J.F. and Krawetz, R., 2015. Evaluating endogenous repair of focal cartilage defects in C57BL/6 and MRL/MpJ mice using 9.4T magnetic resonance imaging: A pilot study. *Magnetic Resonance Imaging*, 33(5), pp.690–694.

Marenah, M., Li, J., Kumar, A. and Murrell, W., 2018. Quality assurance and adverse event management in regenerative medicine for knee osteoarthritis: Current concepts. *Journal of Clinical Orthopaedics and Trauma*.

Marmotti, a., Bonasia, D.E., Bruzzone, M., Rossi, R., Castoldi, F., Collo, G., Realmuto, C., Tarella, C. and Peretti, G.M., 2013a. Human cartilage fragments in a composite scaffold for single-stage cartilage repair: An in vitro study of the chondrocyte migration and the influence of TGF-??1 and G-CSF. *Knee Surgery, Sports Traumatology, Arthroscopy*, 21(8), pp.1819–1833.

Marmotti, a., Castoldi, F., Rossi, R., Marenco, S., Risso, a., Ruella, M., Tron, a., Borrè, a., Blonna, D. and Tarella, C., 2013b. Bone marrow-derived cell mobilization by G-CSF to enhance osseointegration of bone substitute in high tibial osteotomy. *Knee Surgery, Sports Traumatology, Arthroscopy*, 21(1), pp.237–248.

Marsell, R. and Einhorn, T.A., 2011. The biology of fracture healing. *Injury*, 42(6), pp.551–5.

Martinez, R., Figueroa, D., Calvo, R., Conget, P., Gallegos, M., Figueroa, F. and Ahumada, X., 2015. Osteochondral lesion mouse model: An alternative for experimental work. *Revista Española de Cirugía Ortopédica y Traumatología (English Edition)*, 59(1), pp.9–13.

Martins, A., Han, J. and Kim, S.O., 2010. The multifaceted effects of granulocyte colony-stimulating factor in immunomodulation and potential roles in intestinal immune homeostasis. *IUBMB life*, 62(8), pp.611–7.

Matsuoka, M., Onodera, T., Sasazawa, F., Momma, D., Baba, R., Hontani, K. and Iwasaki, N., 2015. An Articular Cartilage Repair Model in Common C57Bl/6 Mice. *Tissue engineering. Part C, Methods*, 21(8), pp.767–72.

Mendes, S.C., Robin, C. and Dzierzak, E., 2005. Mesenchymal progenitor cells localize within hematopoietic sites throughout ontogeny. *Development*, 132(5), pp.1127–1136.

Méndez-Ferrer, S., Michurina, T. V, Ferraro, F., Mazloom, A.R., Macarthur, B.D., Lira, S. a, Scadden, D.T., Ma'ayan, A., Enikolopov, G.N. and Frenette, P.S., 2010. Mesenchymal and haematopoietic stem cells form a unique bone marrow niche. *Nature*, 466(7308), pp.829–834.

Mignone, J.L., Kukekov, V., Chiang, A.-S., Steindler, D. and Enikolopov, G., 2004. Neural stem and progenitor cells in nestin-GFP transgenic mice. *The Journal of Comparative Neurology*, 469(3), pp.311–324.

Miltenyi, S., Müller, W., Weichel, W. and Radbruch, A., 1990. High gradient magnetic cell

separation with MACS. *Cytometry*, 11(2), pp.231–238.

Minagawa, T., Tabata, Y., Oyama, A., Furukawa, H., Yamao, T. and Yamamoto, Y., 2014. Controlled release of granulocyte colony-stimulating factor enhances osteoconductive and biodegradable properties of Beta-tricalcium phosphate in a rat calvarial defect model. *International journal of biomaterials*, 2014, p.134521.

Mithoefer, K., McAdams, T., Williams, R.J., Kreuz, P.C. and Mandelbaum, B.R., 2009. Clinical efficacy of the microfracture technique for articular cartilage repair in the knee: an evidence-based systematic analysis. *The American journal of sports medicine*, 37(10), pp.2053–2063.

Mithoefer, K., Venugopal, V. and Manaqibwala, M., 2016. Incidence, Degree, and Clinical Effect of Subchondral Bone Overgrowth After Microfracture in the Knee. *The American Journal of Sports Medicine*, 44(8), pp.2057–2063.

Mobasheri, A., Rayman, M.P., Gualillo, O., Sellam, J., van der Kraan, P. and Fearon, U., 2017. The role of metabolism in the pathogenesis of osteoarthritis. *Nature Reviews Rheumatology*, 13(5), pp.302–311.

Morelli, A.E., 2006. The Immune Regulatory Effect of Apoptotic Cells and Exosomes on Dendritic Cells: Its Impact on Transplantation. *American Journal of Transplantation*, 6(2), pp.254–261.

Morikawa, S., Mabuchi, Y., Kubota, Y., Nagai, Y., Niibe, K., Hiratsu, E., Suzuki, S., Miyauchi-Hara, C., Nagoshi, N., Sunabori, T., Shimmura, S., Miyawaki, A., Nakagawa, T., Suda, T., Okano, H. and Matsuzaki, Y., 2009. Prospective identification, isolation, and systemic transplantation of multipotent mesenchymal stem cells in murine bone marrow. *The Journal of Experimental Medicine*, 206(11), pp.2483–2496.

Morrison, S.J. and Scadden, D.T., 2014. The bone marrow niche for haematopoietic stem cells. *Nature*, 505(7483), pp.327–334.

Mowry, R., 1956. Alcian blue technics for the histochemical study of acidic carbohydrates. *J Histochem Cytochem*, (4), p.407.

Muguruma, Y., Yahata, T., Miyatake, H., Sato, T., Uno, T., Itoh, J., Kato, S., Ito, M., Hotta, T. and Ando, K., 2006. Reconstitution of the functional human hematopoietic microenvironment derived from human mesenchymal stem cells in the murine bone marrow compartment. *Blood*, 107(5), pp.1878–1887.

Mussano, F., Lee, K.J., Zuk, P., Tran, L., Cacalano, N.A., Jewett, A., Carossa, S. and Nishimura, I., 2010. Differential effect of ionizing radiation exposure on multipotent and differentiation-restricted bone marrow mesenchymal stem cells. *Journal of Cellular Biochemistry*, 111(2), pp.322–332.

Narcisi, R., Cleary, M.A., Brama, P.A.J., Hoogduijn, M.J., Tüysüz, N., ten Berge, D. and van Osch, G.J.V.M., 2015. Long-term expansion, enhanced chondrogenic potential, and suppression of endochondral ossification of adult human MSCs via WNT signaling modulation. *Stem cell reports*, 4(3), pp.459–72.

Németh, K., Leelahavanichkul, A., Yuen, P.S.T., Mayer, B., Parmelee, A., Doi, K., Robey, P.G., Leelahavanichkul, K., Koller, B.H., Brown, J.M., Hu, X., Jelinek, I., Star, R.A. and Mezey, É., 2009. Bone marrow stromal cells attenuate sepsis via prostaglandin E2–dependent reprogramming of host macrophages to increase their interleukin-10 production. *Nature Medicine*, 15(1), pp.42–49.

NICE, 2017. Autologous chondrocyte implantation for treating symptomatic articular cartilage defects of the knee | Guidance and guidelines | NICE.

OARSI, 2016. *OARSI White Paper- OA as a Serious Disease | Osteoarthritis Research Society International (OARSI)*. [online] Available at: <https://www.oarsi.org/education/oarsi-resources/oarsi-white-paper-oa-serious-disease> [Accessed 26 Sep. 2018].

Ok Bozkaya, I., Azik, F., Tavil, B., Koksal, Y., Ozguner, M., Tunc, B. and Uckan Cetinkaya, D., 2015. The Effect of Granulocyte Colony–Stimulating Factor on Immune-Modulatory Cytokines in the Bone Marrow Microenvironment and Mesenchymal Stem Cells of Healthy Donors. *Biology of Blood and Marrow Transplantation*, 21(11), pp.1888–1894.

Okano, T., Mera, H., Itokazu, M., Okabe, T., Koike, T., Nakamura, H. and Wakitani, S., 2014. Systemic Administration of Granulocyte Colony-Stimulating Factor for Osteochondral Defect Repair in a Rat Experimental Model. *Cartilage*, 5(2), pp.107–113.

Omatsu, Y., Sugiyama, T., Kohara, H., Kondoh, G., Fujii, N., Kohno, K. and Nagasawa, T., 2010. The Essential Functions of Adipo-osteogenic Progenitors as the Hematopoietic Stem and Progenitor Cell Niche. *Immunity*, 33(3), pp.387–399.

Oono, T., Specks, U., Eckes, B., Majewski, S., Hunzelmann, N., Timpl, R. and Krieg, T., 1993. Expression of type VI collagen mRNA during wound healing. *The Journal of investigative dermatology*, 100(3), pp.329–34.

Orozco, L., Munar, A., Soler, R., Alberca, M., Soler, F., Huguet, M., Sentís, J., Sánchez, A. and García-Sancho, J., 2013. Treatment of Knee Osteoarthritis With Autologous Mesenchymal Stem Cells. *Transplantation Journal*, 95(12), pp.1535–1541.

Ortiz, L.A., DuTreil, M., Fattman, C., Pandey, A.C., Torres, G., Go, K. and Phinney, D.G., 2007. Interleukin 1 receptor antagonist mediates the antiinflammatory and antifibrotic effect of mesenchymal stem cells during lung injury. *Proceedings of the National Academy of Sciences*, 104(26), pp.11002–11007.

Owen, M. and Friedenstein, A.J., 1988. Stromal stem cells: marrow-derived osteogenic

precursors. *Ciba Foundation symposium*, 136, pp.42–60.

Paletta, G.A., Arnoczky, S.P. and Warren, R.F., 1992. The repair of osteochondral defects using an exogenous fibrin clot. *The American Journal of Sports Medicine*, 20(6), pp.725–731.

Panaroni, C., Tzeng, Y., Saeed, H. and Wu, J.Y., 2014. Mesenchymal Progenitors and the Osteoblast Lineage in Bone Marrow Hematopoietic Niches. *Current Osteoporosis Reports*, 12(1), pp.22–32.

Parmar, K., Mauch, P., Vergilio, J.-A., Sackstein, R. and Down, J.D., 2007. Distribution of hematopoietic stem cells in the bone marrow according to regional hypoxia. *Proceedings of the National Academy of Sciences*, 104(13), pp.5431–5436.

Passegué, E., Jamieson, C.H.M., Ailles, L.E. and Weissman, I.L., 2003. Normal and leukemic hematopoiesis: are leukemias a stem cell disorder or a reacquisition of stem cell characteristics? *Proceedings of the National Academy of Sciences of the United States of America*, 100 Suppl 1(suppl 1), pp.11842–9.

Păunescu, V., Deak, E., Herman, D., Siska, I.R., Tănasie, G., Bunu, C., Anghel, S., Tatu, C.A., Oprea, T.I., Henschler, R., Rüster, B., Bistrian, R. and Seifried, E., 2007. In vitro differentiation of human mesenchymal stem cells to epithelial lineage. *Journal of cellular and molecular medicine*, 11(3), pp.502–8.

Peng, C., Chen, Y., Shan, Y., Zhang, H., Guo, Z., Li, D. and Li, S., 2012. LSK Derived LSK– Cells Have a High Apoptotic Rate Related to Survival Regulation of Hematopoietic and Leukemic Stem Cells. *PLoS ONE*, 7(6), p.e38614.

Perez, J.R., Kouroupis, D., Li, D.J., Best, T.M., Kaplan, L. and Correa, D., 2018. Tissue Engineering and Cell-Based Therapies for Fractures and Bone Defects. *Frontiers in bioengineering and biotechnology*, 6, p.105.

Phinney, D.G., Hill, K., Michelson, C., DuTreil, M., Hughes, C., Humphries, S., Wilkinson, R., Baddoo, M. and Bayly, E., 2006. Biological Activities Encoded by the Murine Mesenchymal Stem Cell Transcriptome Provide a Basis for Their Developmental Potential and Broad Therapeutic Efficacy. *Stem Cells*, 24(1), pp.186–198.

Pineda, S., Pollack, A., Stevenson, S., Goldberg, V. and Caplan, A., 1992. A semiquantitative scale for histologic grading of articular cartilage repair. *Acta anatomica*, 143(4), pp.335–40.

Pittenger, M.F., Mackay, A.M., Beck, S.C., Jaiswal, R.K., Douglas, R., Mosca, J.D., Moorman, M.A., Simonetti, D.W., Craig, S. and Marshak, D.R., 1999. Multilineage potential of adult human mesenchymal stem cells. *Science (New York, N.Y.)*, 284(5411), pp.143–7.

Ponte, A.L., Ribeiro-Fleury, T., Chabot, V., Gouilleux, F., Langonné, A., Hérault, O., Charbord, P. and Domenech, J., 2012. Granulocyte-Colony-Stimulating Factor Stimulation of Bone

Marrow Mesenchymal Stromal Cells Promotes CD34+ Cell Migration Via a Matrix Metalloproteinase-2-Dependent Mechanism. *Stem Cells and Development*, 21(17), p.120724080005007.

Pridie, K. and Gordon, G., 1959. A method of resurfacing osteoarthritic knee joints. *Journal of Bone and Joint Surgery*, 41(3), pp.618–619.

Puchtler, H., Meloan, S.N. and Terry, M.S., 1969. On the history and mechanism of alizarin and alizarin red s stains for calcium. *Journal of Histochemistry & Cytochemistry*, 17(2), pp.110–124.

Punzi, L., Galozzi, P., Luisetto, R., Favero, M., Ramonda, R., Oliviero, F. and Scanu, A., 2016. Post-traumatic arthritis: overview on pathogenic mechanisms and role of inflammation. *RMD Open*, 2(2), p.e000279.

Ramírez-Zacarías, J.L., Castro-Muñozledo, F. and Kuri-Harcuch, W., 1992. Quantitation of adipose conversion and triglycerides by staining intracytoplasmic lipids with Oil red O. *Histochemistry*, 97(6), pp.493–7.

Reinisch, A., Etchart, N., Thomas, D., Hofmann, N.A., Fruehwirth, M., Sinha, S., Chan, C.K., Senarath-Yapa, K., Seo, E.-Y., Wearda, T., Hartwig, U.F., Beham-Schmid, C., Trajanoski, S., Lin, Q., Wagner, W., Dullin, C., Alves, F., Andreeff, M., Weissman, I.L., Longaker, M.T., Schallmoser, K., Majeti, R. and Strunk, D., 2015. Epigenetic and in vivo comparison of diverse MSC sources reveals an endochondral signature for human hematopoietic niche formation. *Blood*, 125(2), pp.249–260.

Reyes, E., García-Castro, I., Esquivel, F., Hornedo, J., Cortes-Funes, H., Solovera, J. and Alvarez-Mon, M., 1999. Granulocyte colony-stimulating factor (G-CSF) transiently suppresses mitogen-stimulated T-cell proliferative response. *British Journal of Cancer*, 80(1–2), pp.229–235.

Roelofs, A.J., Zupan, J., Riemen, A.H.K., Kania, K., Ansboro, S., White, N., Clark, S.M. and De Bari, C., 2017. Joint morphogenetic cells in the adult mammalian synovium. *Nature Communications*, 8, p.15040.

Rustad, K.C. and Gurtner, G.C., 2012. Mesenchymal Stem Cells Home to Sites of Injury and Inflammation. *Advances in wound care*, 1(4), pp.147–152.

Ryd, L., Brittberg, M., Eriksson, K., Jurvelin, J.S., Lindahl, A., Marlovits, S., Möller, P., Richardson, J.B., Steinwachs, M. and Zenobi-Wong, M., 2015. Pre-Osteoarthritis. *CARTILAGE*, 6(3), pp.156–165.

Sacchetti, B., Funari, A., Michienzi, S., Di Cesare, S., Piersanti, S., Saggio, I., Tagliafico, E., Ferrari, S., Robey, P.G., Riminucci, M. and Bianco, P., 2007. Self-Renewing Osteoprogenitors in Bone Marrow Sinusoids Can Organize a Hematopoietic Microenvironment. *Cell*, 131(2),

pp.324–336.

Sandell, L.J., 2012. Etiology of osteoarthritis: genetics and synovial joint development. *Nature Reviews Rheumatology*, 8(2), pp.77–89.

Sasaki, K., Kuroda, R., Ishida, K., Mifune, Y., Kinoshita, K., Kubo, S., Tei, K., Fujita, N. and Kurosaka, M., 2008. Granulocyte colony-stimulating factor promotes osteogenesis in human mesenchymal stem cells. In: *54th Annual Meeting of the Orthopaedic Research Society*. p.860.

Sasaki, T., Akagi, R., Akatsu, Y., Fukawa, T., Hoshi, H., Yamamoto, Y., Enomoto, T., Sato, Y., Nakagawa, R., Takahashi, K., Yamaguchi, S. and Sasho, T., 2017. The effect of systemic administration of G-CSF on a full-thickness cartilage defect in a rabbit model MSC proliferation as presumed mechanism: G-CSF for cartilage repair. *Bone & joint research*, 6(3), pp.123–131.

Sato, T. and Clevers, H., 2013. Growing Self-Organizing Mini-Guts from a Single Intestinal Stem Cell: Mechanism and Applications. *Science*, 340(6137), pp.1190–1194.

Saw, K.-Y., Anz, A., Merican, S., Tay, Y.-G., Ragavanaidu, K., Jee, C.S.Y. and McGuire, D.A., 2011. Articular cartilage regeneration with autologous peripheral blood progenitor cells and hyaluronic acid after arthroscopic subchondral drilling: a report of 5 cases with histology. *Arthroscopy : the journal of arthroscopic & related surgery : official publication of the Arthroscopy Association of North America and the International Arthroscopy Association*, 27(4), pp.493–506.

Saw, K.-Y., Anz, A., Siew-Yoke Jee, C., Merican, S., Ching-Soong Ng, R., Roohi, S.A. and Ragavanaidu, K., 2013. Articular cartilage regeneration with autologous peripheral blood stem cells versus hyaluronic acid: a randomized controlled trial. *Arthroscopy : the journal of arthroscopic & related surgery : official publication of the Arthroscopy Association of North America and the International Arthroscopy Association*, 29(4), pp.684–694.

Saw, K.-Y., Hussin, P., Loke, S.-C., Azam, M., Chen, H.-C., Tay, Y.-G., Low, S., Wallin, K.-L. and Ragavanaidu, K., 2009. Articular cartilage regeneration with autologous marrow aspirate and hyaluronic Acid: an experimental study in a goat model. *Arthroscopy : the journal of arthroscopic & related surgery : official publication of the Arthroscopy Association of North America and the International Arthroscopy Association*, 25(12), pp.1391–1400.

Schaefer, B.C., Schaefer, M.L., Kappler, J.W., Marrack, P. and Kedl, R.M., 2001. Observation of Antigen-Dependent CD8+ T-Cell/ Dendritic Cell Interactions in Vivo. *Cellular Immunology*, 214(2), pp.110–122.

Schindelin, J., Arganda-Carreras, I., Frise, E., Kaynig, V., Longair, M., Pietzsch, T., Preibisch, S., Rueden, C., Saalfeld, S., Schmid, B., Tinevez, J.-Y., White, D.J., Hartenstein, V., Eliceiri, K., Tomancak, P. and Cardona, A., 2012. Fiji: an open-source platform for biological-image analysis. *Nature Methods*, 9(7), pp.676–682.

Schlundt, C., El Khassawna, T., Serra, A., Dienelt, A., Wendler, S., Schell, H., van Rooijen, N., Radbruch, A., Lucius, R., Hartmann, S., Duda, G.N. and Schmidt-Bleek, K., 2018. Macrophages in bone fracture healing: Their essential role in endochondral ossification. *Bone*, 106, pp.78–89.

Schmittgen, T.D. and Livak, K.J., 2008. Analyzing real-time PCR data by the comparative CT method. *Nature Protocols*, 3(6), pp.1101–1108.

Schmitz, N., Laverty, S., Kraus, V.B. and Aigner, T., 2010. Basic methods in histopathology of joint tissues. *Osteoarthritis and Cartilage*, 18, pp.S113–S116.

Schneeberger, C., Speiser, P., Kury, F. and Zeillinger, R., 1995. Quantitative detection of reverse transcriptase-PCR products by means of a novel and sensitive DNA stain. *PCR methods and applications*, 4(4), pp.234–8.

Schofield, R., 1978. The relationship between the spleen colony-forming cell and the haemopoietic stem cell. *Blood cells*, 4(1–2), pp.7–25.

Schuettpelz, L.G., Borgerding, J.N., Christopher, M.J., Gopalan, P.K., Romine, M.P., Herman, A.C., Woloszynek, J.R., Greenbaum, A.M. and Link, D.C., 2014. G-CSF regulates hematopoietic stem cell activity, in part, through activation of Toll-like receptor signaling. *Leukemia*, 28(9), pp.1851–60.

Scuteri, A., Miloso, M., Foudah, D., Orciani, M., Cavaletti, G. and Tredici, G., 2011. Mesenchymal Stem Cells Neuronal Differentiation Ability: A Real Perspective for Nervous System Repair? *Current Stem Cell Research & Therapy*, 6(2), pp.82–92.

Sekhar, R. V, Culbert, S., Hoots, W.K., Klein, M.J., Zietz, H. and Vassilopoulou-Sellin, R., 2001. Severe osteopenia in a young boy with Kostmann's congenital neutropenia treated with granulocyte colony-stimulating factor: suggested therapeutic approach. *Pediatrics*, 108(3), p.E54.

Semerad, C.L., Christopher, M.J., Liu, F., Short, B., Simmons, P.J., Winkler, I., Levesque, J.P., Chappel, J., Ross, F.P. and Link, D.C., 2005. G-CSF potently inhibits osteoblast activity and CXCL12 mRNA expression in the bone marrow. *Blood*, 106(9), pp.3020–3027.

Seol, D., McCabe, D.J., Choe, H., Zheng, H., Yu, Y., Jang, K., Walter, M.W., Lehman, A.D., Ding, L., Buckwalter, J.A. and Martin, J.A., 2012. Chondrogenic progenitor cells respond to cartilage injury. *Arthritis & Rheumatism*, 64(11), pp.3626–3637.

Shah, J.M.Y., Omar, E., Pai, D.R. and Sood, S., 2012. Cellular events and biomarkers of wound healing. *Indian journal of plastic surgery : official publication of the Association of Plastic Surgeons of India*, 45(2), pp.220–8.

Shapiro, F., Koide, S. and Glimcher, M.J., 1993. Cell origin and differentiation in the repair of

full-thickness defects of articular cartilage. *The Journal of bone and joint surgery. American volume*, 75(4), pp.532–53.

da Silva Meirelles, L., Caplan, A.I. and Nardi, N.B., 2008. In Search of the In Vivo Identity of Mesenchymal Stem Cells. *Stem Cells*, 26(9), pp.2287–2299.

Sims, N.A. and Martin, T.J., 2014. Coupling the activities of bone formation and resorption: a multitude of signals within the basic multicellular unit. *BoneKEy Reports*, 3, p.481.

Singh, P., Hu, P., Hoggatt, J., Moh, a and Pelus, L.M., 2012. Expansion of bone marrow neutrophils following G-CSF administration in mice results in osteolineage cell apoptosis and mobilization of hematopoietic stem and progenitor cells. *Leukemia*, 26(11), pp.2375–2383.

Sinusas, K., 2012. Osteoarthritis: diagnosis and treatment. *American family physician*, 85(1), pp.49–56.

Sivaraj, K.K. and Adams, R.H., 2016. Blood vessel formation and function in bone. *Development*, 143(15), pp.2706–2715.

Skinner, R.A., Hickmon, S.G., Lumpkin, C.K., Aronson, J. and Nicholas, R.W., 1997. Decalcified Bone: Twenty Years of Successful Specimen Management. *Journal of Histotechnology*, 20(3), pp.267–277.

Smeriglio, P., Dhulipala, L., Lai, J.H., Goodman, S.B., Dragoo, J.L., Smith, R.L., Maloney, W.J., Yang, F. and Bhutani, N., 2015. Collagen VI enhances cartilage tissue generation by stimulating chondrocyte proliferation. *Tissue engineering. Part A*, 21(3–4), pp.840–9.

Steadman, J.R., Rodkey, W.G. and Briggs, K.K., 2010. Microfracture: Its History and Experience of the Developing Surgeon. *Cartilage*, 1(2), pp.78–86.

Steadman, J.R., Rodkey, W.G., Singleton, S.B. and Briggs, K.K., 1997. Microfracture technique forfull-thickness chondral defects: Technique and clinical results. *Operative Techniques in Orthopaedics*, 7(4), pp.300–304.

Steinberg, J., Brooks, R.A., Southam, L., Bhatnagar, S., Roumeliotis, T.I., Hatzikotoulas, K., Zengini, E., Wilkinson, J.M., Choudhary, J.S., McCaskie, A.W. and Zeggini, E., 2018. Widespread epigenomic, transcriptomic and proteomic differences between hip osteophytic and articular chondrocytes in osteoarthritis. *Rheumatology*, 57(8), pp.1481–1489.

Sugiyama, T., Kohara, H., Noda, M. and Nagasawa, T., 2006. Maintenance of the Hematopoietic Stem Cell Pool by CXCL12-CXCR4 Chemokine Signaling in Bone Marrow Stromal Cell Niches. *Immunity*, 25(6), pp.977–988.

Szarko, M. and Xia, Y., 2012. Direct Visualisation of the Depth-Dependent Mechanical Properties of Full-Thickness Articular Cartilage. *Open journal of orthopedics*, 2.

Taichman, R.S. and Emerson, S.G., 1994. Human osteoblasts support hematopoiesis through the production of granulocyte colony-stimulating factor. *The Journal of experimental medicine*, 179(5), pp.1677–1682.

Taichman, R.S., Reilly, M.J. and Emerson, S.G., 1996. Human osteoblasts support human hematopoietic progenitor cells in vitro bone marrow cultures. *Blood*, 87(2), pp.518–524.

Talwadekar, M.D., Kale, V.P. and Limaye, L.S., 2015. Placenta-derived mesenchymal stem cells possess better immunoregulatory properties compared to their cord-derived counterparts–a paired sample study. *Scientific Reports*, 5(1), p.15784.

Tavassoli, M. and Crosby, W.H., 1968. Transplantation of Marrow to Extramedullary Sites. *Science*, 161(3836), pp.54–56.

Thompson, Z., Miclau, T., Hu, D. and Helms, J.A., 2002. *A model for intramembranous ossification during fracture healing*. *Journal of Orthopaedic Research*, .

Tiku, M.L. and Sabaawy, H.E., 2015. Cartilage regeneration for treatment of osteoarthritis: a paradigm for nonsurgical intervention. *Therapeutic Advances in Musculoskeletal Disease*, 7(3), pp.76–87.

Touw, I.P. and van de Geijn, G.-J.M., 2007. Granulocyte colony-stimulating factor and its receptor in normal myeloid cell development, leukemia and related blood cell disorders. *Frontiers in bioscience : a journal and virtual library*, 12, pp.800–15.

Towbin, H., Staehelin, T. and Gordon, J., 1979. Electrophoretic transfer of proteins from polyacrylamide gels to nitrocellulose sheets: procedure and some applications. *Proceedings of the National Academy of Sciences of the United States of America*, 76(9), pp.4350–4.

Uccelli, A., Moretta, L. and Pistoia, V., 2008. Mesenchymal stem cells in health and disease. *Nature Reviews Immunology*, 8(9), pp.726–736.

UniProt, 2018. *UniProtKB - Q99062 (CSF3R_HUMAN)*. [online] 2018. Available at: <https://www.uniprot.org/uniprot/Q99062> [Accessed 26 Sep. 2018].

United Nations, 2017. *World Population Prospects The 2017 Revision*.

Vasiliadis, H.S. and Wasiak, J., 2010. Autologous chondrocyte implantation for full thickness articular cartilage defects of the knee. *Cochrane Database of Systematic Reviews*, (10), p.CD003323.

Visnjic, D., Kalajzic, Z., Rowe, D.W., Katavic, V., Lorenzo, J. and Aguila, H.L., 2004. Hematopoiesis is severely altered in mice with an induced osteoblast deficiency. *Blood*, 103(9), pp.3258–3264.

Vonk, L.A., van Dooremalen, S.F.J., Liv, N., Klumperman, J., Coffer, P.J., Saris, D.B.F. and

Lorenowicz, M.J., 2018. Mesenchymal Stromal/stem Cell-derived Extracellular Vesicles Promote Human Cartilage Regeneration *In Vitro*. *Theranostics*, 8(4), pp.906–920.

Wang, Y., Chen, X., Cao, W. and Shi, Y., 2014. Plasticity of mesenchymal stem cells in immunomodulation: pathological and therapeutic implications. *Nature Immunology*, 15(11), pp.1009–1016.

Weinstein, Y., Ihle, J.N., Lavu, S. and Reddy, E.P., 1986. Truncation of the c-myb gene by a retroviral integration in an interleukin 3-dependent myeloid leukemia cell line. *Proceedings of the National Academy of Sciences of the United States of America*, 83(14), pp.5010–4.

WHO, 2016. WHO | Chronic rheumatic conditions. *WHO*.

Wieland, H.A., Michaelis, M., Kirschbaum, B.J. and Rudolphi, K.A., 2005. Osteoarthritis - an untreatable disease? *Nature reviews. Drug discovery*, 4(4), pp.331–344.

Wilgus, T.A., Roy, S. and McDaniel, J.C., 2013. Neutrophils and Wound Repair: Positive Actions and Negative Reactions. *Advances in Wound Care*, 2(7), pp.379–388.

Williams, R., Khan, I.M., Richardson, K., Nelson, L., McCarthy, H.E., Analbelsi, T., Singhrao, S.K., Dowthwaite, G.P., Jones, R.E., Baird, D.M., Lewis, H., Roberts, S., Shaw, H.M., Dudhia, J., Fairclough, J., Briggs, T. and Archer, C.W., 2010. Identification and Clonal Characterisation of a Progenitor Cell Sub-Population in Normal Human Articular Cartilage. *PLoS ONE*, 5(10), p.e13246.

de Windt, T.S., Vonk, L.A., Slaper-Cortenbach, I.C.M., Nizak, R., van Rijen, M.H.P. and Saris, D.B.F., 2017. Allogeneic MSCs and Recycled Autologous Chondrons Mixed in a One-Stage Cartilage Cell Transplantion: A First-in-Man Trial in 35 Patients. *STEM CELLS*, 35(8), pp.1984–1993.

Winkler, I.G., Pettit, a R., Raggatt, L.J., Jacobsen, R.N., Forristal, C.E., Barbier, V., Nowlan, B., Cisterne, a, Bendall, L.J., Sims, N. a and Lévesque, J.-P., 2012. Hematopoietic stem cell mobilizing agents G-CSF, cyclophosphamide or AMD3100 have distinct mechanisms of action on bone marrow HSC niches and bone formation. *Leukemia*, 26(7), pp.1594–1601.

Winkler, I.G., Sims, N. a, Pettit, A.R., Barbier, V., Nowlan, B., Helwani, F. and Ingrid, J., 2010. Bone marrow macrophages maintain hematopoietic stem cell (HSC) niches and their depletion mobilizes HSC Bone marrow macrophages maintain hematopoietic stem cell (HSC) niches and their depletion mobilizes HSC. 116(23), pp.4815–4829.

Wittwer, C.T., Herrmann, M.G., Moss, A.A. and Rasmussen, R.P., 1997. Continuous fluorescence monitoring of rapid cycle DNA amplification. *BioTechniques*, 22(1), pp.130–1, 134–8.

van der Woude, J.-T.A.D., Wiegant, K., van Roermund, P.M., Intema, F., Custers, R.J.H.,

Eckstein, F., van Laar, J.M., Mastbergen, S.C. and Lafeber, F.P.J.G., 2017. Five-Year Follow-up of Knee Joint Distraction: Clinical Benefit and Cartilaginous Tissue Repair in an Open Uncontrolled Prospective Study. *CARTILAGE*, 8(3), pp.263–271.

Wu, L., Leijten, J.C.H., Georgi, N., Post, J.N., van Blitterswijk, C.A. and Karperien, M., 2011. Trophic effects of mesenchymal stem cells increase chondrocyte proliferation and matrix formation. *Tissue engineering. Part A*, 17(9–10), pp.1425–36.

Wu, L., Prins, H.-J., Helder, M.N., van Blitterswijk, C.A. and Karperien, M., 2012. Trophic effects of mesenchymal stem cells in chondrocyte co-cultures are independent of culture conditions and cell sources. *Tissue engineering. Part A*, 18(15–16), pp.1542–51.

Xie, L., Zeng, X., Hu, J. and Chen, Q., 2015. Characterization of Nestin, a Selective Marker for Bone Marrow Derived Mesenchymal Stem Cells. *Stem cells international*, 2015, p.762098.

Xu, J., Li, Z., Hou, Y. and Fang, W., 2015. Potential mechanisms underlying the Runx2 induced osteogenesis of bone marrow mesenchymal stem cells. *American journal of translational research*, 7(12), pp.2527–35.

Yang, Y., Pang, D., Hu, C., Lv, Y., He, T., An, Y., Tang, Z. and Deng, Z., 2015. Nestin Positive Bone Marrow Derived Cells Responded to Injury Mobilize into Peripheral Circulation and Participate in Skin Defect Healing. *PLOS ONE*, 10(12), p.e0143368.

Zengini, E., Hatzikotoulas, K., Tachmazidou, I., Steinberg, J., Hartwig, F.P., Southam, L., Hackinger, S., Boer, C.G., Styrkarsdottir, U., Gilly, A., Suveges, D., Killian, B., Ingvarsson, T., Jonsson, H., Babis, G.C., McCaskie, A., Uitterlinden, A.G., van Meurs, J.B.J., Thorsteinsdottir, U., Stefansson, K., Davey Smith, G., Wilkinson, J.M. and Zeggini, E., 2018. Genome-wide analyses using UK Biobank data provide insights into the genetic architecture of osteoarthritis. *Nature Genetics*, 50(4), pp.549–558.

Zhang, J., Niu, C., Ye, L., Huang, H., He, X., Tong, W.-G., Ross, J., Haug, J., Johnson, T., Feng, J.Q., Harris, S., Wiedemann, L.M., Mishina, Y. and Linheng, L., 2003. Identification of the haematopoietic stem cell niche and control of the niche size. *Nature*, 425(October), pp.836–841.

Zhang, W., Ouyang, H., Dass, C.R. and Xu, J., 2016. Current research on pharmacologic and regenerative therapies for osteoarthritis. *Bone research*, 4, p.15040.

Zhou, B.O., Yue, R., Murphy, M.M., Peyer, J.G. and Morrison, S.J., 2014. Leptin-receptor-expressing mesenchymal stromal cells represent the main source of bone formed by adult bone marrow. *Cell stem cell*, 15(2), pp.154–68.

Zhou, S., Cui, Z. and Urban, J.P.G., 2004. Factors influencing the oxygen concentration gradient from the synovial surface of articular cartilage to the cartilage-bone interface: A modeling study. *Arthritis & Rheumatism*, 50(12), pp.3915–3924.

10. APPENDIX

10.1. Patient Details

Patient ID	*Source*	*Age*	*Sex*
Pt 329	Addenbrooke's Hospital Patient	89 years	Female
Pt 398	Addenbrooke's Hospital Patient	55 years	Female
Pt 399	Addenbrooke's Hospital Patient	72 years	Female
L27766	Lonza	23 years	Female
L30654	Lonza	22 years	Male
L29518	Lonza	31 years	Male

10.2. Human qRT-PCR Housekeeping Gene Stability Data

Raw qRT-PCR data (average CT values shown for three technical replicates) of BMSCs cultured to 70% confluency and then serum starved overnight before the addition of 10% FCS, 100 ng/mL G-CSF or 50 ng/mL G-CSF.

Gene name	*No serum*	*10% FCS*	*100 ng/mL G-CSF*	*50 ng/mL G-CSF*
HPRT	23.65	24.27	24.10	23.96
GAPDH	17.59	18.37	17.55	17.44
B2M	17.38	18.50	17.96	17.79

NormFinder results using the data above.

Gene name	*Stability value*	*Standard error*
HPRT	0.013	0.007
GAPDH	0.014	0.007
B2M	0.008	0.009

10.3. qRT-PCR Primers

Target Gene	*Sequence*	*Validation*			
		Sample	***Slope***	***R^2***	***Efficiency percentage***
MURINE PRIMERS					
Bglap	Fw:GGGCAATAAGGTAGTGAACAG Rv:GCAGCACAGGTCCTAAATAGT	D10 osteo D1ORLUVA	-3.366	0.99	98.181
Runx2	Fw:CGGCCCTCCCTGAACTCT Rv:TGCCTGCCTGGGATCTGTA	D7 osteo D1ORLUVA	-3.301	0.997	100.864
Sp7	Fw:ATGGCGTCCTCTCTGCTTGA Rv:GAAGGGTGGGTAGTCATTTG	D10 osteo D1ORLUVA	-3.244	0.997	103.363
Col1a2	Fw:GTAACTTCGTGCCTAGCAACA Rv:CCTTTGTCAGAATACTGAGCAGC	D10 osteo D1ORLUVA	-3.157	0.997	107.361
Col2a1	Fw:CGAGTGGAAGAGCGGAGACT Rv:AACTTTCATGGCGTCCAAGGT	Mouse costal chondrocytes	-3.247	0.998	103.229
Sox9	Fw:AGTACCCGCATCTGCACAAC Rv:ACGAAGGGTCTCTTCTCGCT	Mouse costal chondrocytes	-3.311	0.998	100.454
Tgfβ	Fw:GAGCCCGAAGCGGACTACTA Rv:TGGTTTTCTCATAGATGGCGTTG	D7 chondro D1ORLUVA	-3.004	0.984	115.196
Lpl	Fw:GGGAGTTTGGCTCCAGAGTTT Rv:TGTGTCTTCAGGGGTCCTTAG	D7 adipo D1ORLUVA	-3.192	0.988	105.719
Fabp4	Fw:AAAGAAGTGGGAGTGGGCTT Rv:CTCTTGTGGAAGTCACGCCT	D7 adipo D1ORLUVA	-3.154	0.953	107.543
Pparγ	Fw:GGTGAGGAGAGCTCTGGAAG Rv:GACTGAGGAAGGGCTGGAAG	D7 adipo D1ORLUVA	-3.312	0.972	100.395
Flt3	Fw:GAGCGACTCCAGCTACGTC Rv:ACCCAGTGAAAATATCTCCCAGA	Primary lineage negative BM	-3.533	0.952	91.876
Hck	Fw:TCCTCCGAGATGGAAGCAAG Rv:ACAGTGCGACCACAATGGTAT	Primary lineage positive BM	-3.307	0.925	100.631
Ptprc	Fw:CATGTGCTCCAGCTACAACTATAGATT	Primary lineage positive BM	-3.668	0.976	87.345

	Rv:TGCAGTCATGTAGCGAAAACTTG				
Cfsr3	Fw:CTGATCTTCTTGCTACTCCCCA Rv:GGTGTAGTTCAAGTGAGGCAG	Primary lineage positive BM	-3.053	0.984	112.602
Hprt	Predesigned QuantiTect Qiagen primers				
HUMAN PRIMERS					
RUNX2	Fw:GGTTAATCTCCGCAGGTCAC Rv:GTCACTGTGCTGAAGAGGCT	Primers validated by other lab members			
ALP	Fw:CCCAAAGGCTTCTTCTTG Rv:CTGGTAGTTGTTGTGAGCAT				
VEGF	Fw:GAGCCTTGCCTTGCTGCTCTAC Rv:CACCAGGGTCTCGATTGGATG				
HIF1α	Fw:CCACAGGACAGTACAGGATG Rv:TCAAGTCGTGCTGAATAATACC				
IL-6	Fw:TTCAATGAGGAGACTTGCCTG Rv:ACAACAACAATCTGAGGTGCC				
CCL2	Fw:TCATAGCAGCCACCTTCATTC Rv:TAGCGCAGATTCTTGGGTTG				
CXCL10	Fw:TGGCATTCAAGGAGTACCTCTC Rv:CGTGGACAAAATTGGCTTGC				
IDO	Fw:CAAAGGTCATGGAGATGTCC Rv:CCACCAATAGAGAGACCAGG				
SOX9	Fw:GCAGGCGGAGGCAGAGGAG Rv:GGAGGAGGAGTGTGGCGAGTC				
COL2A	Fw:AACCAGATTGAGAGCATCCGC Rv:CGATAACAGTCTTGCCCCACTTAC				
ACAN	Fw:TCCCCACGGTCTCTCTTGTAG Rv:GCCCACTTAGGTCCAGAAATCC				
COMP	Fw:AACAGTGCCCAGGAGGAC Rv:TTGTCTACCACCTTGTCTGC				

HPRT	Fw:TGACACTGGCAAAACAATGCA Rv:GGTCCTTTTCACCAGCAAGCT
GAPDH	Fw:CTCTGCTCCTCCTGTTCGACA Rv:ACGACCAAATCCGTTGACTC
B2M	Predesigned QuantiTect Qiagen primers
STAT3	Predesigned SYBR green primers from Sigma
EFNB2	Predesigned SYBR green primers from Sigma
FGG	Predesigned SYBR green primers from Sigma